IX-24
FEDD
30513

NASA Contractor Report 194969

(NASA-CR-194969) BENCHMARK PANELS Final Technical Report (Boeing Commercial Airplane Co.) 235 p
LIMIT DOMESTIC

X94-10518

Unclas

G4/24 0030513



Benchmark Panels

T. H. Walker, L. B. Ilcewicz, J. B. Bodine, D. P. Murphy, and E. F. Dost
Boeing Commercial Airplane Group, Seattle, Washington

Contract NAS1-19349
August 1994

National Aeronautics and
Space Administration
Langley Research Center
Hampton, Virginia 23681-0001

Approved for public release

Foreword

This document is the final technical report on fabrication and analysis efforts relating to advanced composite design concepts for transport aircraft crown structure conducted in response to the statement of work for Contract 19349, Task 2, "Benchmark Panels." The work was conducted from March 1992 through December 1993. Jim Nelson was the Contracting Officer's Technical Representative, and Mark Shuart and Jim Starnes were the Technical Monitors, all from Langley Research Center, Hampton, Virginia. Contributors to this effort are contained in the list below.

Use of commercial products or names of manufacturers in this report does not constitute official endorsement of such products or manufacturers, either expressed or implied, by the National Aeronautics and Space Administration.

Program Management
- R. Horton
- J. Olson

Principal Investigator
- E. Dost

Technical Monitoring
- T. Walker
- L. Ilcewicz
- J. Bodine
- D. Polland

Benchmark Panel Fabrication
- K. Willden
- M. Gessel
- C. Grant (Hercules)
- T. Brown (Hercules)
- G. Sharpless (Fiber Innovations)
- S. Goodwin (Fiber Innovations)

Benchmark Panel Finite Element Analysis
- D. Murphy

Strain Softening Development
- B. Dopker

Frame/Skin Bondline Analysis and Test
- M. Fedro
- P. Minguet
- J. Awerbuch (Drexel University)
- A. Wang (Drexel University)

Table of Contents

FOREWORD I

1.0 SUMMARY 1

2.0 INTRODUCTION 4

3.0 BENCHMARK PANEL DEFINITION 9

4.0 PANEL FABRICATION 12

4.1 Skin and Stringer Charges 12

4.2 Frames 12

4.3 Panel Assembly and Cure 13

4.4 Inspection 14

4.5 Attachment of Frames, Failsafe Chords 15

4.6 Edge Doublers 15

5.0 BENCHMARK PANEL FINITE ELEMENT ANALYSIS 19

5.1 Modeling Details 19

5.2 Design Support 25

5.3 Model Results 26

5.4 Comparison with Panel 11b Test Results 29

6.0 STRAIN SOFTENING MODEL DEVELOPMENT 31

6.1 Background 31

6.2 Justification 32

6.3 Developments and Findings 37

7.0 FRAME/SKIN BONDLINE ANALYSIS AND TEST 45

7.1 Introduction 45

7.2 Clamped Pulloff Tests 47

7.3 Global Pressure Pillowing Analysis 52

7.4 Pulloff Tests Using a Modified (Simply Supported) Fixture 55

7.5 Failure Mechanisms 59

7.6 Detailed Failure Analysis 63

7.7 Preliminary Fatigue Testing 66

7.8 Preliminary Moused Frame Pulloff Tests 67

8.0 CONCLUSIONS AND RECOMMENDATIONS 71

9.0 REFERENCES 73

Table of Contents (Concluded)

Appendix A	Panel Bond, Cutting Diagram, and Panel Assembly Drawings for Panel 1
Appendix B	Panel Bond, Cutting Diagram, and Panel Assembly Drawings for Panel 2
Appendix C	Panel Bond, Cutting Diagram, and Panel Assembly Drawings for Panel 3
Appendix D	Panel Bond, Cutting Diagram, and Panel Assembly Drawings for Panel 4
Appendix E	Panel Bond, Cutting Diagram, and Panel Assembly Drawings for Panel 5
Appendix F	Frame Fabrication Drawing
Appendix G	Finite Element Results for Undamaged Panel 1
Appendix H	Finite Element Results for Undamaged Panel 2
Appendix I	Finite Element Results for Undamaged Panel 3
Appendix J	Finite Element Results for Undamaged Panel 4
Appendix K	Finite Element Results for Undamaged Panel 5

1.0 Summary

Benchmark Panel Fabrication. Five curved stiffened panels representative of ATCAS fuselage crown design alternatives were fabricated to provide test specimens for the pressure-box test fixture and for frame/skin bondline strength evaluations. These panels augmented ATCAS pressure-box panels by providing an opportunity for tests of alternate damage scenarios (e.g., large circumferentially-oriented notches, barely visible impact damage), attractive alternate design concepts, and other panel locations.

The designs were characterized by a 122 in. radius, tow-placed skins, hot-drape-formed hat-section stringers, and braided/RTM J-section frames. Attractive design alternatives contained in the panel designs included intraply hybrid skins, higher-stiffness stringers, and bolted frames with smaller mouseholes.

Pulse-echo inspection of the panels revealed no anomalies, however a repeatable pattern was observed in the skins of all panels. The pattern was hypothesized to be a result of thickness variations caused by consistent non-uniformities in band thickness being magnified when the bands of similarly-oriented plies were stacked.

Pulse-echo inspection of the braided frames indicated localized defective regions in the inner chord of six frames. Photomicrographs taken in the defect areas of the frame trim revealed microcracks at the laminate midplane. Three of the frames were trimmed such that all defect regions fell in the trim areas. Fasteners were installed in the inner frame chord of the other three to prevent any delamination growth during testing. The microcracks were hypothesized to be caused by increased residual stresses due to a higher percentage of 0° yarns and a somewhat higher fiber volume fraction than in the other twelve frames.

Load-introduction doublers were fabricated for each pressure-box test panel and provided, with appropriate fasteners, to NASA Langley Research Center for installation. Doubler designs varied with specific panel configuration and loading requirements. Slots were included in all between-frame doublers and the longer between-stringer doublers to maximize decoupling of axial and hoop loads.

Benchmark Panel Finite Element Analysis. Geometrically nonlinear finite element analysis was conducted to support the development of test fixturing, and provide predictions of undamaged panel response. The model utilized shell, brick, and beam elements to properly simulate the panel and load introduction fixturing. The undamaged model contained 2,500 elements and 13,900 degrees-of-freedom. Results were used to refine panel edge-doubler designs to minimize their influence on the central panel bays. Successful nonlinear analyses of panels with high axial load requirements could not be obtained, despite significant efforts. Forces normal to the panel at the hoop-edge grips were observed to reverse sign with each iteration.

Comparisons of similar ATCAS models with test results implied that the representation of the test fixturing requires improvements. Higher strains in the central stringers and

higher radial deflection than predicted suggest that the stiffness of the hoop restraints may be the cause.

Strain Softening Model Development. General shell elements and an orthotropic strain softening material model were used to analyze laminate test results from the ATCAS fracture database, concentrating on uniaxial load conditions perpendicular to the axis of blunt notches. Parametric studies indicated that the maximum stress level and initial unloading portions of a strain softening curve have the strongest effect on small notch strength for coupon sizes typically used for composites. The energy associated with the rest of the strain softening curve is most important to large-notch strengths, due to larger notch tip damage zones allowed by larger specimen widths. These analyses confirmed the experimental observation that small fracture coupons do not provide material properties.

Comparison of strain softening analyses with models based on linear elastic fracture mechanics indicated the superiority of the strain-softening approach in predicting the ATCAS test database, including specimen size effects and residual strengths over a wide range of notch sizes. Differences in strain-softening response can also explain differences observed between tow-placed and tape laminates.

Frame/Skin Bondline Analysis and Test. Bonded frame pulloff tests and analyses were performed to support the baseline crown design including a mousehole detail at the intersection between frames and hat stiffeners. Based on the finite element analysis of the ATCAS crown panel under an internal pressurization load, two critical areas for the frame-to-skin bond were identified: along the length of the frame near the middle of bay, and the gap between the frame and the stiffener in the mousehole area.

Initial tests for conditions in the middle of the frame (away from the mousehole) were performed with a clamped fixture that has been used in the past to evaluate bonded element pulloff. Results from these tests indicated that the type of 'noodle' material used at the end of the frame web, adhesive or braided inserts, had little effect on failure. In most clamped fixture test cases, damage started to propagate unsymmetrically from each of the frame edges but subsequent noodle damage initiated and became the dominant mode leading to final failure. Membrane forces that occur in the clamped specimen as pulloff loads increase may have been the cause for a shift in the dominant damage location. Detailed finite element analysis used to predict damage initiation in clamped specimens compared reasonably well with experiments.

A simply supported test fixture was also designed to determine frame pulloff failure loads and modes for areas away from the mousehole. This improved fixture was statically determinate. In most test cases with the simply supported fixture, damage initiated and propagated unsymmetrically from each of the frame edges leading to final failure at loads less than that observed with the clamped fixture. Some of the specimens tested exhibited manufacturing anomalies with the frame sinking into the skin and causing some waviness in the top plies. This often caused delaminations to propagate deeper into the skin and resulted in lower failure loads. Based on the results, it appears that the frame pull-off load itself is not the best way to report data but

that the skin bending moment at the tip of the frame was the most important load resultant. In view of the static data obtained and the predicted skin bending moments from the finite element analysis, it appears that an adequate margin of safety is obtained for bonded frame pulloff away from the mousehole. Preliminary fatigue tests also indicated that adequate margins exist with the current design.

A frame pulloff test fixture was also designed for testing the mouseholed design detail. For these tests, failure originated under the frame noodle near the stiffener and propagated as a delamination under the frame. Based on the results of the finite element analyses, it would appear that the loads obtained in the test of the mousehole region are not sufficient to reach design ultimate load, although more refined local analysis and test instrumentation may be required to confirm this.

2.0 Introduction

This task was motivated by the need for additional understanding of structural performance to support design of thin-gage fuselage structure from advanced composite materials. It directly supports the efforts of the NASA/Boeing Advanced Technology Composite Aircraft Structure (ATCAS) program (contract NAS1-18889), which, in turn, is an integral part of the NASA Advanced Composites Technology (ACT) initiative. The objective of the ACT initiative is to develop composite primary structure for commercial airplanes with 20-25% less cost and 30-50% less weight than equivalent metallic structure. The ATCAS activities within the ACT framework are focused on fuselage structure, specifically the section immediately aft of the main landing gear wheel-well on a 777-sized airplane. A thorough description of the program is contained in References 1 (AB), 2 (AA), and 3 (AC).

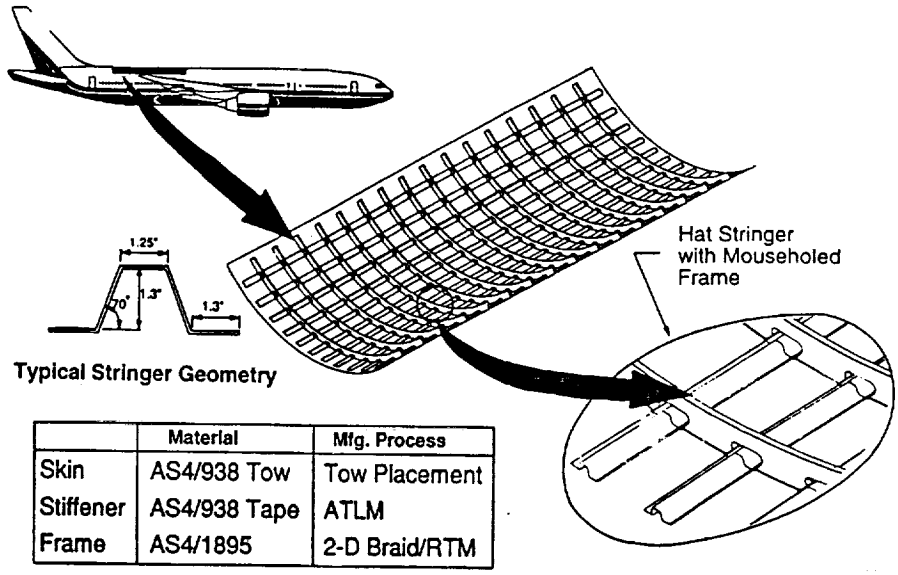
The ATCAS study section was divided into four quadrants based on primary loading considerations. The internal pressure is reacted primarily as hoop tension, and is effective in all quadrants. Critical axial loads are primarily tension in the crown and compression in the keel, with shear being dominant in the side. The upper and lower portions of the side panel have significant regions of combined tension-shear and compression-shear, respectively. The lower side has the additional issue of major load redistribution around cargo door and wheel-well cutouts.

Design studies were conducted for the crown quadrant to determine concepts that meet cost and weight goals as well as structural integrity requirements. Evaluations considered a range of structural concepts, geometries, and materials. The design concept selected for more detailed evaluation is shown in Figure 1. The skins are tow placed using AS4/938 material. The hat stringers are hot drape formed from tow-placed AS4/938 charges and are cocured to the skin on 14 in. centers. The J-section frames consist of a triaxially braided AS4 fiber preform that are resin transfer molded (RTMed) using Shell RSL1895 resin. The frames are cobonded to the skin, and contain cutouts, referred to as a "mouseholes," at the intersection with the continuous stringers.

The design studies identified both axial and hoop damage tolerance as major design drivers (Ref. 4). Axial damage tolerance is the condition of a circumferentially oriented notch subjected primarily to loads along the fuselage length. Hoop damage tolerance is a similar condition, except with a longitudinally oriented notch and hoop loading. Also identified as a critical issue was the performance of the frame/stringer intersection region.

ATCAS testing efforts have addressed axial damage tolerance in a flat regime, ignoring the theoretically-small adverse curvature effects. Hoop damage tolerance is being evaluated using a pressure-box test setup, illustrated in Figure 2. This fixture creates a biaxial-tension loading state through the application of longitudinal loads and internal

pressure to a 63 in. x 72 in. curved panel. The intent was to simulate crown region loads that exist in the full fuselage shell.



	Material	Mfg. Process
Skin	AS4/938 Tow	Tow Placement
Stiffener	AS4/938 Tape	ATLM
Frame	AS4/1895	2-D Braid/RTM

Figure 1: ATCAS Baseline Crown Concept

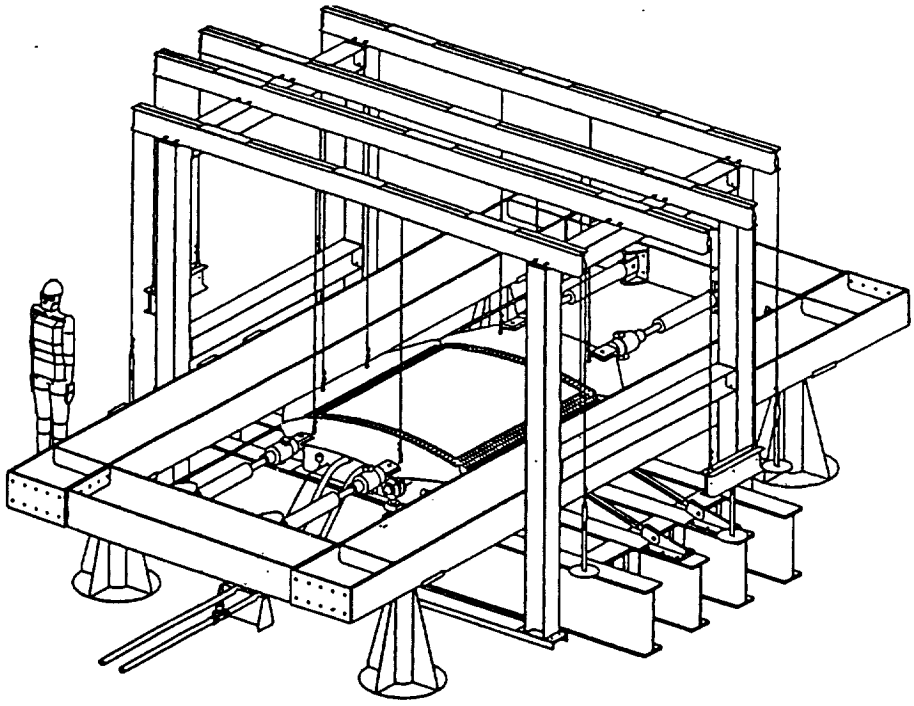


Figure 2: Pressure-Box Test Fixture

At the time of this writing, two ATCAS panels have been tested in the fixture, and another two are planned. The configurations of these four panels are detailed in

Table 1. The preliminary test plans for the three stiffened panels are contained in Table 2. The test results from Panels 13 and 11b are discussed in References 5 and 6. Both panels were tested with a 22 in. longitudinally-oriented notch severing the skin and central stiffening element. The Panel 12 test will provide data similar to that of Panel 11b, except with a *cobonded* frame and with less stiff stringers. Panel 11a will contain a similar 22 in. damage, but that has been repaired.

	Panel 13	Panel 11B	Panel 12	Panel 11A
Skin				
Material	AS4/938 Tow	AS4/938 Tow	AS4/938 Tow	AS4/938 Tow
Mat'l Nominal Fiber Volume	0.57	0.57	0.57	0.57
Layup	[45, -45, 90, 0, 60, -60, 90, -60, 60, 0, 90, -45, 45]	[45, -45, 90, 0, 60, -60, 90, -60, 60, 0, 90, -45, 45]	[45, -45, 90, 0, 60, -60, 90, -60, 60, 0, 90, -45, 45]	[45, -45, 90, 0, 60, -60, 90, -60, 60, 0, 90, -45, 45]
No. of Plies	13	13	13	13
Nominal Thickness	0.096	0.096	0.096	0.096
Stringers				
No. of Stringers	0	4	4	4
Material	N/A	AS4/938 tow	AS4/938 tow	AS4/938 tow
Mat'l Nominal Fiber Volume	N/A	0.57	0.57	0.57
Layup	N/A	[45, -45, 0, 0, 90, 0, 0, 0, 90, 0, 0, -45, 45]	[45, 90, -45, 0, 45, -45, 0, 90, 0, -45, 45, 0, -45, 90, 45]	[45, 90, -45, 0, 45, -45, 0, 90, 0, -45, 45, 0, -45, 90, 45]
No. of Plies	N/A	13	15	15
Nominal Thickness	N/A	0.096	0.111	0.111
Stringer/Skin Attachment	N/A	Cocured	Cocured	Cocured
Frames				
No. of Frames	0	3	3	3
Material	N/A	AS4/RSL1895	AS4/RSL1895	AS4/RSL1895
Braid Architecture	N/A	66.5° Braid Angle, 37.4% Axial Tows	66.5° Braid Angle, 37.4% Axial Tows	66.5° Braid Angle, 37.4% Axial Tows
Fiber Volume	N/A	0.543	0.543	0.534
Nominal Web Thickness	N/A	0.141	0.141	0.141
Nominal Flange Thickness	N/A	0.071	0.071	0.071
Mousehole Configuration	N/A	Wide	Wide	Wide
Frame/Skin Attachment	N/A	Mechanically Fastened	Cobonded	Cobonded
Tear Straps Beneath Frame	BMS 8-256 3K-70-PW fabric, t = 0.07	None	None	None

Table 1: ATCAS Pressure-Box Test Panel Configuration Summary

Panel	ULTIMATE		LIMIT	
	Load Case	Damage	Load Case	Damage
11b	• Pressure: 18.2 psi, Axial: None	None	Pressure: 8.85 psi, Axial: 0.54 kips/in compr.	Loss of Structural Unit (Severed Skin and Frame)
12	• Pressure: 13.8 psi, Axial: 0.84 kips/in. compr. • Pressure: 18.2 psi, Axial: None	Critical Damage at Frame/Skin Interface Between Stringers	Pressure: 8.85 psi, Axial: 0.54 kips/in compr.	Loss of Structural Unit (Severed Skin and Frame)
11a	• Pressure: 18.2 psi, Axial: None • Pressure: 13.8 psi, Axial: 0.84 kips/in. compr. • Pressure: 13.8 psi, Axial: TBD kips/in. tens.	Repaired Failed Structural Unit (Severed Skin and Frame)	None	None

Table 2: Preliminary Test Plans for ATCAS Pressure-Box Panels

The purpose of the task being reported in this document was to augment ATCAS activities towards the understanding of critical performance issues in the crown region. The task was composed of four major activities: (1) benchmark panel fabrication, (2) benchmark panel finite element analysis, (3) strain-softening model development, and (4) frame/skin bondline analysis and test. The following sections of this document discuss each of these activities in detail.

Fabrication of five pressure-box test panels was pursued to enhance the ATCAS test database on panel performance in a pressurized environment. These panels provided an opportunity to test alternate damage scenarios (e.g., large circumferentially-oriented notches, barely visible impact damage), attractive alternate design concepts (e.g., intraply hybrid skins, higher-stiffness stringers, bolted frames with smaller mouseholes), and other panel locations (e.g., forward end of crown study section).

Finite element analysis of these benchmark panels was pursued to provide an initial evaluation of undamaged panel response in the pressure-box test fixture. Additional analyses are required to determine damaged panel response.

Strain softening model development was pursued to extend promising work conducted under ATCAS. Extensive testing within ATCAS had identified the inability of linear elastic fracture mechanics to properly predict fracture in composites (Refs. 7 and 8). Initial finite element analyses conducted on simple coupon geometries indicated the ability of strain softening models to predict finite-width and notch-size effects. The efforts under the current task allowed (1) further understanding of the relationship between material laws and panel performance, and (2) initial attempts at extending the method to structural configurations.

Analysis and test of the frame/skin bondline was pursued to enhance the limited database on the subject obtained in ATCAS. Extensive finite element analysis allowed

the definition of a specimen configuration that accurately replicates the boundary conditions present in the pressurized panel. Oversizing of the benchmark panels provided an opportunity to fabricate those test coupons using scaled-up manufacturing processes.

3.0 Benchmark Panel Definition

Appendices A through E contain the panel bond, cutting diagram, and panel assembly drawings for Panels 1 through 5, respectively. Appendix F contains the drawings for frame fabrication. The panel dimensions of 80 in. x 72 in. were selected to provide a 63 in. x 72 in. pressure-box test article and several frame/skin bond test specimens from each panel. The details of the pressure-box test panels are summarized in Table 3. It should be noted that a manufacturing error resulted in the +45° and -45° plies being switched in the stringers of Panels 1, 2, and 3. Table 3 contains the correct orientations, while the appendix drawings indicate the intended configuration.

Panels 1, 2, and 3 are representative of the baseline design concept. Panels 1 and 2 are aft-end configurations and Panel 3 is a forward-end design. Panel 1 has four stringers to allow testing for hoop damage tolerance with a longitudinal notch centered between two stringers. Panels 2 and 3 have three stringers to allow axial damage tolerance testing with a circumferentially-oriented notch that severs the central stringer. Panels 4 and 5 are forward-end and aft-end configurations, respectively, of an alternate design concept with intraply hybrid skins, higher stiffness stringers, and mechanically-fastened higher-stiffness frames with smaller mouseholes. The fiberglass tear straps beneath the frames were sized to allow the frames to continue over the stringer flange without a joggle. Additionally, they provided increased hoop damage tolerance and provided isolation from the graphite skin if aluminum frames had been used. Metallic frames were an attractive design option from both a stiffness and cost standpoint, and were a fallback position in the event that the fabrication of the higher-stiffness braid/RTM frames had not been successful.

The preliminary test conditions for each panel, as of the writing of this document, are contained in Table 4. These plans differ somewhat from those originally envisioned. Modifications have been made based on further understanding of the structural issues relating to the specific design concepts and the limitations of the pressure-box test fixture (obtained by evaluating Panel 11b test results). These plans are intended to be further revised as necessary when additional test results are obtained. It should be noted that the axial loadings indicated in the table relate to the fuselage loading induced by body bending. The actual axial loads applied by the test fixture are a combination of this component plus that caused by the internal pressure acting on the bulkheads.

	Panel 1	Panel 2	Panel 3	Panel 4	Panel 5
Skin					
Material	AS4/938 Tow	AS4/938 Tow	AS4/938 Tow	75% AS4/938 25% S2/938 Intraply Hybrid	75% AS4/938 25% S2/938 Intraply Hybrid
Mat'l Nominal Fiber Volume	0.57	0.57	0.57	0.57	0.57
Layup	[45, -45, 90, 0, 60, -60, 90, -60, 60, 0, 90, -45, 45]	[45, -45, 90, 0, 60, -60, 90, -60, 60, 0, 90, -45, 45]	[45, -45, 90, 0, 60, -60, 45, -45, 90, -45, 45, -60, 60, 0, 90, -45, 45]	[45, -45, 90, 0, 45, -45, 30, -30, 90, -30, 30, -45, 45, 0, 90, -45, 45]	[45, -45, 90, 0, 45, -45, 90, -45, 45, 0, 90, -45, 45]
No. of Plies	13	13	17	17	13
Nominal Thickness	0.096	0.096	0.126	0.126	0.096
Stringers					
No. of Stringers	4	3	3	4	4
Material	AS4/3501-6 Tape	AS4/3501-6 Tape	AS4/938 Tow	IM6/3501-6 Tape	IM6/3501-6 Tape
Mat'l Nominal Fiber Volume	0.57	0.57	0.57	0.57	0.57
Layup	[-45, 90, 45, 0, -45, 45, 0, 90, 0, 45, -45, 0, 45, 90, -45]	[-45, 90, 45, 0, -45, 45, 0, 90, 0, 45, -45, 0, 45, 90, -45]	[-45, 90, 45, 0, -45, 0, 45, 0, 90, 0, 0, 90, 0, 45, 0, -45, 0, 45, 90, -45]	[45, 0, -45, 90, 0, 0, 45, 0, -45, 0, 0, 90, -45, 0, 45]	[45, 0, -45, 90, 0, 0, 45, -45, 0, 0, 90, -45, 0, 45]
No. of Plies	15	15	20	15	14
Nominal Thickness	0.111	0.111	0.148	0.111	0.104
Stringer/Skin Attachment	Cocured	Cocured	Cocured	Cocured	Cocured
Frames					
No. of Frames	3	3	3	3	3
Material	AS4/RSL1895	AS4/RSL1895	AS4/RSL1895	AS4/RSL1895	AS4/RSL1895
Braid Architecture	66.5° Braid Angle, 37.4% Axial Tows	66.5° Braid Angle, 37.4% Axial Tows	66.5° Braid Angle, 37.4% Axial Tows	66.5° Braid Angle, 44.4% Axial Tows	66.5° Braid Angle, 44.4% Axial Tows
Fiber Volume	0.543	0.543	0.543	0.534	0.534
Nominal Web Thickness	0.141	0.141	0.141	0.161	0.161
Nominal Flange Thickness	0.071	0.071	0.071	0.076	0.076
Mousehole Configuration	Wide	Wide	Wide	Narrow	Narrow
Frame/Skin Attachment	Cobonded	Cobonded	Cobonded	Mechanically Fastened	Mechanically Fastened
Tear Straps Beneath Frame	None	None	None	Fiberglass	Fiberglass

Table 3: Benchmark Pressure-Box Test Panel Configuration Summary

Panel	ULTIMATE		LIMIT	
	Load Case	Damage	Load Case	Damage
1	• Pressure: 13.8 psi, Axial: 5 kips/in tens.	Critical Damage at Frame/Skin Interface Between Stringers	Pressure: 8.85 psi, Axial: 3.37 kips/in tens.	Loss of Structural Unit (Severed Skin and Frame)
2	Recommend Panel Be Cutup for Building Block Tests (Mouseholed Pressure Pillowing Test Elements)			
3	• Pressure: 13.8 psi, Axial: 0.84 kips/in compr. • Pressure: 18.2 psi, Axial: None	Critical Damage (TBD based on pressure pillowing element studies)	None	None
4	TBD (Candidate Conditions Listed) • Repair of Axial Structural Unit Failure (including severed hat damage) • Skin Penetration or Other Small Impact Damage		Pressure: 8.85 psi, Axial: 0.54 kips/in compr., including dynamic loading	Loss of Structural Unit (Severed Skin and Frame)
5	• Pressure: 18.2 psi, Axial: None	None	Pressure: 8.85 psi, Axial: 0.54 kips/in compr.	Loss of Structural Unit (Severed Skin and Frame)

Table 4: Preliminary Test Plans for Benchmark Panels

4.0 Panel Fabrication

4.1 Skin and Stringer Charges

The skins charges for all panels were tow-placed using the Hercules 7-axis fiber placement machine using the 4th generation 32-tow Band Cut and Add (BCA) head on a curved (122 in. radius) winding mandrel. Twenty-four tows were used in each band. The bands used for the AS4/S2/938 intraply hybrid skins of Panels 4 and 5 consisted of 3 groups of 8 tows, with each group comprised of 6 adjacent AS4 tows next to 2 adjacent S2 tows. The stringer charges were fabricated on a flat mandrel using hand layup (for the tape material) or tow placement (for the tow material).

The fiber description and nominal tow widths required to maintain uniform ply thickness (0.0074 in.) and fiber volume (57.6%) are shown in Table 5. Resin rich areas between tows and intermingling of tow types were to be minimized while maintaining a uniform ply thickness. Gaps between tow bands were not to exceed 0.10 in. No lapping of tow bands was allowed. Individual tows could be end spliced, but no two end splices within a single band could occur within 3 in. Band-pass locations on similarly oriented plies were stacked, not offset.

Fiber Type	Fiber Description	Tow Width (in.)
AS4	6K	0.0896
S2	20 End Glass, OCF S-2, 750 yd/LB	0.0968

Table 5: Fiber Description and Tow Spread Widths

The stringer charges were hot-drape-formed at Hercules over rubber cure mandrels. The maximum temperature during the drape was 150°F. The stringers and mandrels were placed into the aluminum female stringer tool, a bag placed over the aluminum tool, and vacuum pulled.

4.2 Frames

The frames were fabricated by Fiber Innovations. The fiber preforms were fabricated on a 144-carrier braider. A swing arm was used to drive the braiding mandrel through the center of the braider at a controlled speed to maintain fiber orientation. The preform consisted of six plies of triaxial braided AS4 fiber. The bias ±66° fibers consisted of 6K tow and the axial fibers of 18K tows (Panels 1, 2, and 3) or 24K tows (Panels 4 and 5). Preform distortion from handling was minimized by integrating the mandrel as part of the RTM mold. The mandrel and attached preform were inserted into the RTM mold cavity. Prior to closing the mold, a simple cut and fold operation was performed on the three outer plies to form the bottom flanges of the two J frames fabricated in each batch. The braided preform was impregnated with Shell RSL1895

resin and cured in a convection oven. Strip heaters were also attached to the outside of the tool for preferential heating.

4.3 Panel Assembly and Cure

A peel ply was placed onto an INVAR cure tool with 122 in. radius. The skin was then transferred onto the cure tool, with precautions being taken to avoid panel wrinkling during this transfer. Film adhesive was placed on the skin at the stringer-flange locations, with the backing paper on the upper surface of the adhesive. The stringers were then located onto the adhesive (with the backing paper still on the adhesive) with the assistance of a full-coverage graphite caul sheet. The stringer mandrel ends were then secured, the caul sheet removed, and the adhesive backing paper removed from beneath the stringer flanges by slightly lifting the stringer flanges and reverse peeling.

For Panels 1, 2, and 3, film adhesive was then placed on the frame flange surfaces, and the frames located using frame clamps. An additional adhesive layer was placed over the tapered portion of the frame flange. Stringer traps were then located at the stringer-frame intersections.

For Panels 4 and 5, adhesive was placed on the skin and over the stringer skin-flange at the frame tear-strap locations. The lower and upper portions of the tear-straps were then located onto the adhesive.

The IML caul plates, which were thin graphite/epoxy laminates with a flexible viton region near the frame locations, were then located. For Panels 1, 2, and 3, the silicone rubber mousehole plugs were then placed and the butt joints of the caul plates at the end of the frames beyond the panel edge were sealed. The thermocouples were placed prior to locating the silicone bag, then the caul and mousehole-plug locations were verified. The nylon bag was placed over the entire assembly and cured in accordance with the following:

1. Apply vacuum to the bag.
2. Pressurize the autoclave to 15 psig.
3. Heat at 2-5°F per minute to 225 ± 10°F (based on leading part thermocouple).
4. Hold at 225 ± 10°F and 15 psig for 15 ± 5 minutes (based on leading part thermocouple).
5. Pressurize the autoclave to 135 ± 15 psig, venting the bag to atmospheric pressure when 30 psig autoclave pressure is reached.
6. Hold at 225 ± 10°F and 135 ± 15 psig for 45 ± 5 minutes.
7. Heat at 2-5°F per minute to 350 ± 10°F (based on lagging part thermocouple).
8. Hold at 350 ± 10°F and 135 ± 15 psig for 120 ± 5 minutes (based on lagging part thermocouple).
9. Cool the autoclave at 5°F per minute maximum to below 150°F before releasing autoclave pressure.

The nylon and silicone bags, and the mousehole plugs, cauls, and silicone stringer mandrels were removed.

4.4 Inspection

Each panel was non-destructively inspected using pulse echo and through transmission ultrasonics. No anomalies were identified. However, a repeatable pattern was observed in the skins of all panels using pulse echo. A map representative of Panels 1, 2, and 3 is shown in Figure 3. The pattern could be due to either density or thickness variations. Visual observations confirm that the IML surface varies radially in a pattern similar to that seen in the inspection, accounting for at least a portion of the inspection result. Since the pattern repeats at a distance similar to the band width, it is hypothesized that consistent non-uniformities in band thickness were magnified when the bands of similarly-oriented plies were stacked. Band thicknesses implied by limited measurements of intraband tow locations support this hypothesis.

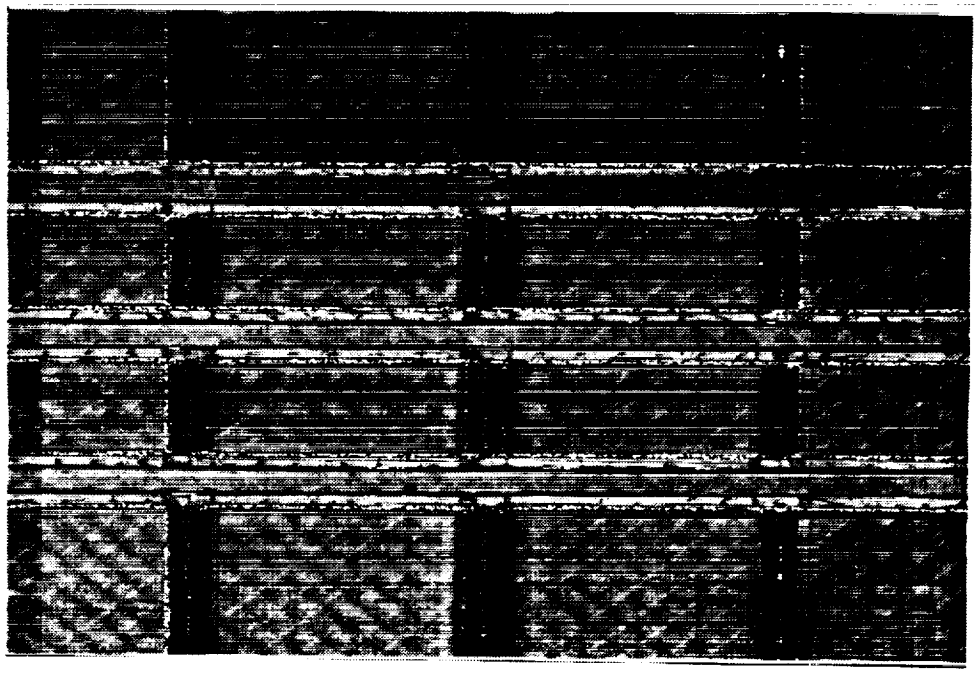


Figure 3: Pulse Echo Amplitude Map for Panel 3 (5 Mz, 12 dB Whiteout)

Pulse-echo inspection of the braided frames indicated localized defective regions in the inner chord of the six frames with modified fiber architecture (24k axial tows were used in place of 18k tows to increase the frame axial stiffness) fabricated for Panels 4 and 5. Photomicrographs taken in the defect areas of the frame trim revealed microcracks at the laminate midplane as shown in Figure 4. For comparison, Figure 5 shows a similar micrograph taken from a defect-free region. It is believed that these microcracks, which were only evident on the frames with a higher percentage of 0° yarns, were caused by residual stresses developed during molding. A contributing factor to the creation of

microcracks may be the increased fiber volume in the INVAR mold, which was not modified to accommodate the thicker preforms, causing the tool to bulge during the RTM process. Three of the frames were trimmed such that all defect regions fell in the trim areas and these frames were mechanically attached to Panel 4. Fasteners (3/16 in. diameter) were installed in the inner frame chord of Panel 5 as shown in Figure 6 to prevent any delamination growth during testing.

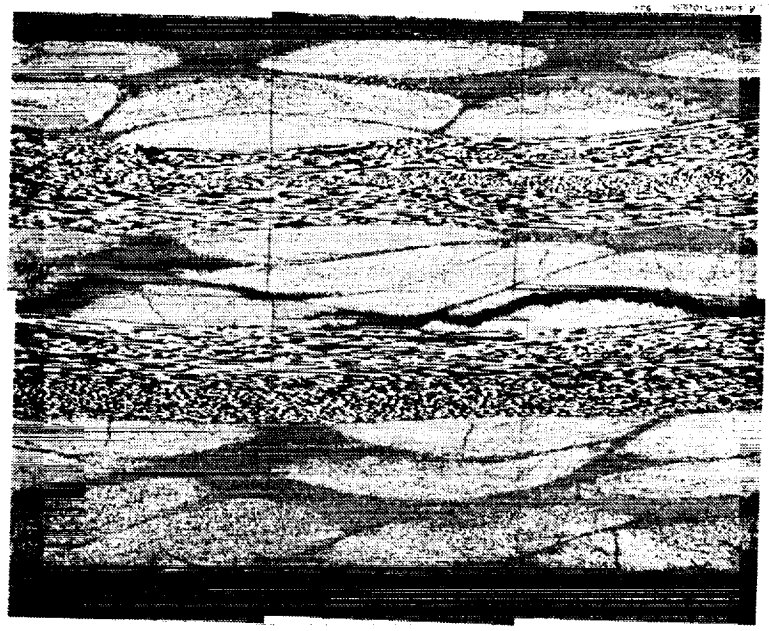


Figure 4: Micrograph of Inner Frame Chord - Defect Region

4.5 Attachment of Frames, Failsafe Chords

The frames for Panels 4 and 5 were mechanically attached to the skin through the fiberglass tear straps using 1/4 in. removable stainless steel Hi-Loks. The failsafe chord were mechanically attached to the frames of each panel using 3/16 in. removable stainless steel Hi-Loks.

4.6 Edge Doublers

Load-introduction doublers were fabricated for each pressure-box test panel and provided, with appropriate fasteners, to NASA Langley Research Center (LaRC) for installation. The doubler configurations for each panel are detailed on the panel assembly drawings contained in Appendices A through E.

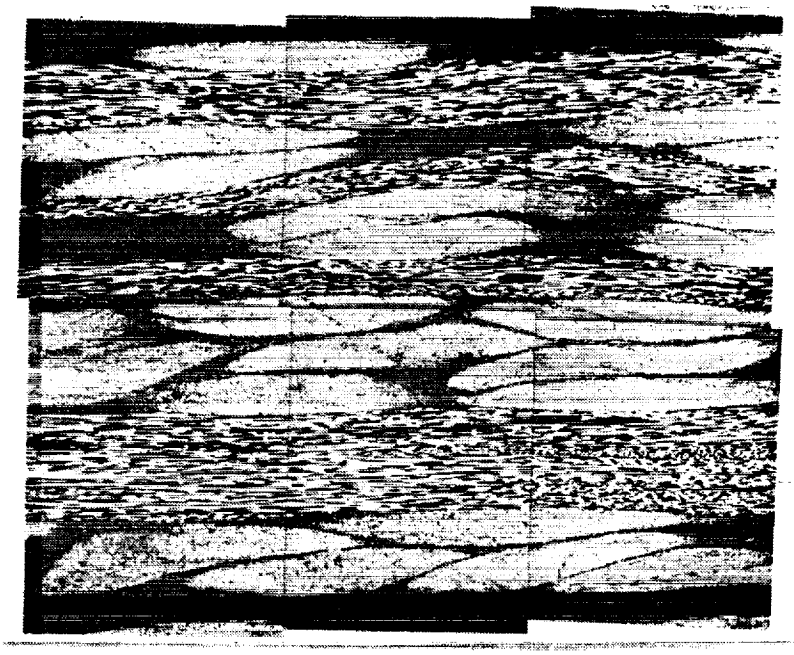


Figure 5: Micrograph of Inner Frame Chord - Defect-Free Region

The doublers located between the frames are needed to reduce fastener bearing stresses in the skin under hoop loads induced by 18.2 psi pressure. These doublers are identical for all five benchmark panels. They extend in from the panel edge approximately 5 in. and are made of constant thickness (0.071 in.) tempered aluminum. They are attached to the skin using 5/16 in. diameter steel fasteners, at a minimum fastener-to-fastener spacing of 5 diameters, and a minimum fastener-to-edge spacing of 2.5 diameters. The doublers also contain circumferential slots at close intervals to minimize their axial stiffness, and therefore their influence on axial load distributions.

The doublers located between the stringers along the curved edge serve a dual purpose, both resulting from the absence of load introduction directly into the stringer caps. First, they adjust the neutral axis of the axially loaded section to match that of the combined stringer/skin-pitch, thereby minimizing localized edge bending moments on the panel when applying an axial loading. Second, these doublers serve as beams between two adjacent stringers and assist the skin in distributing axial loading to the stringer flanges; these beams behave with a measure of end-fixity at their connection to the stringer flanges.

The thickness and length of between-stringer doublers vary for each panel, depending on the required neutral axis shift and the axial load requirements. All of these doublers are step-tapered tempered aluminum, with the thickest step at the curved edge of the panel and the thinnest step nearest the frame. Between the stepped doublers and the skin, a standard gauge aluminum sheet whose thickness exceeds the stringer flange

thickness is to be installed to create a shimmable gap between the stepped doubler and the flange.

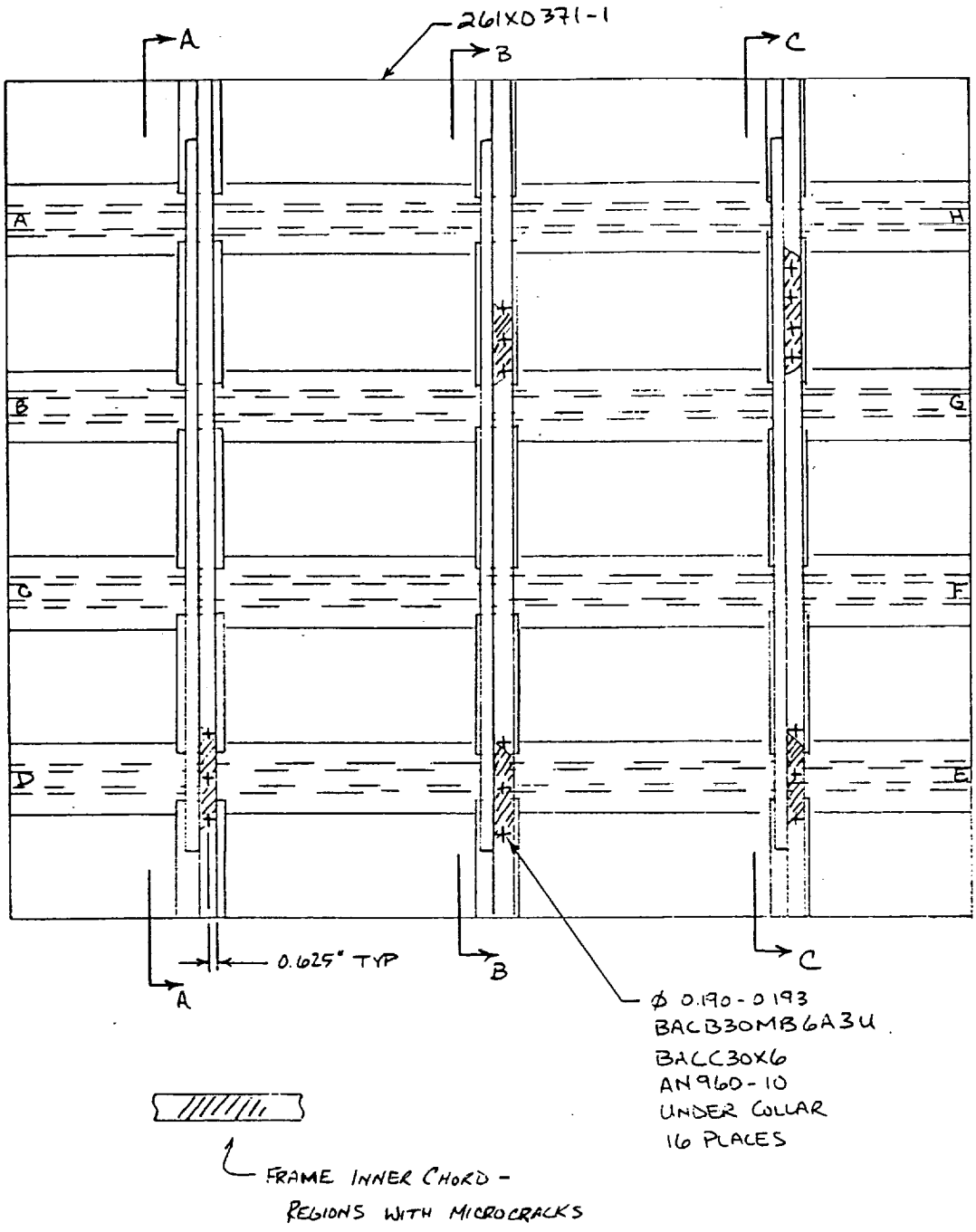


Figure 6: Location of Delamination-Containment Fasteners on Panel 5 Inner Frame Chords

The doublers for Panels 2 through 5 extend approximately half the distance from the panel edges to the outer frames. This distance is sufficient to properly introduce the maximum axial load (1110 lb./in.) that is required for these panels. They are attached to the skin using 5/16 in. diameter steel fasteners, at a minimum fastener-to-fastener spacing of 5 diameters, and a minimum fastener-to-edge spacing of 2.5 diameters.

The higher axial load requirement for Panel 1 (5000 lb./in.), requires that several modifications be incorporated in the doubler design. First, the doublers are extended to the outer frame flanges to increase the load transfer area. Second, the doublers are bonded using room-temperature adhesive to avoid a severe bearing/bypass condition encountered with a bolted configuration in conjunction with the higher axial loads. Third, the two thinnest steps of the doublers are slotted in the longitudinal direction to reduce the hoop stiffness, and thereby avoid adversely affecting the panel test-section strain distribution. The two thickest steps are not slotted in order to preserve the integrity of the stringer-to-stringer beam concept.

The doublers in the corner skin bays are required to perform the functions of both the between-frame and between-stringer doublers. In addition, coupling of the axial and hoop loading must be minimized. The doubler details vary for each panel, but have similar configuration. The thickness profile in the longitudinal direction, the attachment method (i.e., mechanically fastened or bonded), and the longitudinal slotting for a given panel's corner doublers are identical to its between-stringer doublers. The standard gauge aluminum sheet is also present to create the shimmable gap between the doubler and the stringer flange.

5.0 Benchmark Panel Finite Element Analysis

Finite element analysis was conducted to support the development of test fixturing, and provide predictions of undamaged panel response. Modeling had also accompanied earlier ATCAS pressure-box development activities, including (a) box design, (b) test fixturing design, and (c) undamaged and damaged predictions for Panels 13 and 11b. For completeness, the following discussions contain descriptions of work conducted under ATCAS and this contract. Modeling activities were closely coupled, as lessons learned from ATCAS activities were applied to the current modeling effort.

The pressure-box test fixture was developed to study the effects of combined loading on curved fuselage panels. Of specific concern are the influence of the combined loading and the curvature on axial and hoop damage tolerance. The fixture is shown in Figure 2. Loading is applied to the test panel through axial load actuators and pressure on panel's inner surface. The pressure is reacted in the hoop direction by skin and frame restraints.

In developing the test fixture under ATCAS funding, it was desired to simulate the boundary conditions present in a full fuselage shell. A full-shell model, with estimated properties was developed and analyzed at NASA LaRC. Due to the coarseness of the mesh and the approximate properties, only limited comparisons of test panel response were made with this model. Some additional limited studies were made with the test panel model by removing the test fixturing, extending the model several bays in both the hoop and axial direction, and then applying symmetric boundary conditions along these edges. Most comparisons, however, were made with results obtained by applying symmetrical boundary conditions along the edges of the test panel, after the test fixturing was removed. This is the least accurate of the three "reference" solutions, but was the most accessible and cost-effective choice.

5.1 Modeling Details

The models are based on an assumption of two mutually perpendicular planes of symmetry, intersecting at the geometric center of the test apparatus. As shown in Figures 7 and 8, this makes it possible to confine the area of the models to one quarter of the actual structure. Note that this assumption restricts the models to damage scenarios which are symmetric about the panel centerlines. Several element types are used in the models as described below:

Composite test panel skins, stringers and frames	4-noded shells
Composite skin damage region	8-noded shells
Steel axial and hoop load plates	4-noded shells
Load introduction doublers	8-noded solid bricks
Finger grips	3D beams
Load Actuators	3D beams

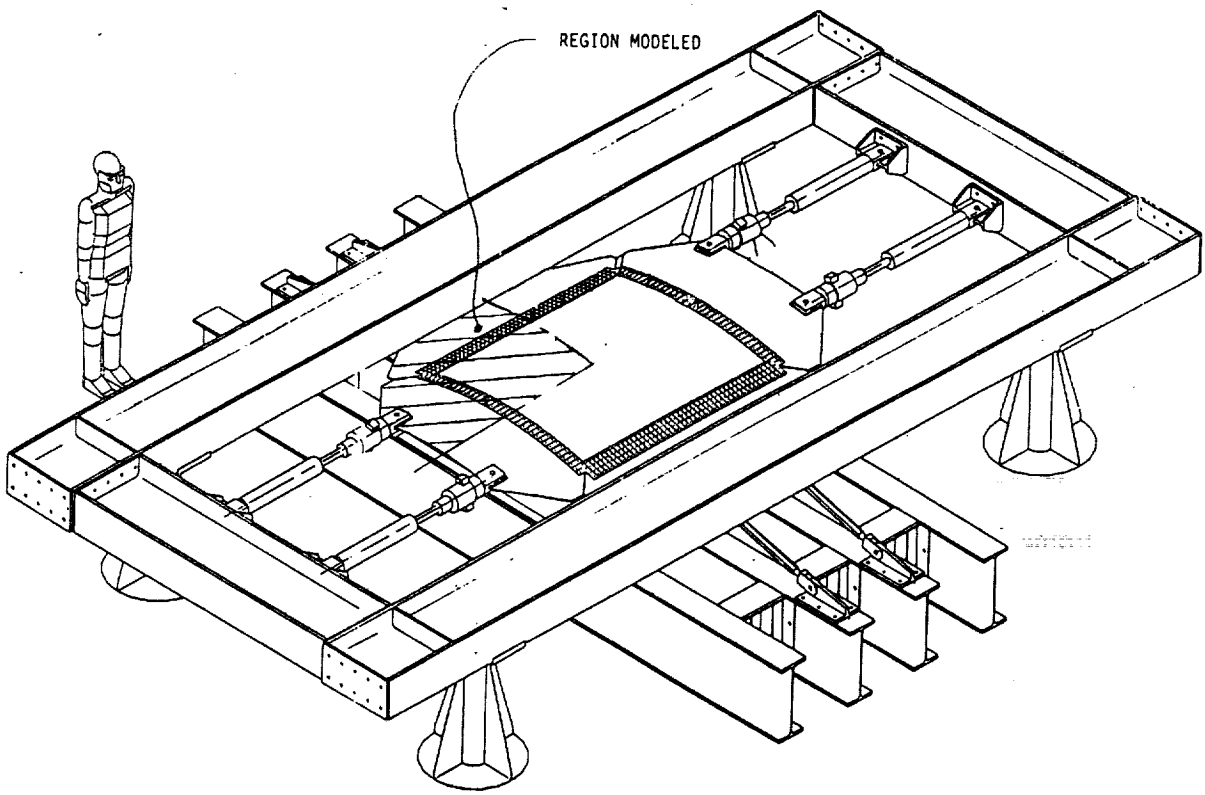


Figure 7: Modeled Region of Pressure-Box Test Setup

As an example of model size, the undamaged Panel 11b model has approximately 2,500 elements and 13,900 active degrees of freedom, while the damaged model has 2,650 elements and 15,600 active degrees of freedom.

Figure 9 illustrates the model global coordinate system. The test panel represents a section of a 20-foot diameter cylindrical fuselage structure. The origin of the model's global coordinate system lies on the axis of that cylinder. Axial strains were designated e_{11} for any part of the model which can sustain axial response. All hoop responses are designated e_{22}. Frame webs have their radial response components designated e_{11}. This convention eliminates confusion in interpreting response contour plots for the entire panel. For example, plots of strain component e_{22} is hoop strain in the skins and frame webs.

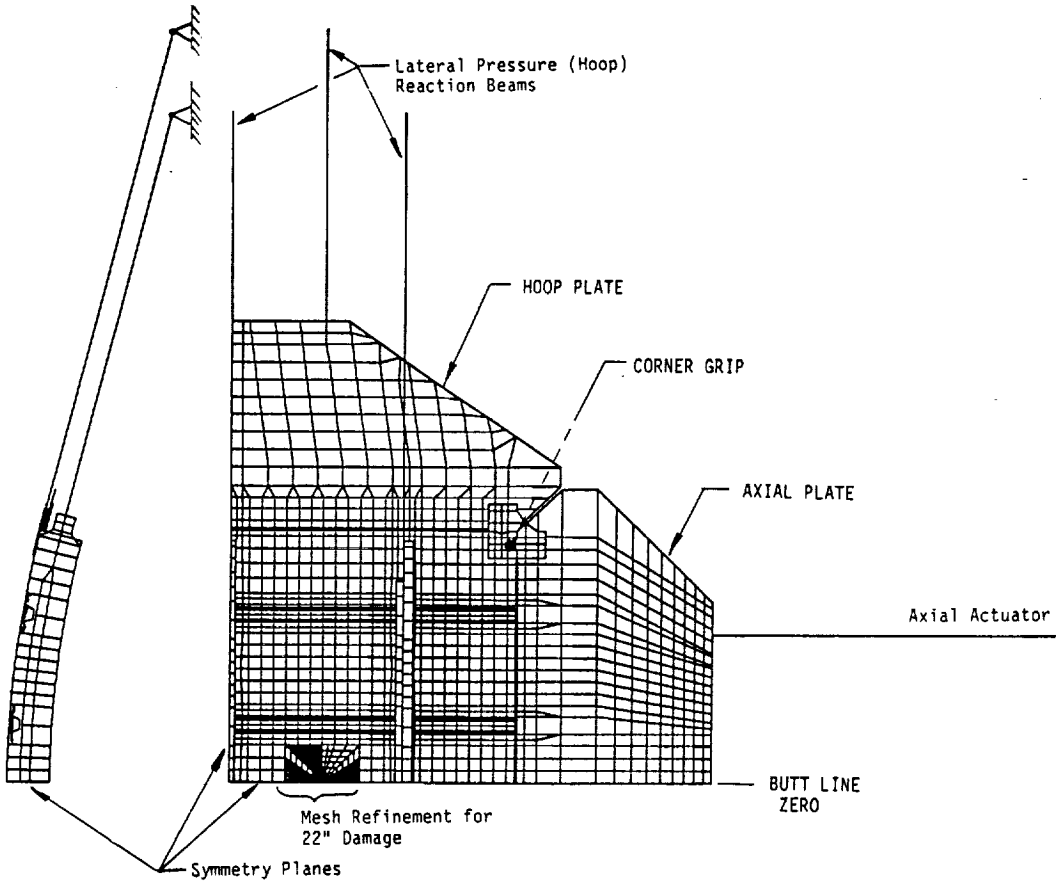


Figure 8: Finite Element Model of Pressure-Box Test Setup

A very important modeling detail is the simulation of the load introduction region along the panel's edges. The modeling strategy for the hoop edges is shown in Figure 10. The laminate skins and load plates are modeled with shell elements, the doublers with solid elements, load grips with beam elements. The fasteners are treated as perfectly rigid, allowing the pieces in the grip region to be linked using constraint equations through ABAQUS Multi-Point Constraints (MPC) Type 7. Successive analyses confirmed the need to discretely model grips on both sides of the panel, with each grip located at its correct radial distance from the centerline of the cylinder. The constraints representing the fasteners through the slotted grip holes were accomplished with equations connecting the hoop and radial displacements of pairs of nodes together while leaving their relative axial displacements and all rotations unconstrained. The constraints representing the fasteners through unslotted holes connected all three translations but not the rotations of two specified nodes.

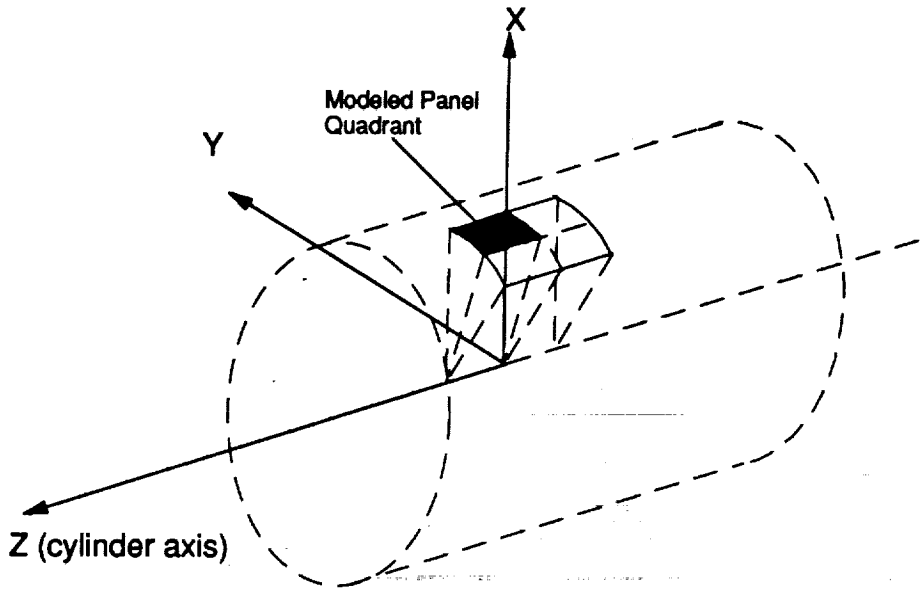


Figure 9: Global Coordinate System for Finite Element Model

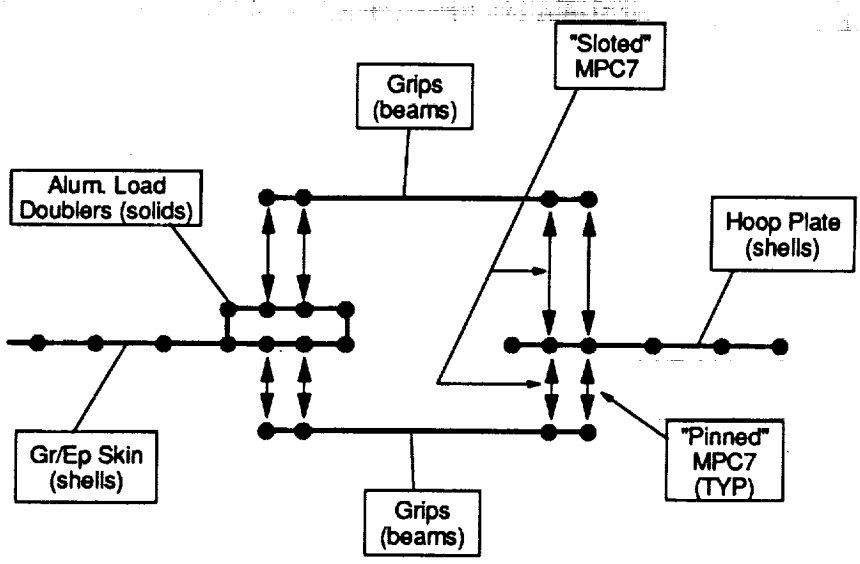


Figure 10: Modeling Strategy for Hoop Edges

Figure 11 illustrates another interesting feature of this model. When modeling relatively thin monocoque shell structure, a significant reduction in computational time is achieved by sharing nodes between skin elements and frame and stringer flange elements. This reduces the number of nodes in the model, the bandwidth of the stiffness matrix, and eliminates the tedious "tying" of discretely modeled elements

(MPC's, bar elements, etc.). The lack of offset between the skin and flange elements was found to have only a small effect on the overall accuracy of the results.

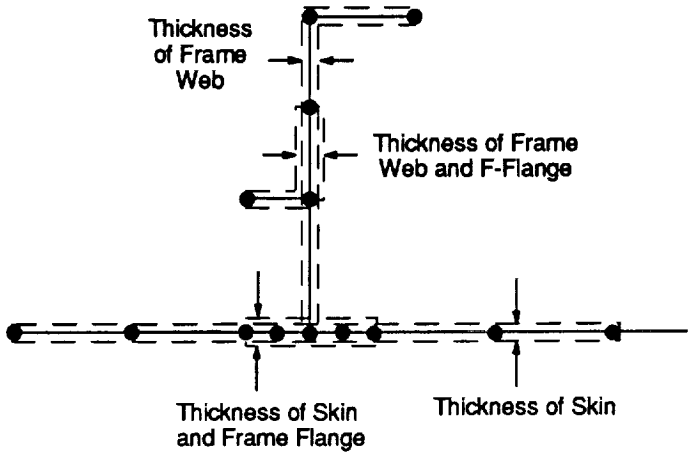


Figure 11: Modeling Strategy for Interfaces Between Skin, Frame Flange, and Stringer Flange Sections: Shell Elements Sharing Nodes

Figure 12 illustrates details of the fine notch-tip mesh used in ATCAS models with the 22" notch severing the skin and central frame. In the region of the crack tip, shell element dimensions are just slightly larger than the thickness of the laminated skin (~ 0.091 in.). In addition, the elements nearest the crack tip have second order shape functions (8 node shells). The primary reasons for this additional refinement are: (1) increased accuracy of a higher order element in a region of very high strain gradients and local bending, (2) the four integration points of the 8-node shell provide a calculated strain value at a point closer to the crack tip, and (3) the option of simulating a local singularity (e.g., infinite stress) at the crack tip by moving the mid-side nodes of the elements adjacent to the crack tip to quarter point positions.

Load is introduced into the model through pressure acting perpendicular to the inner panel surface and through the loads simulating the actuators. The importance of locating the load actuators to align with the vertical centroid of the panel cross-section cannot be overstated, since misalignment causes a pitch bending moment on the panel to which the axial strain distribution is very sensitive. When calculating this vertical centroid, the area of the slotted hoop-edge doublers should be neglected since their slotting renders them ineffective in carrying axial load.

The skin, stringer, and frame properties used in the analyses are contained in Tables 6, 7, and 8, respectively. These skin and stringer laminate properties were calculated using lamination theory based on the ply properties given in Table 9 and the layups defined previously in Table 3.

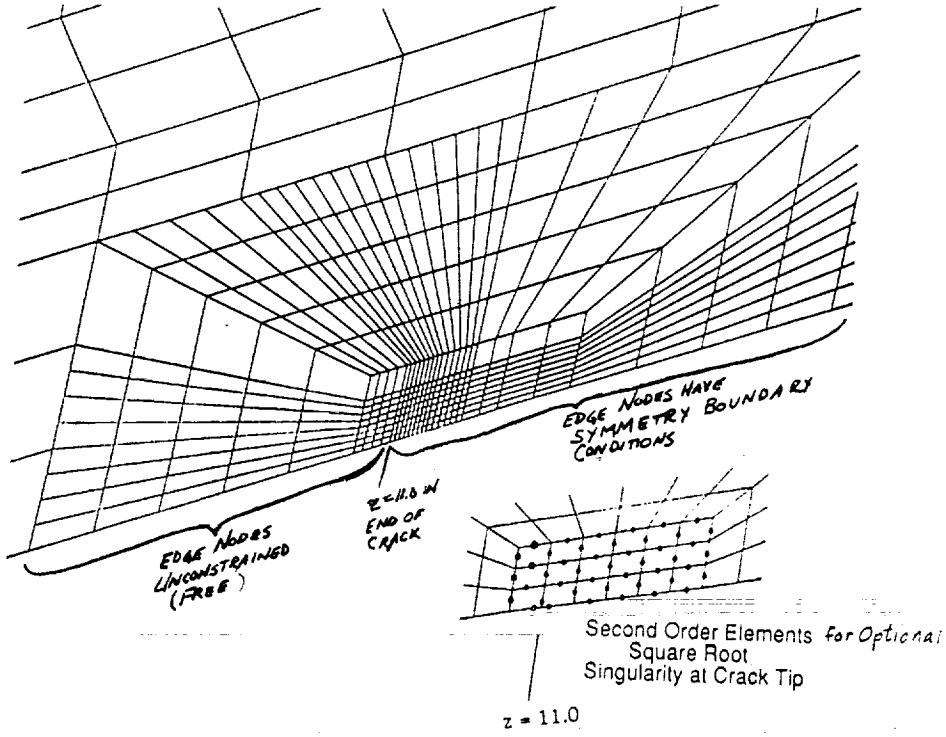


Figure 12: Refined Crack-Tip Mesh

	E_{axial} (msi)	E_{hoop} (msi)	$G_{axial\text{-}hoop}$ (msi)	$\nu_{axial\text{-}hoop}$
Panel 1	5.37	9.11	3.06	0.271
Panel 2	5.37	9.11	3.06	0.271
Panel 3	5.00	7.65	3.55	0.351
Panel 4	5.98	5.24	3.05	0.445
Panel 5	5.34	6.33	2.94	0.361

Table 6: Skin Laminate Stiffness Properties Used in Finite Element Analyses

	E_{axial} (msi)	E_{hoop} (msi)	$G_{axial\text{-}hoop}$ (msi)	$\nu_{axial\text{-}hoop}$
Panel 1	7.89	6.80	3.04	0.365
Panel 2	7.89	6.80	3.04	0.365
Panel 3	10.05	6.58	2.45	0.315
Panel 4	11.82	5.66	2.59	0.383
Panel 5	11.16	5.92	2.72	0.384

Table 7: Stringer Laminate Stiffness Properties Used in Finite Element Analyses

	E_{hoop} (msi)	$E_{transverse}$ (msi)	$G_{hoop\text{-}transverse}$ (msi)	$\nu_{hoop\text{-}transverse}$
Panel 1	7.76	8.02	1.99	0.187
Panel 2	7.76	8.02	1.99	0.187
Panel 3	7.76	8.02	1.99	0.187
Panel 4	9.05	7.28	1.86	0.188
Panel 5	9.05	7.28	1.86	0.188

Table 8: Frame Stiffness Properties Used in Finite Element Analyses

	E_{11} (msi)	E_{22} (msi)	G_{12} (msi)	ν_{12}
AS4/938 Tow	19.80	1.37	0.68	0.32
AS4/3501-6 Tape	19.80	1.37	0.68	0.32
IM6/3501-6 Tape	21.09	1.34	0.70	0.33
75% AS4/938 25% S2/938 Intraply Hybrid	16.60	1.51	0.70	0.31

Table 9: Ply Stiffness Properties Used to Calculate Skin and Stringer Laminate Stiffnesses

Geometrically nonlinear analyses were pursued to capture the interaction of the internal loads and the panel deformations. Of particular concern for the undamaged conditions evaluated under this contract were the outward deflection of the skin between the stiffening elements (i.e., pillowing) and the rigid radial motion of the test panel. The panel response's dependence on this load-deformation interaction was confirmed by results. For example, the linear-elastic mid-bay hoop strain in Panel 5 was found to be 3065 μin./in., while for a geometrically nonlinear solution, it was 2525 μin./in., a 20% reduction. The nonlinear results were also found to more accurately predict the test response of Panel 11b.

5.2 Design Support

The finite element models were used to support the development of test fixturing, specifically the panel-edge doublers. Analyses indicated that the between-frame doublers were acting as axial load sinks, causing the axial strain to vary significantly across the panel width. Circumferential slots were added at close intervals to axially soften these doublers. The slotting was simulated using an orthotropic material and reducing the axial stiffness by two orders of magnitude. Nonlinear simulations with this modification produced significantly more uniform strain distributions in the test panels and considerable reduction in load build-up in the doublers.

Development of the doublers along the panels' curved edges was also very closely coupled with the finite element models. As discussed previously (Section 4.6, Edge Doublers), these doublers are necessary to adjust the neutral axis of the axially loaded section to match that of the combined stringer/skin-pitch and to beam loads into the stringers. The stringer caps are not loaded directly, and receive loading only through shear transfer from the attached flanges. In initial designs, these doublers extended from the panel edge to the outer edge of the frame flanges. Even with stepped thicknesses, the analyses indicated significant influence on the strain distributions in the central bays, which constitute the test section. To overcome this and still provide for load transfer into the stringer flanges, the doubler region over the skin was "scalloped" back approximately half the distance to the edge. The doublers still extended along the stringer flanges to the outer frame flanges. Analyses indicated a significant improvement in the central-bay strain distributions. This concept was used on Panel 11b.

Further modifications in these doublers were indicated by analyses of the Panels 1 through 5. For Panels 2 through 5, the reduced axial load requirements allowed the doubler extensions along the stringer flanges to be eliminated. The high axial load associated with Panel 1, however, required a return to the original doubler design that extended to the outer frame flanges. Predictions indicated these doublers were adversely affecting the hoop strain distributions. Longitudinally oriented slots were therefore added to the thinnest two steps to reduce the hoop-direction stiffness. The doublers were modeled with eight elements comprising the total axial length, and the four elements nearest the outside frame were softened progressively toward the frame by reducing the hoop modulus of elasticity. The reduced modulus values were manually calculated to include the inplane bending and inplane shear of the fingers acting as cantilever beams, as well as the effects of circumferential tension and inplane bending of the non-slotted portion of the doubler.

5.3 Model Results

Finite element results for Panels 1 through 5 are contained in Appendices G through K, respectively. These results consist of strain plots, as identified in Table 10. As indicated, most of the results are from nonlinear elastic analyses. The end bay results are from linear elastic analyses, which differed only slightly from nonlinear analyses. Panel 1 results are also for linear elastic analysis due to convergence difficulties with the nonlinear case (discussed below).

	Panel Number				
	1	2	3	4	5
Appendix containing results	G	H	I	J	K
Axial Load (lb./in.)	5000	1110	1110	1110	1110
Pressure (psi.)	13.8	18.2	18.2	18.2	18.2
Axial, complete panel	Linear	Nonlin.	Nonlin.	Nonlin.	Nonlin.
Axial, skin OML(1), all bays	Linear	Nonlin.	Nonlin.	Nonlin.	Nonlin.
Axial, skin IML(2), all bays	Linear	Nonlin.	Nonlin.	Nonlin.	Nonlin.
Hoop, complete panel	Linear	Nonlin.	Nonlin.	Nonlin.	Nonlin.
Hoop, skin OML(1), all bays	Linear	Nonlin.	Nonlin.	Nonlin.	Nonlin.
Hoop, skin IML(2) all bays	Linear	Nonlin.	Nonlin.	Nonlin.	Nonlin.
Axial, stringer, end bay	Linear	Linear	Linear	Linear	Linear
Axial, doublers, end bay	Linear	Linear	Linear	Linear	Linear
Hoop, doublers, end bay	Linear	Linear	Linear	Linear	Linear

Notes: (1) OML Plots Denoted "Section Point 1"
(2) IML Plots Denoted "Section Point 5"

Table 10: Finite Element Strain Plots Contained in Appendices

The strain plots for the undamaged versions of the 3-stringer configurations (Panels 2 and 3) and for the 4-stringer configurations (Panels 4 and 5) illustrate the behavior of the major elements of the panels. All of these responses agree with the expected results. For example:

- skin pillowing is plainly visible between frames and stringers as well as between end frames and axial doublers
- bending of the stringers as beams transmitting some of the pressure load to the frames is evident
- mousehole-induced bending in the frames, predominantly hoop tension members, is minimal
- strain concentration in the stringer flange at the edge of the mousehole for Panels 2 and 3 is reduced by the narrower mousehole configuration for Panels 4 and 5

Panel 1 is unique among these panels due to its high axial-load requirement. The strain plots for the undamaged version of this 4-stringer configuration illustrate how the axial strains dominate the panel cross-section. The Poisson effect is such that the skin tightens over the stringers, applying forces on the stringers large enough to overcome

the forces from internal pressure, thus bending the stringers inward. Skin pillowing is practically eliminated by the combination of high axial loading and Poisson effect. The high axial strain in the skin at the tip of the end frame was unexpected and has persisted throughout the model development; slotting the hoop edge doublers reduced this strain by about 10%, but it remains the maximum strain in the skin, It should be noted that bolt holes are needed in this region for the attachment of pressure box grips. This high strain is likely a result of the inability of the corner axial doubler to gradually transfer applied tension load into the panel over the length of the end bay. The doubler behaves instead as a tension strap between its loaded end and the end near the frame. Between-stringer doublers can beam applied loads to the stringers, but the corner doubler is located between a stringer and the unstiffened panel edge which works to a high strain due to its low area as a doubler beam support.

The higher axial-load condition associated with Panel 1 (i.e., 13.8 psi internal pressure and 5000 lbs./in. axial load) caused solution difficulties. This axial load is 6 times the bulkhead load associated with 13.8 psi internal pressure. The combination of large axial loads and the edge moments induced by the axial-load doublers led to extreme convergence problems with the radial forces in the hoop grips. Forces normal to the panel at these grips were observed to reverse sign with each iteration.

Significant effort was expended to obtain a complete solution of this panel configuration and loading. Among the approaches attempted were:

1. Applying the internal pressure and axial load separately (two step solution).
2. Applying the pressure and equivalent bulkhead axial load, followed by the remaining axial load (two step solution).
3. Permutations of the above two schemes (three step solutions).
4. Direct dynamic integration of the system with a variety of damping schemes.

In all cases, the solution was unable to progress beyond approximately 38% of the total axial load, (i.e., 1900 lbs./in. or 2.3 times bulkhead load). A very similar problem was encountered when Panel 5 was modeled with high axial loads. In this case, the solution was terminated after 2 hours of CPU time (at approximately 4 times the bulkhead load) since the step size had become excessively small.

These solution difficulties may imply local "snap through" or other unstable behavior along the hoop edge of Panel 1. Close observation during testing may confirm this.

The cost of a nonlinear analysis can vary significantly, but in general, a simulation in which the axial load is equal to the equivalent bulkhead pressure runs roughly 5 to 6 times as long as the linear case. When running on Boeing Computer Services' CRAY YMP, the CPU time for a linear run is approximately 85 seconds, while a "well behaved" nonlinear run takes approximately 480 seconds. Computation time increased considerably for nonlinear simulations of test panels with large cracks and severed

frames, or with large axial loads were performed. For some of the less well-behaved runs, 3600 CPU seconds was observed.

5.4 Comparison with Panel 11b Test Results

The following paragraphs discuss comparisons of the pretest finite element predictions with measured results obtained during the undamaged testing of Panel 11b. In instances that test measurements were taken at corresponding locations in multiple quadrants of the panel, the average of these values is compared to the prediction.

Skins. Correlation to measured hoop-direction skin strains was quite good, generally being within 10% for both Outer Mold Line (OML) and Inner Mold Line (IML) strains. Strain gages for measuring hoop strains were arranged along a meridian through the center of the panel, also known as butt line zero (BL0). Gages were located in the centers of the skin bays as well as adjacent to the frame members. In all cases, the analysis predicted positive in-plane bending moment due to hoop strains (i.e., OML strains were larger than IML strains). This proved to be the case for five out of the six locations at which hoop strains were measured.

The predicted axial strains compare more closely to measured IML strains than OML strains. In addition, significant variations of corresponding quadrant-to-quadrant strains indicated a lack of symmetry in the fixture and the loads. In spite of this, the correlation was within 20% for the four skin bays which flank the two center bays. In the center bays (i.e., along BL0), the predicted IML strains were 17% low, on average, while the predicted IML axial strains averaged 37% less than measured strains.

Stringers. Axial strains along the stringers were measured on the outer skin surface coincident with the stringers and on the innermost surface of the stringer cap. Observed bending strains were qualitatively as predicted, being (a) positive between the frames and (b) negative in the mousehole region. The axial strains along all four stringers were predicted to be similar. Test strains were within 15% of the predicted values for the outer stringers, but were between 200% and 300% higher than predicted for the inner stringers.

Frames. The analysis consistently underpredicted the hoop strains in the frame flanges and webs, being approximately 20% low in the two end frames and 50% low in the center frame.

Loads and Deflections. The analysis substantially underpredicts the loads in the frame reaction beams and the radial deflection of the panel. In particular, the deflections along BL0 are 100% larger than predicted while those between the inner and outer stringers were between 25% and 50% greater than predicted.

Discussion. The larger deflection observed along BL0 for the actual panel, along with greater axial loads and bending for the inner stringers suggest that the test fixture differed somewhat from that assumed in the model. Good correlation between predictions and actual strains in the skin and much of the stringers indicates that the

skins, stringers, frames, steel plates, loading grips, and aluminum doublers were accurately modeled. Possible causes of the differences include:

1. Differences between assumed and actual location of the axial actuator with respect to the neutral axis of bending of the test panel
2. Differences between assumed and actual stiffnesses of the skin and frame hoop reaction beams.
3. Mechanical slack in the hoop reaction systems
4. Bending of the hoop reaction pins
5. Preload in the hoop reaction systems

A brief parametric study was performed to evaluate the second of these mechanisms. Linear elastic analyses were conducted with varying hoop reaction stiffnesses. Improved correlation with experimental results was obtained, specifically with reduced stiffness of the skin restraint beam and increased stiffness of the center-frame restraint beam. Nonlinear large deflection analyses would be required to confirm the trends and quantify the optimal modifications.

6.0 Strain Softening Model Development

6.1 Background

Structural damage tolerance analysis consists of four interrelated steps, as shown in Figure 13. Structural configuration factors relate the stresses or strains in the damaged structure to a relatively simple reference configuration (e.g., unstiffened flat plate with infinite width) as a function of structural parameters (e.g., stringer type, spacing, stiffening ratio), and are typically determined from analytical simulations augmented with experimental measurements. Progressive damage models determine, for any damage condition, the load level that causes damage growth and the direction in which growth will occur. Load redistribution analyses quantify stresses shared with adjacent elements as a function of damage size. This, in conjunction with progressive damage models, determines the stability and arrestment of the damage growth. Finally, as damage growth continues, structural failure occurs when an insufficient amount of load redistribution capability exists in the remaining structure.

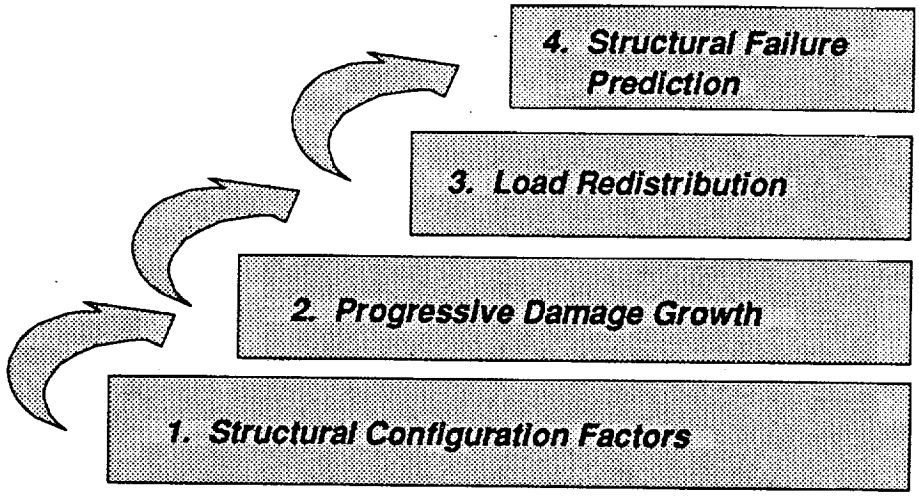


Figure 13: Interrelated Steps for Structural Damage Tolerance Analysis

Extensive thin-laminate testing within ATCAS identified significant limitations of current methods to predict tension fracture response in composites for a wide range of notch sizes, materials, laminate layups, and specimen geometries. Semi-emperical failure criteria for composite laminates have routinely used curve fits of notched strength data corrected by elastic finite width correction (EFWC) factors. Significant errors in this approach are possible, and are related to the size of the notch tip damage zone, specimen geometry, and the assumed EFWC factor. Specimen geometry effects for several materials and layups were found to be much stronger than predicted by EFWC factors. Those materials and layups most strongly affected by specimen size were

found to have relatively low small-notch strength, but relatively high large-notch strength and decreased notch sensitivity.

Figure 14 schematically poses an explanation for residual strength data trends that deviate from LEFM for relatively small notches. The solid residual strength curve shown in the left schematic is representative of much of the fracture data collected for ATCAS. Note that the curve does not follow LEFM for most notch sizes. Empirical modifications to LEFM using point stress or strain characteristic dimensions were also unable to correlate with test data for the wide range of notch sizes studied. When allowing the characteristic dimension to vary with notch size (essentially the same approach as pictured in the right schematic), empirical fits of test data were possible.

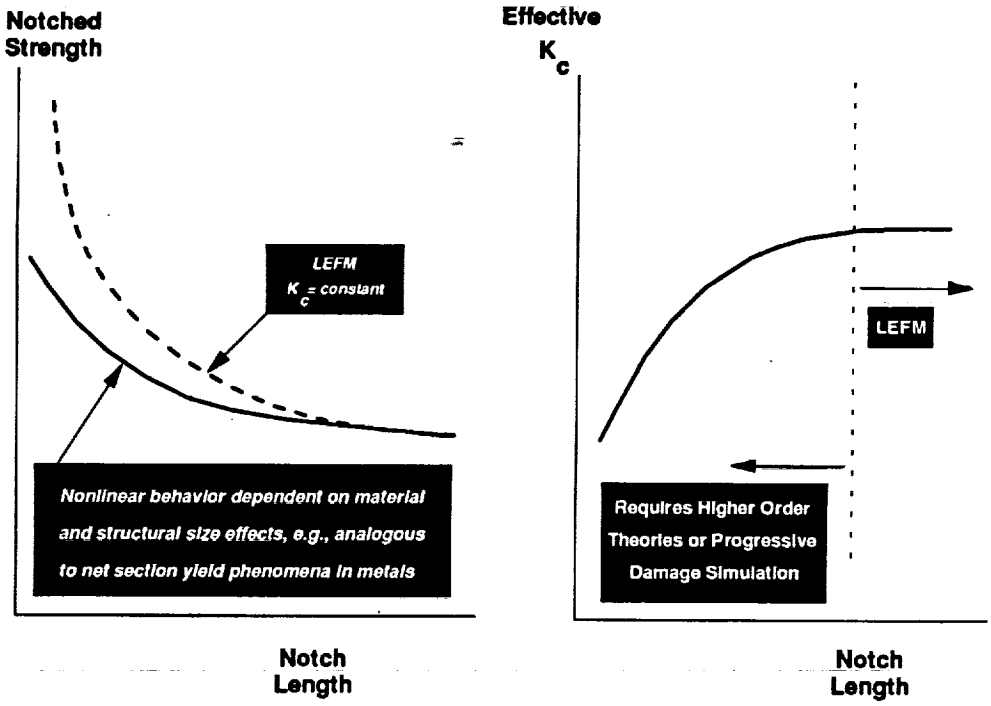


Figure 14: Schematics of thin laminate fracture behavior based on observations from the ATCAS database (Ref. 8).

6.2 Justification

Analysis and tests to quantify progressive damage in composite laminates is crucial to interpreting results from coupon data. In structures, damage accumulation in the skin affects load redistribution to stiffening elements, the associated stable or unstable growth, and residual strength. It is desirable to develop an accurate and efficient method of simulating progressive damage growth, suitable for the analysis of configured composite structures.

Three advanced methods for simulating the effects of composite microstructure and progressive damage growth have been studied during the course of ATCAS crown tension fracture studies. Each model used finite element formulations to account for specimen size effects. These included Cosserat mechanics (Cairns, et al, Ref. 9), Stanford University progressive damage analysis (Shahid and Chang, Ref. 10), and strain softening laws (e.g., Ref. 11). The current work focuses on strain softening analyses. Results from studies with the other two models will be summarized when appropriate.

Materials that exhibit a strain softening response can appear brittle in tests that involve limited load redistribution. For example, composite materials tested in coupons subjected to static uniform load conditions tend to fail abruptly at a maximum stress level. Figure 15 shows stress versus strain curves for two strain softening materials, each responding in a similar manner until a maximum stress level (point B). Between points O and A, linear elastic response is evident. Uniform damage accumulation would occur for the materials subjected to stress levels between points A and B. In the case of uniformly loaded specimens, damage would localize for each material shown in the figure at the same maximum stress level, resulting in failure. Those portions of the specimens in which damage localizes would dynamically unload at failure along the downward slopes shown in Figure 15. The rest of the specimen would retract elastically, suggesting an apparent brittle response. Unless special instrumentation was used to capture locally high strains occurring during the dynamic unloading event, little difference between the two materials shown in Figure 15 can be observed under static uniform load test conditions.

Differences in a material's strain softening response is more easily observed in notched coupons or in structures capable of load redistribution following damage localization. Damage is forced to localize near the stress concentration in a notched coupon. As shown schematically in Figure 15, characteristics of the unloading curve will effect the notch tip damage zone which develops to redistribute local stresses prior to failure. The observed notched strength will depend on specific characteristics of the strain softening curve, notch size, and specimen geometry. Several studies have shown the merits of using strain softening analysis to predict notched tension and compression properties of composite laminates (e.g., Refs. 12-14). A more complete documentation of the use of strain softening methods for analyzing the fracture and collapse of engineering structures is discussed in a book by Bazant and Cedolin (Ref. 11). As in the case of difficult stability problems, efficient nonlinear solution schemes must be applied to obtain accurate and timely results. To date, most engineering applications using strain softening analysis have come in analyzing inhomogeneous materials used in the building industry (e.g., concrete).

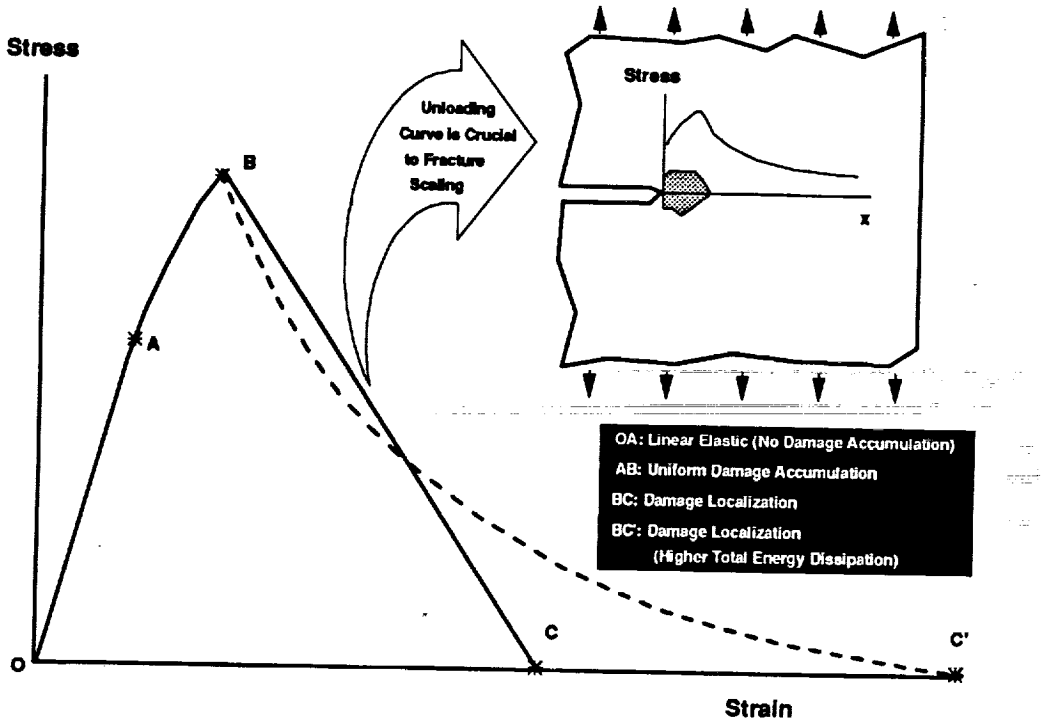


Figure 15: Stress-strain curves for strain softening materials

Composite damage mechanisms that would effect the strain softening curves shown in Figure 15 include matrix cracking, delamination, fiber failure, fiber bundle pullout, and local scissoring of angle plies. Distributed damage occurring between points A and B of the strain softening curves in Figure 15 have little effect on the overall stiffness. Composite laminate damages occurring in this part of the curves are limited to matrix cracking, delamination, and isolated fiber breaks. Beyond point B, large drops in the stiffness are evident, suggesting significant fiber failure. Initial unloading portions of the strain softening curve for different composite laminates may be predicted using micromechanical considerations of the statistical nature of fiber failure and a shear lag model for fiber/matrix interaction (Ref. 13). Methods to predict failures when a complex damage state exists near the ends of a strain softening curve (over the large strains approaching points C or C' in Figure 15) appear less feasible. For example, delaminated angle plies that contain matrix splits may undergo large deflections and twisting when uncoupled from the constraint of axial fibers. Although such energy dissipation mechanisms seem insignificant, later discussions will show that the end of the strain softening curve can have a pronounced effect on large notch strength.

The progressive damage analysis developed at Stanford University (Ref. 10) under an ATCAS subcontract simulates local laminate stiffness reduction associated with matrix cracking, splitting, and fiber failures on a ply-by-ply basis. The Stanford progressive damage analysis has shown reasonably good correlation with the ATCAS database for

unstiffened coupons with notch sizes up to 2.5 in. To date, results have not been obtained for larger specimens and configured panels. The Stanford finite element analysis may not prove efficient when directly applied to configured structures that have large damage growth, load redistribution, and competing failure modes. However, the tool could prove valuable for determining the laminate strain softening curves suitable for structural progressive damage analysis. Since a method to account for the effects of delamination has not yet been added to the Stanford finite element code, some experimental fracture data may also be needed to quantify the complete strain softening curve.

Fiber failure must occur in laminate layups typical of composite structures to justify the large strains and reduced stiffness assumed as damage localizes in a strain softening simulation. As shown in the schematic of Figure 15, a concentrated stress state and load redistribution to surrounding elastic material allows the stable development of a damage zone and local unloading to occur. Material taken from a notch tip damage zone provides a direct method for determining if strain softening is occurring prior to failure. Some ATCAS fracture tests were stopped short of failure to characterize notch tip damage occurring in composite laminates. The largest test stopped short of failure was a curved tear strap panel (122 in. radius) with an initial notch size of 22 in. (Panel 13). This panel was loaded in a pressure box to 85% of the predicted failure load (Ref. 5). Ultrasonic inspection (pulse echo and flexural wave dispersion) and x-ray of the panel was used to map damage size. Figure 16 shows a schematic of the notch tip damage zones and additional experiments performed to characterize the localized damage states.

Fiber failure maps and tensile tests performed with specimens cut from the pressure box panel are shown in Figures 17 and 18, respectively. Significant fiber failure was evident in six of the thirteen plies. The fiber failures spanned most of the damage zone width measured by ultrasonic methods. Note the discontinuous distribution of fiber failures for the tow-placed laminate tested. Figure 18 shows the stiffness measured for undamaged specimens were within 10% of the predicted laminate modulus. The undamaged specimens failed at a strain level near 0.01 in/in. Test measurements for specimens cut from the damaged zone indicated significantly reduced stiffness. The damaged specimens did not fail when taken to strains above 0.02 in/in. This strain level is much higher than the tensile fiber failure strain of AS4. In addition, the extensometer used for these tests had a gage length of 1 in., which is probably much larger than the length of the fiber failure zone over which the highest unloading strains would be measured. Another interesting characteristic of the notch tip damage zone was that the specimen cut closest to the notch tip did not have the lowest reduced stiffness (see Figures 16 and 18). This may indicate a microstructural effect present prior to the onset of damage or that damage closest to the notch tip is more localized (resulting in lower strains measured over the 1 in. gage length). The fiber failure deply maps and reduced stiffness measurements from tensile tests are characteristic of a strain softening material.

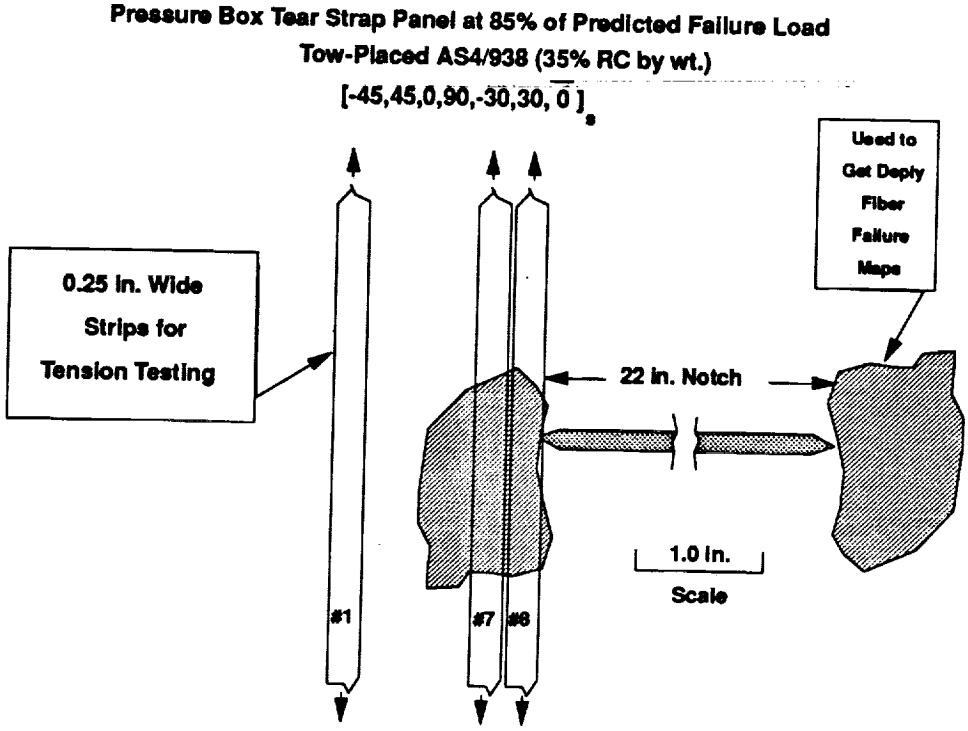


Figure 16: Experiments Performed to Characterize Notch Tip Damage Zones Occurring in Composite Laminates

Nonlinear elastic analysis and test results obtained for the curved tear strap panel prior to the onset of damage accumulation indicated large notch tip bending strains caused by the pressure load conditions (Ref. 5). As damage accumulated at the notch tip, strain gage readings showed a shift in the peak strains to an area outside the damage zone. This is believed to be an indication that less load is being carried through the softened material. Direct measurements of the high inelastic strains occurring within the damage zone would require the strain gage length to be centered over an area equal to or smaller than that in which fiber failure localizes. Figure 17 shows that there was only a slight tendency for fiber failures to localize towards the laminate outer surface despite significantly higher initial tensile strains. This suggests that notch tip damage accumulation and the associated strain softening curve may be complex for pressure-induced bending, with delamination playing an important role in isolating plies. A discrete model simulating such a complex damage state seems unreasonable. Perhaps some combination of micromechanics for predicting initial failures and fracture experiments would lead to the development of a strain softening curve suitable for simulating bending failures for a given material and laminate layup. Strain softening analysis efforts in the current paper are limited to developments for inplane load conditions.

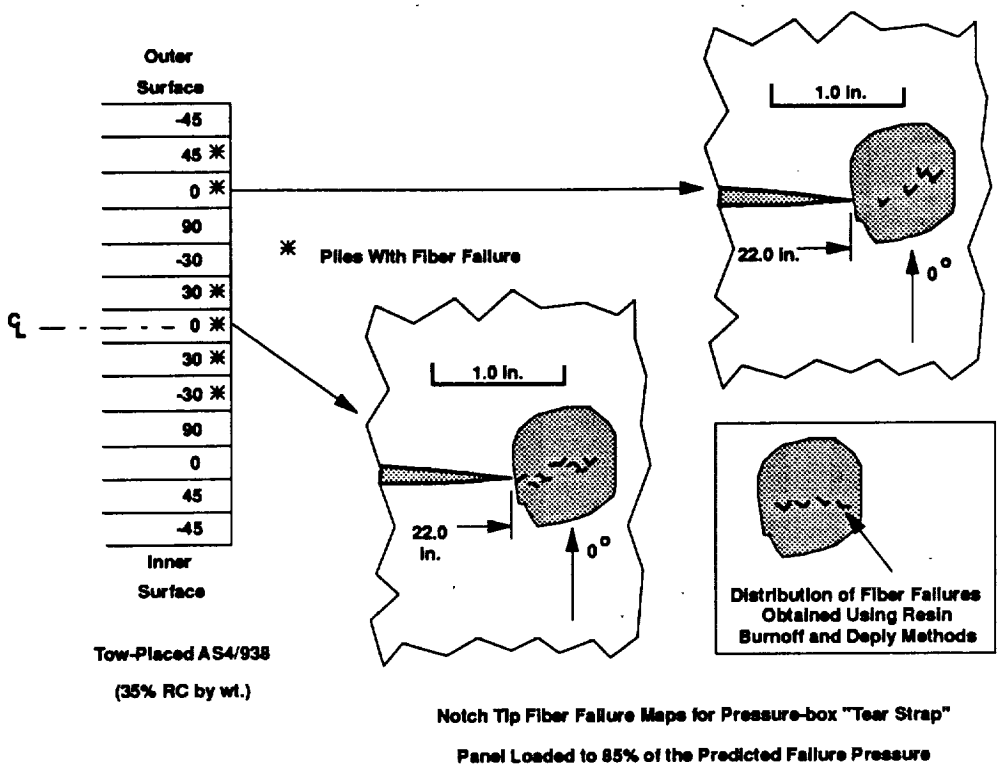


Figure 17: Fiber Failure Maps of the Notch Tip Damage Zone

6.3 Developments and Findings

In order to implement a practical progressive damage model for composite laminates, it was desirable to employ existing, commercially available finite elements with the versatility necessary for modeling configured fuselage structure. The code ABAQUS was selected because it has a variety of robust, nonlinear solution algorithms and is capable of modeling strain softening response for orthotropic materials. Typical nonlinear incremental loading schemes would not provide solutions for problems involving strain softening because of an inability to track global unloading. The Riks solution algorithm was employed with some success in early efforts. This method was found to have numerical stability problems when applied to strain softening laws which change abruptly by shifting to a steep negative slope after reaching the maximum stress level (e.g., unload portion of dashed curve following point B in Figure 15). Such curves, which were characteristic of some graphite/epoxy laminates, were simulated with the help of dynamic nonlinear solution schemes.

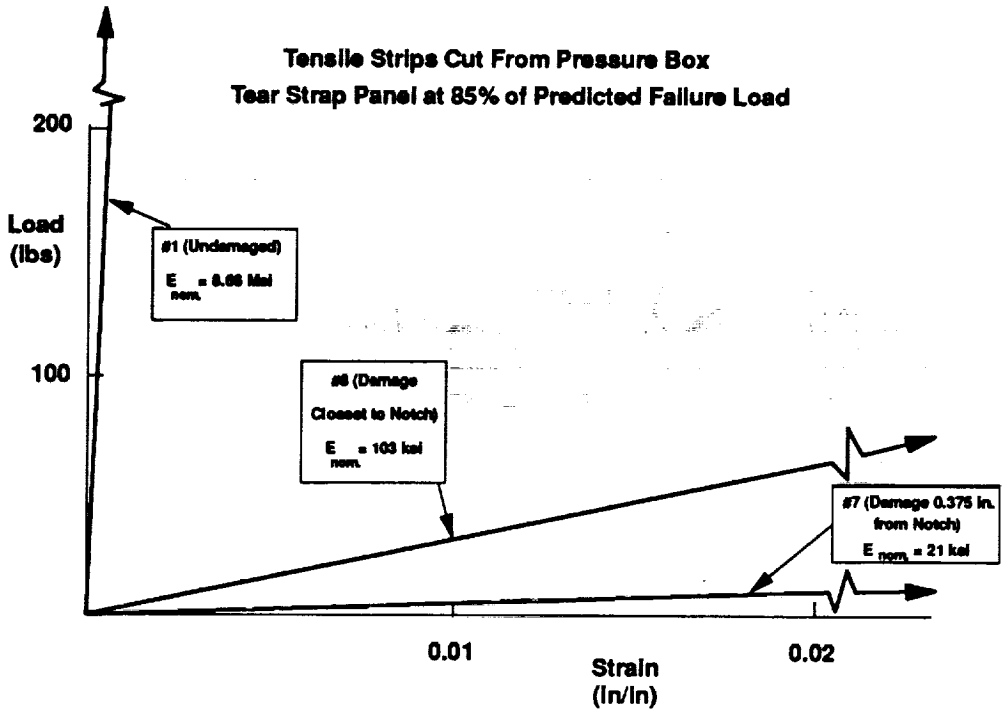


Figure 18: Tensile Test Results Indicating the Reduced Stiffness of Strips Cut From Notch Tip Damage Zone

General shell elements and an orthotropic strain softening material model from ABAQUS were used to analyze laminate test results from the ATCAS fracture database. These investigations concentrated on uniaxial load conditions perpendicular to the axis of blunt notches. A Hill yield function was selected to simulate strain softening as a function of any direction within an element; however, the choice of interaction terms in this criterion were found to have little effect on the problems studied.

Parametric studies were performed to determine how different characteristics of the strain softening law relate to specimen size effects and notched strength. These studies indicated that the maximum stress level and initial unloading portions of a strain softening curve have the strongest effect on small notch strength for coupon sizes typically used for composites. When considering larger coupon sizes typical of large notch tests performed in ATCAS, energy associated with the rest of the strain softening curve becomes much more important to residual strength. This relates to an interaction between notch tip damage development and finite specimen width. In small coupons, less notch tip softening is able to occur (i.e., incomplete unloading results in a smaller damage zone) prior to specimen collapse. Strain softening analyses confirms the experimental observation that small fracture coupons do not provide material properties.

Figure 19 shows typical results from strain softening analyses as compared to the point strain failure criterion and ATCAS test results for flat unstiffened panels (Ref. 8). Strain softening analyses were performed using finite element models of the specific specimen geometry. The material and laminate layup in the figure are characteristic of that used for minimum gage skin areas of the ATCAS crown design (see Figure 17). The first part of the strain softening curve (initial modulus and maximum stress level) used to make predictions in Figure 19 was developed based on unnotched strength tests. Results from the parametric strain softening study was used to determine initial characteristics of the unloading curve that best represent small notch test data trends (up to 2.5 in.). The average test result for 2.5 in. notch specimens with W/D = 4 was used to establish the final unloading part of the strain softening curve and the point strain fracture parameter. The point strain parameter determined in this manner is shown to over predict and under predict small and large notch test results, respectively. When using smaller notches to determine the point strain fracture parameter, predictions of large notch properties become even more conservative. The strain softening analysis method seems to accurately predict small notch results but also underestimates the large notch property.

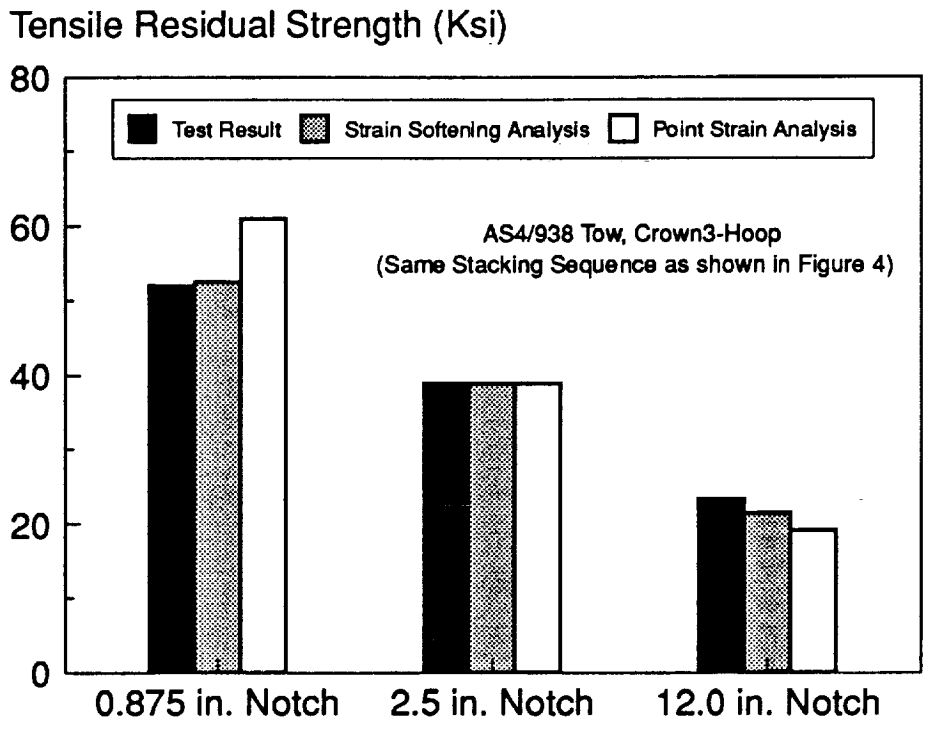


Figure 19: Notched Residual Strength Analysis and Test Results

Figure 20 compares strain softening and point strain analyses for another material and laminate from the ATCAS test database (Ref. 8). The same procedure discussed in the previous paragraph was used to determine a strain softening curve and point strain

fracture parameter for the laminate. Note that the specimens used to get an average strength for a 1.25 in. notch in Figure 20 has W/D = 8. Despite the smaller notch size, the average strength for a 0.875 in. notch (W/D = 4) is less than that for the 1.25 in. notch. This indicates that a specimen size effect was stronger than the notch size effect, giving the appearance of notch insensitivity. Past literature (Refs. 7, 15, and 16) has shown notch insensitivity with very soft layups (e.g., $[\pm 45]_{ns}$) but little has been done to quantify the relationship with specimen size.

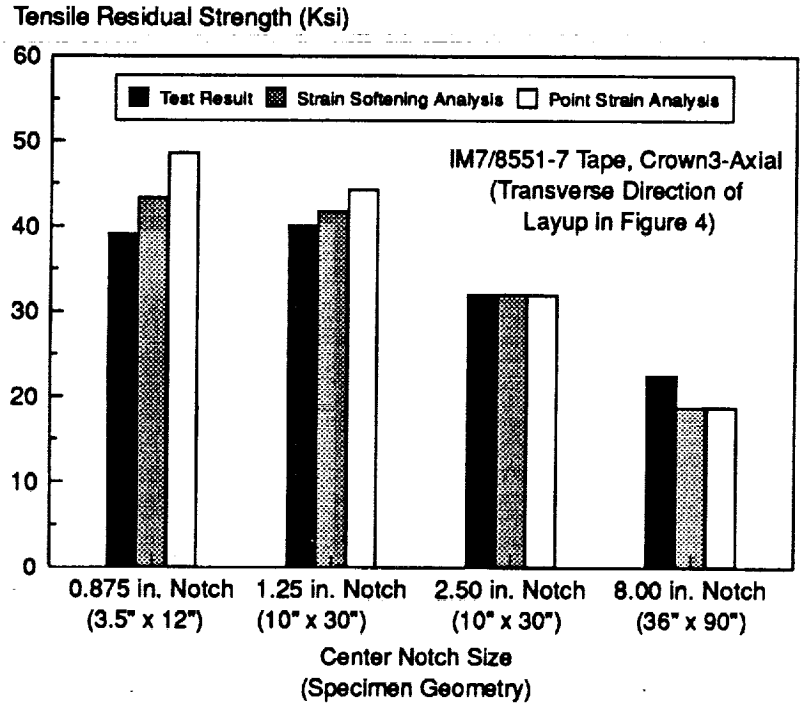


Figure 20: Comparison of Specimen Size Effects for Notched Residual Strength Analysis and Test Results.

Analysis comparisons with test data in Figure 20 indicate that the strain softening methods had better correlation with small notch test results than did the point strain approach. This included the ability to better predict the specimen size effect leading to the apparent notch insensitivity exhibited by the two smallest notch sizes in Figure 20. As was the case in earlier work by the authors with notched composite failure criteria (Refs. 7 and 8), progressive damage analysis methods studied in ATCAS are being judged based on an ability to scale relatively small notch test results to large notch properties. Figure 20 indicates that both strain softening and point strain analyses underpredict the largest notch result for "soft layups". The fracture parameter for point strain analysis would have to empirically vary with crack length and specimen size to predict all results in Figure 20. This would limit its use to interpolation and it could not

be used with confidence for scaling small test results to accurately predict large panel performance.

A laminate strain softening curve that is suitable for large panel scaling analyses may be characterized from more complete test data correlation with a range of small notches and differing coupon sizes. Such an engineering approach would benefit from additional parametric studies to understand how various parts of a strain softening curve affect fracture strength as a function of specimen size. This approach would only be practical if it results in less test and analysis costs than an empirical database that includes large notch data. The method of determining strain softening curves used in current studies was strongly dependent on the 2.5 in. notch fracture data. Conservative predictions of large notch strength appear to be a direct result of this constraint. Some additional dependence on results from other small specimen sizes would have changed the initial unloading slope and increased total energy under the curve such that it still matched with test data for the 2.5 in. notch. Greater energy under the curve would increase strain softening predictions for the largest notch shown in Figure 20.

Significant differences in the fracture residual strength curves for ATCAS tow-placed and hand laid tape laminates have been measured (Refs. 7, 8, and 17). These laminates consisted of the same volume ratios of identical fiber and matrix types. Differences were found to be negligible for unnotched and small notch coupons (D = 0.25 in.). Tow-placed laminate fracture strength was significantly higher in the range, 0.75 in. $\leq$ D $\leq$ 2.5 in. (W/D = 4). Figure 21 shows strain softening curves which were found to predict differences in fracture strength measured for the two manufacturing processes. The laminate layup is the same as that shown in Figure 17.

The strain softening material response is identical for the cases in Figure 21 until a point where significantly more energy is evident in the tow-placed laminate unloading curve. Experimental measurements for larger tow and tape fracture tests (D = 2 in., W/D = 4) confirmed that damage initiated in both material forms at the same stress level (Ref. 17); however, the tow-placed laminate specimens were able to sustain higher loads. This is consistent with physical reasoning posed earlier that the end portions of the strain softening curve do not become important until larger notch and specimen sizes are considered. Figure 22 shows additional evidence of differences in tow and tape failure mechanisms observed in laminate impact damage. The heterogeneous fiber failure, also noted for tow-placed laminate notch tip damage zones (see Figure 17), is thought to be a function of a repeatable inhomogeneity produced at the scale of tows used to form the laminate during automated placement processes. Hypothetically, the tow placed material architecture results in more fracture energy absorption due to dispersed fiber/matrix failures and additional unloading strains from uncoupled plies.

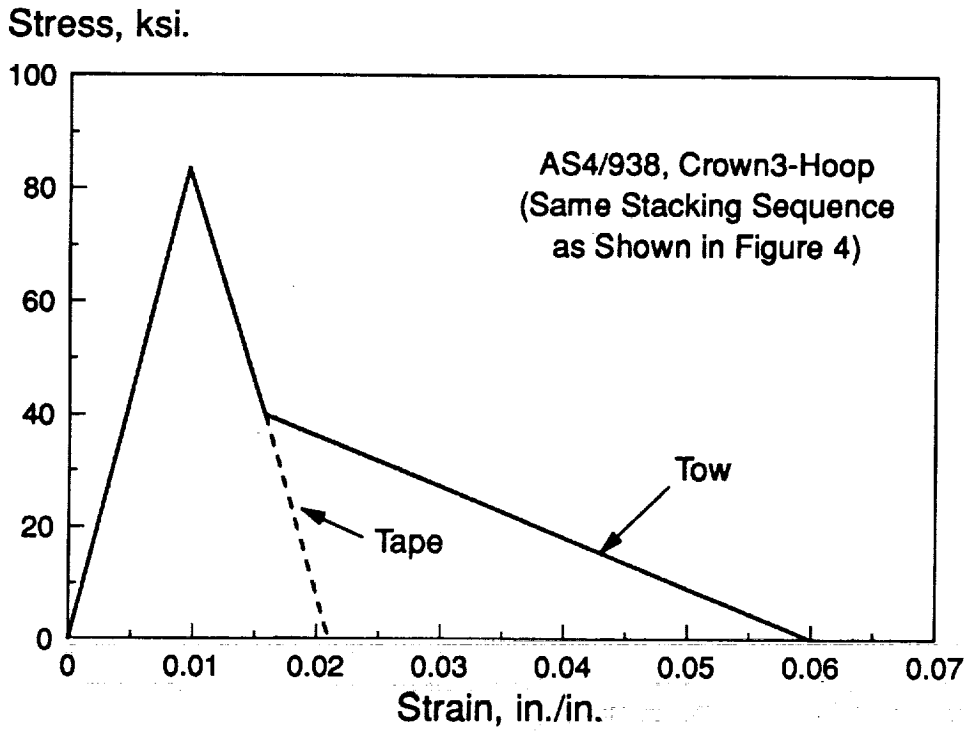
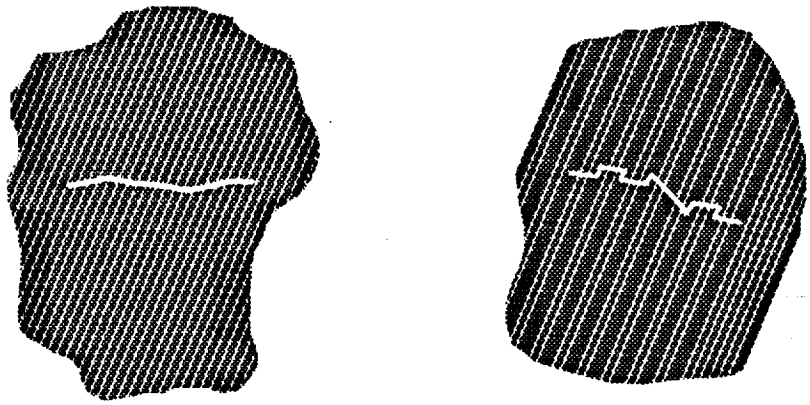


Figure 21: Differences in Strain Softening Laws for Tow-Placed and Hand Laid Tape Laminates



Homogeneous
Tape Material

Inhomogeneous
Tow Placed Material

Figure 22: Differences in Tow and Tape Fiber Deply Maps Measured for Impacted Laminates (Ref. 18)

Figure 23 illustrates extremes of the "strength versus toughness trade" observed in tension fracture tests for materials and laminates from the ATCAS database (Refs. 1, 7, and 8). The solid curve is characteristic of a hard laminate layup for the toughened matrix material, IM7/8551-7. The dashed curve illustrates the apparent notch insensitive behavior of a soft, tow-placed laminate layup consisting of an intraply hybrid material, 25%S2/75%AS4/938. The strain softening curves shown in the upper right portion of Figure 23 predict the trends shown in the residual strength curves.

The material response denoted "hard brittle behavior" in Figure 23 yields the highest small-notch strengths, relatively small notch tip damage zones, insignificant specimen size effects, and a low fracture toughness. These traits are characteristic of a strain softening curve with relatively high maximum stress but low total fracture energy. Progressive damage analysis for this material would only benefit small coupon predictions since the material response quickly converges with a LEFM curve. The material response denoted "soft tough behavior" in Figure 23 yields low apparent small-notch strengths, relatively large notch tip damage zones, significant specimen size effects, and a high fracture toughness. These traits are characteristic of a strain softening curve with relatively low maximum stress but high total fracture energy. Progressive damage analysis for this material is essential because the entire residual strength curve is strongly dependent on specimen size effects. High toughness observed for intraply hybrids suggest that progressive damage analysis would be crucial for even large structural scales.

Some ATCAS efforts have utilized strain softening analysis for progressive damage growth in configured structures. Debugging of models that combine progressive damage growth simulation and nonlinear geometric effects (caused by large local deflections occurring with load redistribution in notched structure) has proved labor intensive. Finite element substructuring also appears necessary to reduce computing time. Future ATCAS efforts will explore:

1. economical and fast solution schemes for composite structures
2. experimental and analytical methods for determining strain softening laws and interaction curves.

Similar trends to those shown in Figure 23 are likely to occur for notched composite laminates loaded in compression. Future ATCAS studies will also explore the use of strain softening analysis for compression. Generally lower unnotched compression strengths for composites suggest stronger specimen size effects than noted for tension. Some work on compression size effects for composites has been published (Ref. 14). Also note that strain softening laws have been applied as a scaling method to predict the inelastic collapse of building materials used in compression loaded structures (Ref. 11).

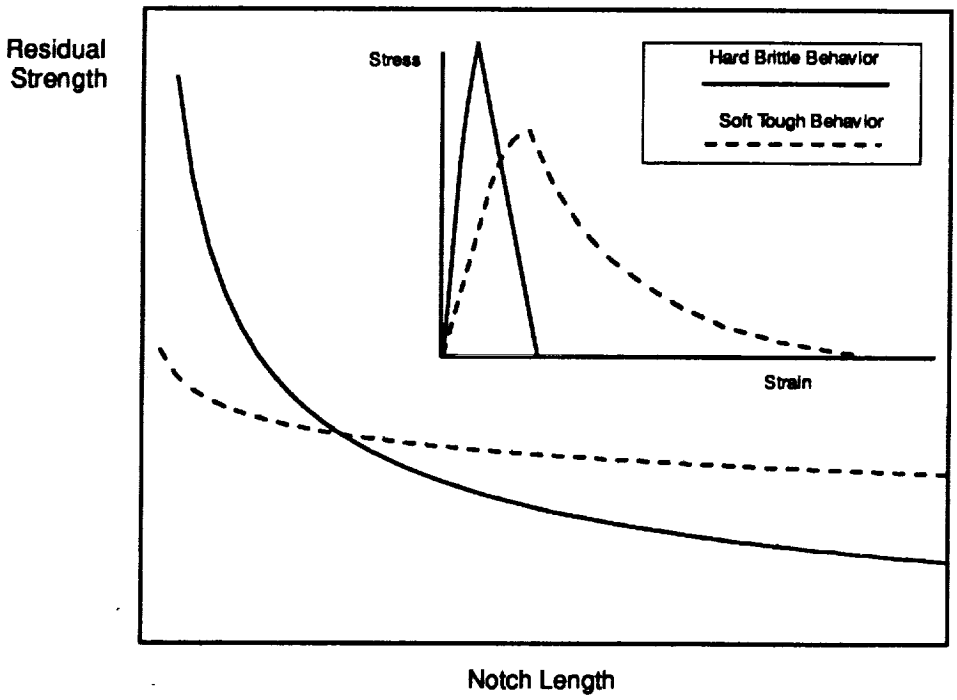


Figure 23: Schematic of Strain Softening Laws That Predict the Apparent "Strength Versus Toughness Trade" Observed in the ATCAS Database (Refs. 1, 7, and 8).

7.0 Frame/Skin Bondline Analysis and Test

7.1 Introduction

The Boeing ATCAS program selected a Family C (bonded stringers and frames) design as baseline for the fuselage crown quadrant due to projected cost and weight savings potential (Ref. 19). The baseline design configuration mouseholed the bonded frame over the cocured hat stiffener as shown in Figure 24. Significant cost savings were projected with this design that does not have stringer clips due to:

1. Elimination of clip fabrication costs
2. Elimination of costs for clip attachment to stringer and frame
3. Simplified panel cure tooling at the frame/stringer intersection (due to the enlarged mousehole opening)
4. The ability to use hat-stringers which have lower fabrication costs (as compared to blades or Js which are better for clip attachment)
5. The potential for wider stringer spacing with the more stable hat geometry (significant cost savings documented in Ref. 20).

These cost considerations warranted technical studies of the mouseholed design detail to judge whether a stringer clip or some other design modification would be needed to meet performance requirements. Note that the cost savings described items 3, 4, and 5 from above may be possible with a design modification simpler than a traditional stringer clip (e.g., strip that mechanically attaches frame and stringer flanges).

A composite structure consisting of bonded stiffener and frame elements requires control of the bonding processes and technical understanding of the related performance issues. A key manufacturing issue for the concept shown in Figure 24 is the control of cobonded frame processes for selected design details. The related technical issue is the frame/skin bond integrity associated with loads from pressure pillowing and compression postbuckled skins. The current study concentrated on pressure pillowing loads since compression stability issues were not as strong an influence for the crown quadrant design (i.e., this area of the fuselage is dominated by tension load cases).

Several technical groups coordinated efforts to study pressure pillowing of the bonded frame design detail characteristic of the ATCAS crown panel. A number of design modifications and process variables were considered in early ATCAS fabrication trials. This provided parts for initial ATCAS frame pulloff tests (using a clamped fixture) at Drexel University (J. Awerbuch and A. Wang subcontract funded by NAS1-18889). Subsequent analysis performed at Boeing Helicopters (M. Fedro and P. Menguet) and Drexel (funded by NAS1-19349) lead to a concern that the clamped test fixture used to produce initial ATCAS results could not be directly related to pressure pillowing load conditions in the fuselage. A new test fixture was developed for frame skin bond

strength assessment away from the mousehole design detail (referred to as the modified frame pulloff test fixture). Another new test fixture was designed for frame skin bond strength assessment at the mousehole. Both new fixtures were analyzed and designed under NAS1-19349. The fixtures were fabricated at NASA Langley. Initial tests with these new fixtures were performed by the Mechanics of Materials Branch at NASA (R. Martin and T. K. O'Brien). Test and analysis correlation was performed under NAS1-19349. A technical paper was presented at the 4th ACT Conference (Ref. 21) to summarize global analysis (supporting design of the new fixtures and data reduction) and static frame pulloff tests. Other supporting activities performed by Drexel University subcontracts have included local finite element analysis of frame pulloff fracture mechanisms and preliminary fatigue tests, respectively. The mechanics of Materials, Computational Structural Mechanics (J. Wang), and Aircraft Structures (M. Shuart) Branches at NASA Langley also helped perform analysis and data interpretation.

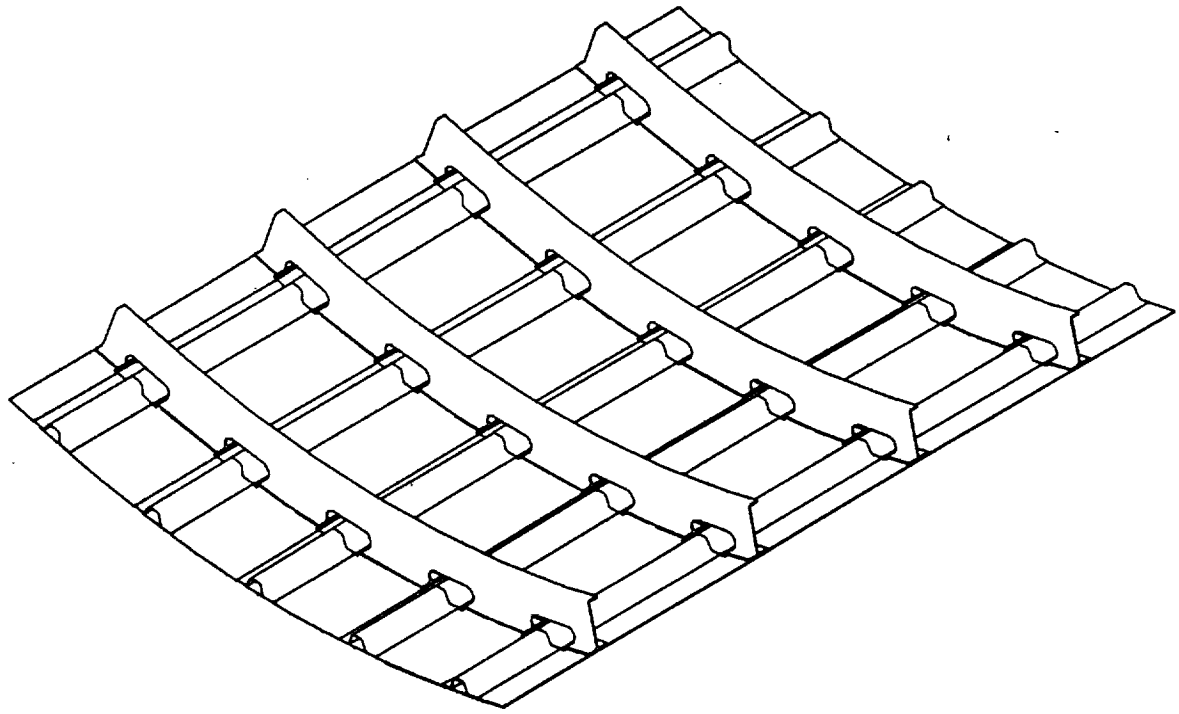
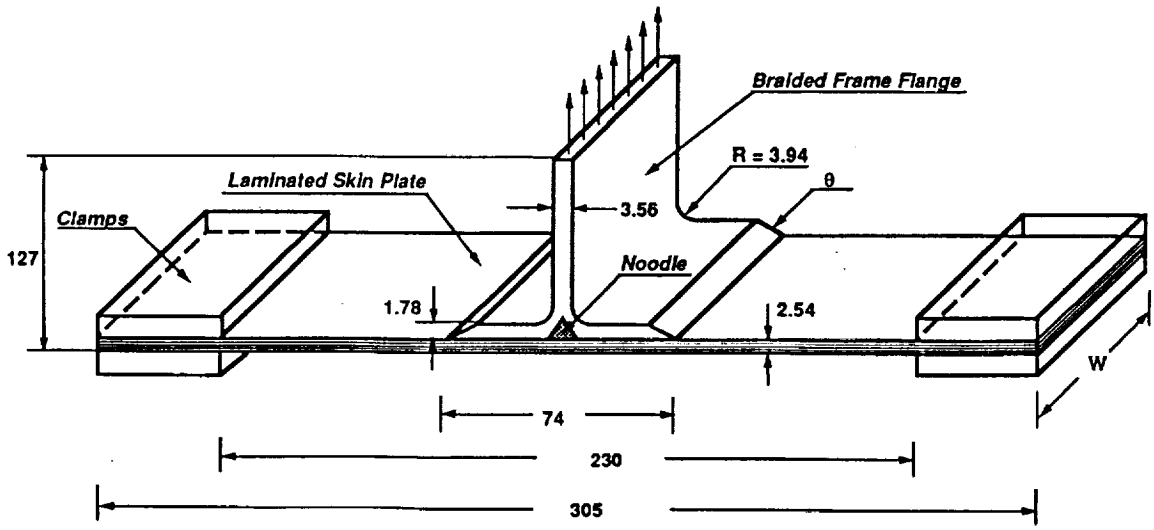


Figure 24: Baseline ATCAS Crown Concept With a Mouseholed Frame Design Detail

The following documentation summarizes all studies that have addressed frame pressure pillowing analysis and tests for the ATCAS crown panel design. This provides a complete history of the technical work performed to date. The efforts of groups funded by NAS1-19349, Task 2 will be highlighted.

7.2 Clamped Pulloff Tests

Test elements for initial frame pulloff testing were machined from panels produced while developing manufacturing processes for the ATCAS crown design. Figure 25 shows the specimen geometry and its dimensions. The skin plate consists of a 13 ply AS4/938 [±45/90/0/±60/90/±60/0/90/±45] laminate (nominal ply thickness = 0.0074 in). The top flange of the J-frame was machined off, resulting in an inverted 'T' for testing. As discussed in previous sections of this report, the crown frame is fabricated via the resin-transfer-molding (RTM) process. The frame preform is a 2-D braided architecture, with ±66° bias angle AS4 tows and 37% axial AS4 tows. The RTM resin system is Shell's 1895, which is similar in performance to Hercules 3501-6. Assembly of the frame/skin configuration is achieved via a cobonding and cocuring process. The frame was cobonded to the skin plate with a 9 mil film adhesive of BASF Narmco 1515. A triangular shaped 'noodle' was inserted at the base of the frame to fill the void created during assembly. Materials used to create the 'noodle' were either the same braided material used in the frame or the BASF Narmco 1515 adhesive. In certain coupons, a thin flange plate was inserted between the frame and the skin plate.



Dimensions are given in mm.

Figure 25: Clamped Frame Pulloff Test Specimen

Initial ATCAS specimens were designated by four groups (J, K, L, and M), depending on when they were received by the Composite Mechanics Laboratory at Drexel. Each group was different in either specimen design or in the manufacturing process. Variations in the design included geometry, 'noodle' type, and the addition of a flange plate. A total of 28 specimens were tested, as listed in Table 11.

SPECIMEN NO.	NOODLE TYPE	CRACK INITIATION LOAD [N (lbf)]	MAXIMUM APPLIED LOAD [N (lbf)]	SITE OF FIRST CRACK[a]	DOMINANT CRACK[b]	DOMINANT DAMAGED AREA[c]
J-1	Adhesive	810 (182)	1383 (311)	L	R	S
J-3	Adhesive	503 (113)	1259 (283)	L	R	S
J-5[d]	Adhesive	729 (164)	1338 (301)	L	L	S
J-6[d]	Adhesive	667 (150)	1428 (321)	R	R	S
J-8[d]	Adhesive	778 (175)	1148 (258)	R	R	S
J-9	Braided	640 (144)	1156 (260)	R	R	S
J-11	Braided	689 (155)	1379 (310)	R	R	S
J-12	Braided	885 (199)	1401 (315)	L	L	S
J-13[d]	Braided	547 (123)	1205 (271)	L	R	S
J-14[d]	Braided	489 (110)	1236 (278)	R	L	S
J-16[d]	Braided	512 (115)	1165 (262)	L	L	S
K-1	Braided	867 (195)	1148 (258)	L	L	S, F, N
K-2	Braided	1169 (263)	1481 (333)	R, L	L	S
K-3	Braided	1108 (249)	1592 (358)	R, L	C	S, F, N
K-4	Braided	983 (221)	1739 (391)	L	R	S, F, N
K-1A	Adhesive	956 (215)	1396 (314)	C	C	S, F, N
K-2A	Adhesive	1054 (237)	1375 (309)	C	C	F, N
K-3A	Adhesive	992 (223)	1352 (304)	L	R	S
K-4A	Adhesive	987 (222)	1317 (296)	R	L	S, N
L-1[e]	Adhesive	1081 (243)	4315 (970)	L	C	S, F, N
L-2	Adhesive	721 (162)	1833 (412)	L	C	S, F, N
L-3	Adhesive	756 (170)	1744 (392)	L	C	S, F, N
M-A[e]	Adhesive	1472 (331)	3078 (692)	L	C	S, F, N
M-B[e]	Adhesive	1953 (439)	3216 (723)	C	C	F, N
M-C[e]	Adhesive	1223 (275)	2647 (595)	R	C	S, F, N
M-D[e]	Adhesive	1721 (387)	3523 (792)	R	C	S, F, N
M-E[e]	Adhesive	1415 (318)	2673 (601)	R	R	S
M-F[e]	Adhesive	1544 (347)	3803 (855)	R	C	S, N

a. R, L, C... Crack initiation site occurred along the Right or Left edge of base of frame, or at the Center of frame (around noodle), respectively.

b. R, L, C... Dominant crack progressed from Right or Left edge of base of frame towards the center of test element, or from Center (around noodle), towards the right and/or left hand side of frame, respectively.

c. S, F, N... Faliure occurred inside Skin plate, Frame, and 'Noodle', respectively.

d. Test element contained also an additional flange plate inserted between the frame and the skin plate.

e. Width of specimen = 127.0 mm (5.0 inch). Width of all other specimens = 76.2 mm (3.0 inch).

Table 11: Clamped Frame Pulloff Test Results

The J-series specimens shown in Table 11 were broken into four additional separate sub-groups: a) Adhesive noodle, without flange plate; b) Adhesive noodle, with flange plate; c) Braided noodle, without flange plate, and d) Braided noodle, with flange plate. There were two different groups of the K-series specimens; those made with a braided noodle and those made with an adhesive noodle. The L and M-series specimens were all made with an adhesive noodle. No flange plates were used in the K, L and M-series specimens. The J-series specimens were cut from small manufacturing trial panels, while the K, L and M-series specimens were cut out from larger fuselage crown panels.

Initial ATCAS frame pulloff testing was performed using the clamped fixture shown in Figure 26. A fixture similar to this has been used in past composite element pulloff studies (Ref. 22). The load was applied along the web of the frame through two plates which were affixed to the web. The specimens were loaded under the "clamp-clamp" conditions. All testing was performed under stroke controlled mode on an electro-mechanical testing machine (Instron, Model 4206). The specimens were subjected to tensile quasi-static loading/unloading cycles, incrementally increasing the load up to failure. Immediately upon damage initiation (observed optically and by acoustic emission), the specimens were unloaded rapidly to approximately 50-80% of the previous maximum load and accurate measurements of the crack extension and state-of-damage were taken. In order to determine the effect of loading rate, three different crosshead rates were used: 0.0254 mm/min. (0.001 in./min.), 0.1270 mm/min. (0.005 in./min.), and 1.270 mm/min. (0.05 in./min.). Complete failure was determined when the specimen could no longer sustain any load.

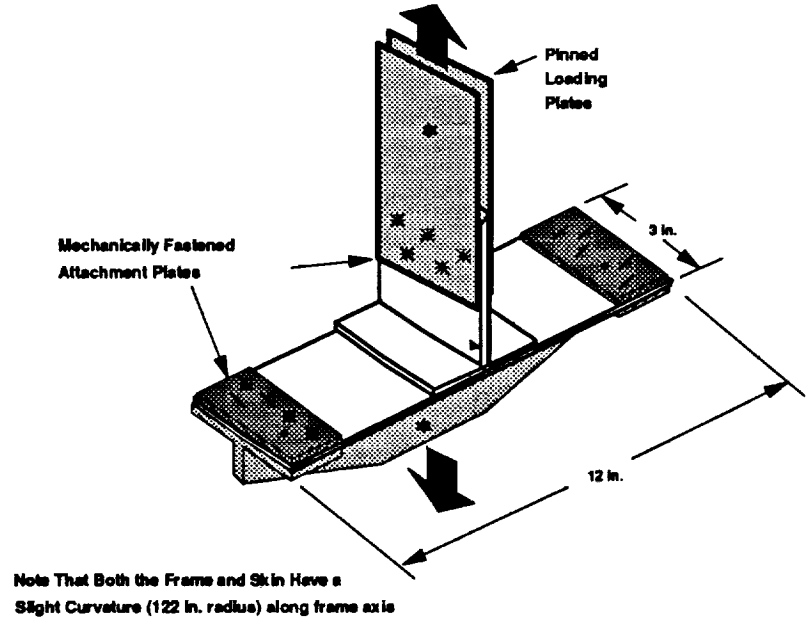


Figure 26: Clamped Frame Pulloff Test Fixture

Damage initiation and progression were monitored continuously throughout loading using a high magnification (150X) closed circuit television system (CCTV). The length of the cracks emanating from both ends of the frame and/or the 'noodle' region were measured with a resolution of approximately 0.2 mm (0.008 in.).

For all specimens tested at Drexel, acoustic emission (AE) was used as an early warning device for detecting damage initiation. For selected specimens, a detailed AE data analysis has been performed and a correlation between acoustic emission and the actual damage progression has been established. Special emphasis has been placed on identifying the emission generated by grating among the fracture surfaces. For selected specimens, the fracture surface morphologies along the frame/skin bond line were examined via the scanning electron microscope and X-radiographs were taken in order to determine whether the crack front progressed uniformly across the width of the specimen.

A typical load-displacement curve obtained during loading/unloading cycles of a clamped frame pulloff test is shown in Figure 27. The specimen was unloaded immediately following the detection of damage growth (via optical observations and from acoustic emission). Each damage growth was accompanied by a sudden drop in load which resulted from the fact that loading was conducted under stroke controlled mode. The sharp decrease in load is indicative of unstable crack growth. This phenomena can be seen in every load-displacement curve, usually in the later loading/unloading cycles. Initially, the specimen behaved linearly, as expected. The nonlinear behavior during the unloading and reloading phases of each of the loading cycles should be attributed primarily to the presence of damage in the test element. In some specimens there is clearly a hysteresis phenomenon, indicating energy loss during the load cycle. The amount of hysteresis decreases with load cycle. It should be noted, however, that the load-displacement behavior incorporates the lumped effect of the testing machine, the large deformation of the thin skin plate, and the extensive damage growth. It is interesting to note that when the applied load reached the previous maximum load, following each damage growth, the specimen resumed its linear behavior. This behavior continues until the load reached its maximum. Beyond that point, massive damage had occurred, to the extent that the frame and skin where partially separated.

Following each unloading the extent of damage was measured optically through the closed-circuit television system. Failure initiated either along the edge of the base of the frame (defined here as frame termination point) or inside the 'noodle' region. In the first case, the crack progressed along the specimen at the vicinity of the frame/skin interface. A typical crack extension plot for that case is shown in Figure 28. The figure clearly indicates that cracks had initiated at both ends of the base of the frame simultaneously and during the first few loading cycles they progressed approximately at similar rates. With further increase of the load the crack on the right hand side of the frame progressed rapidly, in an unstable manner, while the crack on the left hand side was arrested. This unsymmetrical crack growth behavior occurred in all test elements in which the crack progressed along the frame/skin interface. This is expected since

material inhomogeneities and the lack of perfect symmetry in either the far-field load or in the crack-tip front, or a combination thereof, may cause different rates of progression of the cracks in either side of the frame.

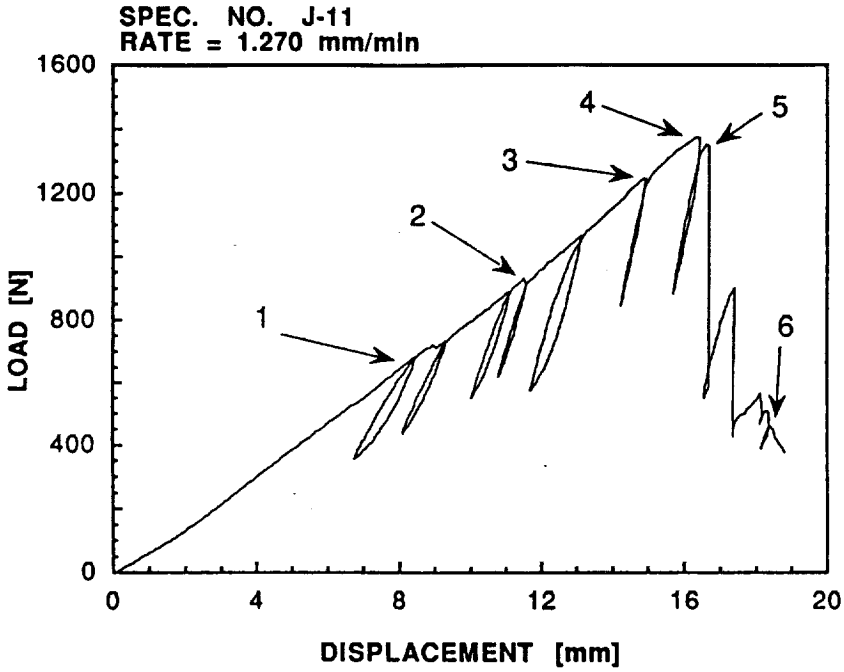


Figure 27: Load-Displacement Curve Showing the Applied Loading/Unloading Sequence.

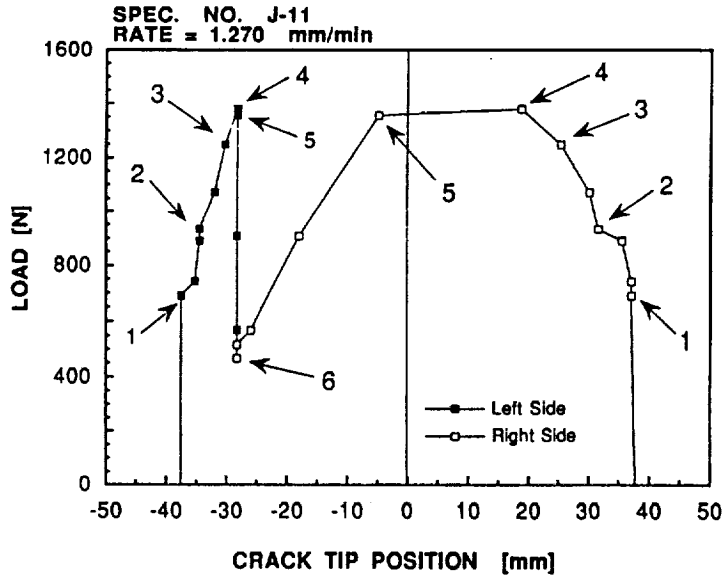


Figure 28: Crack Growth Along the Frame/Skin Interface as a Function of Far-Field Applied Load for the Same Test Element Shown in Figure 27.

The main disadvantage of the clamped frame pulloff test fixture shown in Figure 26 is that the specimen is statically indeterminate. As will be discussed later, the bending moment at the tip of the frame flange is the primary load leading to failure and cannot be determined directly. This bending moment can be determined through more detailed analysis, but the accuracy is then dependent on stiffness properties and exact boundary conditions. Another potential difficulty is that some of the nonlinearity was observed in the load versus displacement curve due to in-plane membrane forces caused by the large out-of-plane deflection and the deflection reduces the bending moment at the tip as illustrated in Figure 29.

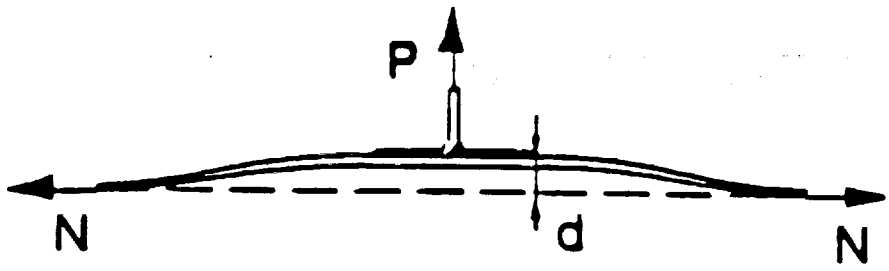


Figure 29: Illustration of Geometric Non-Linearity Due to Membrane Loads.

7.3 Global Pressure Pillowing Analysis

A finite element model was developed to understand pressure pillowing load redistribution near the bonded frame detail of the ATCAS baseline crown design. This model helped define and interpret additional frame pulloff experiments performed in support of design development. Since the local stress distribution was of interest, rather than the overall loads in the whole fuselage, a detailed model of one typical bay of the frame and stringer grid was represented. Furthermore, symmetry considerations were used to reduce the size of the model to one quarter of such a bay. A view of the model, where 1575 laminated composite shell elements were used, is shown in Figure 30. Different variations of this model were used to analyze different sections of the crown panel. While the frame spacing remains constant at 22 in. throughout the crown quadrant, the stiffener spacing varies between 14 in. at the top of the panel, and 18 in. near the edge of the panel. Also, the skin gage increases, adding plies to the layup, moving from aft to forward sections of the crown panel. However, based on the results shown later, the thinner skin of the aft crown panel appeared more critical and is used in the results shown here. The layup of the aft crown panel skin is [±45/90/0/±60/90/± 60/0/90/±45], while the hat-stiffener layup is [$\pm45/0_2/90/\pm15/90/0_2/\pm45$].

Loading in the aft crown panel consists mostly of the aircraft internal pressure and the axial load due to global fuselage bending. Two load cases were considered: the first one consists of a pressure level of 13.8 psi (1.5 times the maximum level of 9.1 psi) with an axial tension load of 5500 lb./in. The second load case consists of an ultimate

pressure of 18.2 psi (twice the normal level) acting alone with an axial bulkhead reaction load of 1110 lb./in. for a 122 in. radius fuselage.

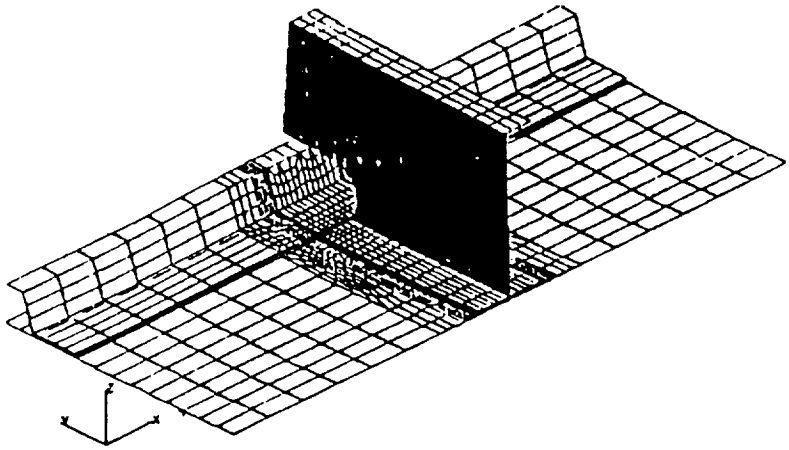


Figure 30: Finite Element Model of Crown Panel Bay.

Different views of the deformed structure for the ultimate pressure load case are shown in Figure 30. The overall deformation pattern shows the skin bulging at the center of each bay as expected. The maximum radial deflection is 0.247 in. at the center of a bay for the 14 in. stiffener spacing and 0.315 in. for the 18 in. spacing. The radial deformation under the frame is 0.147 in. for the 14 in. spacing and 0.130 in. for 18 in. spacing. Both the frame web and top flange deform out-of-plane. This is due to the high axial load in the curved upper flange that induces normal loads and flange curling. Another area of interest is the gap between the stiffener flange and the base of frame inside the mousehole. High local curvatures can be seen in this area.

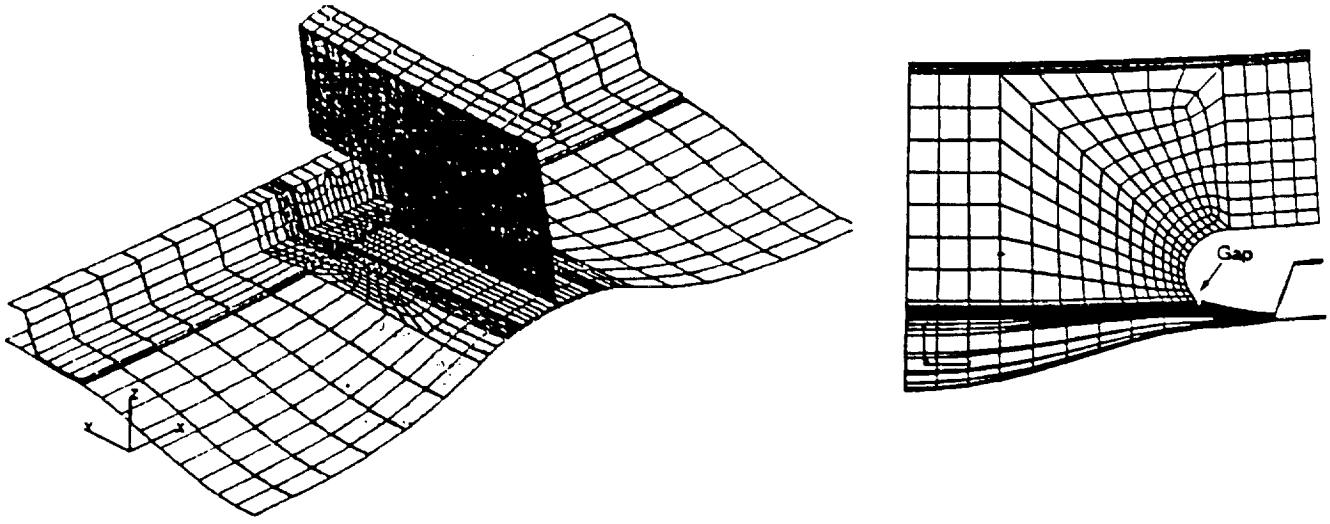


Figure 31: Deformed Panel Under Ultimate Pressure Condition.

When pressure is applied on the panel, most of the load is reacted by hoop tension stresses in the skin. However, some load is reacted from each skin panel through transverse shear and bending in the stiffener and frame. This is due to the mismatch in radial compliance between the different components. The stiffener can then be viewed as a continuous beam supported at each frame. Transverse load on the stiffener is reacted into each frame through skin in the narrow gap between the two components.

The first area of interest is the bondline along the length of the frame. Based on the test data that will be shown later, the skin bending moment at the attaching frame flange edge is the most important loading to initiate failure because it is responsible for most of the adhesive peel and shear stresses.

Ultimate over-pressure of 18.2 psi is the critical load case, causing maximum bending moments along the frame length. The moment distribution along the attaching frame flange edge is shown in Figure 32, going from the middle of the bay towards the stiffener. Values shown in this figure were obtained for stiffener spacing of 18 in. and 14 in. In each plot, two curves are shown representing the moment distribution on either side of the frame. The small difference in moment between the two sides is due to the fact that the frame section is not symmetrical and tends to twist as previously described. The presence of the axial load tends to contribute only slightly to the local moments because of the local asymmetry created by the thickness change between the skin and skin-plus-frame flange area. For further reference, note that the peak bending moment is about 22 in.-lb./in. near the middle of the bay for the 18 in. spacing. This stiffener spacing gave the highest moment because of the larger size of each bay.

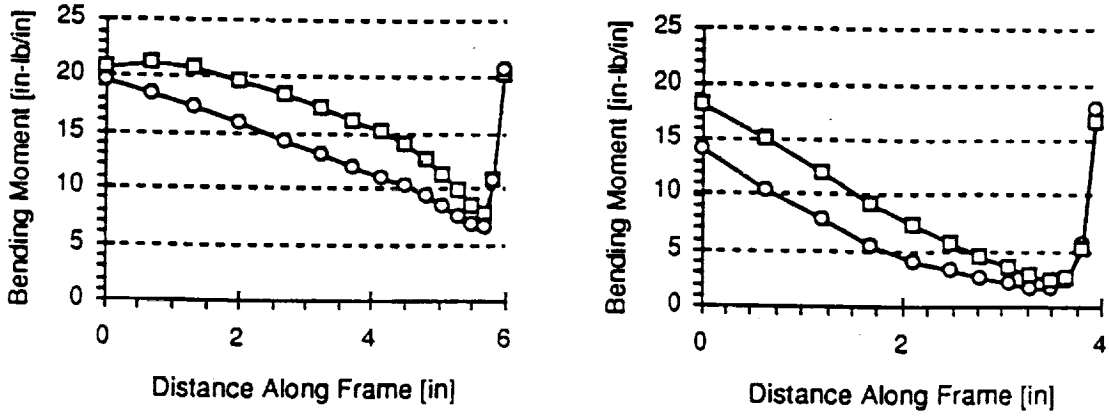


Figure 32: Skin Bending Moments Along both Edges of the Attaching Frame Flange for Stiffener Spacings of 18 in. (left) and 14 in. (right).

The second critical area considered in reviewing analysis results is the skin inside the mousehole at the frame and stiffener intersection. As shown in Figure 33, a large bending moment is predicted in the skin mostly due to the transverse load being transferred from the stiffener to the frame. This moment is such that it tends to peel the

skin away from the frame. Another contributor to the moment is the local asymmetry due to the termination of the frame flange. The maximum pressure load case is also critical for this area, while the stiffener spacing has less influence than in the previous area. The peak moment is reached at the center of the mousehole and is about 140 in.-lb./in. However, this FE model based on shell elements may be less accurate in this narrow region and a more detailed local three-dimensional model may be necessary to capture the actual stress distribution.

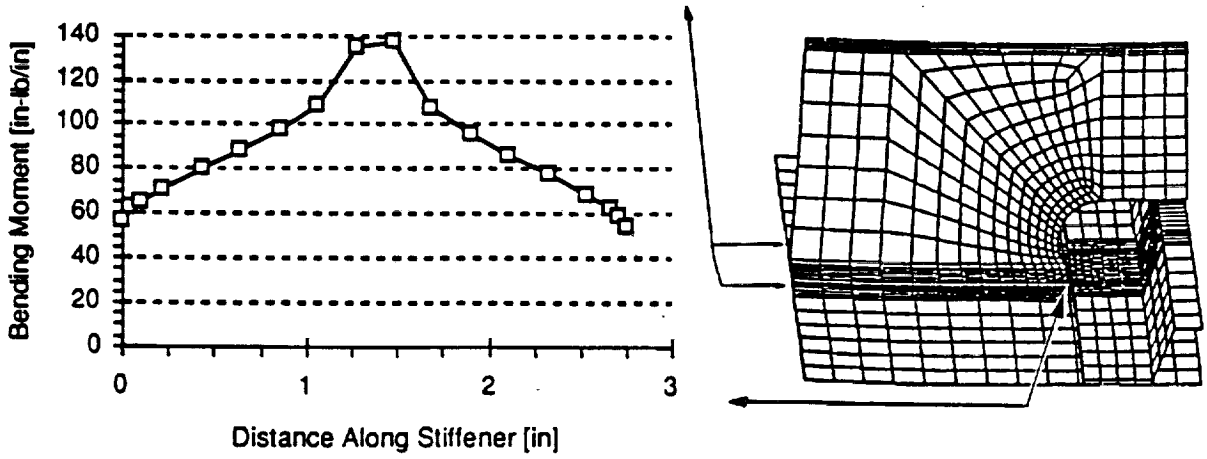


Figure 33: Bending Moment in the Skin Gap between Stiffener and Mouseholed Frame.

7.4 Pulloff Tests Using a Modified (Simply Supported) Fixture

A modified loading fixture was designed to test the same specimen geometry shown earlier. As discussed, the main drawback of the clamped frame pulloff fixture is the inability to directly determine the moment at the flange tip. Thus, in the modified fixture, the specimen boundary conditions are changed from clamped to simply supported. The new setup is depicted in Figure 34. Circular rods are used to support the specimen and can be located at different stations to vary the ratio of applied bending moment and transverse shear at the tip of the frame flange. The side plates can also be moved to accommodate different width specimens. Practically no membrane loads are introduced in the specimen since it is free to slide and thus no geometric non-linearity was observed.

For this round of testing, the specimen configuration was similar to the one used above. All the specimens were built with a 20° taper angle at the flange tip and an adhesive filler in the frame noodle. This is the benchmark panel design discussed earlier. All specimens were machined from the benchmark panels fabricated for this task. Most specimens had the same 13 ply skin layup, [±45/90/0/±60/90/±60/0/90/±45], as previously tested (representative of the aft crown), while some were manufactured with a thicker skin that had a 17 ply layup of [±45/90/0/±60/±30/90/±30/±60/0/90/±45] (representative of the forward crown). The effect of specimen width was also

investigated. Specimen width was varied between 0.6 in and 7 in. The moment arm between the load application point and the frame tip was also varied to obtain different ratios of shear and moment. Three values were used: 3.45 in. and 0.85 in., chosen to induce failure at the frame tip, and 0.0 in. (corresponding to the load application point next to the frame tip) chosen to trigger failure in the noodle area.

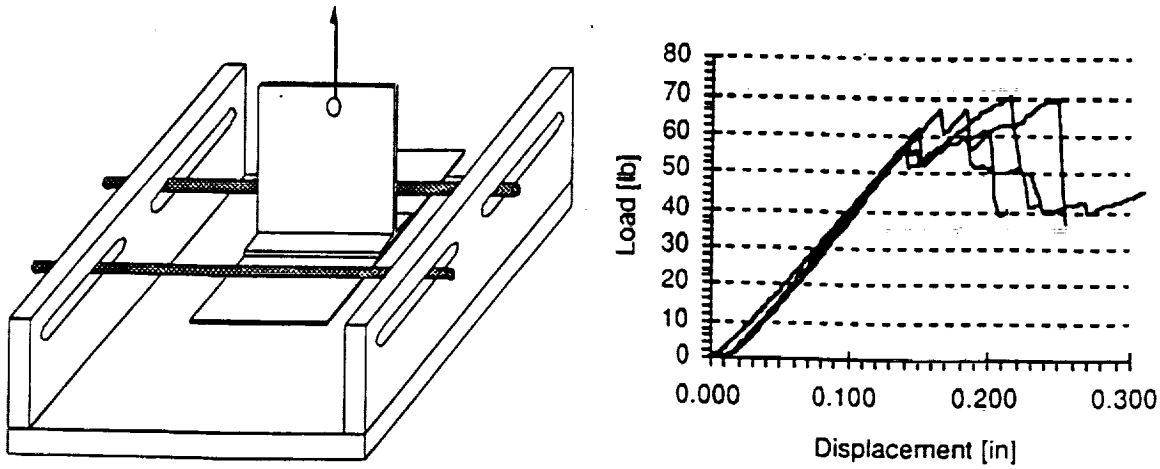


Figure 34: Modified Frame Pull-off Test Fixture and Typical Load versus Displacement Data for Frame Pull-off.

A typical set of load versus web displacement curves are shown in Figure 34. These correspond to four 0.75 in. wide thin skin specimens tested with a short moment arm. The first load drop was always associated with some failure in the frame tip region. After that event, the load was further increased while a delamination started to propagate under the bondline. That growth continued until a maximum load was reached and the delamination grew unstable.

A summary of the frame pulloff data obtained using the simply supported test fixture is shown in the bar chart in Figure 35 for three test configurations: the first two used thin skin (13 plies) specimens and varied the moment arm, while the third one used thick skin (17 plies) specimens with a long moment arm. One of the first observations that can be made is that only reporting the pull-off load, as has been frequently done in previous investigations, is not a good way to present the data. Although the first two configurations are the same specimens, the load is completely different. A better way to analyze the data is to look at the bending moment in the skin calculated at the tip of the frame. When the data is plotted in that fashion, then the results of the first two test configurations are much more consistent. On the moment chart, two values are reported for each group: the moment at which damage initiates and the maximum moment reached in the test.

The skin flexural stiffness appears to have a very strong effect on the results: a 30% increase in skin thickness results in a 95% increase in maximum moment capability. However, it is important to note that the ratio of maximum moment to damage initiation moment is very different between the two groups. In fact, if a criterion such as "no

damage at limit load, no bond failure (i.e., complete separation of frame and skin) at ultimate load" was used, the former would be the designing factor for the thick skin part.

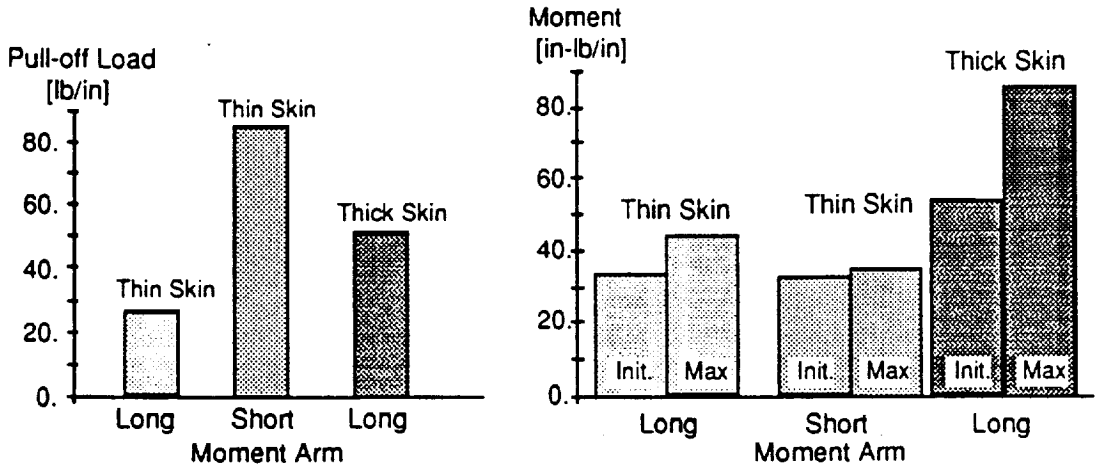


Figure 35: Pull-off Load and Moment Data for Tests Using the Simply Supported Fixture.

The effect of specimen width was also investigated. As shown in Figure 36, fairly consistent results were obtained for specimens up to 3 in. wide. An apparent increase in strength was observed for wider specimens. The main reason for this behavior is that specimens were cut from cylindrical panels. As the width increases, the overall bending stiffness of the curved specimen cross-section becomes higher than that of a specimen with a straight cross-section. For example, in the case of a 7 in. wide specimen, the second moment of inertia of a circular cross-section is about 26% higher than that of a straight cross-section with equal width. This results in a portion of the applied bending moment being carried in the skin by in-plane membrane forces (which do not create severe peel stresses) instead of bending moments.

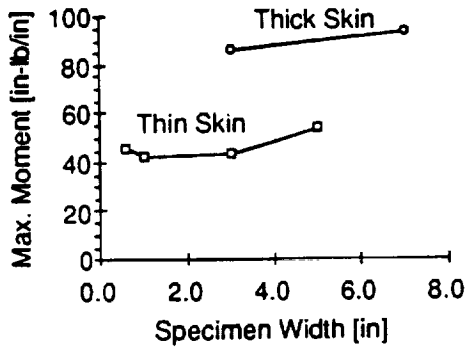


Figure 36: Specimen Width Effect On Frame Pull-off.

Three specimens were also impact-damaged prior to testing with a 5 ft.-lb. energy level. The impact was located on the outside of the skin and centered near the tip of the

frame flange. No clearly visible damage was created, but ultrasonic inspection easily revealed that an approximately one inch diameter delamination was created under the frame flange. During testing, damage spread along the width of the specimen at the tip of the flange in the same manner as the undamaged specimens but at a lower load level. However, the important observation is that the maximum load capability fell within the scatter of the undamaged specimens.

For design purposes, the data collected in frame pulloff tests can be summarized in a failure envelope such as the one shown below in Figure 37. All the data obtained for specimens with thin skins up to 3 in. wide are shown in this figure. The pull-off load is shown on the vertical axis, while the bending moment is shown on the horizontal axis. For damage initiation, the bending moment calculated at the tip of the frame flange is the logical choice since it is the location of failure. For the maximum load, however, the station at which the moment should be calculated is less clear because the delamination has usually spread some distance away from the frame tip when it becomes unstable. Thus, given that the moment at the crack tip is the driving load, the moment shown in the figure below is calculated at the station where the flange taper ends. For long moment arm tests (3.45 in.), the length of the taper, approximately 0.2 in., is not significant. For short moment arm tests (0.85 in.), it makes a significant difference. The points on the vertical axis with zero moment correspond to specimens that failed in the noodle area.

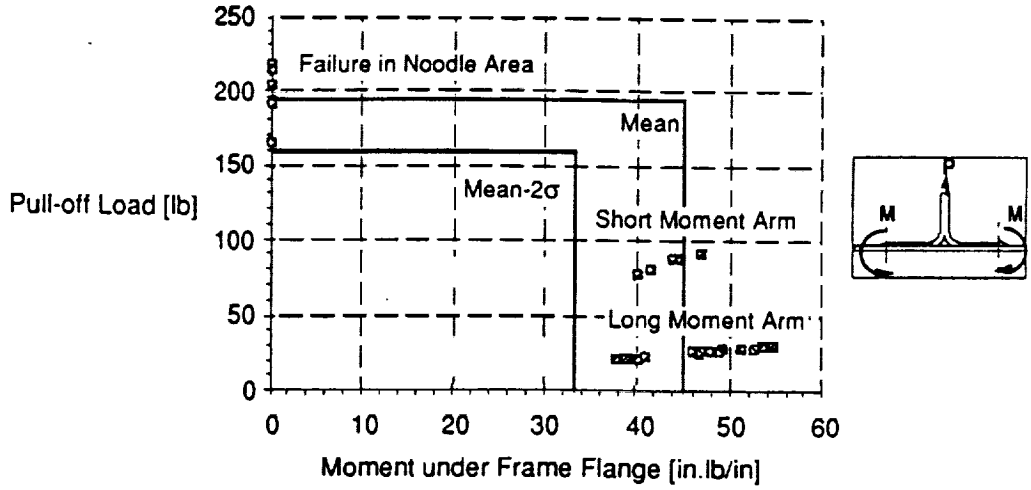


Figure 37: Failure Envelope for Ultimate Load of Thin Skin Specimens.

For all the data points shown in Figure 37, the mean moment at failure is about 44 in.-lb./in. If for design purpose an allowable moment had to be defined, the use of a "mean minus two standard deviations" definition would lead to an allowable of 33 in.-lb./in., which is below all the data points obtained here. Suggested mean failure and allowable envelope are drawn in the figure, although more data are needed to validate them. Recalling that the maximum moment predicted by finite element analysis is about 22 in.-lb./in., this would indicate that an adequate margin of safety is

obtained for this load case along the length of the frame. However, other factors such as elevated temperature, moisture, and fatigue still need to be considered.

7.5 Failure Mechanisms

Failure mechanisms were studied for frame pulloff tests performed with both the clamped and simply supported fixtures. Failure of the test elements initiated at either of the following three different sites: along the edge of the base of the frame (i.e. the frame termination point); around the noodle; and inside the noodle, as shown schematically in Figure 38.

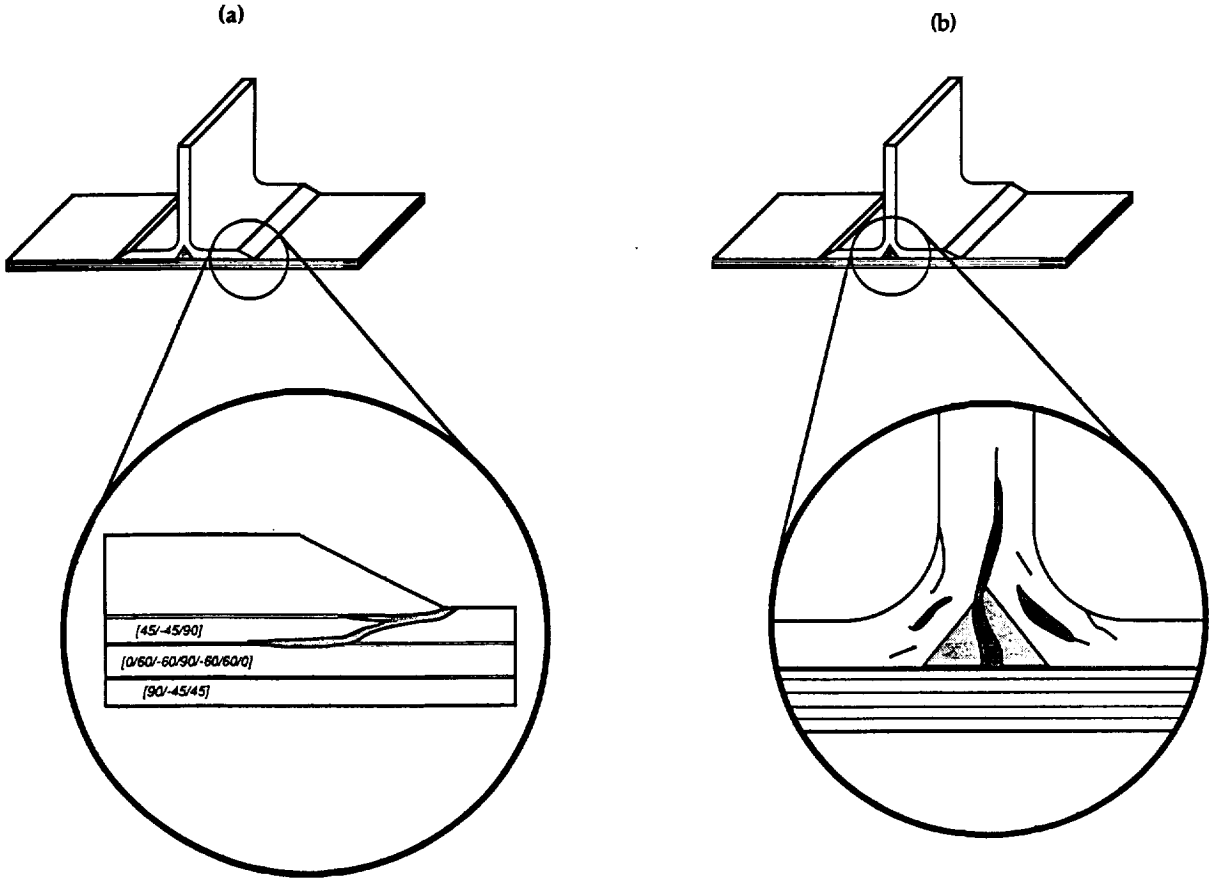


Figure 38: Schematics of Typical Failure of the Test Element: a.) Failure Initiates Along the Frame Edge; b.) Failure Initiates Around and Inside the "Noodle".

An example of failure initiating at the frame edge is shown in Figure 39a. The figure shows a sequence of schematic plots (depicted from the optical observations), illustrating the pattern of damage progression at the vicinity of the frame/skin interface. Note that the plot number indicated in Figure 39a corresponds to the load number shown in Figure 27. In this particular specimen, the crack initiated along both frame termination points and with increasing load they progressed towards the center of the test element. Beyond a certain load level (plot no. 5) the crack on the right hand side

progressed in an unstable manner, which resulted in the corresponding sudden load drop in the load-displacement curve, Figure 27.

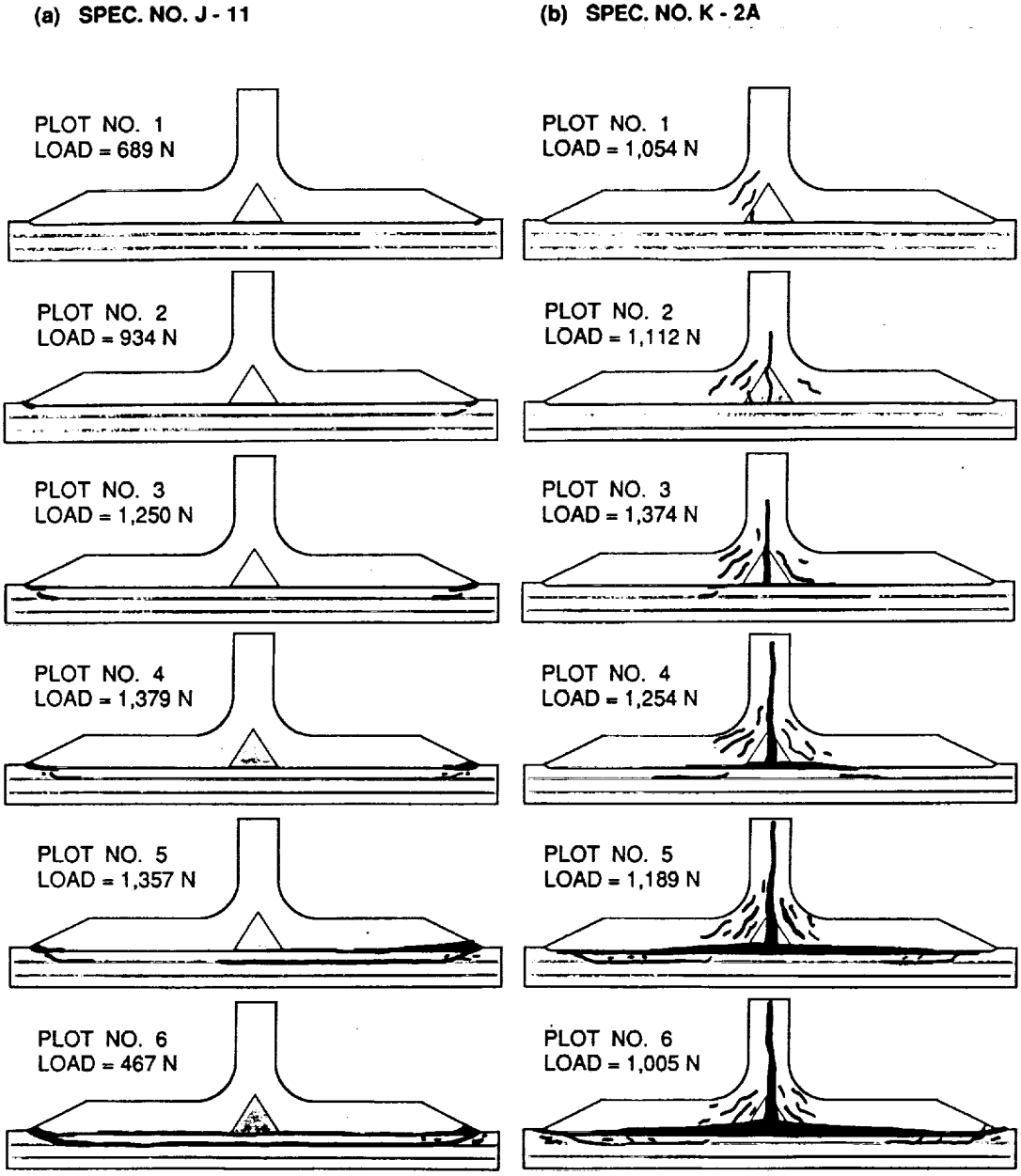


Figure 39: Schematic Plots of Damage Progression Sequence in 2 Test Elements: a.) Failure Initiates Along Frame Edge and Progressed Inward Inside the Skin; b.) Failure Initiates Around & Inside the "Noodle" and Progressed Outward Inside the Skin and Skin/Frame Interface.

It should be noted that optical observations (as well as examinations of the fracture surface morphologies) clearly revealed that the cracks separating skin from frame did not progress within the adhesive layer but rather inside the skin laminate. This probably occurs because the laminated skin material has a lower interlaminar fracture toughness than that of the adhesive layer.

An example showing the damage initiating at the 'noodle' site is shown in Figure 39b. Here, the sequence of schematic plots (depicted from the optical observations) clearly shows that initially damage had occurred inside the braided frame, around the 'noodle'. This damage appeared in the form of several cracks. At a certain load level (plot no. 3) a crack initiated inside the 'noodle', near the skin/frame interface (at the base of the frame), and progressed into the braided frame along the web. This crack always progressed in an unstable manner. The number and length of cracks around the 'noodle' increased with load. Once the cracks reached the skin/frame interface, they progressed rapidly along that interface. Again, in most cases these cracks propagated inside the skin plate.

The initiation sites for each of the 28 clamped specimens tested are listed in Table 11. Results indicate that the type of 'noodle' used (i.e. adhesive versus braided materials) does not affect the site at which the damage initiated. In all the J-group specimens the crack initiated at the frame edge, irrespective of the 'noodle' type or whether an additional flange plate was inserted between the frame and laminated skin. No damage was observed at the 'noodle' site in this group of specimens. Among the other three groups of specimens (i.e. the K, L, and M groups), damage initiated in the 'noodle' for only three specimens. Generally, it seems that there is no correlation between the site of damage initiation and the type of test element used.

On the other hand, there is a clear difference between the J-group and the other three groups of clamped test elements in terms of the site at which the dominant damage had occurred. The dominant damage is that which triggers final failure at maximum load. While damage also initiated at the frame edges in most of the K, L, and M groups of specimens, the dominant damage areas in most of these specimens occurred inside the 'noodle' region. That is, dominant damage growth out of the 'noodle' region usually occurred after cracks had initiated at the frame edge. Membrane loads associated with large deflections in the clamped test fixture may be the cause of this shift in crack growth trends as the pulloff force increases. Clamped specimens were also found to have a greater difference between initiation and failure loads than did the simply supported specimens, suggesting some interaction with the fixture.

Results in Table 11 indicate some scatter in the damage initiation load as should be expected in such composite structures. However, it should be noted that damage was monitored along one edge of the clamped test element, while damage may also have initiated along the other edge, contributing to the scatter in results. Generally, the results listed in Table 11 indicate that neither the damage initiation load nor the maximum load for tests in the clamped fixture are affected by the 'noodle' type. The

'noodle' type would also likely have little influence on simply supported tests performed with a moment arm.

Many frame pulloff specimens showed some manufacturing anomalies in the skin laminate under the frame. The frame flange tended to "sink" into the skin causing some waviness in the top plies most clearly seen in the uppermost 0° ply. In some of the worst cases, the top 2 or 3 plies were severely distorted into an "S" shape. The relative severity of these manufacturing anomalies may also contribute to data scatter.

Figure 40 shows failure initiation in the top 4 skin plies at the frame edge for specimens with and without manufacturing anomalies. For most specimens with little or no manufacturing anomalies, failure initiated in the manner described in the top of Figure 40. These were drawn based on observations of the videos taken during the first batch of tests and of photographs of specimens for which loading had been stopped after the first load drop. Although events occurred very rapidly, failure appeared in most cases to start with a crack in the adhesive pocket at the tip of the frame. This crack usually propagated into the top 45° ply as a transverse crack.

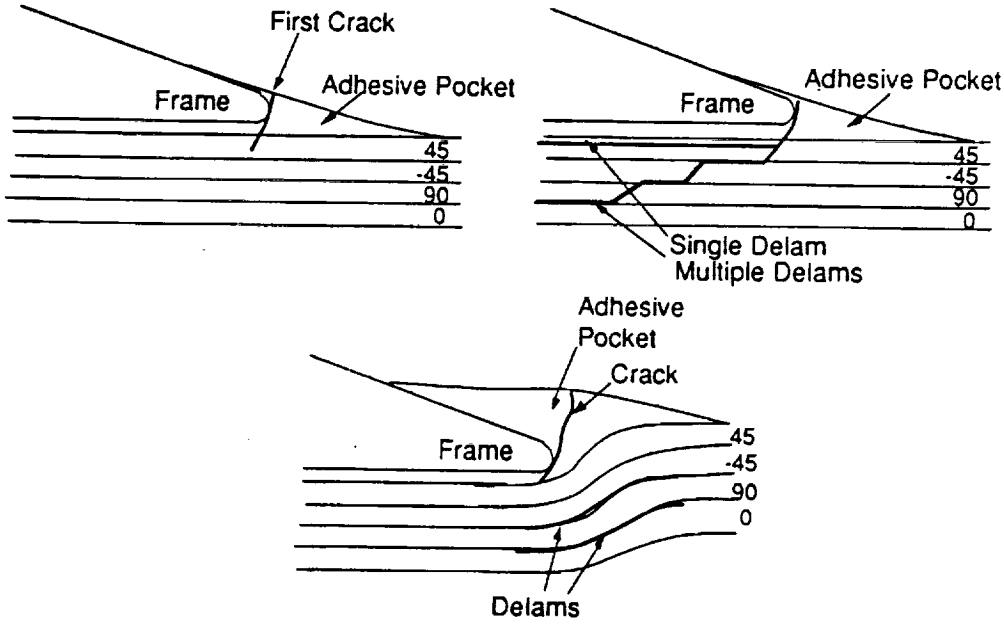


Figure 40: Illustration of Failure Sequence at the Frame Tip for Specimens Without (top) and With (bottom) Manufacturing Anomalies.

As the load increased for specimens with manufacturing anomalies, a delamination formed at various locations. In several cases, a single delamination propagated in the top 45° under the bondline. In other cases, the delamination jumped through transverse cracks at other ply interfaces down to the first 0° ply. However, the key point of these observations is that failure never propagates through the adhesive layer, but always in the skin material. This, in retrospect, makes sense as the fracture toughness of the adhesive is much higher than that of the skin material. After final failure and

separation of the frame and skin, numerous transverse cracks in the top two 45° plies were observed along with delamination.

For specimens with manufacturing anomalies, delaminations seemed to often appear deeper into the skin, sometimes before the crack in the adhesive pocket. Although not always easily visible, transverse cracks appeared to be present in the 45° plies. For specimens with the worst defects, fiber breakage in the top 0° ply was also observed.

Several simply supported specimens were tested with a very short moment arm to prevent failure at the frame tip, forcing failure to occur in the noodle area. For these specimens, the failure modes were similar to those shown in Figure 39b: delamination between braid layers in the frame fillet radius and/or a crack appearing in the noodle and propagating into the frame web as load is increased.

7.6 Detailed Failure Analysis

Some detailed finite element analysis was performed to predict the failure of frame pulloff test specimens. The computer simulation of tests was performed to mimic observed failure initiation. As described in the previous section, damage initiation was observed to occur in two major locations: the frame edge and in/around the noodle. Most of the detailed analysis studies performed to date simulated tests performed with the clamped frame pulloff fixture.

The finite element code VISOCRACK was employed for the simulation of the two types of failure modes identified in the tests listed in Table 11. VISOCRACK is a special purpose finite element code developed under an ATCAS subcontract during the first phase of the Drexel research program. It is capable of modeling a 3-D elastic/viscoelastic laminated composite medium with prescribed propagating crack(s). The code provides the stress/strain/displacement/energy fields as functions of loading history. For the case in which the medium is elastic, the code can provide the same fields as functions of the propagating crack(s).

For failure simulation, the exact lamination structure of the specimens is accounted for in the code, with the material of each lamina assumed elastic/anisotropic. Figure 41 shows the finite element model of the clamped test element under a fixed support (no lateral movement and rotation) condition. Similarly, the case of a partially free support (allowing lateral movement and rotation) has been investigated. However, none of the failure simulations performed to date modeled a specific simply supported test result.

Figure 42 shows the finite element mesh and the locations of three prescribed cracks (numbered 1, 2 and 3). The crack-tip strain-energy release rates in each simulated cracking case are calculated in terms of the applied load and the crack size; the Griffith criterion of fracture is then applied to predict the critical initiation load.

Table 12 shows the predicted critical load at the failure initiation of each clamped test case. Note that the critical load for each test case was calculated based on several assumed G_c values ranging from 87.6 to 350.2 J/m^2. The exact G_c values for the

materials in the various test elements were not available; but it is believed that their probable values are in the range of 175.1 to 350.2 J/m^2. Test observations on the initiation of failure are also shown in Table 12, indicating that the experimental results fall within predicted critical load ranges. Future efforts will attempt to predict damage growth.

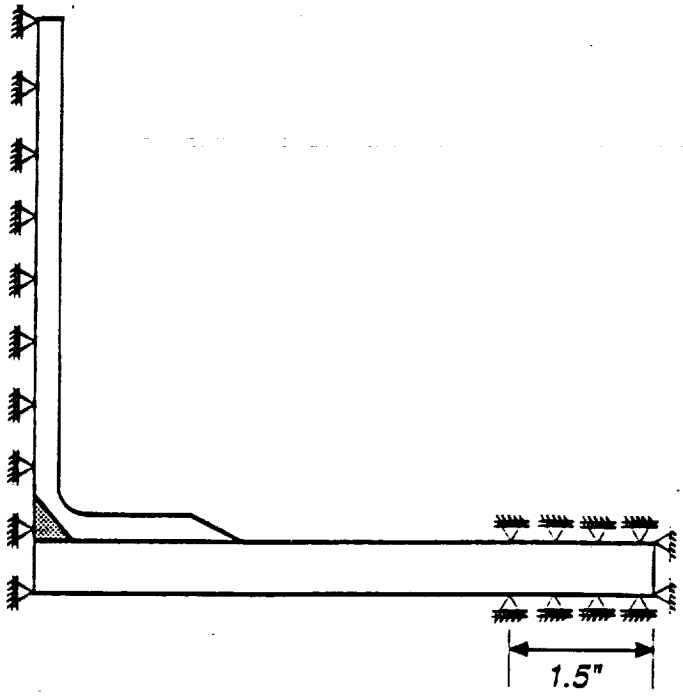


Figure 41: Schematic Showing the Fixed End Boundary Conditions Used in the Finite Element Model.

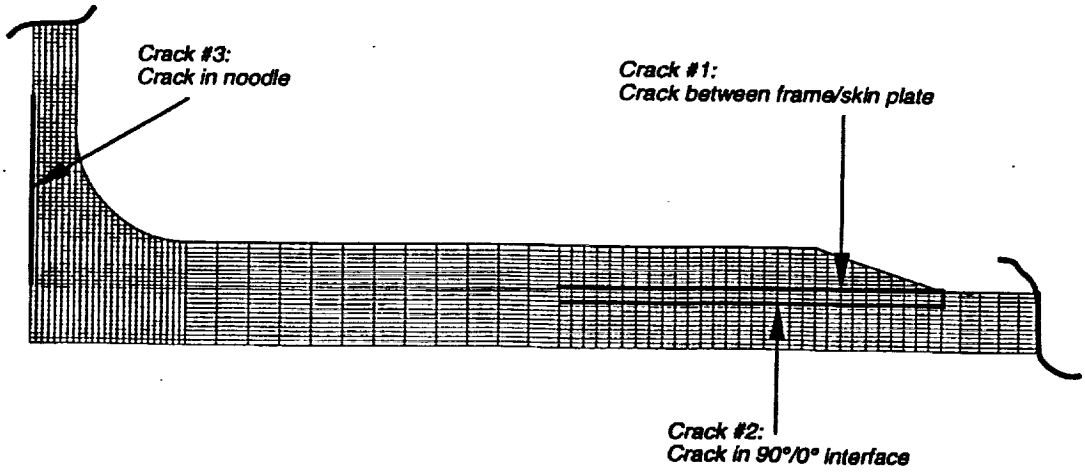


Figure 42: The Finite Element Mesh and Prescribed Crack Growth Lines.

SPECIMEN NO.	CRACK INITIATION LOAD [N (lbf)]	PREDICTED INITIATION LOAD [N (lbf)]			
		G_c=87.6 J/m^2	G_c=175.1 J/m^2	G_c=262.7 J/m^2	G_c=350.2 J/m^2
J-1	810 (182)	553.3 (124.4)	782.4 (175.9)	958.1 (215.4)	1106.2 (248.7)
J-3	503 (113)	553.3 (124.4)	782.4 (175.9)	958.1 (215.4)	1106.2 (248.7)
J-5[d]	729 (164)	553.3 (124.4)	782.4 (175.9)	958.1 (215.4)	1106.2 (248.7)
J-6[d]	667 (150)	553.3 (124.4)	782.4 (175.9)	958.1 (215.4)	1106.2 (248.7)
J-8[d]	778 (175)	553.3 (124.4)	782.4 (175.9)	958.1 (215.4)	1106.2 (248.7)
J-9	640 (144)	553.3 (124.4)	782.4 (175.9)	958.1 (215.4)	1106.2 (248.7)
J-11	689 (155)	553.3 (124.4)	782.4 (175.9)	958.1 (215.4)	1106.2 (248.7)
J-12	885 (199)	553.3 (124.4)	782.4 (175.9)	958.1 (215.4)	1106.2 (248.7)
J-13[d]	547 (123)	553.3 (124.4)	782.4 (175.9)	958.1 (215.4)	1106.2 (248.7)
J-14[d]	489 (110)	553.3 (124.4)	782.4 (175.9)	958.1 (215.4)	1106.2 (248.7)
J-16[d]	512 (115)	553.3 (124.4)	782.4 (175.9)	958.1 (215.4)	1106.2 (248.7)
K-1	867 (195)	553.3 (124.4)	782.4 (175.9)	958.1 (215.4)	1106.2 (248.7)
K-2	1169 (263)	553.3 (124.4)	782.4 (175.9)	958.1 (215.4)	1106.2 (248.7)
K-3	1108 (249)	553.3 (124.4)	782.4 (175.9)	958.1 (215.4)	1106.2 (248.7)
K-4	983 (221)	553.3 (124.4)	782.4 (175.9)	958.1 (215.4)	1106.2 (248.7)
K-1A	956 (215)	600.5 (135.0)	845.1 (190.0)	1,039.9 (233.8)	1201.0 (270.0)
K-2A	1054 (237)	600.5 (135.0)	845.1 (190.0)	1,039.9 (233.8)	1201.0 (270.0)
K-3A	992 (223)	553.3 (124.4)	782.4 (175.9)	958.1 (215.4)	1106.2 (248.7)
K-4A	987 (222)	553.3 (124.4)	782.4 (175.9)	958.1 (215.4)	1106.2 (248.7)
L-1[e]	1081 (243)	922.1 (207.3)	1303.7 (293.1)	1596.8 (359.0)	1843.7 (414.5)
L-2	721 (162)	553.3 (124.4)	782.4 (175.9)	958.1 (215.4)	1106.2 (248.7)
L-3	756 (170)	553.3 (124.4)	782.4 (175.9)	958.1 (215.4)	1106.2 (248.7)
M-A[e]	1472 (331)	922.1 (207.3)	1303.7 (293.1)	1596.8 (359.0)	1843.7 (414.5)
M-B[e]	1953 (439)	1000.8 (225.0)	1414.9 (318.1)	1732.9 (389.6)	2001.2 (449.9)
M-C[e]	1223 (275)	922.1 (207.3)	1303.7 (293.1)	1596.8 (359.0)	1843.7 (414.5)
M-D[e]	1721 (387)	922.1 (207.3)	1303.7 (293.1)	1596.8 (359.0)	1843.7 (414.5)
M-E[e]	1415 (318)	922.1 (207.3)	1303.7 (293.1)	1596.8 (359.0)	1843.7 (414.5)
M-F[e]	1544 (347)	922.1 (207.3)	1303.7 (293.1)	1596.8 (359.0)	1843.7 (414.5)

Table 12: Experimental and Predicted Crack Initiation Loads.

7.7 Preliminary Fatigue Testing

A limited number of fatigue tests were performed at Drexel in the simply supported frame pulloff fixture to develop the test method and observe failure mechanisms. Tests were performed at 80 and 95% of the crack initiation force observed in static tests. As was the case for static tests, fatigue crack initiation and growth was seen to occur unsymmetrically from both frame edges. After some growth, damage was also noted around the 'noodle'. Final failure occurred as one of the cracks starting from the edge became dominant and abruptly grew across the frame width. Figure 43 shows the fatigue crack extension curve for a specimen loaded at 95% of the static crack initiation load. Figure 44 shows the same result as a function of crack tip position.

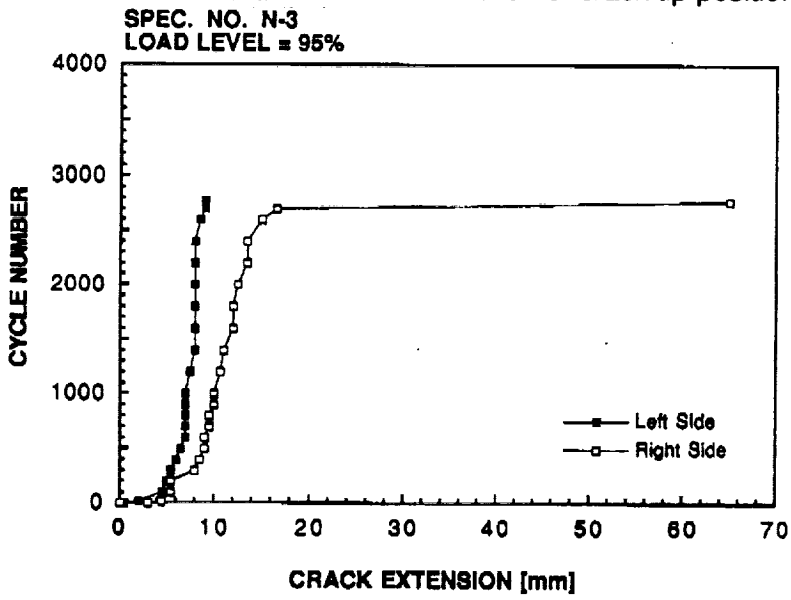


Figure 43: Crack Extension Curve from Initial Fatigue Tests.

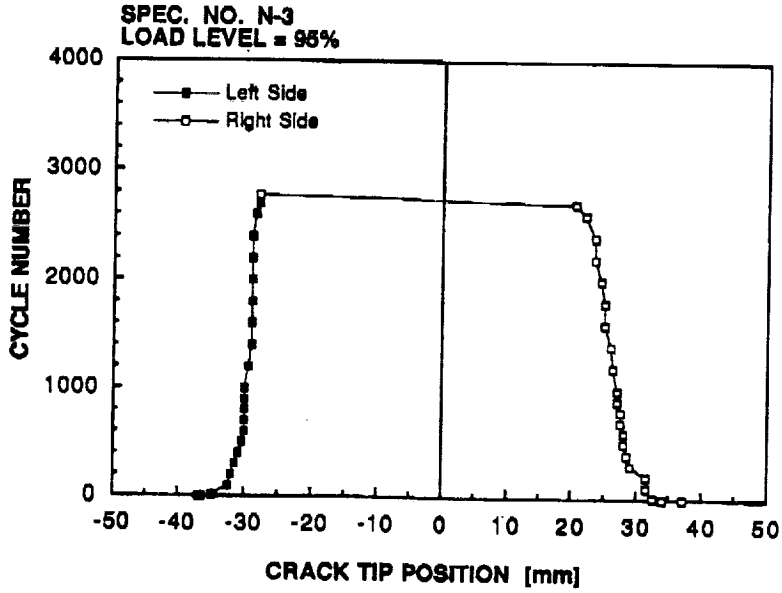


Figure 44: Crack Tip Position Curve from Initial Fatigue Tests.

7.8 Preliminary Mouseholed Frame Pulloff Tests

As mentioned earlier, the mousehole area is a critical location for frame pulloff loads and moments. The fixture shown in Figure 44 is designed to test the load transfer between hat-stiffener and frame. The stiffener is attached at both ends to the base of the test machine, while the frame web is loaded vertically through a clevis arrangement. This setup forces the shear load in the stiffener to pass through the critical skin area into the frame.

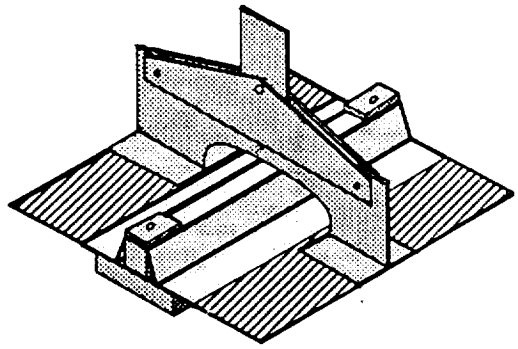


Figure 45: Frame Pulloff Test Fixture for the Mousehole Area.

Unlike the previous test, the target load level to be achieved by the specimen shown in Figure 44 has to be determined through analysis. Two methods of determining that load level were used. In the first one, the load being transferred between frame and stiffener in the test specimen matches that in the actual panel. Using a free-body diagram of the stiffener section located inside the mousehole area, the total load is equal to the sum of the shear forces in the stiffener vertical sides and of the pressure load over the area of the stiffener. Using the results of the FE model of the panel under internal pressure, the sum of the shear flows contributes 473 lb., and the pressure load adds 302 lb., for a total reaction of 775 lb. Another method to calculate the load is to determine the applied force that will match the peak bending moment in the skin between frame and stiffener. Using the same FE model as discussed earlier (see subsection on global pressure pillowing analysis of the crown design) with new boundary conditions to represent the test specimen, a load of approximately 1100 lb. was found to give the same maximum moment as shown in Figure 46. Therefore, it appears that the two methods provide an upper and lower bound on the target load to be reached during testing.

Load versus displacement data was recorded during the test and a typical plot is shown in Figure 47. Some specimens were also instrumented with strain gages at various locations in the mouseholed region. Three of these gages were located on the outside of the skin opposite to the gap between the frame and stiffener, with gage 1 on the centerline opposite to the frame web, and gages 2 and 5 located 1.4 in. and 1.5 in. away. The output of these gages is shown in Figure 48. Because of the location of gage 1, its output is very sensitive to failure initiation, allowing the onset of damage load level to be determined very precisely.

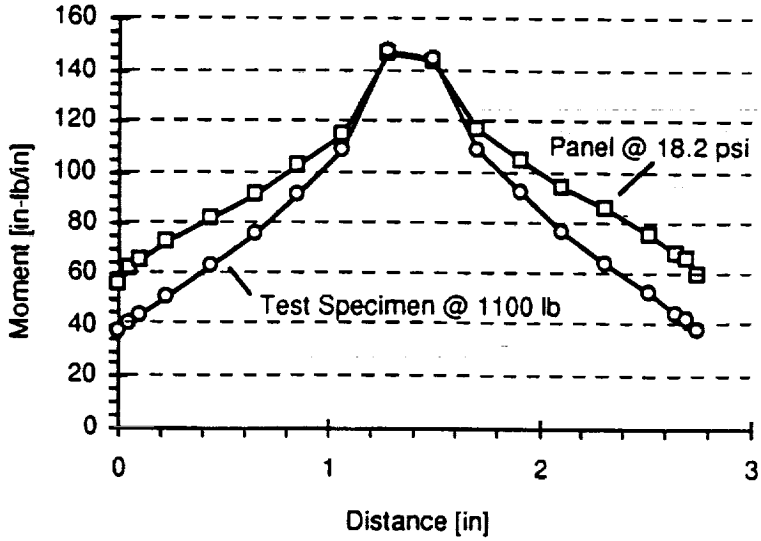


Figure 46: Comparison Between Skin Bending Moment in the Gap Between Frame and Stiffener for Pressurized Panel and Test Specimen.

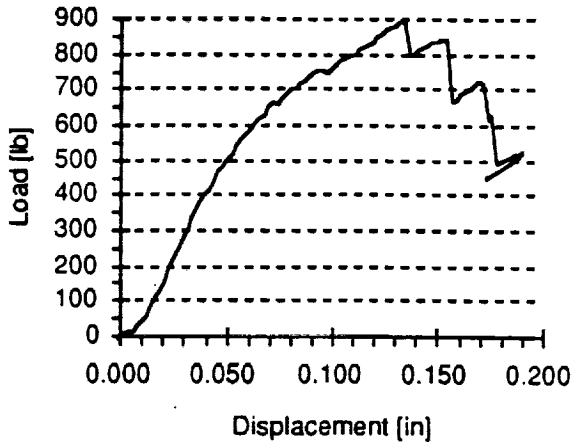


Figure 47: Typical Load-Displacement Curve from Mousehole Pull-off Test.

During several of these tests, loading was stopped after the initiation of damage for inspection. An opaque dye was injected under the frame and X-ray photographs were taken. A semi-elliptical delamination was observed under the frame web next to the stiffener and apparently originated at the interface between the noodle and the skin. When loading was resumed, the delamination spread to the width of the frame flange and then progressed in the hoop direction. Surface cracks were also observed near the mousehole in the resin-rich area located in the frame flange-to-web radius. This can also be seen in the strain gage output in Figure 48 where gages 2 and 5 indicate local failure in succession at increasing load level. This progressive failure also translates into a gradual softening of the load versus displacement behavior shown in Figure 47.

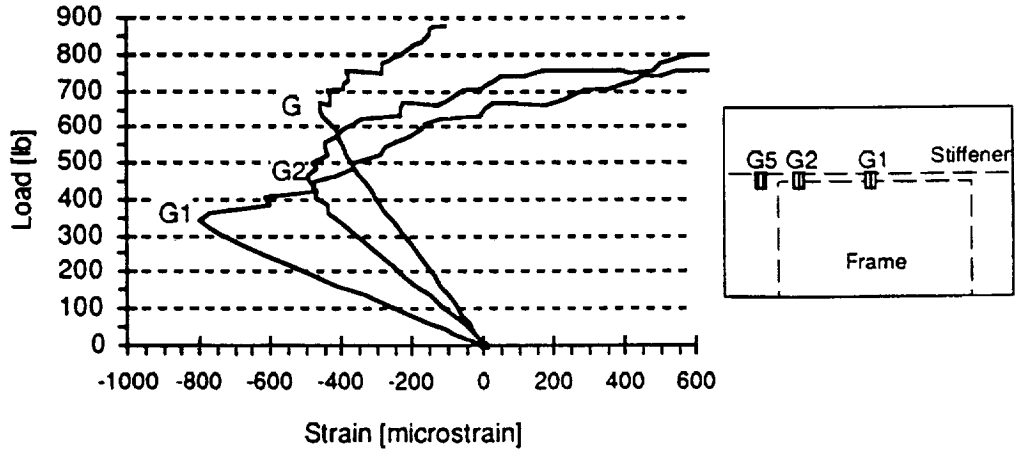


Figure 48: Typical Strain Gage Data from Mousehole Pull-off Test.

Three groups of three specimens each were tested. The first two groups were built with a thin 13 ply skin and the third one with a thicker 17 ply skin. The second group of specimens sustained a 5 ft.-lb. impact on the outside skin opposite to the gap between frame and stiffener. Although no visible damage was present, ultrasonic inspection indicated that some delamination was present.

Results from the tests are summarized in Figure 49 where two load values are reported for each specimen, one corresponding to the onset of damage and one to the maximum load. The average failure load of the thin skin specimens was 700 lb. As in the previous tests, the thick skin specimens performed better with an average failure load of 874 lb., although the increase in strength was not as pronounced. With impact damage present, the average failure load was 624 lb., a fairly small reduction considering the scatter in the data.

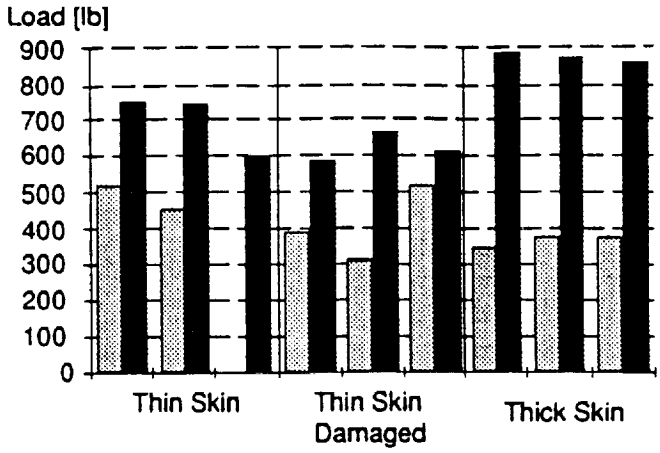


Figure 49: Failure Initiation and Ultimate Load Test Results for Mousehole Area Frame Pulloff.

Based on the load requirement determined from the analysis, thin skin specimens do not appear to meet ultimate load requirements. Thick skin specimens may pass the lower bound of the requirement, but, in both cases, damage initiation occurs well below limit load, which is usually not acceptable. However, a more refined three-dimensional finite element model of both the panel and the test specimen may be necessary to determine the exact stress distribution in that area and perform a better comparison between the two configurations.

8.0 Conclusions and Recommendations

Benchmark Panel Fabrication. The successful fabrication of the five benchmark panels demonstrated the producibility of the ATCAS crown panel design. The range of design variables included in these panels further demonstrated the robust nature of the fabrication process selected. Test of these panels will provide critical data for further crown design refinement. The specific test plans for these panels should, and are intended to be, modified as additional knowledge is gained.

Benchmark Panel Finite Element Analysis. Comparisons of experimental results with models similar to those developed under this task indicate the ability, with proper attention to detail, to model the response of complex test configurations. Additional refinement of the pressure-box load introduction hardware is required to improve correlation with actual panel response. This includes identification and quantification of the critical load-introduction parameters.

Numerical difficulties encountered in geometrically nonlinear analyses of high-axial load conditions may indicate the presence of a snap-through or other unstable phenomenon. Tests of such panels should be carefully monitored to understand the physical implications of such predicted response.

Models are required for each of the test panels that include appropriate damage states. Consideration of predicting damage progression is also required. The ability to predict damage growth and final structural collapse of the test panels provides a measure of current capabilities and direction for future developments.

Further efforts are required to understand the relationship between panel response in the pressure-box test fixture and in the full fuselage shell. Full-shell models that provide sufficient detail in the region of interest are likely to be prohibitively costly, forcing one of several global-local approaches to be adopted. Successful implementation of this capability, however, will provide the ability to properly interpret damage growth and residual strength test results.

Strain Softening Model Development. Strain softening models continue to appear attractive for extending small test results to larger, configured structure, due to its ability to predict tension fracture strengths for a wide range of materials, notch sizes, and specimen geometries. The success of this method stems from its physical basis and its consideration of the interaction between damage accumulation and specimen size.

Maximum stress levels and initial unloading portions of strain softening material laws control small-notch strengths for specimen sizes typically used in composites evaluation. The energy associated with the rest of the strain softening curve is most important to large-notch strengths, due to larger notch tip damage zones allowed by larger specimen widths. Numerical analyses of specimen geometries should be conducted to develop methods for characterizing strain softening laws for specific materials using the minimum number of tests. Such methodology has been

demonstrated for other materials, but must be extended to the anisotropic regime of composite materials.

Development of interaction bending laws are required to extend strain softening into the structural domain. Efforts are also required to determine and overcome computational difficulties encountered in modeling such laws in complex structure.

Frame/Skin Bondline Analysis and Test. Test results indicate that the skin bending moment at the tip of the frame was the most important load resultant, not the pull-off load as is typically reported. Results from clamped-fixture tests indicated that the type of 'noodle' material used at the end of the frame web, adhesive or braided inserts, had little effect on failure. The static and fatigue strength of the skin/frame bondline away from the mousehole regions appears adequate. However, the static strength in the mousehole region does not appear sufficient, although further analysis and test instrumentation is require to confirm this.

Future efforts are needed to evaluate frame bond integrity for the ATCAS baseline design. Detailed analysis of experimental failure modes occurring with the simply supported test fixture would provide a basis for validation of fracture mechanics methodology. Additional long term durability tests are needed to quantify the effects of load frequency, environment, and initial damage conditions. The benchmark panels should be instrumented to provide accurate test measurements of local load transfer. These results should be used to verify the mousehole modeling scheme and, if necessary, modify the design of the single mousehole element test fixture to better simulate pressure loads. Some mousehole design refinement may also be needed to ensure that the crown design has adequate margins of safety.

9.0 References

1. Ilcewicz, L. B., Smith, P. J., and Horton, R. E., "Advanced Composite Fuselage Technology", *Third NASA Advanced Composite Technology Conference*, NASA CP 3178, pp. 97-156, 1992.
2. Ilcewicz, L. B., Smith, P. J., Walker, T. H., and Johnson, R. W., "Advanced Technology Composite Fuselage Structure," *First NASA Advanced Composite Technology Conference*, NASA CP-3104, Part 1, pp. 127-155, 1991.
3. Olson, J. T., Smith, P. J., and Ilcewicz, L. B., "Advanced Composite Fuselage Technology," To be published in the *Proceedings of the Tenth DoD/NASA/FAA Conference on Fibrous Composites in Structural Design*, 1993.
4. Swanson, G.D., Ilcewicz, L.B., Walker, T.H., Graesser, D., Tuttle, M., and Zabinsky, Z., "Local Design Optimization for Composite Transport Fuselage Crown Panels," *Second NASA Advanced Technology Conference*, NASA CP-3154, pp. 243-262, 1991.
5. Smith, P.J., Bodine, J.B., Preuss, C.H., and Koch, W.J., "Design, Analysis, and fabrication of a Pressure Box Test Fixture for Tension Damage Tolerance testing of Curved Fuselage panels," *Third NASA Advanced Technology Conference*, NASA CP-3178, pp. 789-806, 1992.
6. Walker, T.H., Ilcewicz, L.B., Polland, D.R., Bodine, J.B., and Poe, C.C., Jr., "Tension Fracture of Laminates for Transport Fuselage - Part 3: Structural Configurations," *Fourth NASA/DoD Advanced Technology Conference,* NASA CP-3229, 1993.
7. Walker, T.H., Avery, W.B., Ilcewicz, L.B., Poe, C.C., Jr., & Harris, C.E., "Tension Fracture of Laminates for Transport Fuselage - Part 1: Material Screening," *Second NASA Advanced Technology Conference*, NASA CP-3154, pp. 197-238, 1991.
8. Walker, T.H., Ilcewicz, L.B., Polland, D.R., and Poe, C.C., Jr., "Tension Fracture of Laminates for Transport Fuselage - Part 2: Large Notches," *Third NASA Advanced Technology Conference*, NASA CP-3178, pp. 727-758, 1992.
9. Cairns, D.S., Ilcewicz, L.B., Walker, T.H., and Minguet, P.J., "The Consequence of Material Inhomogeneity on Fracture of Automated Tow Placed Structures With Stress Concentrations," *Fourth NASA/DoD Advanced Technology Conference,* NASA CP-3229, 1993.
10. Shahid, I., "Progressive Failure Analysis of Laminated Composites Subjected to In-Plane Tensile and Shear Loads," PhD Dissertation (performed under direction of F.K. Chang, ATCAS Subcontract No. TZ-633037-0A57N), Stanford Univ., 1993.
11. Bazant, Z.P., and Cedolin, L., *Stability of Structures: Elastic, Inelastic, Fracture, and Damage Theories*, Oxford University press, Inc., New York, 1991.
12. Aronsson, C.G., and Backlund, J., "Tension Fracture of Laminates With Cracks," *J. Composite Materials*, Vol. 20, pp. 287-307, 1986.

13. Llorca, J., and Elices, M., "A Cohesive Crack Model to Study the Fracture Behavior of Fiber-Reinforced Brittle-Matrix Composites," *Int. J. of Fracture*, Vol. 54, pp. 251-267, 1992.

14. Sutcliffe, M.P.F., and Fleck, N.A., "Effect of Geometry On Compressive Failure of Notched Composites," *Int. J. of Fracture*, Vol. 59, pp. 115-132, 1993.

15. Awerbuch, J., and Madhukar, M.S., "Notched Strength of Composite Laminates: Predictions and Experiments -- A Review," *J. of Reinforced Plastics and Composites*, Vol. 4, pp. 1-159, 1985.

16. Avery, S.S., *Fracture of Graphite/Polymer Composite Panels With Large Center Cracks,* M.S. Thesis (J. Chaudhuri, advisor) Witchita State University, 1988.

17. Mak, Y.P., *Strain Rate Effects On tensile fracture and Damage Tolerance of Composite Laminates,* M.S. Thesis (performed under direction of H.L. McManus and P.A. Lagace, ATCAS Subcontract No. FZ-282568-0755N), MIT, 1992.

18. Dost, E.F., Avery, W.B., Finn, S.R., Ilcewicz, L.B., Scholz, D.B., and Wishart, R.E., "Impact Damage Resistance of Composite Fuselage Structure, Part 3," *Fourth NASA/DoD Advanced Technology Conference,* NASA CP-3229, 1993.

19. Ilcewicz, L.B., Walker, T.H., Willden, K.S., Swanson, G.D., Truslove, G., Metschan, S.L., and Pfahl, C.L., "Application of a Design-Build-Team Approach to low Cost and Weight Composite Fuselage Structure," NASA CR-4418, December, 1991.

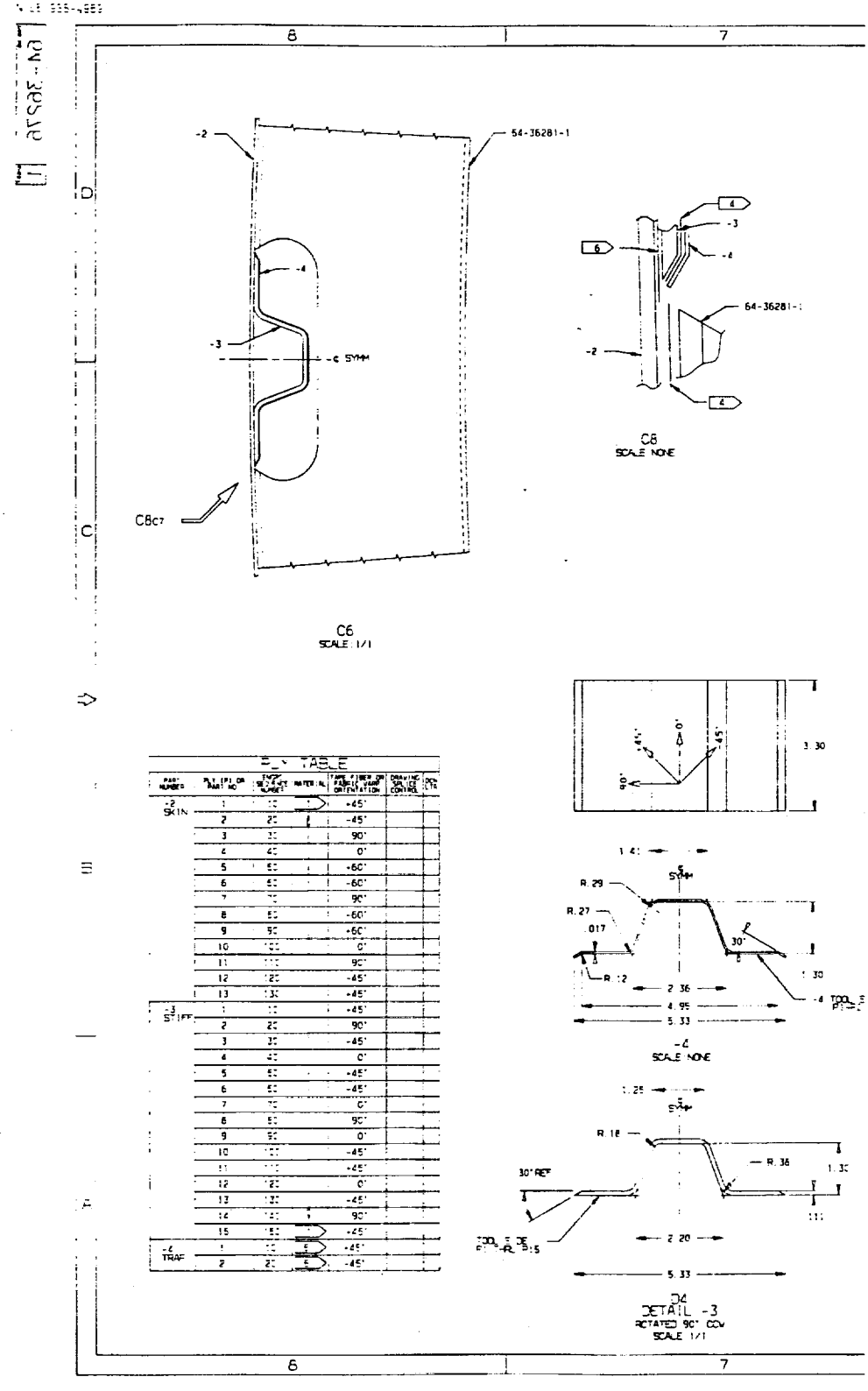
20. Swanson, G.D., Ilcewicz, L.B., Walker, T.H., Graesser, D.L., Tuttle, M.E., and Zabinsky, Z.B., "Local Design optimization for Composite Transport Fuselage Crown Panels," Second NASA Advanced Composite Technology Conference, NASA CP-3154, 1991, pp. 243-262.

21. Menguet, P.J., Fedro, M., O'Brien, T.K., Martin, R., Ilcewicz, L., Awerbuch, J., and Wang, A., "Development of a Structural Test Simulating Pressure Pillowing Effects in a Bonded Skin/Stringer/Frame Configuration," Fourth NASA Advanced Composite Technology Conference, NASA CP-3229, 1993.

22. Deaton, J.W., Kullerd, S.M., Madan, R.C., and Chen, V.L., "Test and Analysis Results for Composite Transport Fuselage and Wing Structures," Second NASA Advanced Composite Technology Conference, NASA CP-3154, 1991, pp. 169-193.

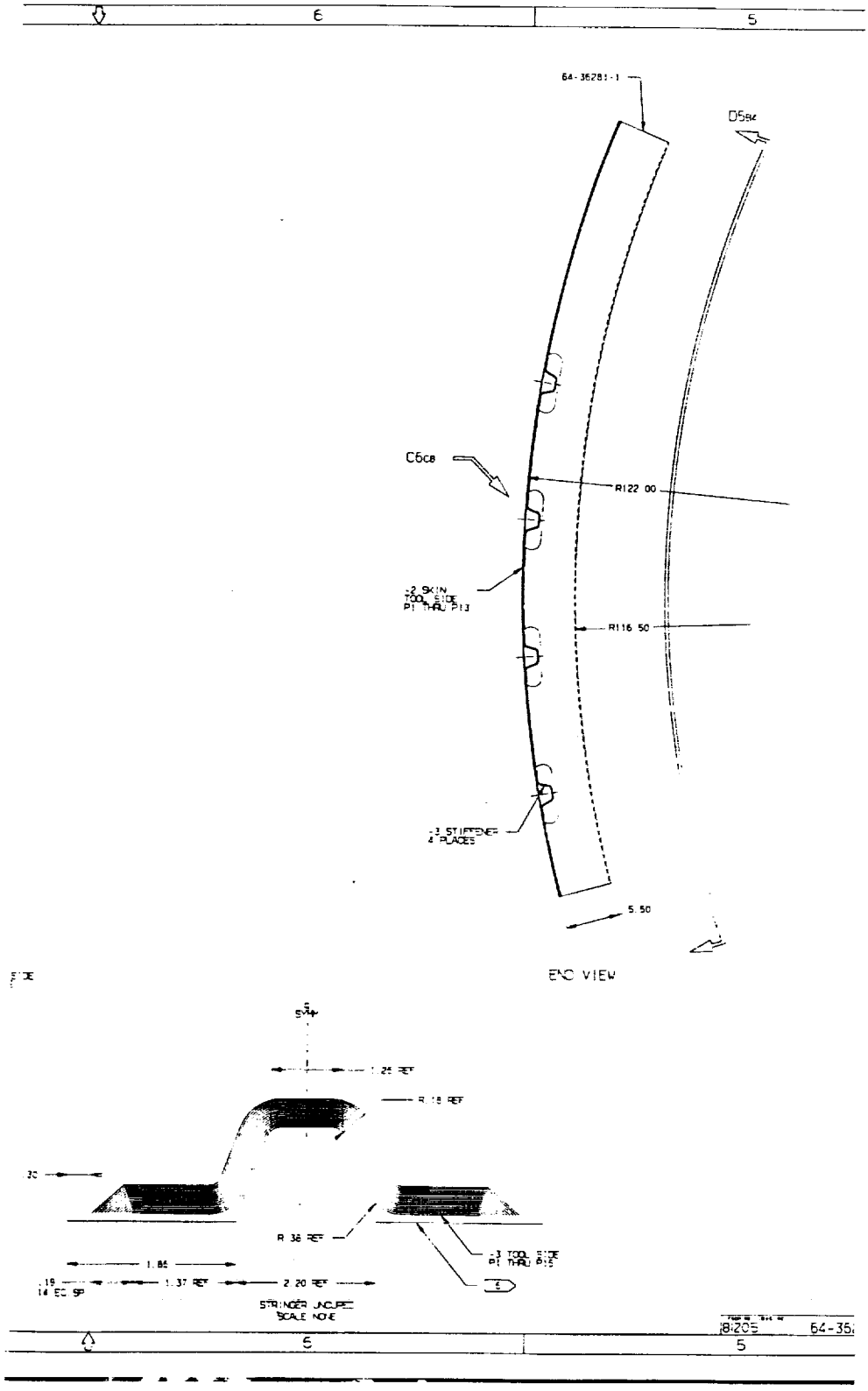
Appendix A

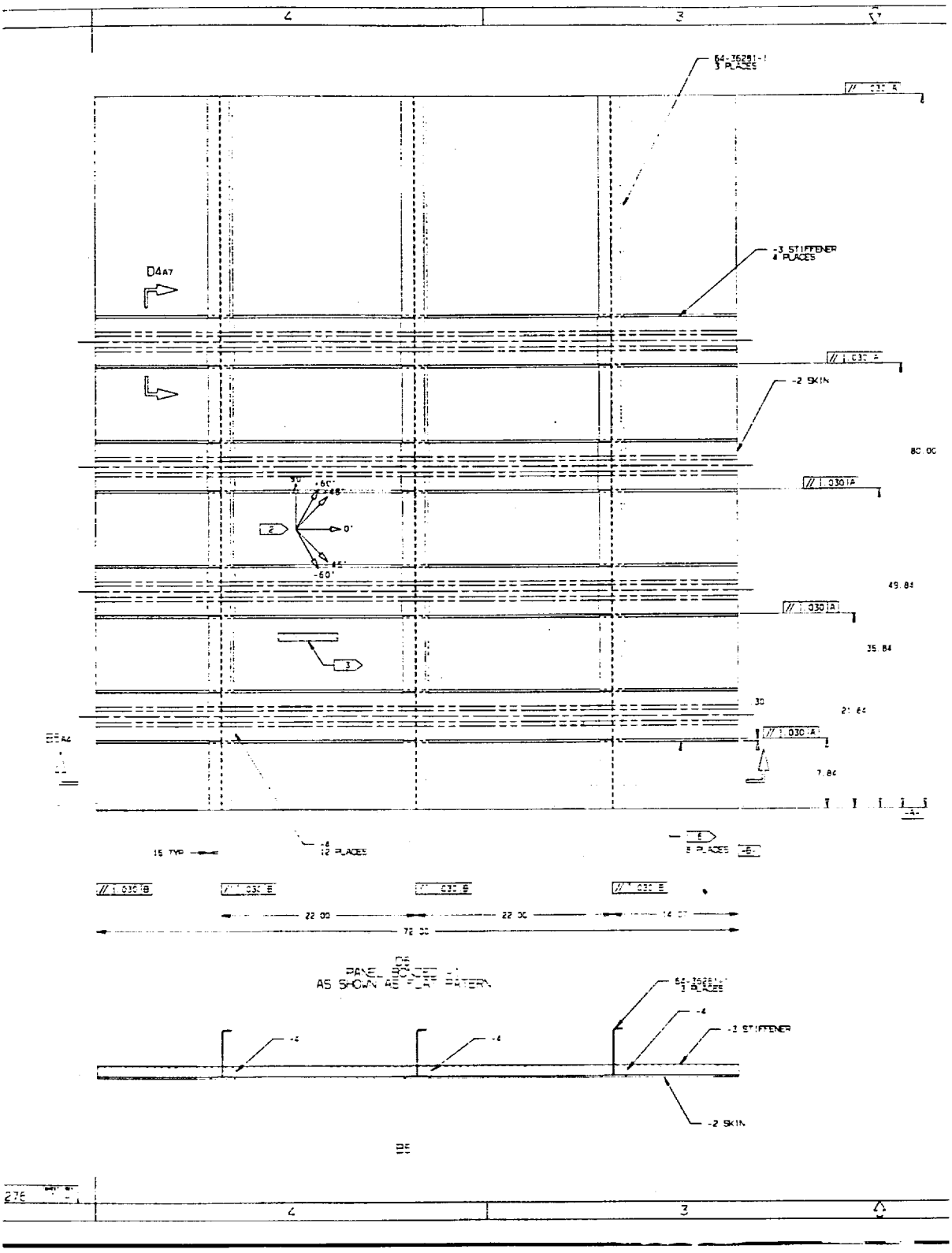
Panel Bond, Cutting Diagram, and Panel Assembly Drawings for Panel 1

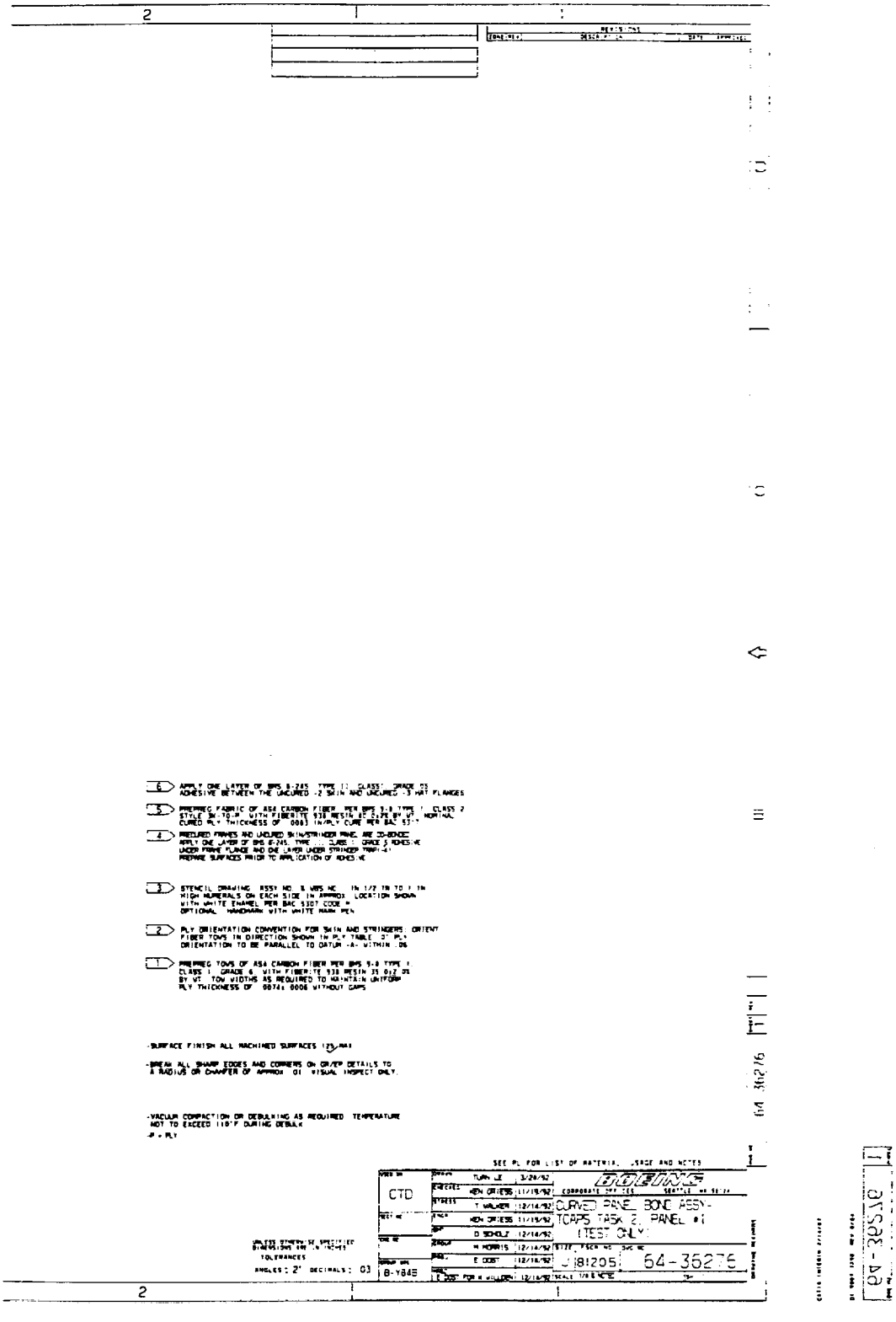


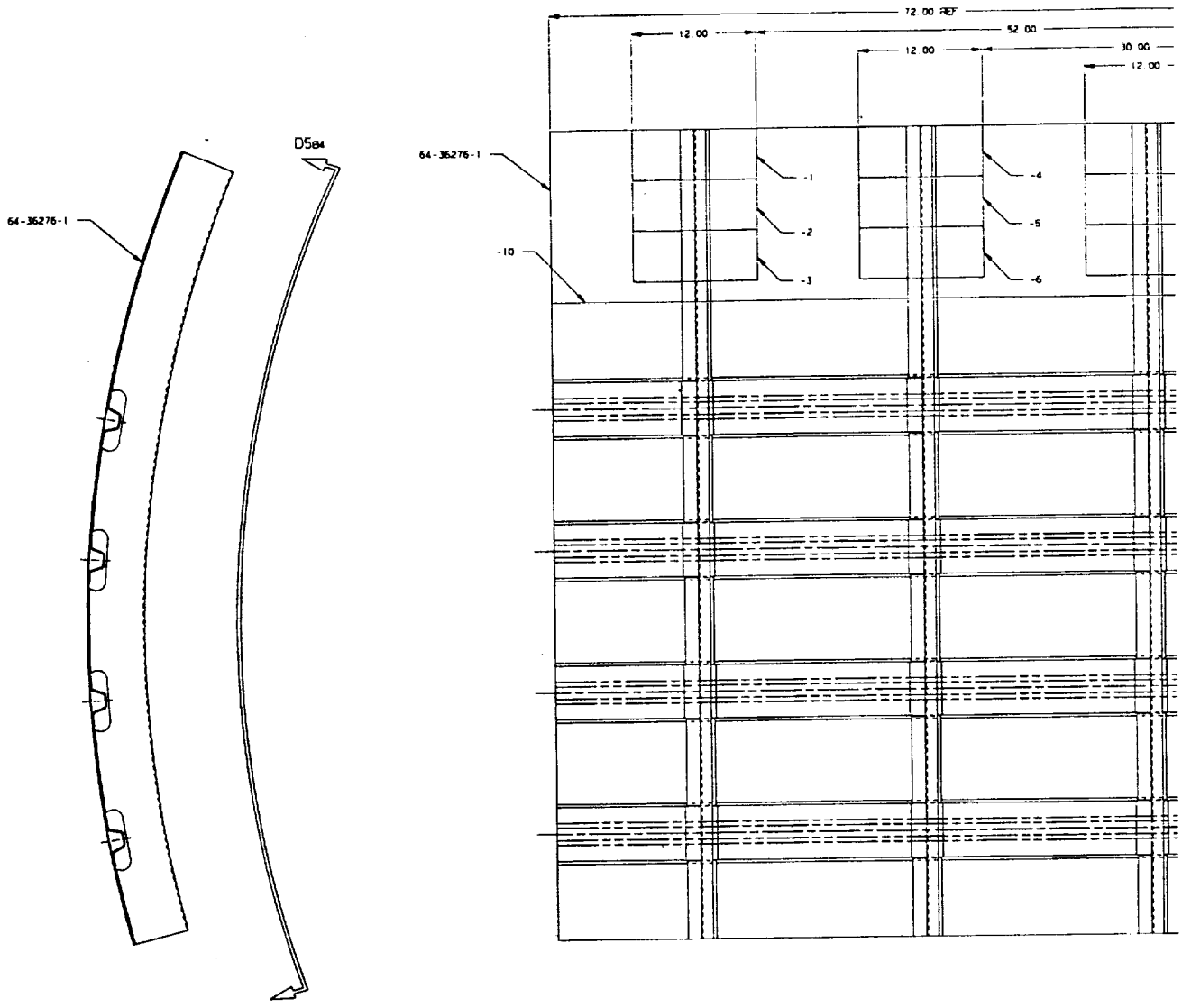
PLY TABLE

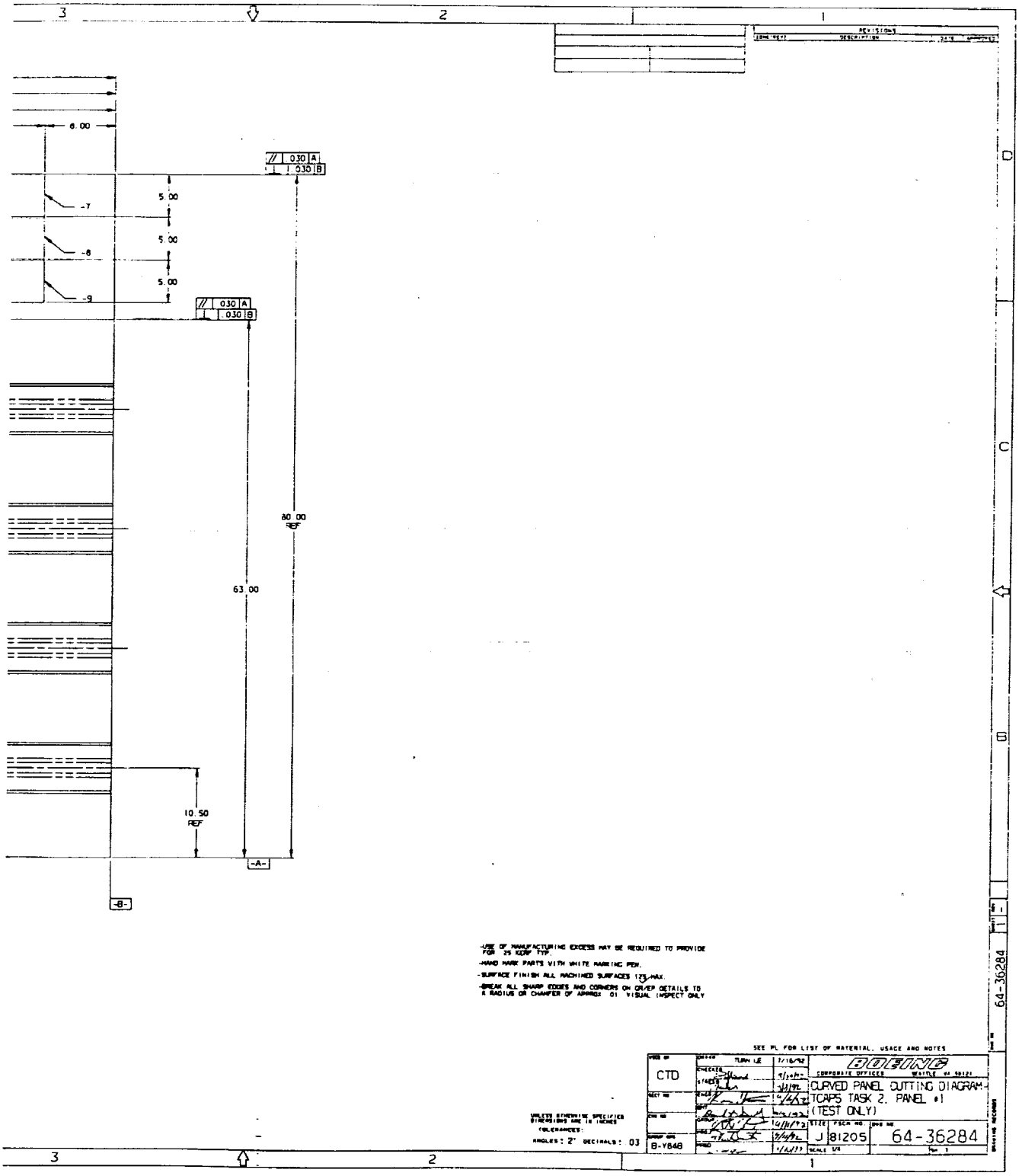
PART NUMBER	PLY ITEM OR PART NO	ENTITY NUMBER	MATERIAL	FIBER OR FABRIC ORIENTATION	DRAWING SOURCE CONTROL	QTY
-2 SKIN	1	1		+45°		
	2	2		-45°		
	3	3		90°		
	4	4		0°		
	5	5		+60°		
	6	6		-60°		
	7	7		90°		
	8	8		-60°		
	9	9		+60°		
	10	10		0°		
	11	11		90°		
	12	12		-45°		
	13	13		+45°		
-3 STIFF	1	1		+45°		
	2	2		90°		
	3	3		-45°		
	4	4		0°		
	5	5		+45°		
	6	6		-45°		
	7	7		0°		
	8	8		90°		
	9	9		0°		
	10	10		-45°		
	11	11		+45°		
	12	12		0°		
	13	13		-45°		
	14	14		90°		
	15	15		+45°		
-4 TRAP	1	1		+45°		
	2	2		-45°		

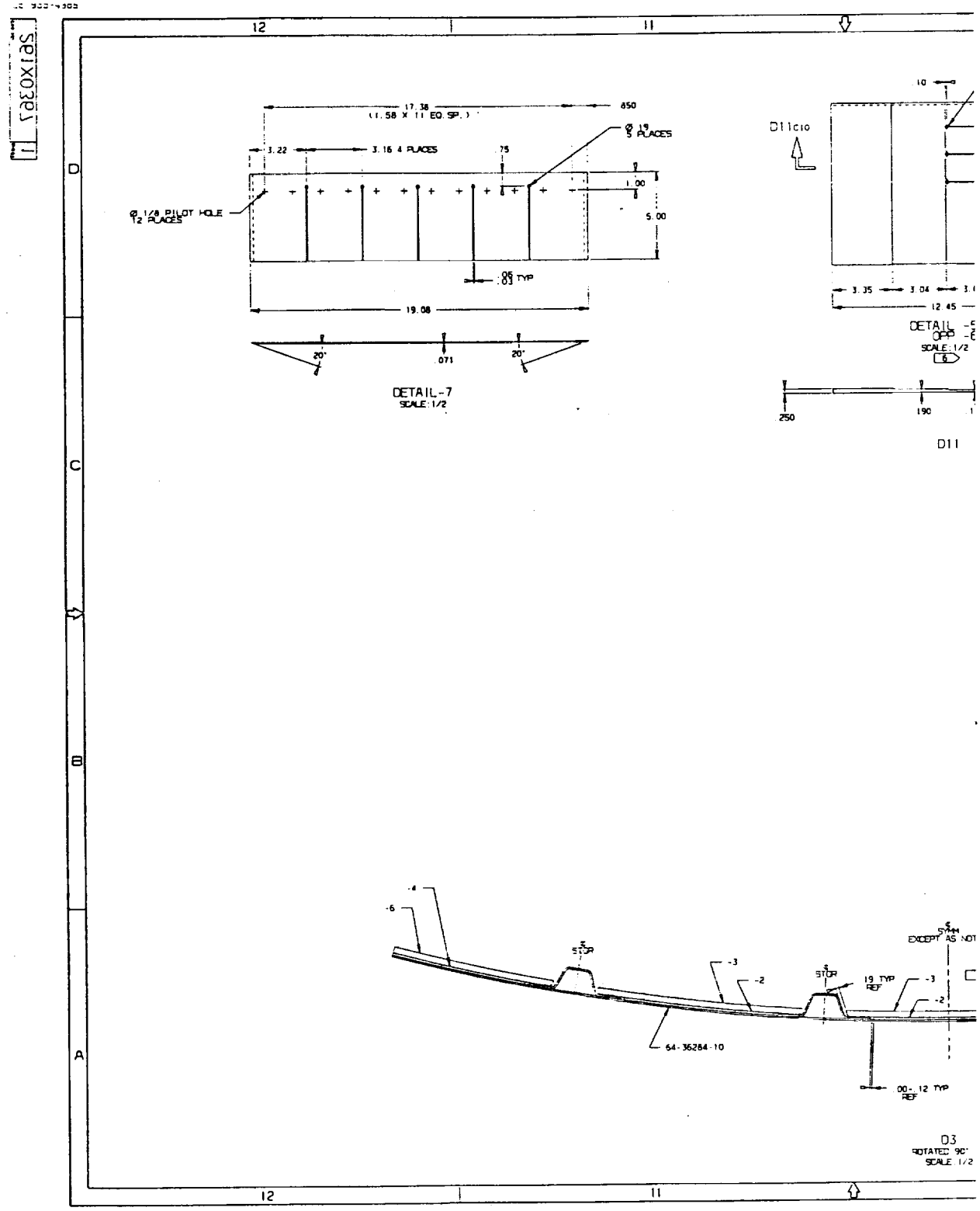

6
5
64-36281-1
D5B4
C6C8
R122 00
-2 SKIN
TOOL SIDE
PT THRU P13
R116 50
-3 STIFFENER
4 PLACES
5.50
END VIEW
1.25 REF
R .18 REF
.30
R .38 REF
-3 TOOL SIDE
PT THRU P15
1.84
.19
14 EQ SP
1.37 REF
2.20 REF
STRINGER JACKPEC
SCALE NONE
8:20S
64-35
6
5

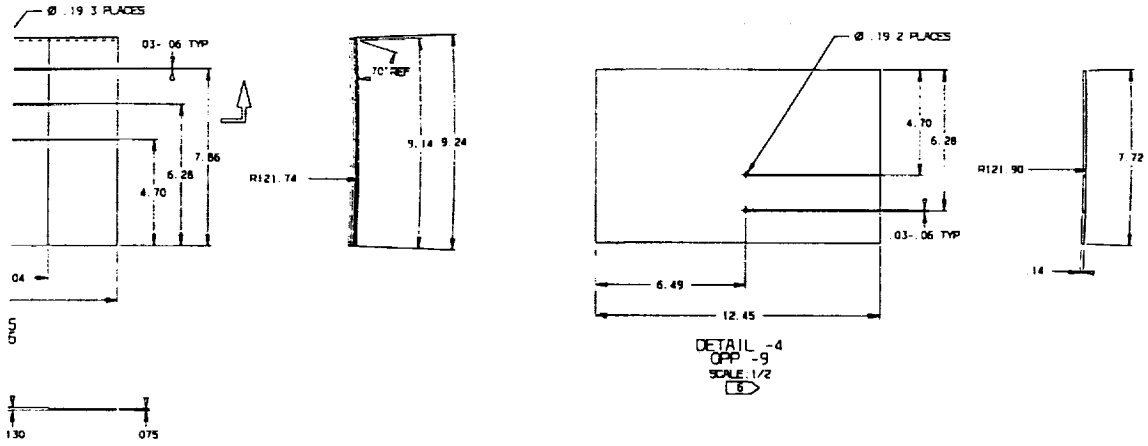

-3 STIFFENER
4 PLACES
-2 SKIN
80.00
49.84
35.84
21.84
7.84
22.00
22.00
72.00
-3 STIFFENER
-2 SKIN

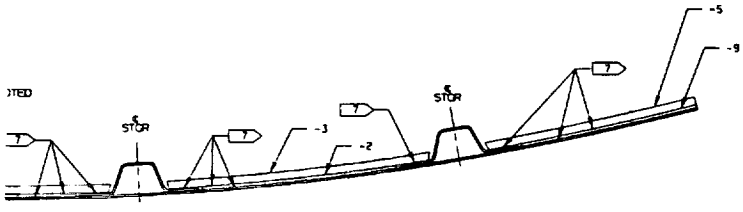

6 APPLY ONE LAYER OF BMS 8-245 TYPE II CLASS I GRADE 05 ADHESIVE BETWEEN THE UNCURED -2 SKIN AND UNCURED -3 HAT FLANGES
5 PREPREG FABRIC OF AS4 CARBON FIBER PER BMS 9-8 TYPE I CLASS 2 STYLE 3K-70-P WITH FIBERITE 938 RESIN AT 35 PCT BY WT NOMINAL CURED PLY THICKNESS OF .0013 IN/PLY CURE PER BAC 5717
4 PRECURED FRAMES AND UNCURED SKIN/STRINGER PANEL ARE CO-BONDED APPLY ONE LAYER OF BMS 8-245 TYPE II CLASS I GRADE 5 ADHESIVE UNDER FRAME FLANGE AND ONE LAYER UNDER STRINGER RUNOUTS PREPARE SURFACES PRIOR TO APPLICATION OF ADHESIVE
3 STENCIL DRAWING ASSY NO & WBS NO IN 1/2 IN TO 1 IN HIGH NUMERALS ON EACH SIDE IN APPROX LOCATION SHOWN WITH WHITE ENAMEL PER BAC 5307 CODE M OPTIONAL HANDMARK WITH WHITE MARK PEN
2 PLY ORIENTATION CONVENTION FOR SKIN AND STRINGERS ORIENT FIBER TOWS IN DIRECTION SHOWN IN PLY TABLE 0° PLY ORIENTATION TO BE PARALLEL TO DATUM -A- WITHIN .06
1 PREPREG TOWS OF AS4 CARBON FIBER PER BMS 9-8 TYPE I CLASS 1 GRADE 6 WITH FIBERITE 938 RESIN 35 0±2 05 BY WT TOW WIDTHS AS REQUIRED TO MAINTAIN UNIFORM PLY THICKNESS OF .0074±.0008 WITHOUT GAPS
-SURFACE FINISH ALL MACHINED SURFACES 125
-BREAK ALL SHARP EDGES AND CORNERS ON DRAWING DETAILS TO A RADIUS OR CHAMFER OF APPROX .01 VISUAL INSPECT ONLY.
-VACUUM COMPACTION OR DEBULKING AS REQUIRED TEMPERATURE NOT TO EXCEED 110°F DURING DEBULK
P = PLY
SEE PL FOR LIST OF MATERIAL, STAGE AND NOTES
CTD
TURN IN 3/20/92
DRAWN HEN GRIESS 11/19/92
CHECKED T WALKER 12/14/92
ENGR HEN GRIESS 11/15/92
QA D SCHOLZ 12/14/92
GROUP M MORRIS 12/14/92
PROJ E COST 12/16/92
LE DOC FOR M WILSON 12/16/92
BOEING
CORPORATE PAT DEV SEATTLE WA 98124
CURVED PANE BOND ASSY-
TCAPS TASK 2 PANEL #1
(TEST ONLY)
SIZE FSCM NO DWG NO
J 81205 54-35276
SCALE 1/8 WEIGHT SHEET
8-9848
UNLESS OTHERWISE SPECIFIED DIMENSIONS ARE IN INCHES
TOLERANCES
ANGLES ± 2° DECIMALS .03
54-35276
54-35276

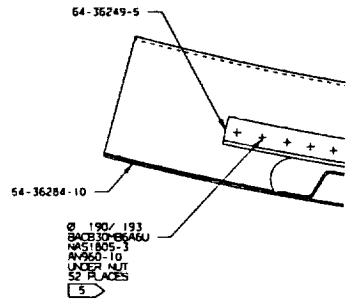

5
4
72.00 REF
12.00
52.00
12.00
30.00
12.00
D5B4
64-36276-1
64-36276-1
-10
-1
-2
-3
-4
-5
-6
END VIEW
D5
SKIN AS SHOWN AS FLATPATERN
DIMENSION MEASURE ON
OUTSIDE MOLD LINE
81205
64-36284
1
-
5
4


6.00
.030 A
.030 B
5.00
5.00
5.00
-7
-8
-9
80.00 REF
63.00
10.50 REF
-A-
-B-
-USE OF MANUFACTURING EXCESS MAY BE REQUIRED TO PROVIDE FOR 25 KSIF TYP.
-HAND MARK PARTS WITH WHITE MARKING PEN.
-SURFACE FINISH ALL MACHINED SURFACES 125 MAX.
-BREAK ALL SHARP EDGES AND CORNERS ON OR/EP DETAILS TO A RADIUS OR CHAMFER OF APPROX .01 VISUAL INSPECT ONLY
SEE PL FOR LIST OF MATERIAL, USAGE AND NOTES
UNLESS OTHERWISE SPECIFIED DIMENSIONS ARE IN INCHES
TOLERANCES:
ANGLES: 2° DECIMALS: .03
CTD
B-Y848
TURN UE
BOEING
CURVED PANEL CUTTING DIAGRAM
TCAPS TASK 2, PANEL #1
(TEST ONLY)
J 81205
64-36284
64-36284


12
11
D
C
B
A
17.38
(11.58 X 11 EQ. SP.)
650
Ø .19
5 PLACES
3.22
3.16 4 PLACES
75
1.00
5.00
Ø.128 PILOT HOLE
12 PLACES
.06
.03 TYP
19.08
20°
.071
20°
DETAIL-7
SCALE: 1/2
D11c10
10
3.35
3.04
12.45
DETAIL
SCALE: 1/2
250
190
D11
-4
-6
STOP
-3
-2
STOP
19 TYP
REF
-3
-2
64-36284-10
.00 .12 TYP
REF
SYMM
EXCEPT AS NOT
D3
ROTATED 90°
SCALE 1/2

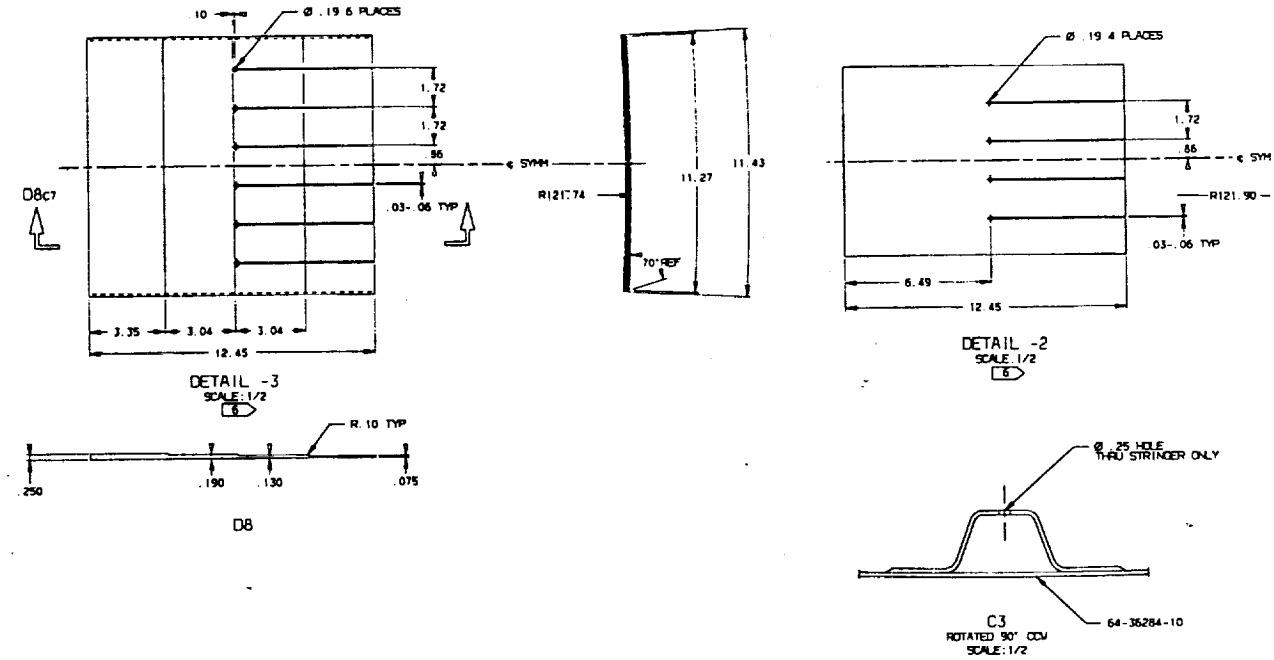


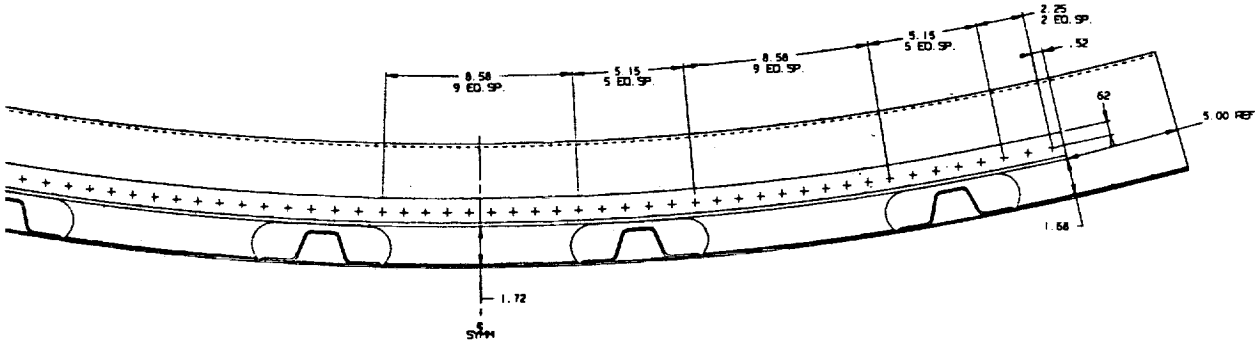




BOEING PROPRIETARY
THE INFORMATION CONTAINED HEREIN IS PROPRIETARY TO THE BOEING COMPANY AND SHALL NOT BE REPRODUCED OR DISCLOSED IN WHOLE OR IN PART OR USED FOR ANY PURPOSE EXCEPT WHEN SUCH USER POSSESSES DIRECT WRITTEN AUTHORIZATION FROM THE BOEING COMPANY

81205 261X0367 1 -

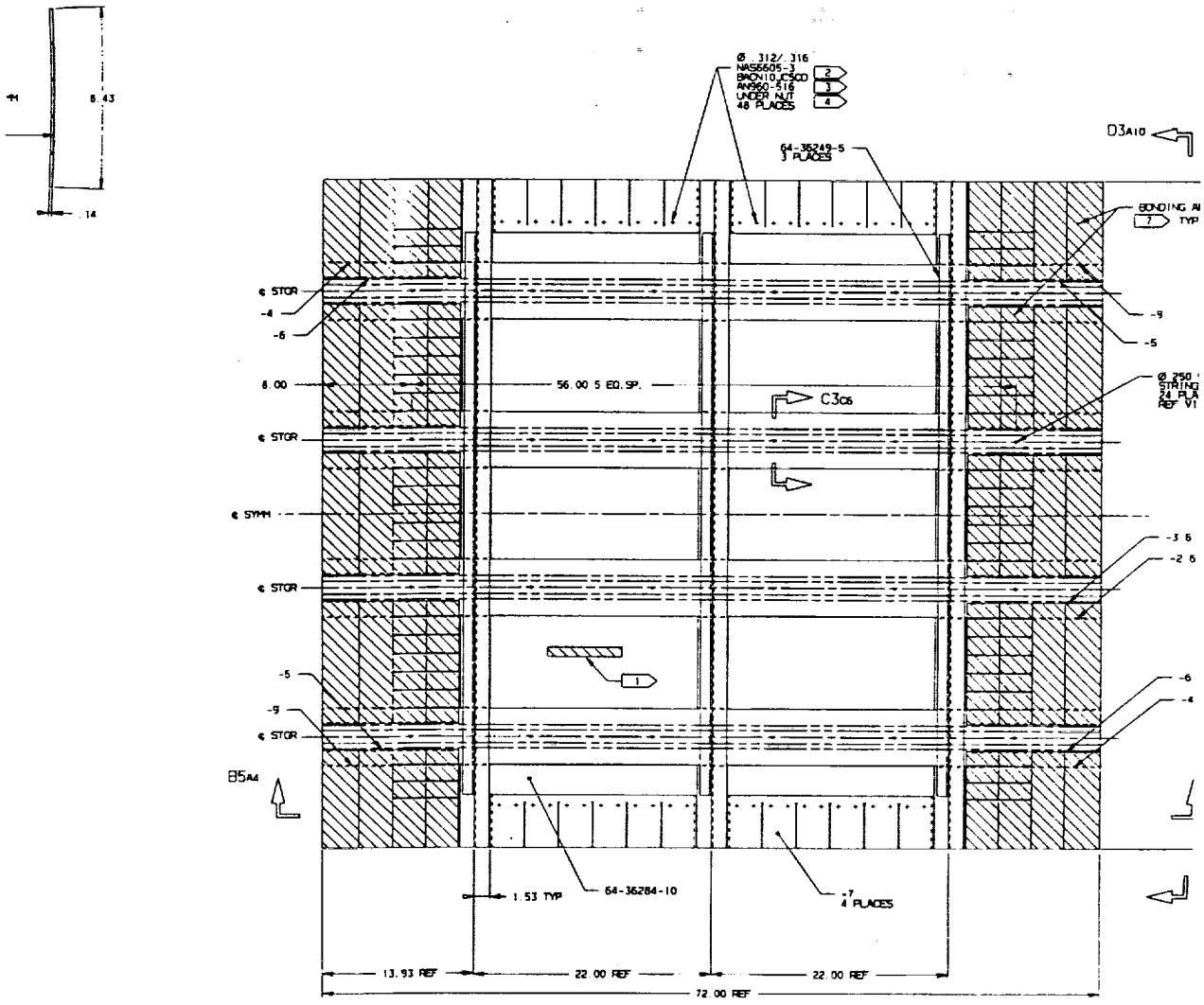




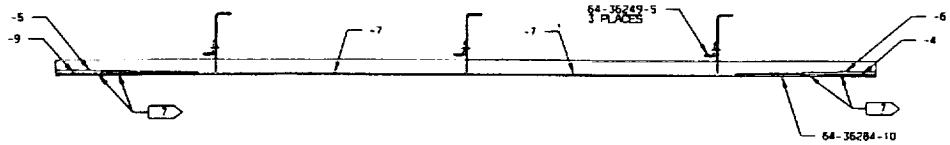
TYPICAL FRAME SECTION
SCALE: 1/2

BOEING PROPRIETARY
THE INFORMATION CONTAINED HEREIN IS PROPRIETARY TO THE BOEING COMPANY AND SHALL NOT BE REPRODUCED OR DISCLOSED IN WHOLE OR IN PART OR USED FOR ANY PURPOSE EXCEPT WHEN SUCH USE POSSESSES DIRECT WRITTEN AUTHORIZATION FROM THE BOEING COMPANY.

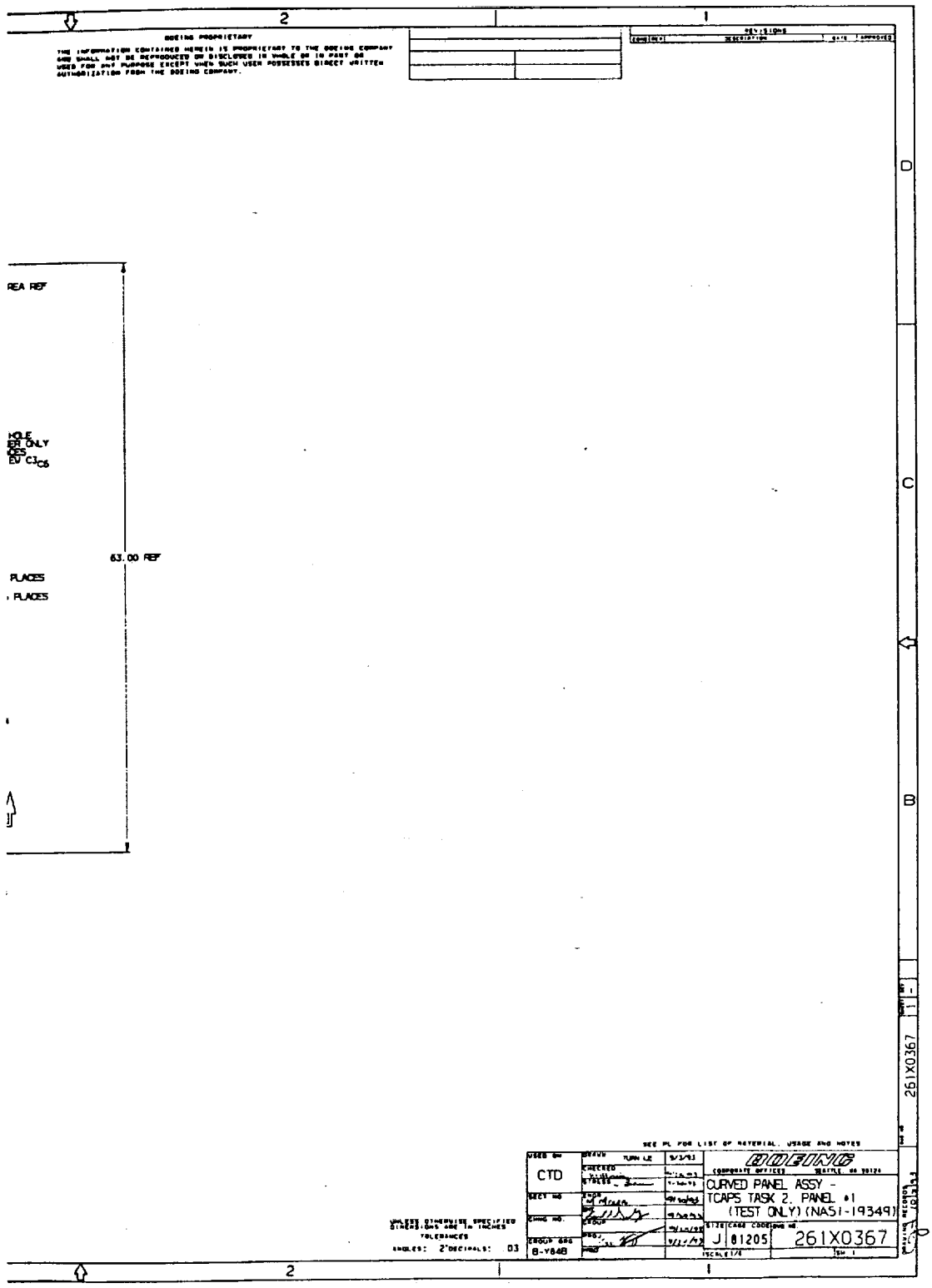
7
6



PANEL ASSY-1
SHOWN AS FLAT PATTERN



B5


BOEING PROPRIETARY
THE INFORMATION CONTAINED HEREIN IS PROPRIETARY TO THE BOEING COMPANY AND SHALL NOT BE REPRODUCED OR DISCLOSED IN WHOLE OR IN PART OR USED FOR ANY PURPOSE EXCEPT WHEN SUCH USER POSSESSES DIRECT WRITTEN AUTHORIZATION FROM THE BOEING COMPANY.
REVISIONS
REA REF
63.00 REF
PLACES
PLACES
SEE PL FOR LIST OF MATERIAL, USAGE AND NOTES
CTD
BOEING
CURVED PANEL ASSY -
TCAPS TASK 2, PANEL #1
(TEST ONLY) (NAS1-19349)
J 81205
261X0367
UNLESS OTHERWISE SPECIFIED DIMENSIONS ARE IN INCHES
TOLERANCES
ANGLES: 2° DECIMALS: .03
8-Y848

PARTS LIST

REVISION STATUS

SHEET	LTR	ADDED SHEETS				SHEET	LTR	ADDED SHEETS			
		SHEET	LTR	SHEET	LTR			SHEET	LTR	SHEET	LTR
1	-										
2	-										
3	-										
4	-										
5	-										

PART NUMBER	APPLICATION			DWG SH NUMBER	REV LTR
	NEXT ASSY	USED ON	EFFECTIVITY		
-1	113X9001	TEST ONLY			

CAD DRAWING
(NO DATASET RELEASED)

ENGINEERING REFERENCE ONLY
CAD FILE NAME: CATIAX.V2R2.NSTGRPAT.MAP
DATASET NAME:261X0367M01-- CURVED PANEL ASSY TCAPS PANEL #1

DWG ORIG BY B-Y84B

CONTR		THE BOEING COMPANY STRUCTURES LABORATORY SEATTLE, WASHINGTON 98124
DRN TUAN LE	9/07/93	
CHK	9/28/93	
ENGR STRESS: J. Bodine	9-29-93	CURVED PANEL ASSY- TCAPS TASK 2, PANEL #1 (TEST ONLY) (NAS1-19349)
ORG		
PROJ	9/29/93	
BMT	9/29/93	CODE IDENT NO 81205 | PL 261X0367 | SH 1 OF 5 | REV LTR -

PARTS LIST	THE BOEING COMPANY STRUCTURES LABORATORY SEATTLE, WASHINGTON 98124	CODE IDENT NUMBER 81205	PL 261X0367	SHEET 2	REV LTR -

REVISIONS				REVISIONS			
LTR	DESCRIPTION	DATE	APPROVED	LTR	DESCRIPTION	DATE	APPROVED

PARTS LIST	THE BOEING COMPANY STRUCTURES LABORATORY SEATTLE, WASHINGTON 98124	CODE IDENT NUMBER 81205	PL 261X0367	SHEET 3	REV LTR –

NOTES

-INSTALL BOLT AND NUT FASTENERS PER BAC 5009 & BAC 5063.

-SURFACE FINISH ALL MACHINED SURFACES 125 MAX.

-TRIM AND MACHINE GR/EP PARTS TO THE REQUIREMENTS OF BAC 5578.

-BREAK ALL SHARP EDGES AND CORNERS ON GR/EP DETAILS TO A RADIUS OR CHAMFER OF APPROX .01. VISUAL INSPECT ONLY.

-FORM, PUNCH, STRAIGHTEN, BREAK SHARP EDGES AND FIT METAL PARTS PER BAC5300.

1. STENCIL DRAWING, ASSY NO. IN 1/2 IN TO 1 IN HIGH NUMERALS ON EACH SIDE IN APPROX. LOCATION SHOWN WITH WHITE ENAMEL PER BAC 5307. OPTIONAL: HANDMARK WITH WHITE MARK PEN.
2. FASTENER HEAD NEAR SIDE.
3. UP TO (2) WASHERS UNDER NUT IS ACCEPTABLE FOR LONGER GRIP LENGTH FASTENERS.
4. TORQUE FASTENERS 90-125 IN-LBS.
5. TORQUE FASTENERS 30-40 IN-LBS.
6. 1- PHOSPHORIC ACID ANODIZE PER BAC 5555.
   2- PRIME WITH BMS 5-89 TYPE I GRADE A PER BAC 5514-589.
7. BOND PER BAC 5010 TYPE 106.

NOTES

PARTS LIST

THE BOEING COMPANY
STRUCTURES LABORATORY SEATTLE, WASHINGTON 98124

CODE IDENT NUMBER 81205 | PL 261X0367 | SHEET 4 | REV LTR -

EAMR NUMBER	QTY REQD	QTY REQD	QTY REQD	QTY REQD	QTY REQD	QTY REQD -1	FIND NUMBER	PART OR IDENTIFYING NUMBER	NOMENCLATURE OR DESCRIPTION	ZONE	MATERIAL AND SPECIFICATION	CODE IDENT NUMBER	HT TR	FINISH	PT MK	REV LTR
						-		-1	TEST PANEL-ASSY	A4-1						
						6		-2	DOUBLER	C6-1	.14 X 8.5 X 12.5 7075-T6 ALUM. SHEET			6	M	
						6		-3	DOUBLER	C7-1	.25 X 11.5 X 12.5 7075-T6 ALUM. PLATE OR T651 BARE OR CLAD			6	M	
						2		-4	DOUBLER	C9-1	.14 X 7.8 X 12.5 7075-T6 ALUM. SHEET			6	M	
						2		-9	OPP-4	C9-1	.14 X 7.8 X 12.5 7075-T6 ALUM. SHEET			6	M	
						2		-5	DOUBLER	C10-1	.25 X 9.3 X 12.5 7075-T6 ALUM. PLATE OR T651 BARE OR CLAD			6	M	
						2		-6	OPP-5	C10-1	.25 X 9.3 X 12.5 7075-T6 ALUM. PLATE OR T651 BARE OR CLAD			6	M	
						4		-7	DOUBLER	C12-1	.071 X 5.1 X 19.1 7075-T6 ALUM. SHEET				M	
						1		64-36284-10	PANEL-ASSY							
						3		64-36249-5	CURVED ANGLE							

PARTS LIST

THE BOEING COMPANY
STRUCTURES LABORATORY SEATTLE, WASHINGTON 98124

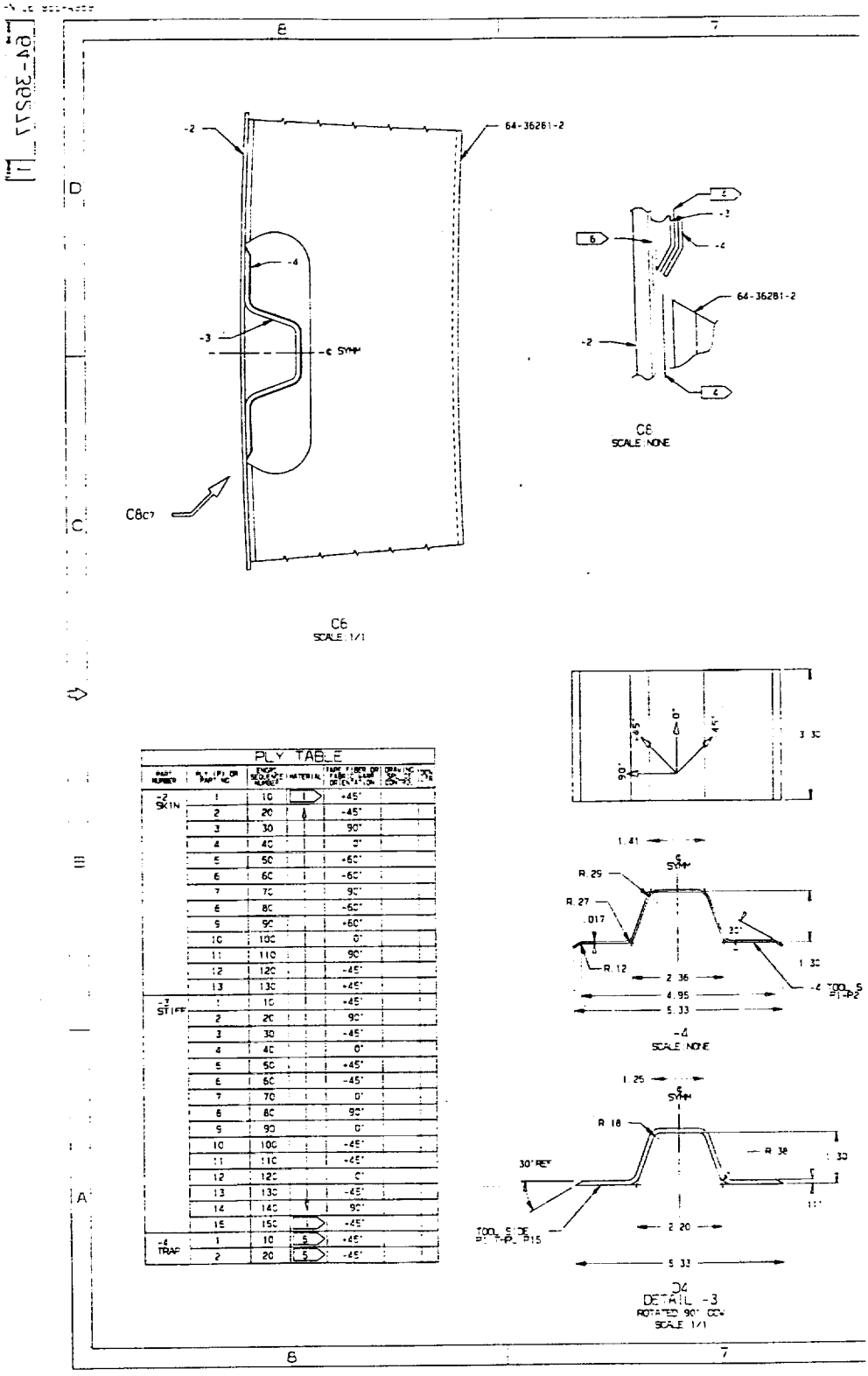
CODE IDENT NUMBER 81205 | PL 261X0367 | SHEET 5 | REV LTR –

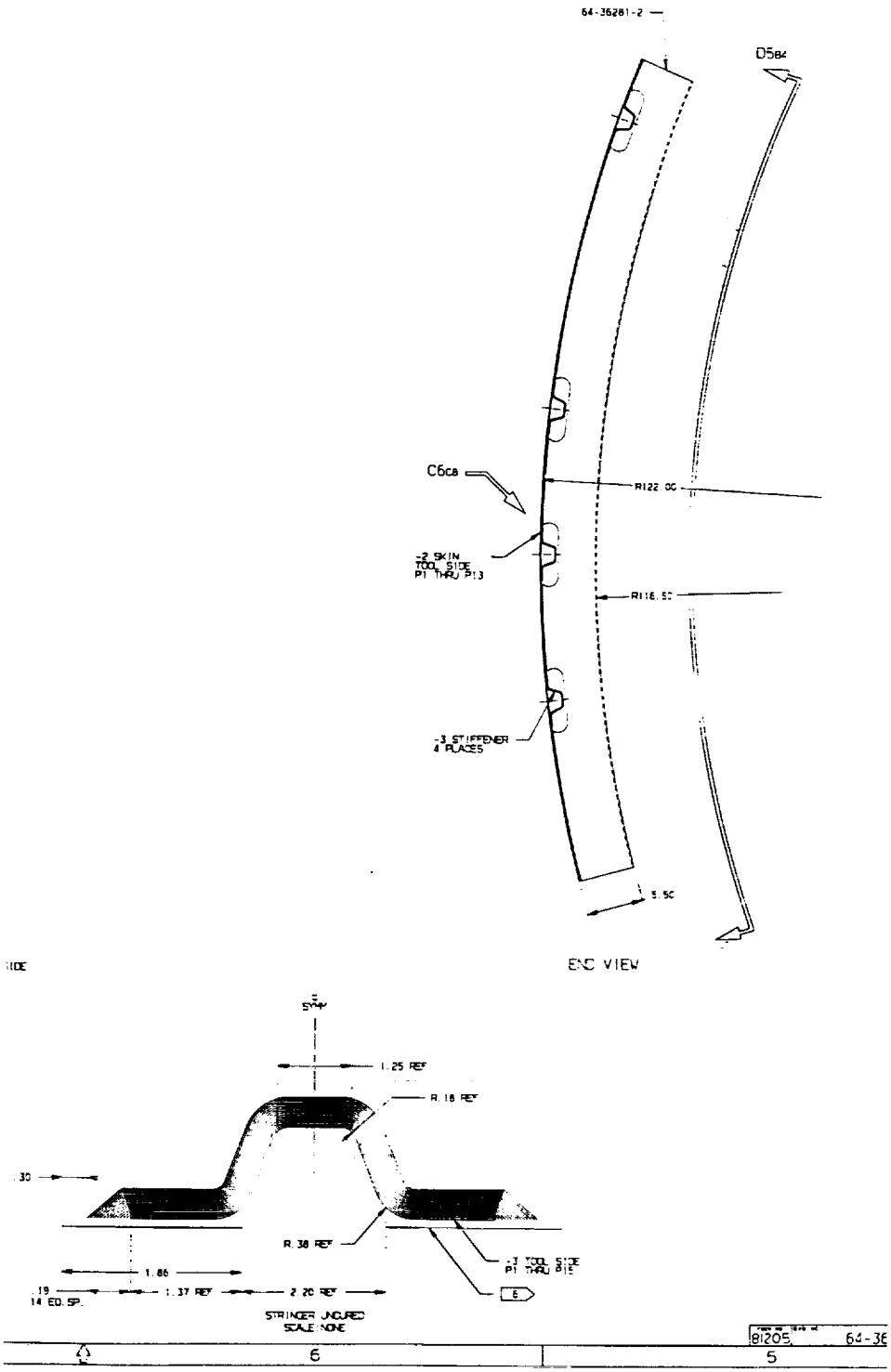
EAMR NUMBER	QTY REQD	QTY REQD	QTY REQD	QTY REQD	QTY REQD	QTY REQD -1	FIND NUMBER	PART OR IDENTIFYING NUMBER	NOMENCLATURE OR DESCRIPTION	ZONE	MATERIAL AND SPECIFICATION	CODE IDENT NUMBER	HT TR	FINISH	PT MK	REV LTR
						156		BACB30MB6A6U	BOLT							
						48		NAS6605-3	BOLT							
						A.R.		AN960-10	WASHER							
						A.R.		AN960-516	WASHER							
						48		BACN10JC5CD	NUT							
						156		NAS1805-3	NUT							

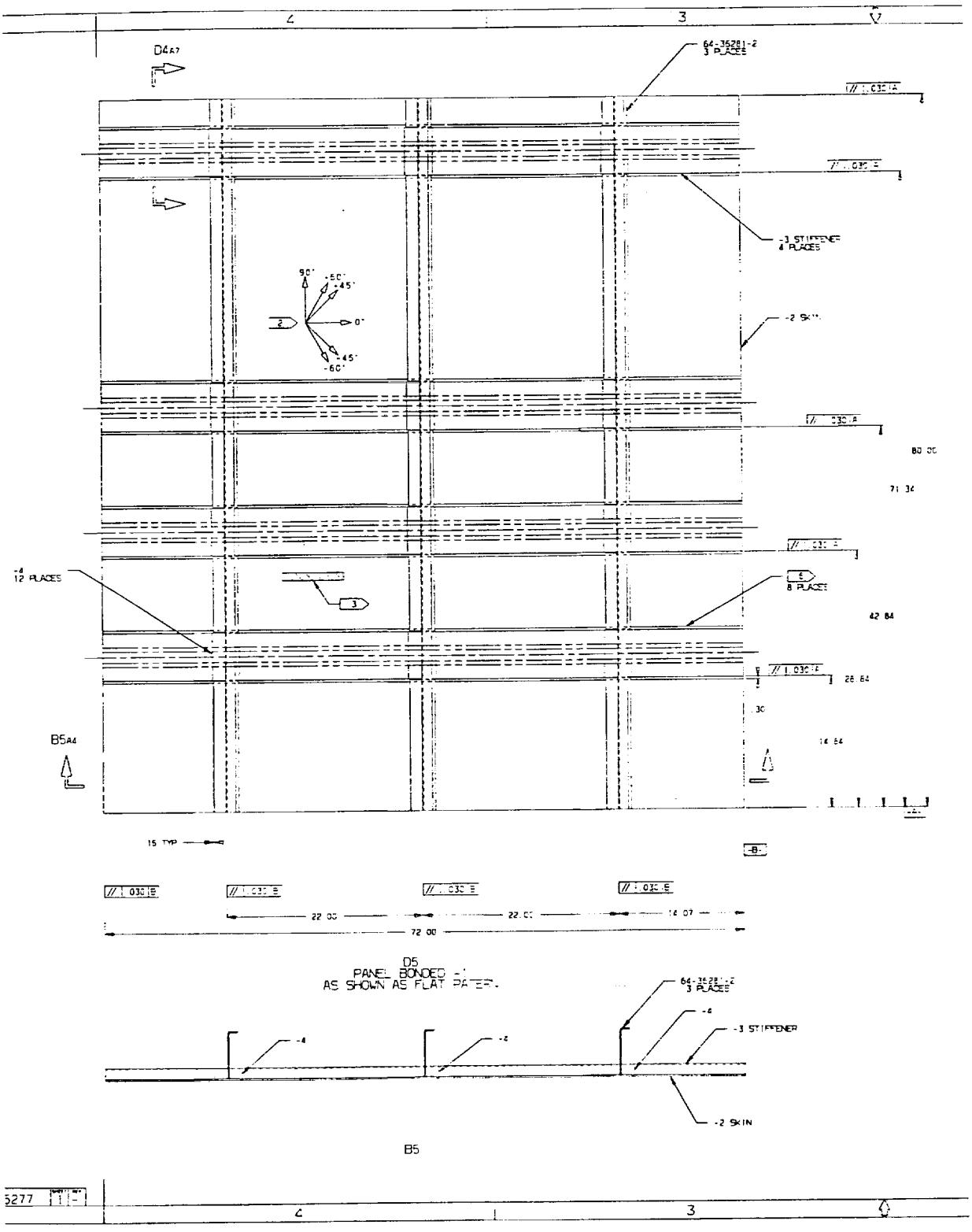
A-16

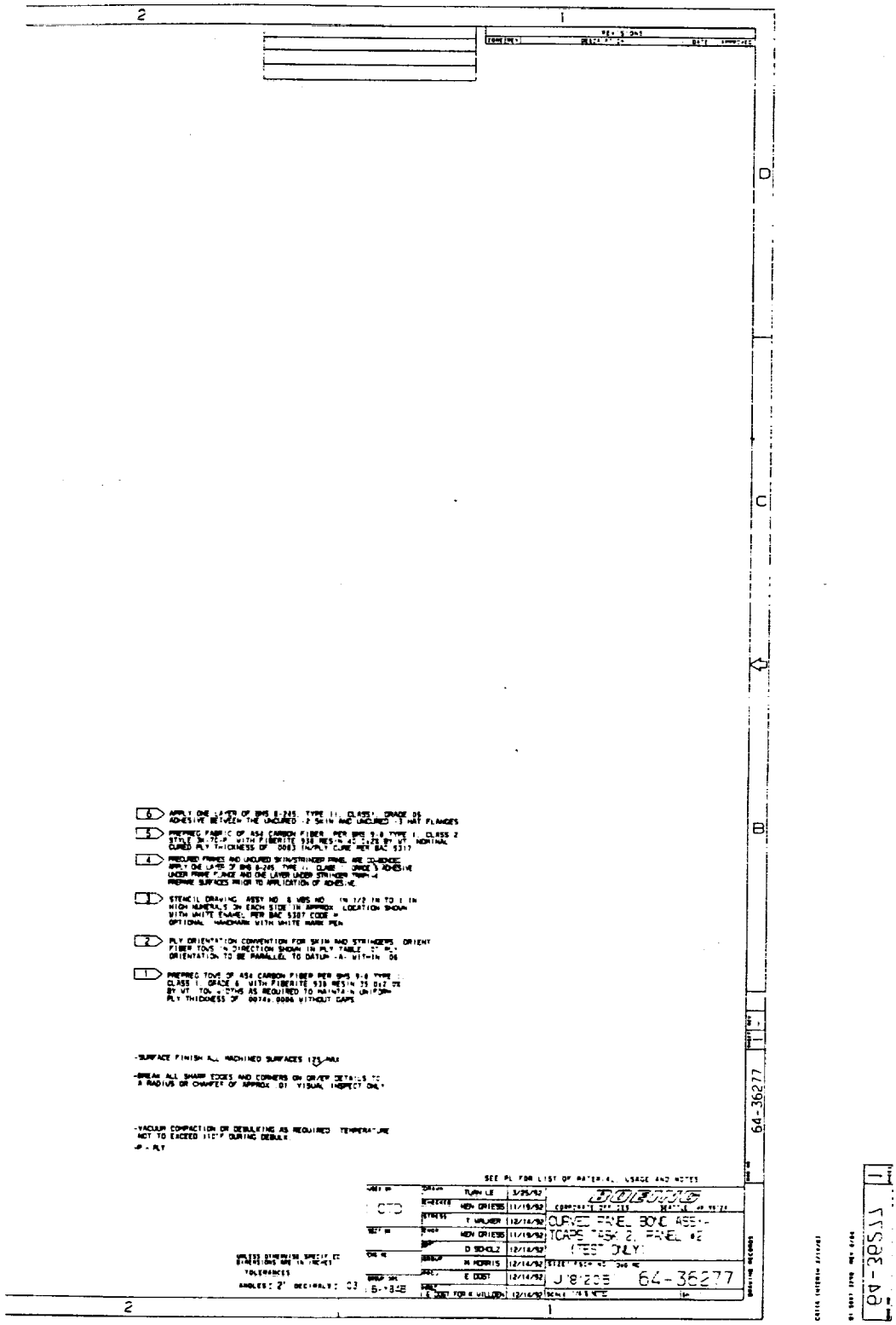
Appendix B

Panel Bond, Cutting Diagram, and Panel Assembly Drawings for Panel 2

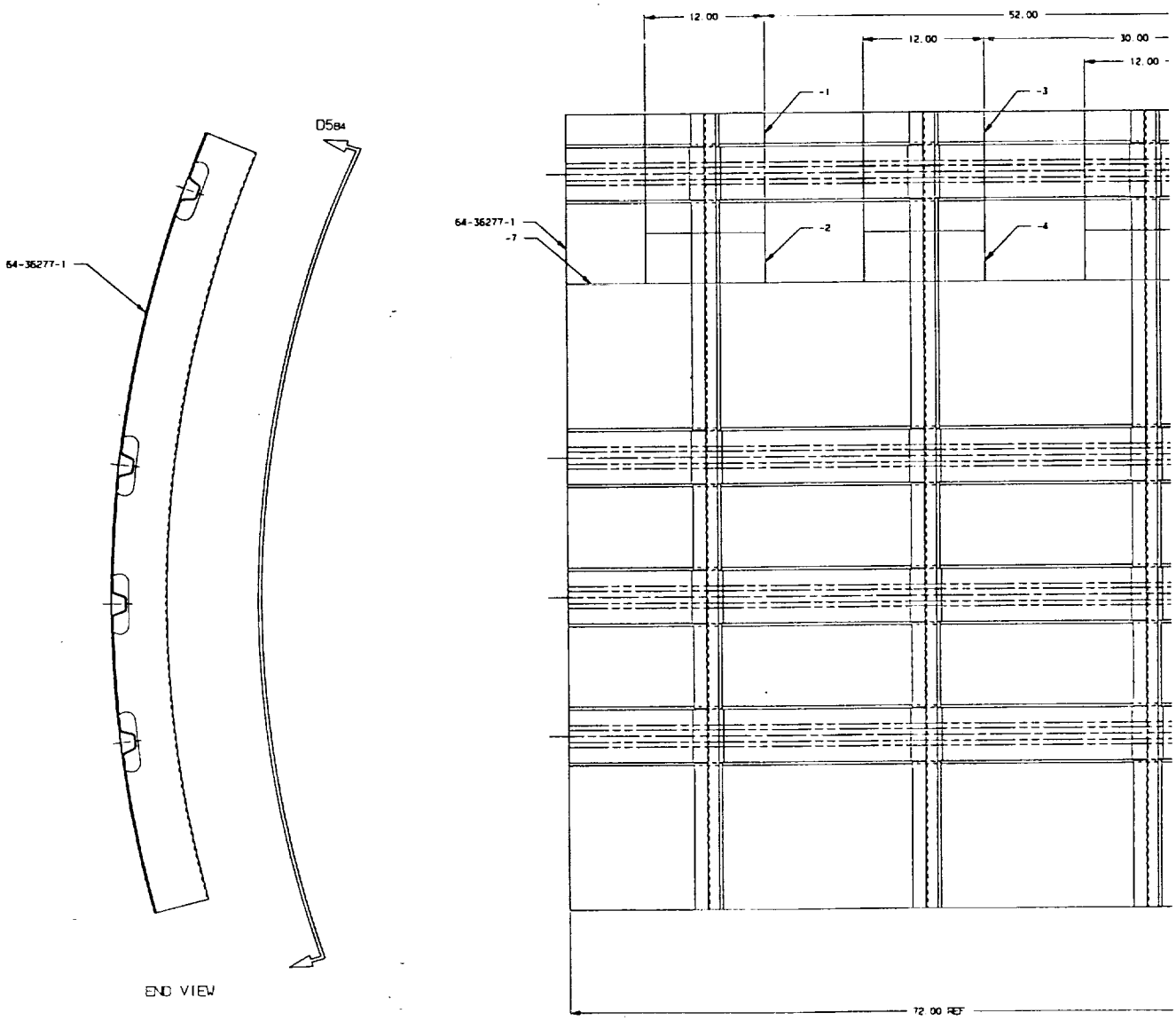

64-36281-2
-2
-4
-3
℄ SYM
C8C7
C6
SCALE 1/1
64-36281-2
C8
SCALE NONE
PLY TABLE
-2 SKIN
-3 STIFF
-4 TRAP
3.30
1.41
R.25
R.27
.017
R.12
2.36
4.95
5.33
-4
SCALE NONE
1.25
R.18
R.38
30° REF
2.20
5.33
D4
DETAIL -3
ROTATED 90° CCW
SCALE 1/1


64-36281-2
D5B4
C6C8
R122.00
-2 SKIN
TOOL SIDE
P1 THRU P13
R116.50
-3 STIFFENER
4 PLACES
5.50
END VIEW
1.25 REF
R.18 REF
.30
R.38 REF
-7 TOOL SIDE
P1 THRU P16
1.86
.19
14 ED. SP.
1.37 REF
2.20 REF
6
STRINGER INCURED
SCALE: NONE


2
3
D4A7
64-36281-2
3 PLACES
-3 STIFFENER
4 PLACES
-2 SKIN
90°
-60°
-45°
0°
45°
60°
80.00
71.36
42.84
28.64
30
14.64
-4
12 PLACES
6
8 PLACES
B5A4
15 TYP
-B-
22.00
22.00
14.07
72.00
D5
PANEL BONDED -
AS SHOWN AS FLAT PATTERN
64-36281-2
3 PLACES
-4
-3 STIFFENER
-2 SKIN
B5
5277

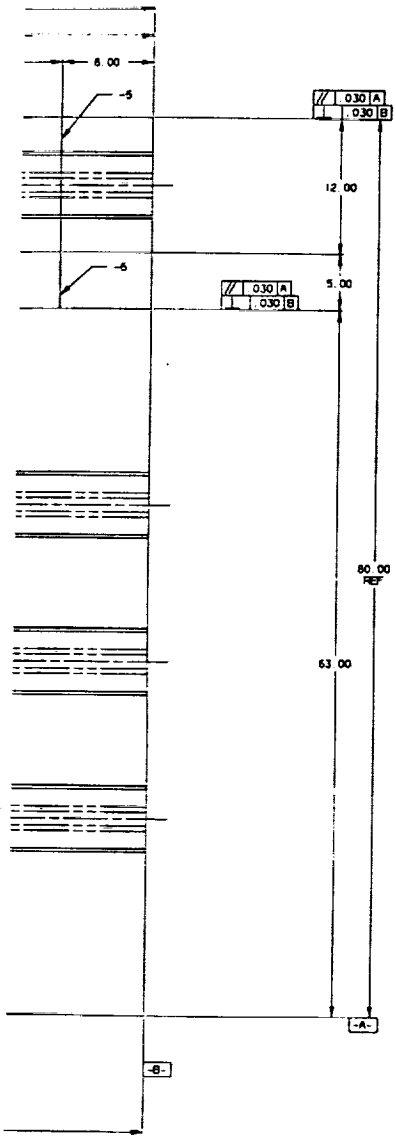

2
1
D
C
B
64-36277
SEE PL FOR LIST OF MATERIAL, USAGE AND NOTES
CTD
TURN LE 3/25/92
MEN ORTEGA 11/19/92
T WALKER 12/14/92
MEN ORTEGA 11/19/92
D SCHOLZ 12/18/92
M MORRIS 12/16/92
E DOST 12/14/92
J 18235
64-36277
TOLERANCES
ANGLES: 2° DECIMALS: .03
B-348
2
1

B-4



D5
SKIN AS SHOWN AS FLATPATERN
DIMENSION MEASURE ON
OUTSIDE MOLD LINE

81205 64-36285 1 -



-USE OF MANUFACTURING EXCESS MAY BE REQUIRED TO PROVIDE FOR 25 KSI/F TYP

-HAND MARK PARTS WITH WHITE MARKING PEN

-SURFACE FINISH ALL MACHINED SURFACES 125 MAX

-BREAK ALL SHARP EDGES AND CORNERS OR CHAMFER DETAILS TO A RADIUS OR CHAMFER OF APPROX .01. VISUAL INSPECT ONLY.

SEE PL FOR LIST OF MATERIAL USAGE AND NOTES

CTD	TURN LE	7/16/92
		9/14/92
		9/11/92
		9/14/92
		11/11/92
B-Y848		1/6/93

BOEING CORPORATE OFFICES SEATTLE, WA 98124

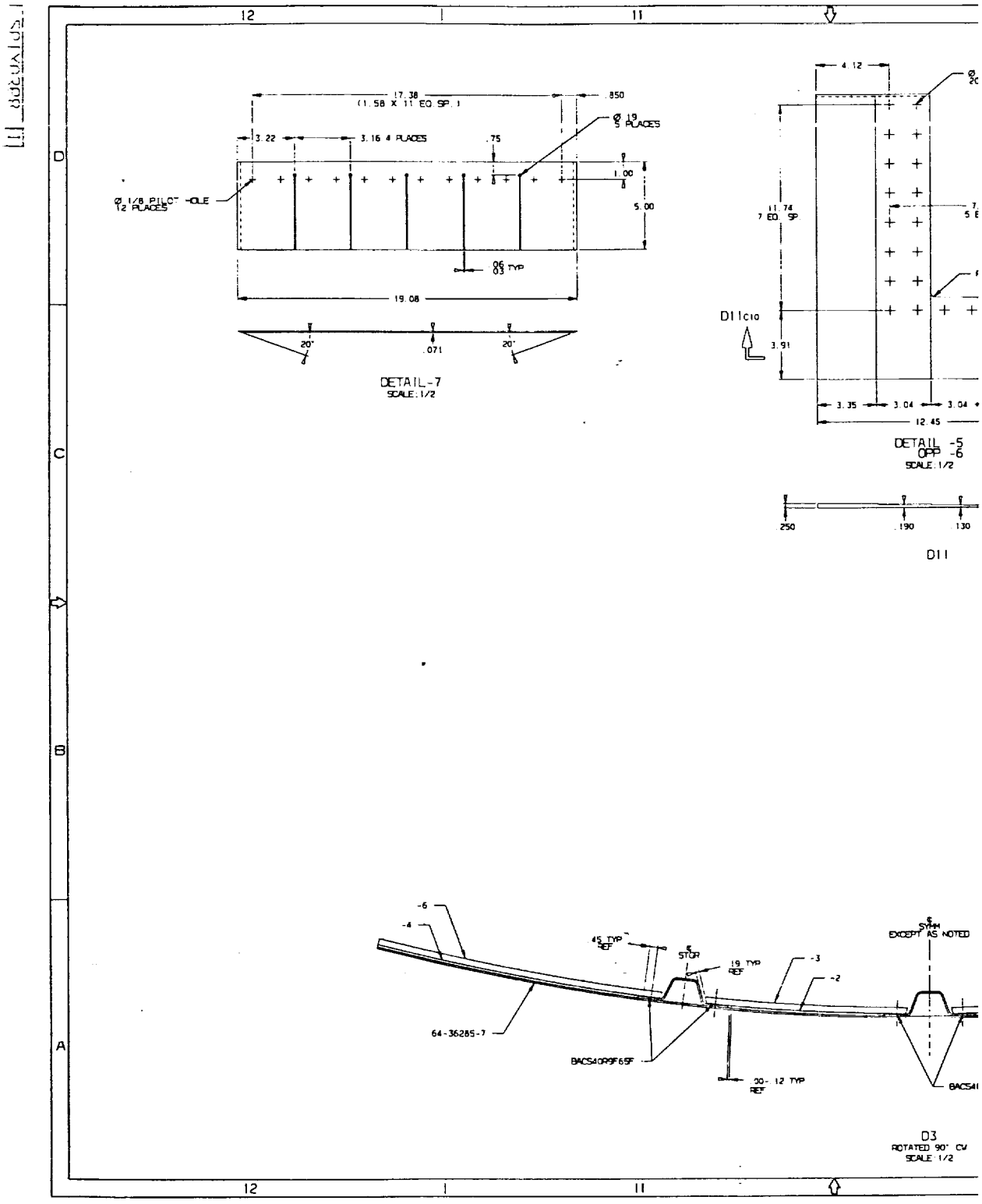
CURVED PANEL CUTTING DIAGRAM-TCAPS TASK 2, PANEL #2 (TEST ONLY)

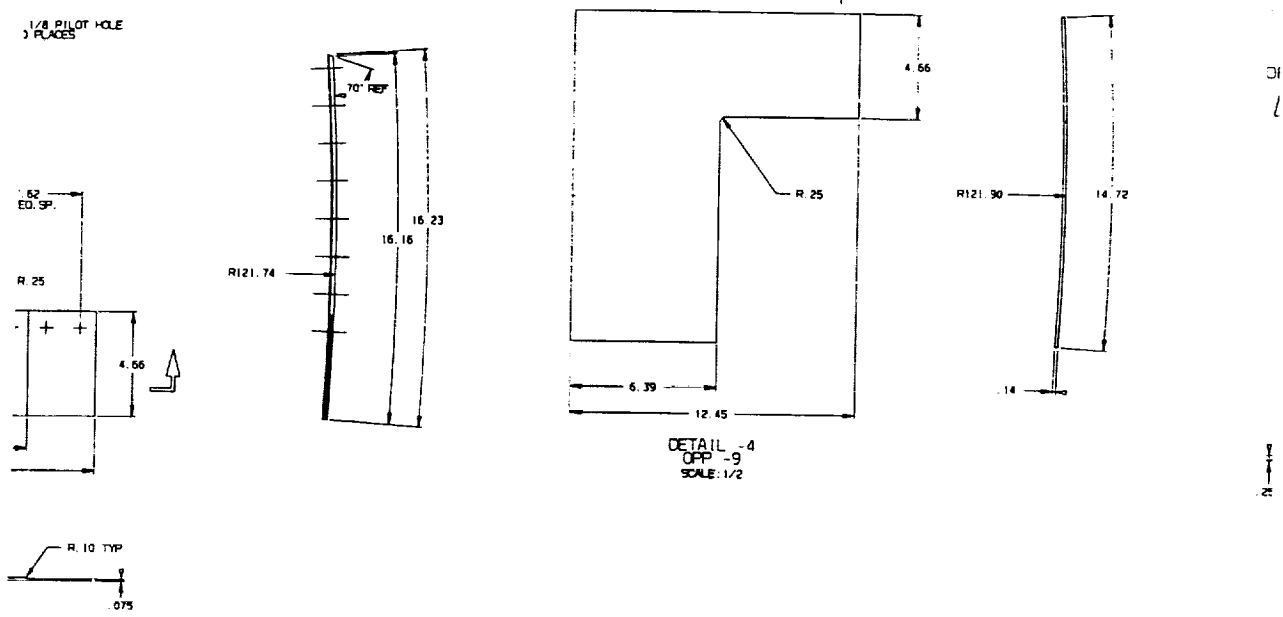
SIZE J | FSCM NO 81205 | DWG NO 64-36285

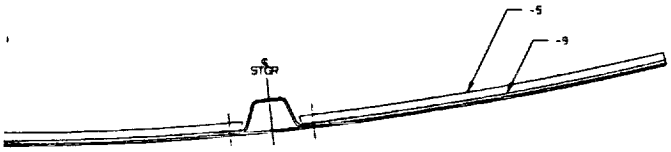
SCALE 1/8

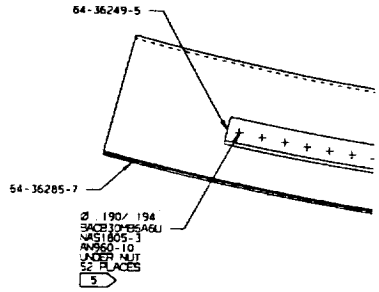
64-36285

UNLESS OTHERWISE SPECIFIED DIMENSIONS ARE IN INCHES
TOLERANCES:
ANGLES ± 2° DECIMALS ± .03


12
11
D
C
B
A
17.38
(11.58 X 1.1 EQ. SP.)
.850
Ø .19
5 PLACES
3.22
3.16 4 PLACES
.75
1.00
5.00
Ø 1/8 PILOT HOLE
12 PLACES
.06
.03 TYP
19.08
20°
.071
20°
DETAIL-7
SCALE: 1/2
4.12
11.74
7 EQ. SP
D11 C10
3.91
3.35
3.04
3.04
12.45
DETAIL -5
OPP -6
SCALE: 1/2
.250
.190
.130
D11
-6
-4
45 TYP
REF
STGR
.19 TYP
REF
-3
-2
64-36285-7
BACS40R9F65F
.30 - 12 TYP
REF
SYM
EXCEPT AS NOTED
D3
ROTATED 90° CW
SCALE: 1/2





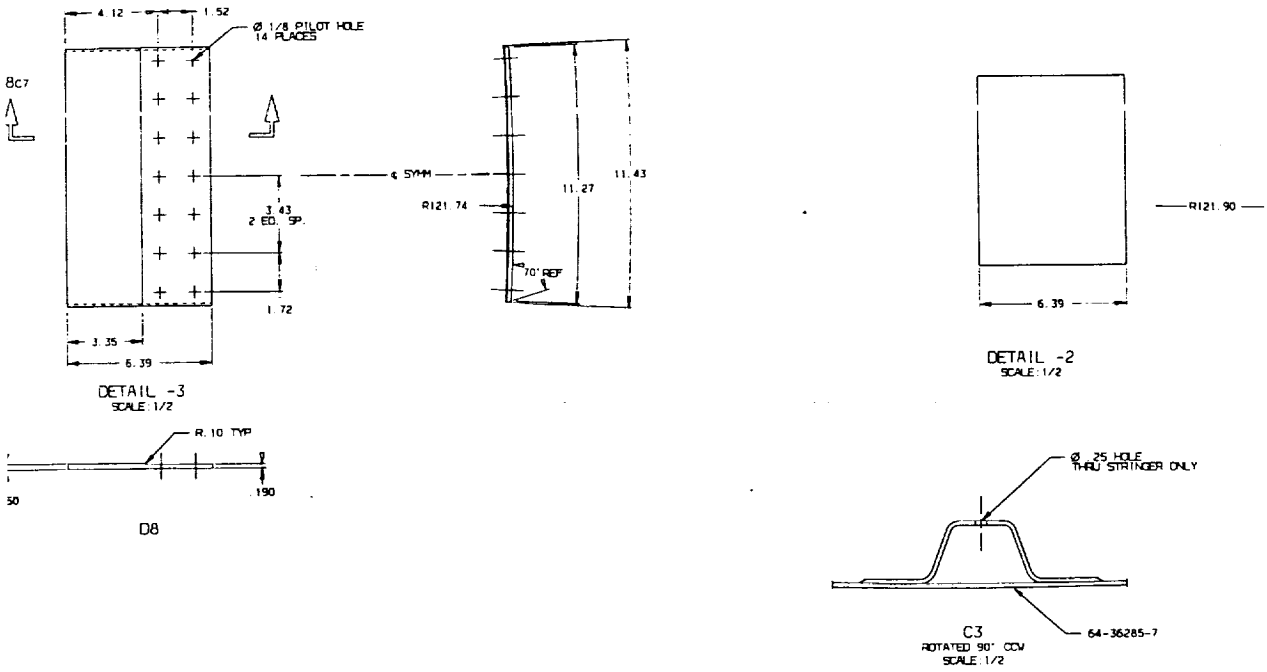


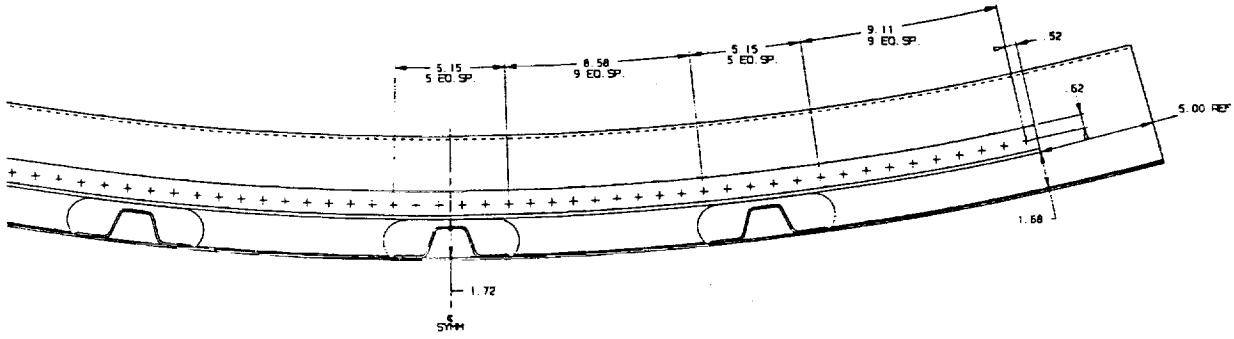
340R9F55F

BOEING PROPRIETARY
THE INFORMATION CONTAINED HEREIN IS PROPRIETARY TO THE BOEING COMPANY AND SHALL NOT BE REPRODUCED OR DISCLOSED IN WHOLE OR IN PART OR USED FOR ANY PURPOSE EXCEPT WHEN SUCH USER POSSESSES DIRECT WRITTEN AUTHORIZATION FROM THE BOEING COMPANY.

81205 261X0368 1 1 -

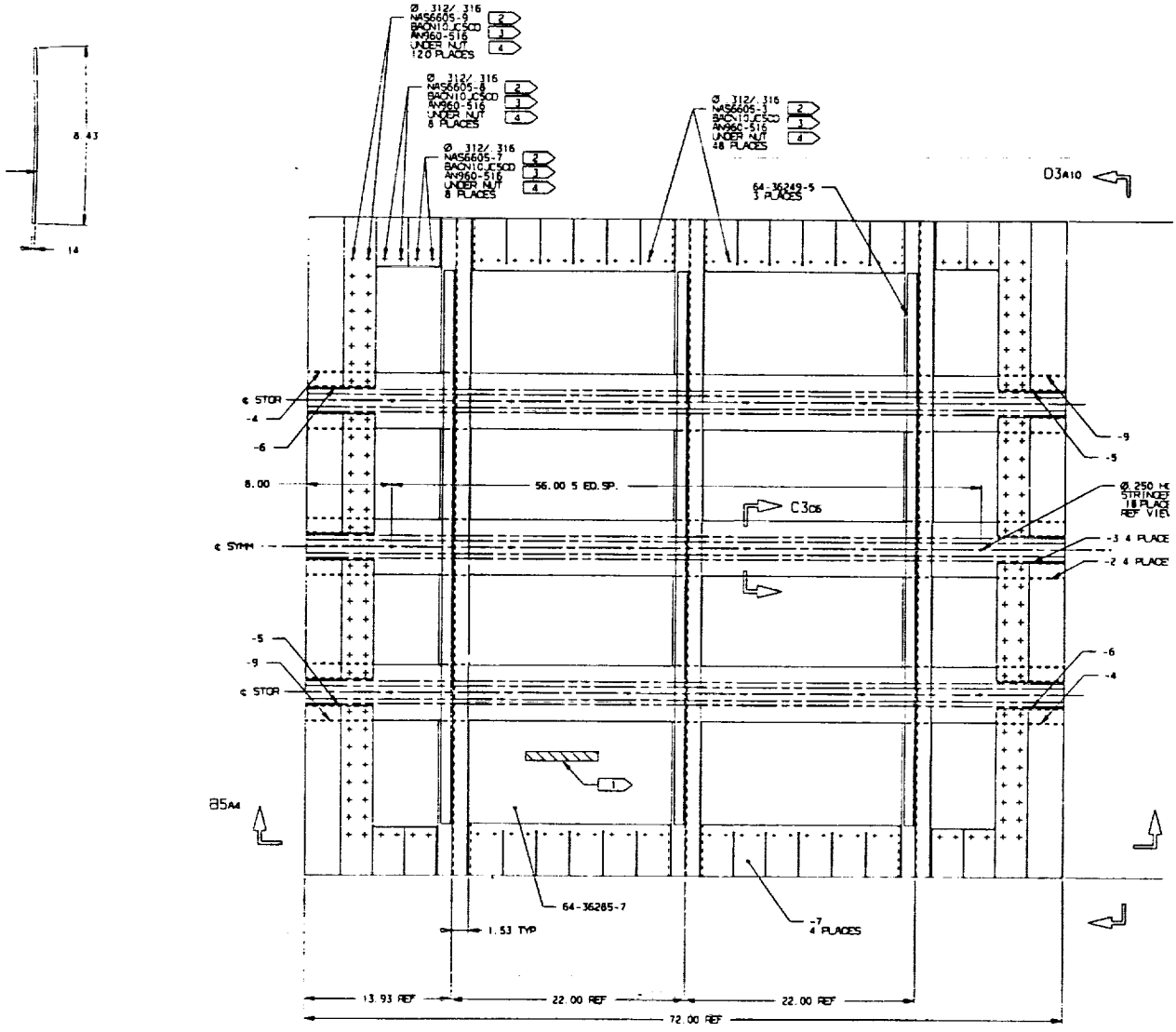
10 9 8

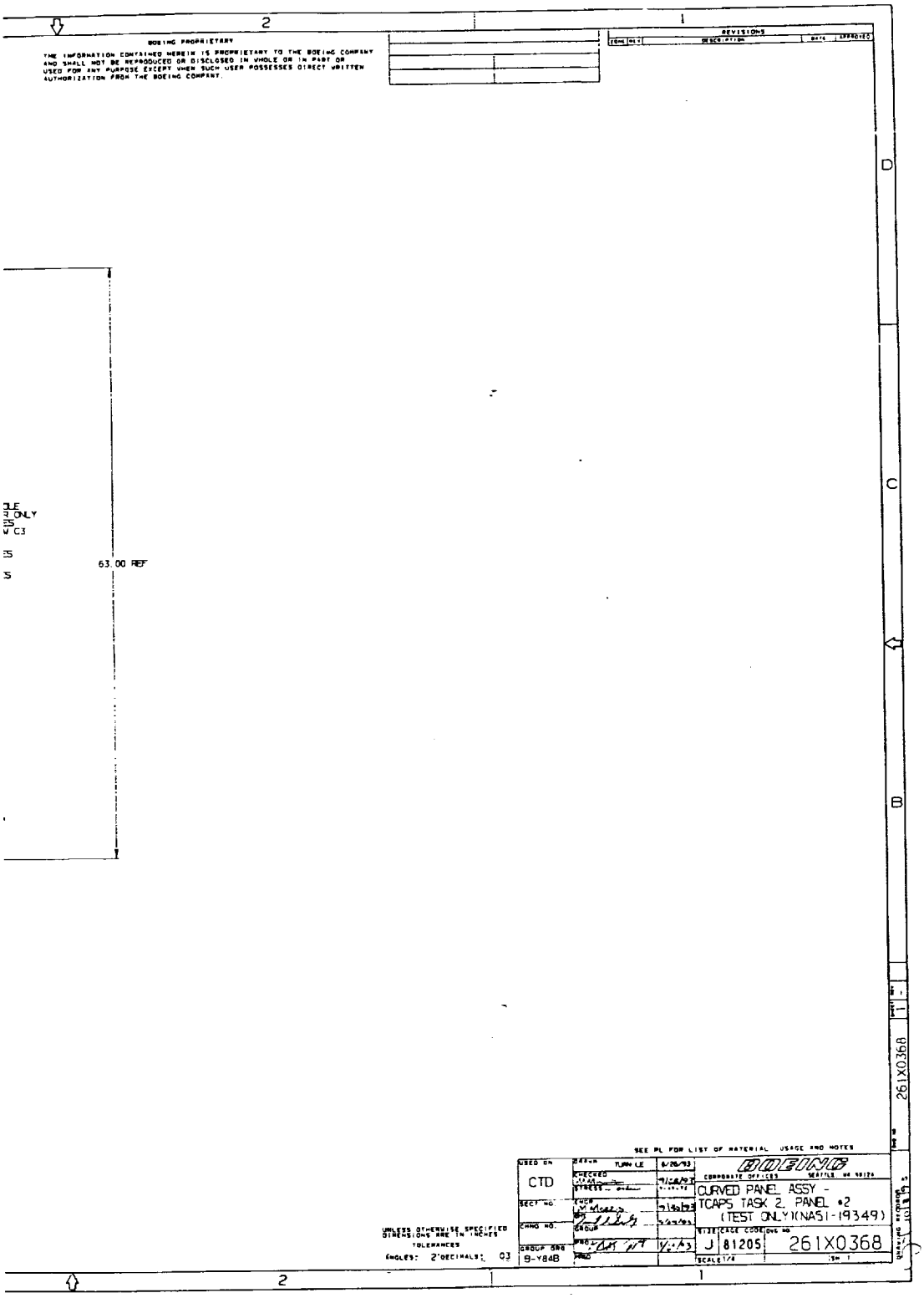




TYPICAL FRAME SECTION
SCALE: 1/2

BOEING PROPRIETARY
THE INFORMATION CONTAINED HEREIN IS PROPRIETARY TO THE BOEING COMPANY AND SHALL NOT BE REPRODUCED OR DISCLOSED IN WHOLE OR IN PART OR USED FOR ANY PURPOSE EXCEPT WHEN SUCH USE POSSESSES DIRECT WRITTEN AUTHORIZATION FROM THE BOEING COMPANY


5
4
3
8.43
14
Ø .312/.316
NAS6605-9
BACN10JC5CD
AN960-516
UNDER NUT
120 PLACES
Ø .312/.316
NAS6605-8
BACN10JC5CD
AN960-516
UNDER NUT
8 PLACES
Ø .312/.316
NAS6605-7
BACN10JC5CD
AN960-516
UNDER NUT
8 PLACES
Ø .312/.316
NAS6605-3
BACN10JC5CD
AN960-516
UNDER NUT
48 PLACES
64-36249-5
3 PLACES
D3A10
℄ STOR
-4
-6
8.00
56.00 5 ED. SP.
C3D6
℄ SYMM
-5
-9
℄ STOR
B5A4
64-36285-7
1.53 TYP
-7
4 PLACES
-9
-5
-3 4 PLACE
-2 4 PLACE
-6
-4
13.93 REF
22.00 REF
22.00 REF
72.00 REF
PANEL ASSY-1
SHOWN AS FLAT PATTERN
-5
-9
-7
-7
64-36249-5
3 PLACES
-6
-4
64-36285-7
B5
81205
251X0368
5
4
3


BOEING PROPRIETARY
THE INFORMATION CONTAINED HEREIN IS PROPRIETARY TO THE BOEING COMPANY AND SHALL NOT BE REPRODUCED OR DISCLOSED IN WHOLE OR IN PART OR USED FOR ANY PURPOSE EXCEPT WHEN SUCH USER POSSESSES DIRECT WRITTEN AUTHORIZATION FROM THE BOEING COMPANY.
REVISIONS
63.00 REF
SEE PL FOR LIST OF MATERIAL USAGE AND NOTES
CTD
CURVED PANEL ASSY -
TCAPS TASK 2, PANEL #2
(TEST ONLY)(NAS1-19349)
J 81205
261X0368
261X036A
UNLESS OTHERWISE SPECIFIED DIMENSIONS ARE IN INCHES
TOLERANCES
ANGLES: 2° DECIMALS: .03
GROUP 286
9-Y84B

PARTS LIST

REVISION STATUS											
		ADDED SHEETS						ADDED SHEETS			
SHEET	LTR	SHEET	LTR	SHEET	LTR	SHEET	LTR	SHEET	LTR	SHEET	LTR
1	-										
2	-										
3	-										
4	-										
5	-										

PART NUMBER	APPLICATION			DWG SH NUMBER	REV LTR
	NEXT ASSY	USED ON	EFFECTIVITY		
-1	113X9002	TEST ONLY			

CAD DRAWING
(NO DATASET RELEASED)

ENGINEERING REFERENCE ONLY
CAD FILE NAME: CATIAX.V2R2.NSTGRPAT.MAP
DATASET NAME: 261X0368M01-- CURVED PANEL ASSY TCAPS PANEL #2

DWG ORIG BY B-Y84B

CONTR		THE BOEING COMPANY STRUCTURES LABORATORY SEATTLE, WASHINGTON 98124
DRN TUAN LE	8/27/93	
CHK M Murray	9/28/93	CURVED PANEL ASSY- TCAPS TASK 2, PANEL #2 (TEST ONLY) (NAS1-19349)
ENGR STRESS: J. Hudnut	9-29-93	
ORG		
PROJ E Ortiz	9/29/93	
BMT	9/29/93	CODE IDENT NO 81205 | PL 261X0368 | SH 1 OF 5 | REV LTR -

PARTS LIST

THE BOEING COMPANY
STRUCTURES LABORATORY SEATTLE, WASHINGTON 98124

CODE IDENT NUMBER		SHEET	REV
81205	PL 261X0368	2	-

REVISIONS

LTR	DESCRIPTION	DATE	APPROVED

REVISIONS

LTR	DESCRIPTION	DATE	APPROVED

NOTES

- INSTALL BOLT AND NUT FASTENERS PER BAC 5009 & BAC 5063.
- SURFACE FINISH ALL MACHINED SURFACES 125 MAX.
- TRIM AND MACHINE GR/EP PARTS TO THE REQUIREMENTS OF BAC 5578.
- BREAK ALL SHARP EDGES AND CORNERS ON GR/EP DETAILS TO A RADIUS OR CHAMFER OF APPROX .01. VISUAL INSPECT ONLY.
- FORM, PUNCH, STRAIGHTEN, BREAK SHARP EDGES AND FIT METAL PARTS PER BAC5300.

1. STENCIL DRAWING, ASSY NO. IN 1/2 IN TO 1 IN HIGH NUMERALS ON EACH SIDE IN APPROX. LOCATION SHOWN WITH WHITE ENAMEL PER BAC 5307. OPTIONAL: HANDMARK WITH WHITE MARK PEN.
2. FASTENER HEAD NEAR SIDE.
3. UP TO (2) WASHERS UNDER NUT IS ACCEPTABLE FOR LONGER GRIP LENGTH FASTENERS.
4. TORQUE FASTENERS 90-125 IN-LBS.
5. TORQUE FASTENERS 30-40 IN-LBS.
6. OPTIONAL P/N.

NOTES

PARTS LIST

THE BOEING COMPANY
STRUCTURES LABORATORY SEATTLE, WASHINGTON 98124

CODE IDENT NUMBER 81205 | PL 261X0368 | SHEET 4 | REV LT –

EAMR NUMBER	QTY REQD	QTY REQD	QTY REQD	QTY REQD	QTY REQD	QTY REQD	FIND NUMBER	PART OR IDENTIFYING NUMBER	NOMENCLATURE OR DESCRIPTION	ZONE	MATERIAL AND SPECIFICATION	CODE IDENT NUMBER	HT TR	FINISH	PT MK	REV LT
						- 1										
						-		-1	TEST PANEL-ASSY	A4-1						
						4		-2	DOUBLER	C6-1	.14 X 6.5 X 8.5 7075-T6 ALUM. SHEET				M	
						4		-3	DOUBLER	C7-1	.25 X 6.5 X 11.5 7075-T6 ALUM. PLATE OR T651 BARE OR CLAD				M	
						2		-4	DOUBLER	C9-1	.14 X 12.5 X 14.8 7075-T6 ALUM. SHEET				M	
						2		-9	OPP-4	C9-1	.14 X 12.5 X 14.8 7075-T6 ALUM. SHEET				M	
						2		-5	DOUBLER	C10-1	.25 X 12.5 X 16.3 7075-T6 ALUM. PLATE OR T651 BARE OR CLAD				M	
						2		-6	OPP-5	C10-1	.25 X 12.5 X 16.3 7075-T6 ALUM. PLATE OR T651 BARE OR CLAD				M	
						4		-7	DOUBLER	C12-1	.071 X 5.1 X 19.1 7075-T6 ALUM. SHEET				M	
						A.R		BACS40R9F65F	SHIM							
						1		64-36285-7	PANEL-ASSY							
						3		64-36249-5	CURVED ANGLE		6					

PARTS LIST

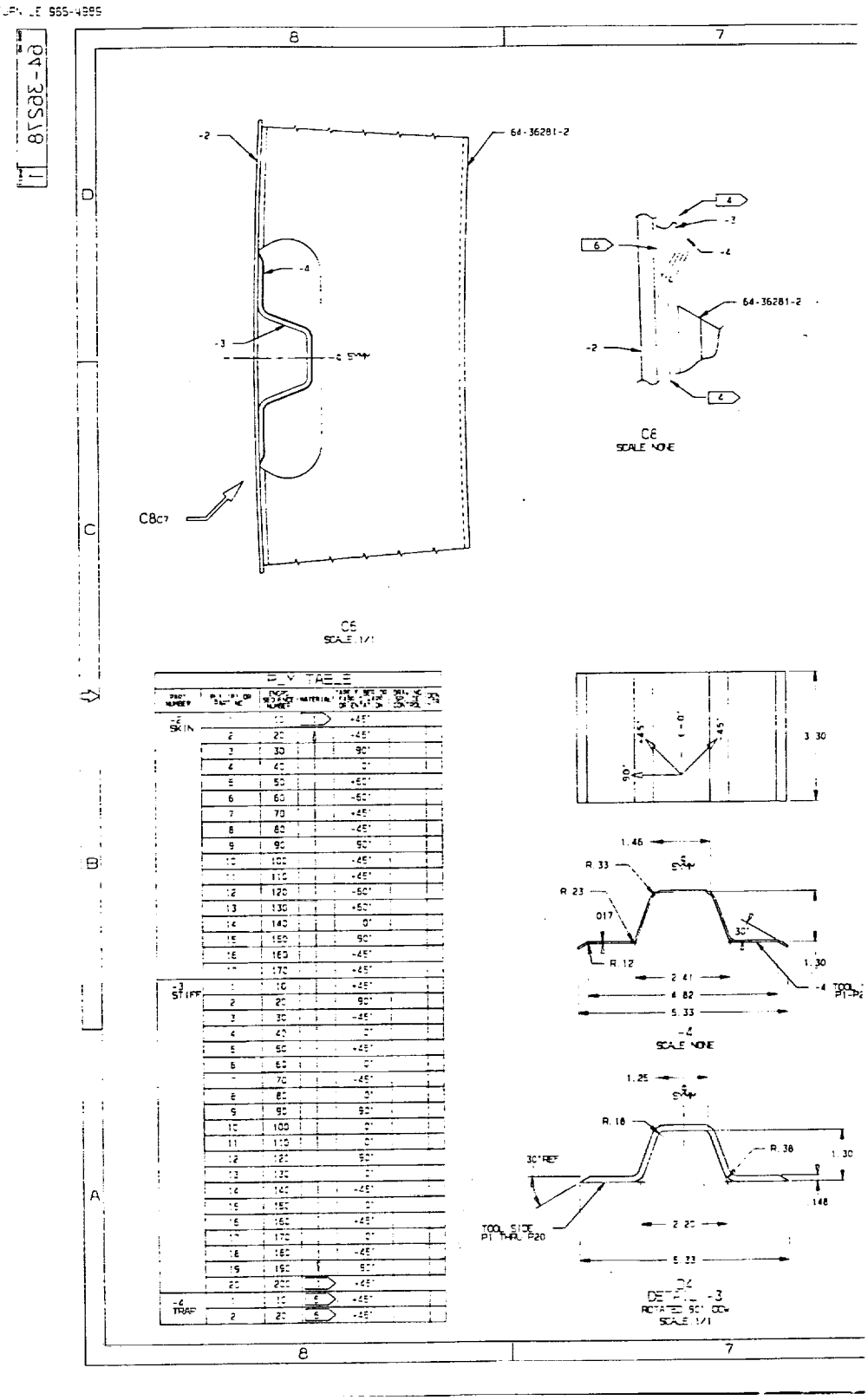
THE BOEING COMPANY
STRUCTURES LABORATORY SEATTLE, WASHINGTON 98124

CODE IDENT NUMBER 81205 | PL 261X0368 | SHEET 5 | REV LTR –

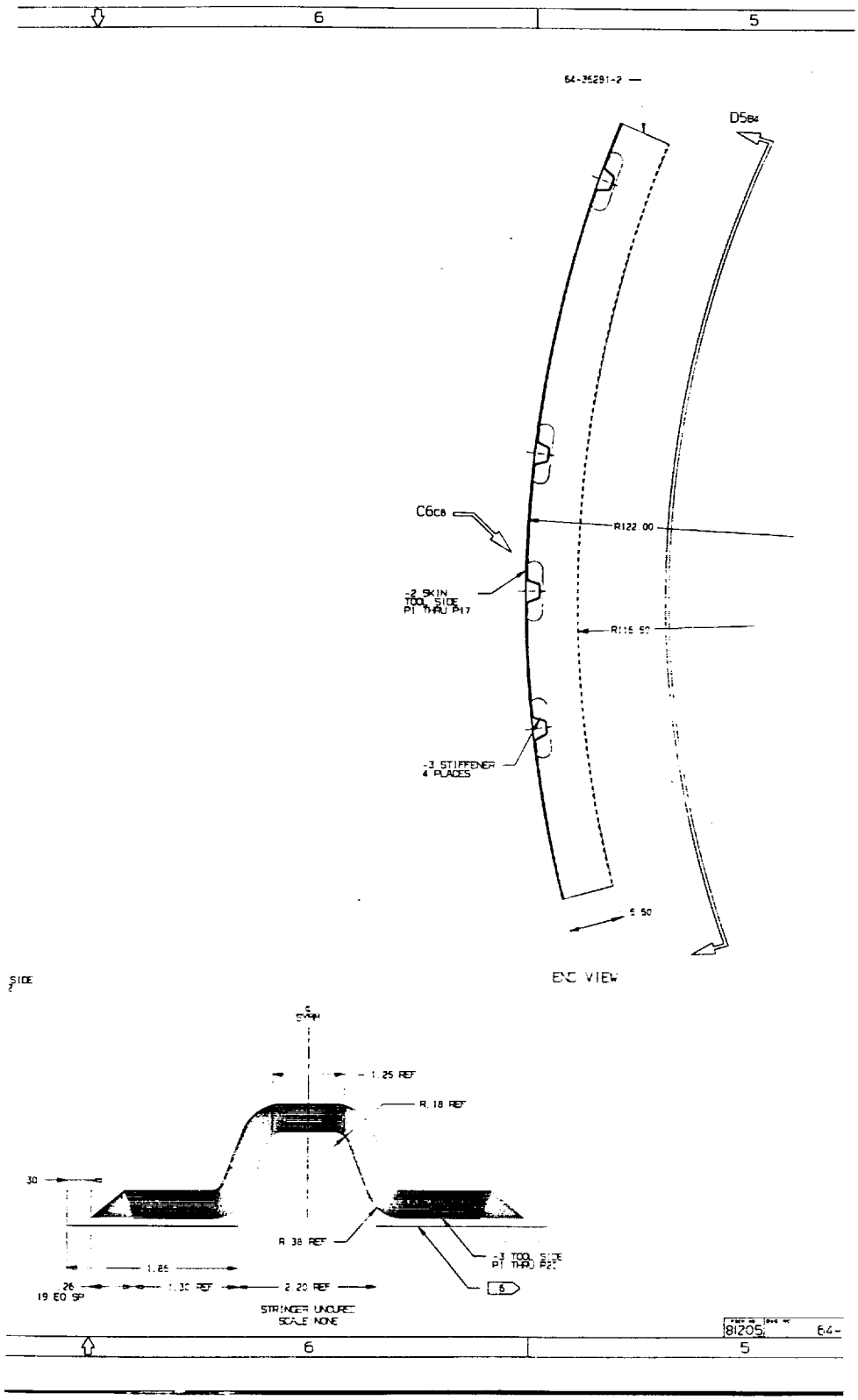
EAHR NUMBER	QTY REQD	QTY REQD	QTY REQD	QTY REQD	QTY REQD	QTY REQD -1	FIND NUMBER	PART OR IDENTIFYING NUMBER	NOMENCLATURE OR DESCRIPTION	ZONE	MATERIAL AND SPECIFICATION	CODE IDENT NUMBER	HT TR	FINISH	PT MK	REV LTR
						156		BACB30MB6A6U	BOLT		6					
						120		NAS6605-9	BOLT							
						8		NAS6605-8	BOLT							
						8		NAS6605-7	BOLT							
						48		NAS6605-3	BOLT							
						A.R.		AN960-10	WASHER		6					
						A.R.		AN960-516	WASHER							
						184		BACN10JC5CD	NUT							
						156		NAS1805-3	NUT		6					

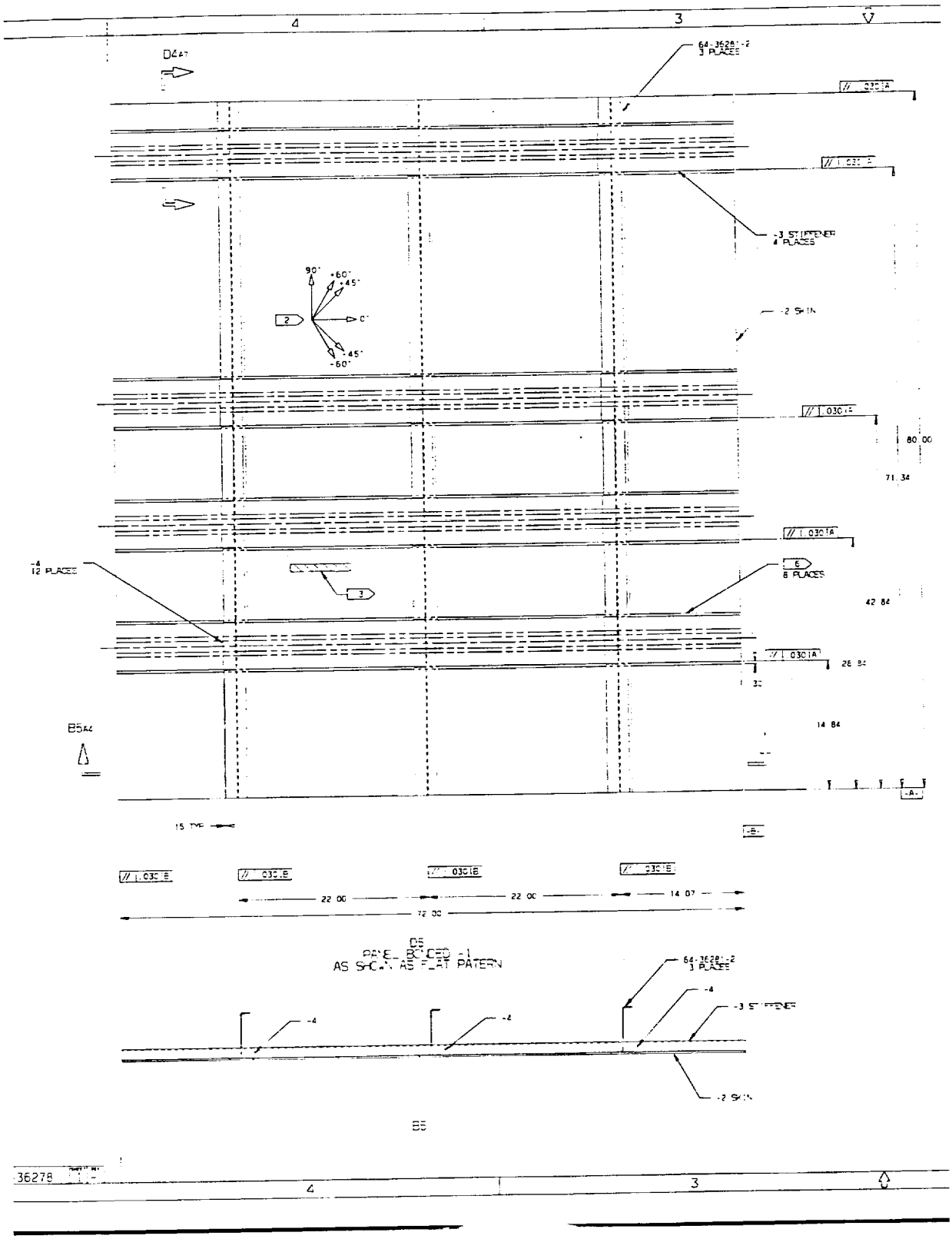
Appendix C

Panel Bond, Cutting Diagram, and Panel Assembly Drawings for Panel 3

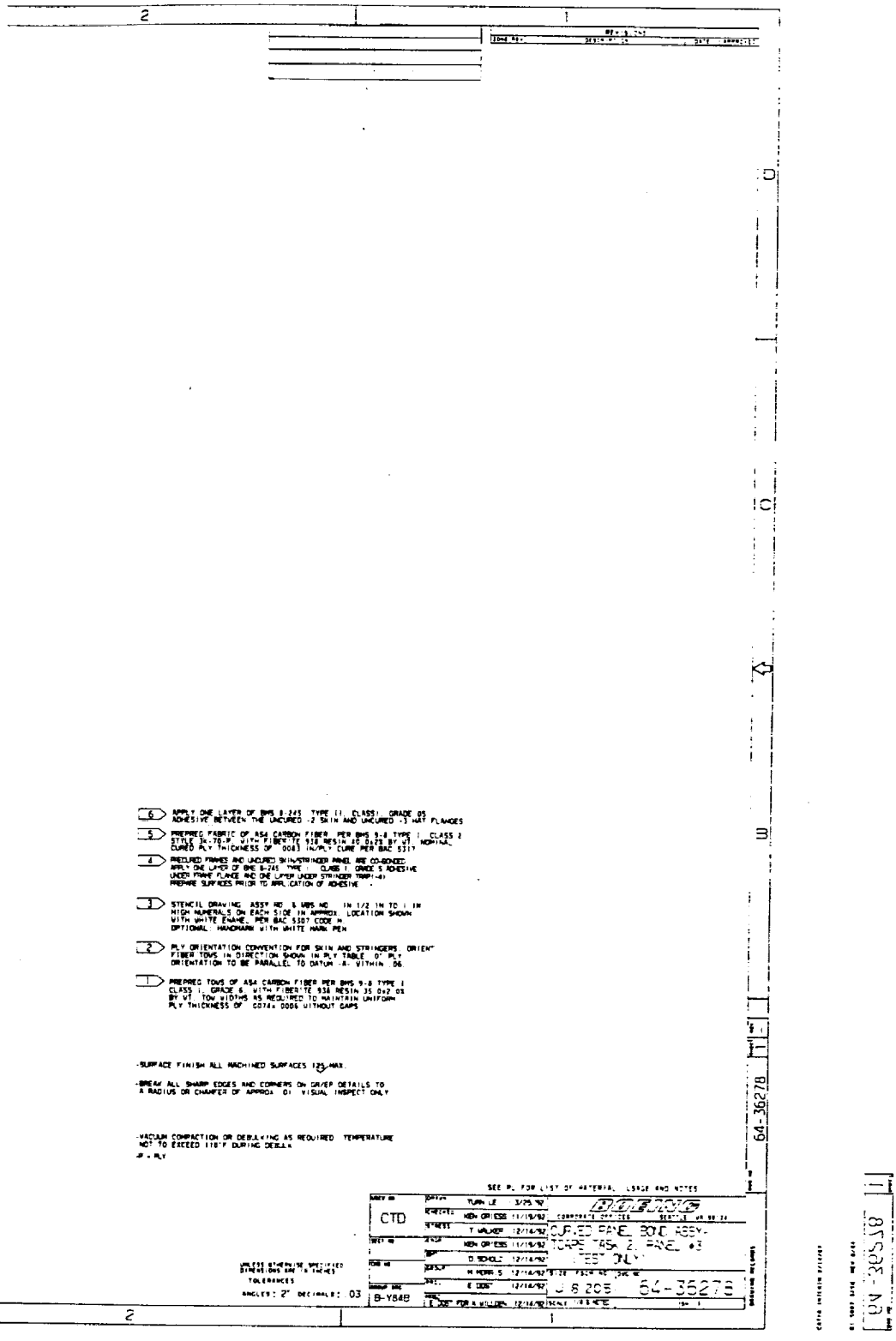


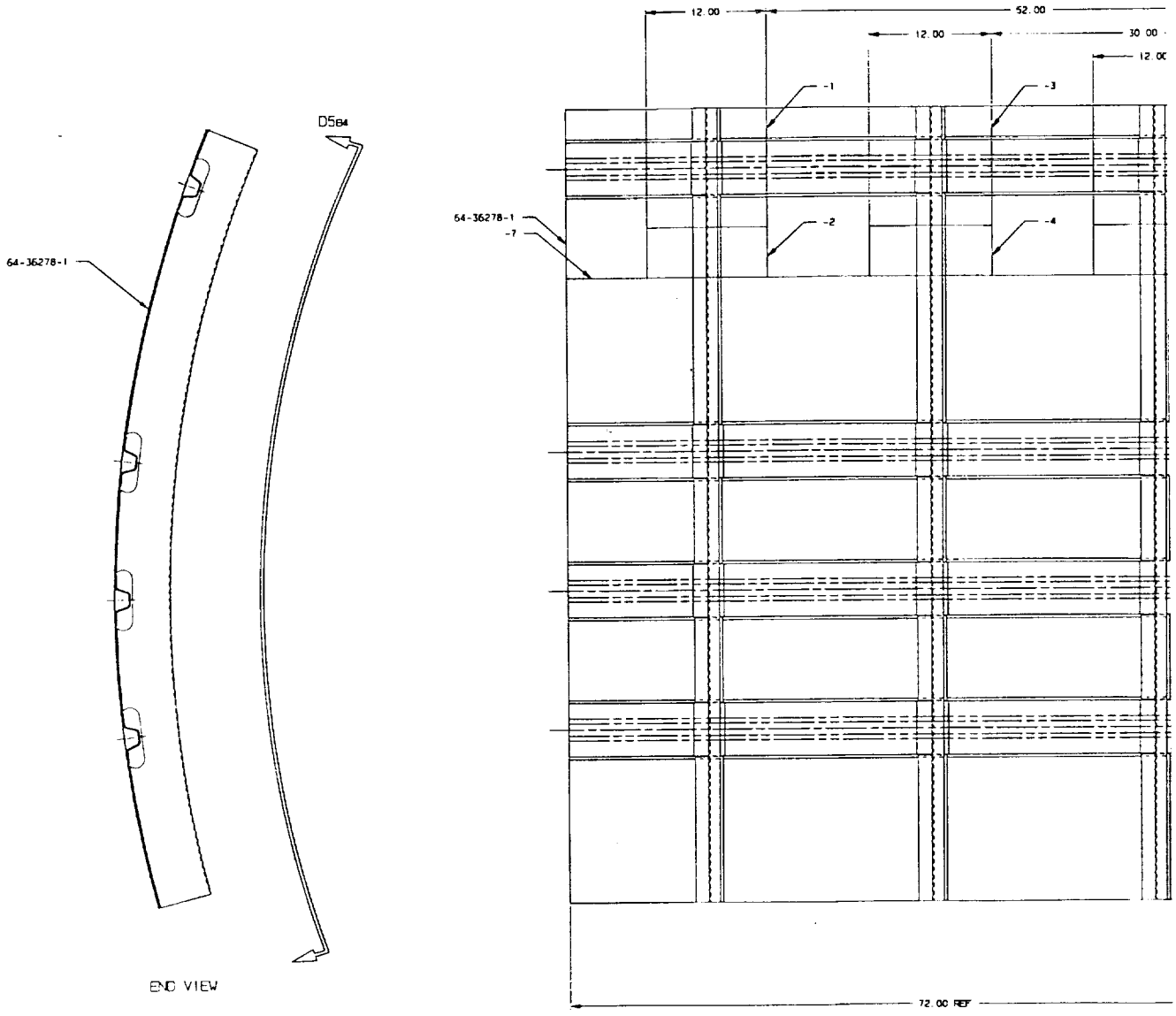
ORIGINAL PAGE IS
OF POOR QUALITY


6
5
64-35281-2
D5B4
C6C8
R122.00
-2 SKIN
TOOL SIDE
PT THRU P17
R115.50
-3 STIFFENER
4 PLACES
5.50
END VIEW
SIDE
1.25 REF
R.18 REF
.30
R.38 REF
-3 TOOL SIDE
PT THRU P23
1.85
.26
19 EQ SP
1.30 REF
2.20 REF
6
STRINGER UNCURED
SCALE NONE
81205
64-
6
5



ORIGINAL PAGE IS
OF POOR QUALITY

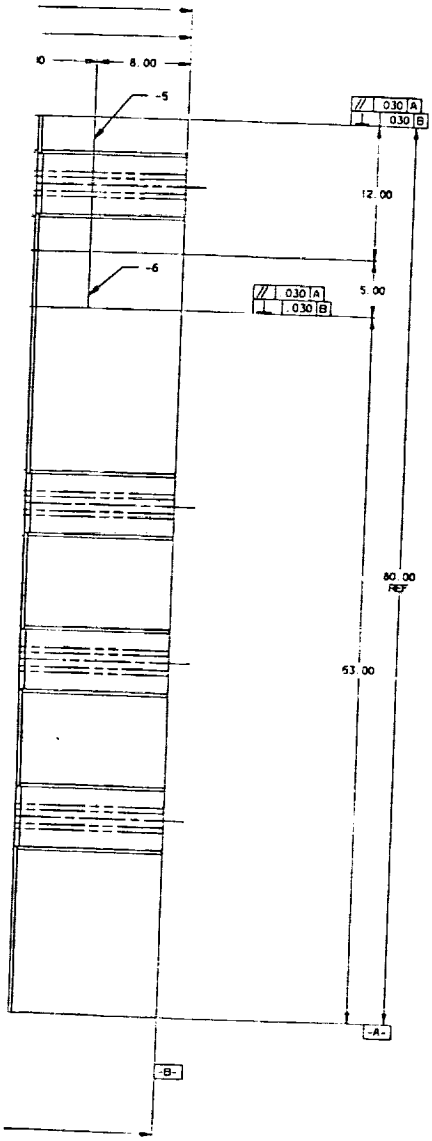

6 APPLY ONE LAYER OF BMS 8-245 TYPE II, CLASS1, GRADE 05 ADHESIVE BETWEEN THE UNCURED 2 SKIN AND UNCURED 1 HAT FLANGES
5 PREPREG FABRIC OF AS4 CARBON FIBER PER BMS 9-8 TYPE I, CLASS 2 STYLE 3K-70-P WITH FIBERITE 938 RESIN 35 0±2% BY WT NOMINAL CURED PLY THICKNESS OF .0083 IN/PLY CURE PER BAC 5317
4 PRECURED FRAMES AND UNCURED SKIN/STRINGER PANEL ARE CO-BONDED APPLY ONE LAYER OF BMS 8-245 TYPE I, CLASS 1 ONDE 5 ADHESIVE UNDER FRAME FLANGE AND ONE LAYER UNDER STRINGER TRAPI-41 PREPARE SURFACES PRIOR TO APPLICATION OF ADHESIVE
3 STENCIL DRAWING, ASSY NO. & MPS NO. IN 1/2 IN TO 1 IN HIGH NUMERALS ON EACH SIDE IN APPROX. LOCATION SHOWN WITH WHITE ENAME, PER BAC 5307 CODE H OPTIONAL: MARDMARK WITH WHITE MARK PEN
2 PLY ORIENTATION CONVENTION FOR SKIN AND STRINGERS ORIENT FIBER TOWS IN DIRECTION SHOWN IN PLY TABLE 0° PLY ORIENTATION TO BE PARALLEL TO DATUM A WITHIN .06
1 PREPREG TOWS OF AS4 CARBON FIBER PER BMS 9-8 TYPE I CLASS 1 GRADE 6 WITH FIBERITE 938 RESIN 35 0±2 0% BY WT TOW WIDTHS AS REQUIRED TO MAINTAIN UNIFORM PLY THICKNESS OF .0074 .0006 WITHOUT GAPS
-SURFACE FINISH ALL MACHINED SURFACES 125 MAX.
-BREAK ALL SHARP EDGES AND CORNERS ON DRAWING DETAILS TO A RADIUS OR CHAMFER OF APPROX .01 VISUAL INSPECT ONLY
-VACUUM COMPACTION OR DEBULKING AS REQUIRED TEMPERATURE NOT TO EXCEED 110°F DURING DEBULK
P = PLY
SEE PL FOR LIST OF MATERIAL, LOCAL AND NOTES
CTD
TURN LE 3/25/92
MEN OR ESS 11/15/92
T WALKER 12/14/92
MEN OR ESS 12/14/92
D SCHOLZ 12/14/92
M MERR S 12/14/92
E DOS 12/14/92
CURED PANEL BOX ASSY-
TORE TAS 2 PANEL #3
TEST ONLY
J 8 205
64-36278
B-Y848
UNLESS OTHERWISE SPECIFIED DIMENSIONS ARE IN INCHES
TOLERANCES
ANGLES: 2° DECIMALS: 03
64-36278
UV-305J30



D5
SKIN AS SHOWN AS FLATPATERN
DIMENSION MEASURE ON
OUTSIDE MOLD LINE

81205	54-36286	1	-

5 4



-USE OF MANUFACTURING EXCESS MAY BE REQUIRED TO PROVIDE FOR .25 RDIF TYP.

-HAND MARK PARTS WITH WHITE MARKING PEN.

-SURFACE FINISH ALL MACHINED SURFACES 125 MAX.

-BREAK ALL SHARP EDGES AND CORNERS ON OP/EP DETAILS TO A RADIUS OR CHAMFER OF APPROX .01. VISUAL INSPECT ONLY.

SEE PL FOR LIST OF MATERIAL, USAGE AND NOTES

UNLESS OTHERWISE SPECIFIED DIMENSIONS ARE IN INCHES
TOLERANCES:
ANGLES: 2° DECIMALS: .03

CTD	TURN LE	7/20/92
		9/4/92
		9/11/92
8-9848		9/11/92

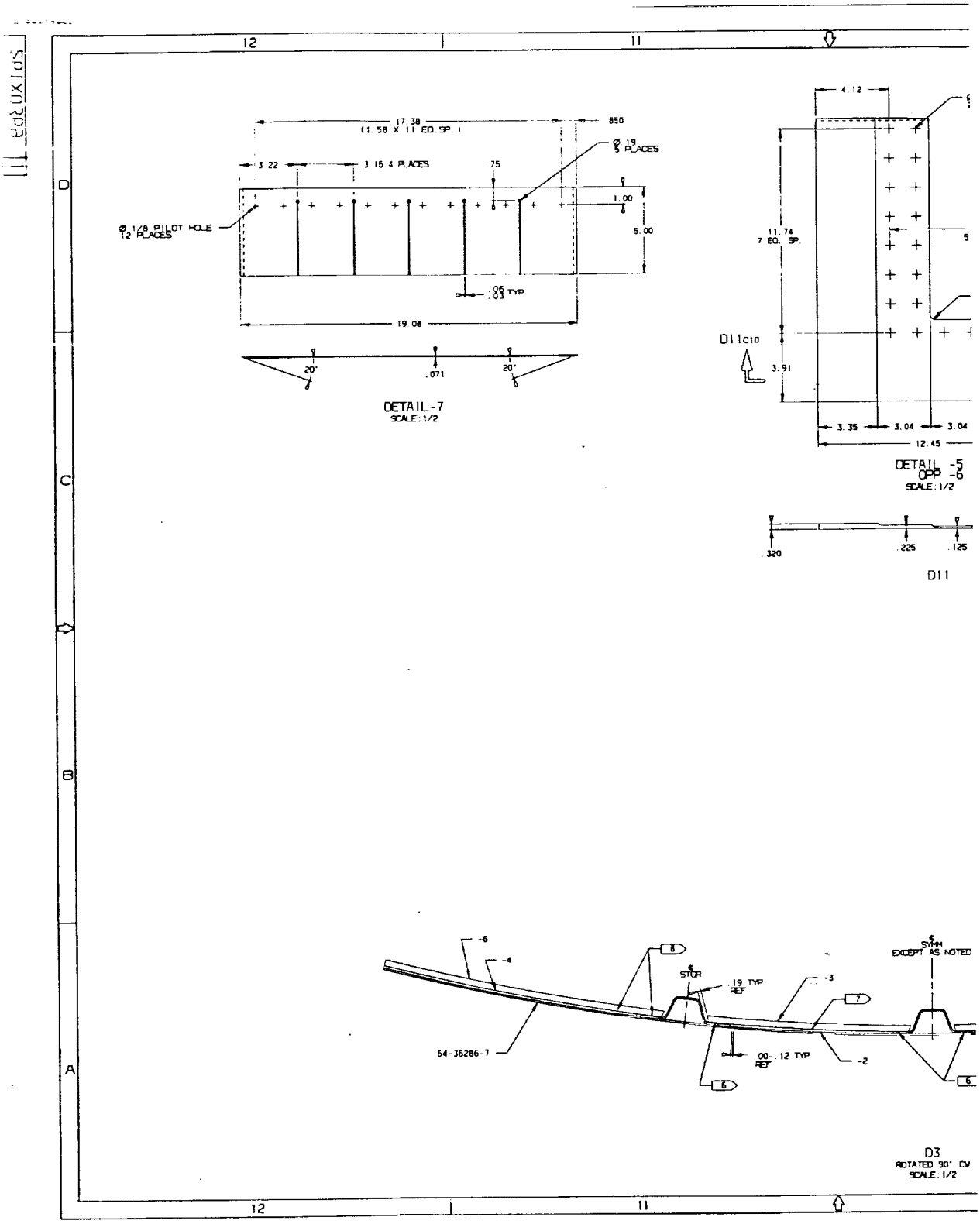
BOEING
COMMERCIAL AIRPLANE GROUP
SEATTLE, WASHINGTON 98124

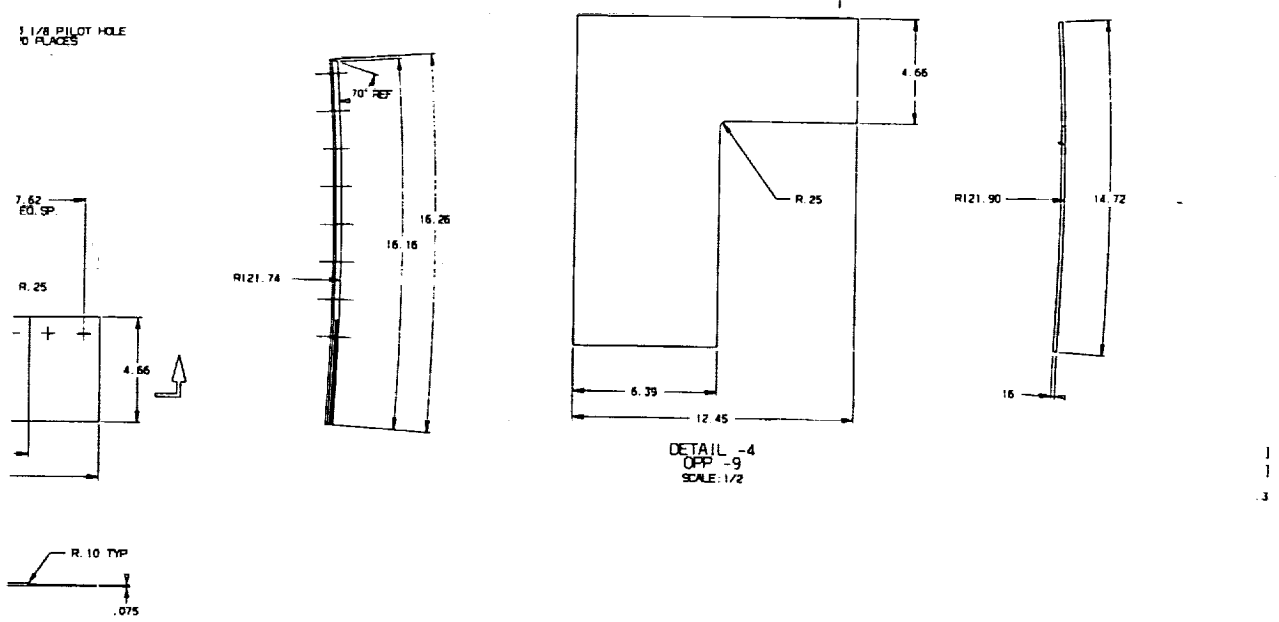
CURVED PANEL CUTTING DIAGRAM-
TCAPS TASK 2, PANEL #3
(TEST ONLY)

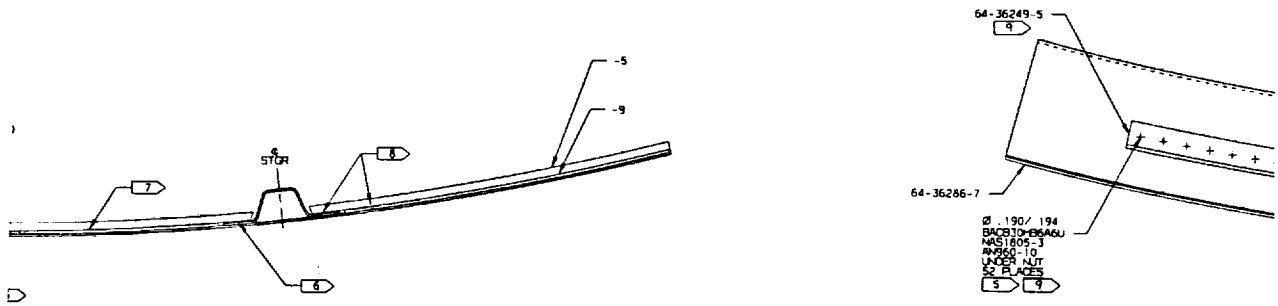
SIZE J | FSCM NO 81205 | DWG NO 64-36286 | REV

SCALE 1/8 | SHT 1

64-36286


12
11
D
C
B
A
17.38
(11.58 X 1.1 EQ. SP.)
.850
3.22
3.15 4 PLACES
.75
Ø .19
5 PLACES
1.00
5.00
Ø.1/8 PILOT HOLE
12 PLACES
.06
.03 TYP
19.08
20°
.071
20°
DETAIL-7
SCALE: 1/2
4.12
11.74
7 EQ. SP.
D11C10
3.91
3.35
3.04
3.04
12.45
DETAIL -5
OPP -6
SCALE: 1/2
.320
.225
.125
D11
-6
-4
8
STOR
.19 TYP
REF
-3
7
SYMM
EXCEPT AS NOTED
64-36286-7
.00-.12 TYP
REF
-2
6
6
D3
ROTATED 90° CW
SCALE: 1/2

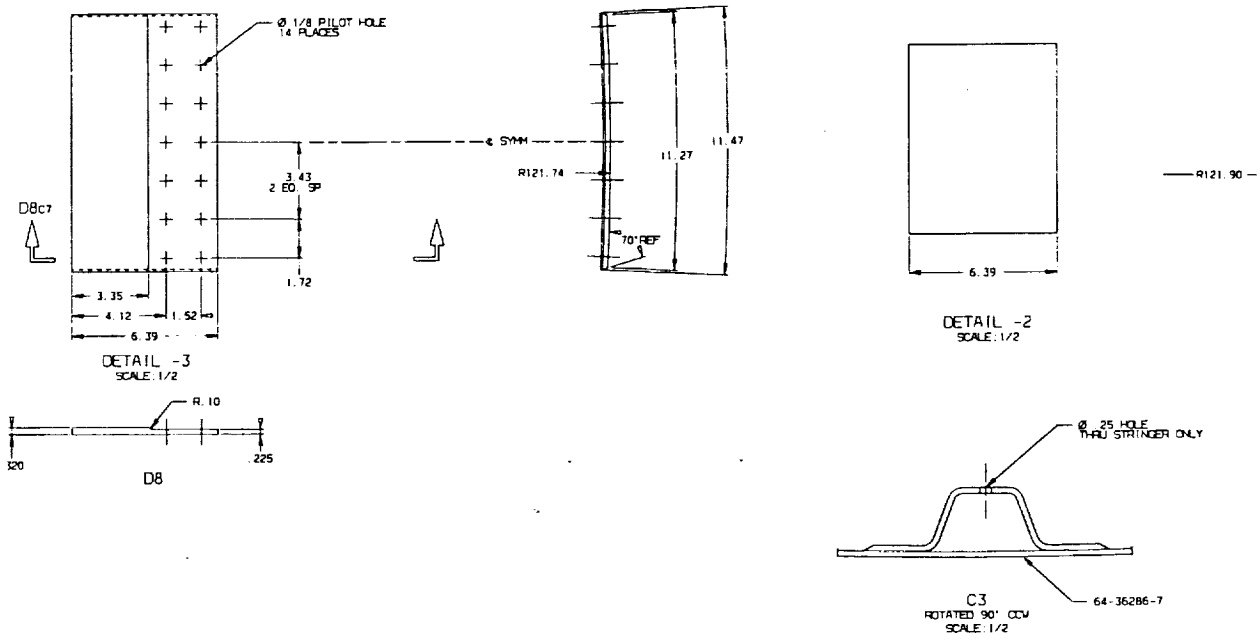


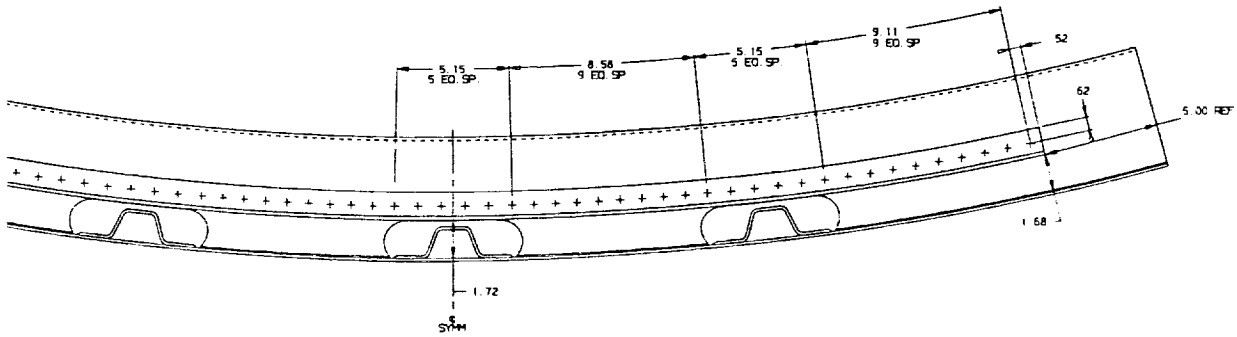


BOEING PROPRIETARY
THE INFORMATION CONTAINED HEREIN IS PROPRIETARY TO THE BOEING COMPANY AND SHALL NOT BE REPRODUCED OR DISCLOSED IN WHOLE OR IN PART OR USED FOR ANY PURPOSE EXCEPT WHEN SUCH USER POSSESSES DIRECT WRITTEN AUTHORIZATION FROM THE BOEING COMPANY

81205	251X0369	SHEET 1	REV -

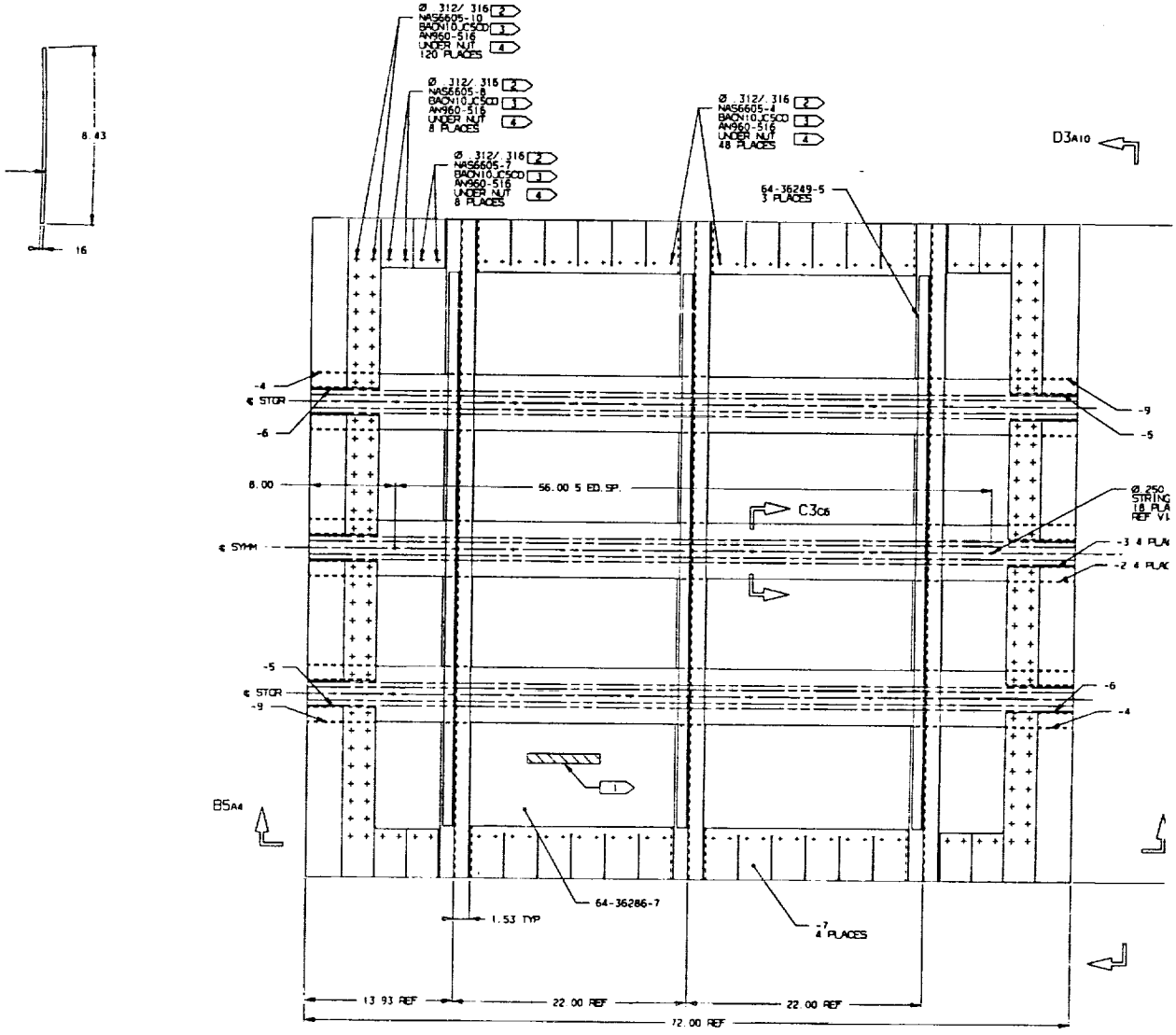
10
9
8

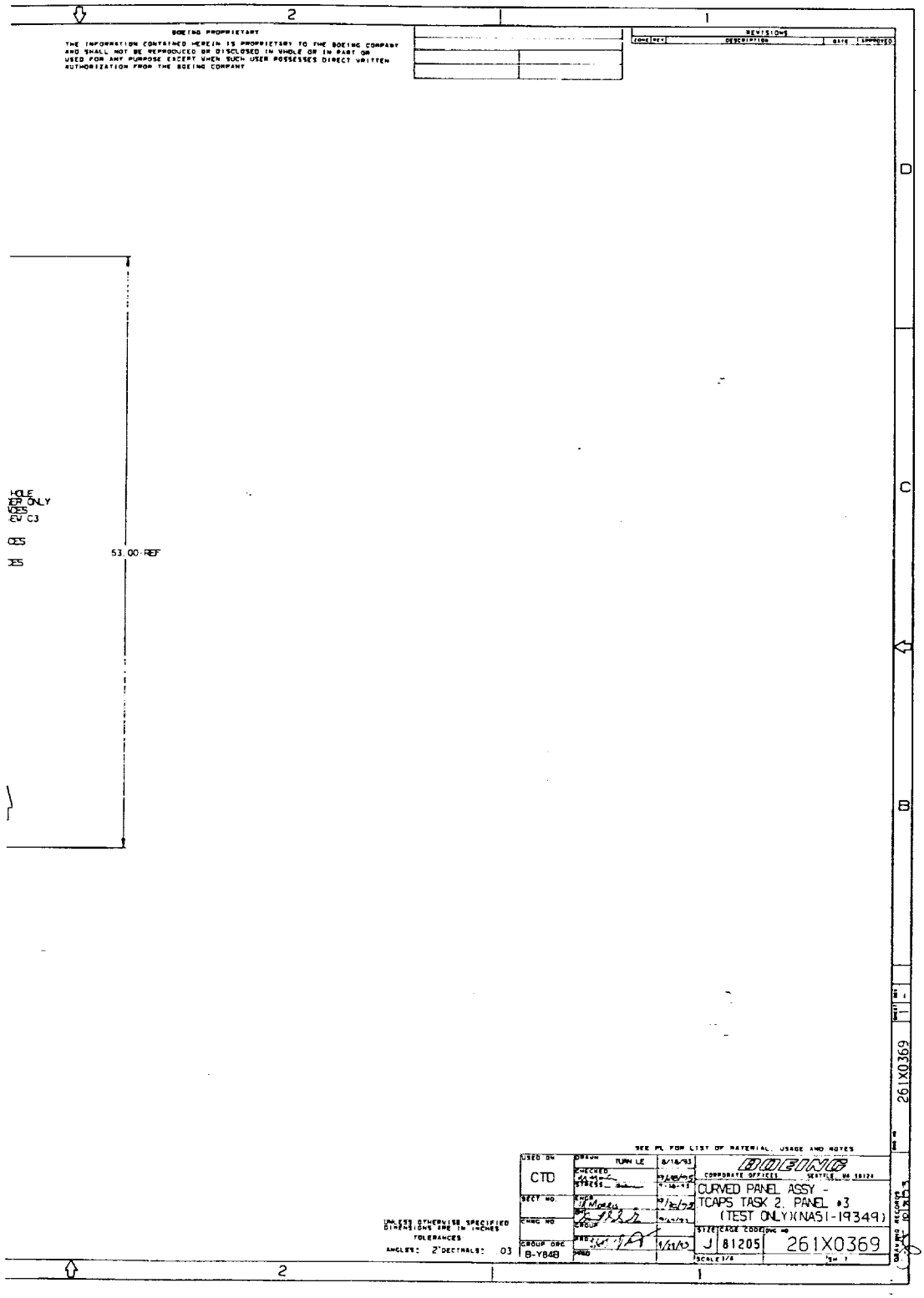




TYPICAL FRAME SECTION
SCALE: 1/2

BOEING PROPRIETARY
THE INFORMATION CONTAINED HEREIN IS PROPRIETARY TO THE BOEING COMPANY AND SHALL NOT BE REPRODUCED OR DISCLOSED IN WHOLE OR IN PART OR USED FOR ANY PURPOSE EXCEPT WHERE SUCH USE POSSESSES DIRECT WRITTEN AUTHORIZATION FROM THE BOEING COMPANY


5
4
3
8.43
16
Ø .312/.316
NAS6605-10
BACN10JC5CD
AN960-516
UNDER NUT
120 PLACES
Ø .312/.316
NAS6605-8
BACN10JC5CD
AN960-516
UNDER NUT
8 PLACES
Ø .312/.316
NAS6605-7
BACN10JC5CD
AN960-516
UNDER NUT
8 PLACES
Ø .312/.316
NAS6605-4
BACN10JC5CD
AN960-516
UNDER NUT
48 PLACES
D3A10
64-36249-5
3 PLACES
-4
℄ STGR
-6
8.00
56.00 5 ED. SP.
C3C6
℄ SYMM
-5
℄ STGR
-9
B5A4
64-36286-7
1.53 TYP
-7
4 PLACES
-9
-5
-6
-4
13.93 REF
22.00 REF
22.00 REF
72.00 REF
PANEL ASSY-1
SHOWN AS FLAT PATTERN
-5
-9
-7
-7
64-36249-5
3 PLACES
-6
-4
64-36286-7
B5
61205
251X0369
5
4
3


BOEING PROPRIETARY
THE INFORMATION CONTAINED HEREIN IS PROPRIETARY TO THE BOEING COMPANY AND SHALL NOT BE REPRODUCED OR DISCLOSED IN WHOLE OR IN PART OR USED FOR ANY PURPOSE EXCEPT WHEN SUCH USER POSSESSES DIRECT WRITTEN AUTHORIZATION FROM THE BOEING COMPANY
REVISIONS
ZONE REV DESCRIPTION DATE APPROVED
HOLE
JER ONLY
OES
EV C3
OES
ES
53.00 REF
SEE PL FOR LIST OF MATERIAL, USAGE AND NOTES
USED ON
CTD
DRAWN TURN LE 8/18/93
CHECKED
STRESS
SECT NO.
ENGR
GROUP
CHNG NO
GROUP ORG
B-Y848
PROJ ENGR
UNLESS OTHERWISE SPECIFIED DIMENSIONS ARE IN INCHES
TOLERANCES
ANGLES: 2° DECIMALS: .03
BOEING
CORPORATE OFFICES SEATTLE, WA 98124
CURVED PANEL ASSY -
TCAPS TASK 2, PANEL #3
(TEST ONLY)(NAS1-19349)
SIZE CAGE CODE DWG NO
J 81205 261X0369
SCALE 1/6
SHT 1
261X0369
SHEET NO 1
DRAWING RECORDS

PARTS LIST

REVISION STATUS												
		ADDED SHEETS						ADDED SHEETS				
SHEET	LTR	SHEET	LTR	SHEET	LTR	SHEET	LTR	SHEET	LTR	SHEET	LTR	
1	-											
2	-											
3	-											
4	-											
5	-											

PART NUMBER	APPLICATION			DVG SH NUMBER	REV LTR
	NEXT ASSY	USED ON	EFFECTIVITY		
-1	113X9003	TEST ONLY			

CAD DRAWING
(NO DATASET RELEASED)

ENGINEERING REFERENCE ONLY
CAD FILE NAME: CATIAX.V2R2.NSTGRPAT.MAP
DATASET NAME: 261X0369M01-- CURVED PANEL ASSY TCAPS PANEL #3

DVG ORIG BY B-Y84B

CONTR		
ORN TUAN LE	8/18/93	
CHK	9/28/93	
ENGR STRESS: J. Bodine	9-29-93	
ORG		
PROJ	9/29/93	
BHT	9/20/93	

THE BOEING COMPANY
STRUCTURES LABORATORY SEATTLE, WASHINGTON 98124

CURVED PANEL ASSY-
TCAPS TASK 2, PANEL #3
(TEST ONLY) (NAS1-19349)

CODE IDENT NO		SH 1 OF 5	REV LTR
81205	PL 261X0369		-

PARTS LIST	THE BOEING COMPANY STRUCTURES LABORATORY SEATTLE, WASHINGTON 98124	CODE IDENT NUMBER 81205	PL 261X0369	SHEET 2	REV -

REVISIONS				REVISIONS			
LTR	DESCRIPTION	DATE	APPROVED	LTR	DESCRIPTION	DATE	APPROVED

PARTS LIST	THE BOEING COMPANY STRUCTURES LABORATORY SEATTLE, WASHINGTON 98124	CODE IDENT NUMBER 81205	PL 261X0369	SHEET 3	REV -

NOTES

-INSTALL BOLT AND NUT FASTENERS PER BAC 5009 & BAC 5063.

-SURFACE FINISH ALL MACHINED SURFACES 125 MAX.

-TRIM AND MACHINE GR/EP PARTS TO THE REQUIREMENTS OF BAC 5578.

-BREAK ALL SHARP EDGES AND CORNERS ON GR/EP DETAILS TO A RADIUS OR CHAMFER OF APPROX .01. VISUAL INSPECT ONLY.

-FORM, PUNCH, STRAIGHTEN, BREAK SHARP EDGES AND FIT METAL PARTS PER BAC5300.

1 STENCIL DRAWING, ASSY NO. IN 1/2 IN TO 1 IN HIGH NUMERALS ON EACH SIDE IN APPROX. LOCATION SHOWN WITH WHITE ENAMEL PER BAC 5307. OPTIONAL: HANDMARK WITH WHITE MARK PEN.

2 FASTENER HEAD NEAR SIDE.

3 UP TO (2) WASHERS UNDER NUT IS ACCEPTABLE FOR LONGER GRIP LENGTH FASTENERS.

4 TORQUE FASTENERS 90-125 IN-LBS.

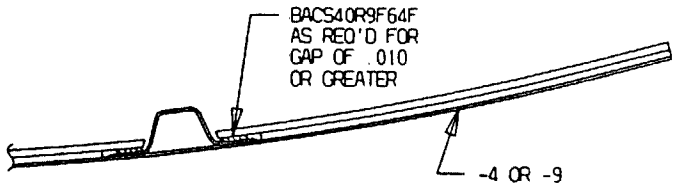
5 TORQUE FASTENERS 30-40 IN-LBS.

6 FOR GAP .010 OR GREATER USE BACS40R9F64F SHIM AS REQ'D. LOCATE AND CENTER TO EXISTING HOLES IN DOUBLERS. Ø .375 HOLE THRU BACS40R9F64F SHIM ONLY.

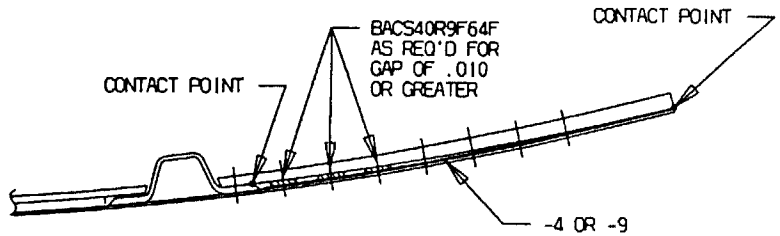
7 FOR GAP .010 OR GREATER USE BACS40R64F84F SHIM AS REQ'D. LOCATE AND CENTER TO EXISTING HOLES IN DOUBLERS. Ø .375 HOLE THRU BACS40R64F84F SHIM ONLY.

NOTES

8 IF -4 OR -9 HIGHER THAN STRINGER FLANGE USE OPT#1 BELOW. IF -4 OR -9 LOWER THAN STRINGER FLANGE USE OPT#2 BELOW. FOR GAP .010 OR GREATER USE BACS40R9F64F SHIM AS REQ'D. LOCATE AND CENTER TO EXISTING HOLES IN DOUBLERS. Ø .375 HOLE THRU SHIMS ONLY.



OPTION #1



OPTION #2

9 OPTIONAL P/N.

PARTS LIST

THE BOEING COMPANY
STRUCTURES LABORATORY SEATTLE, WASHINGTON 98124

CODE IDENT NUMBER 81205 | PL 261X0369 | SHEET 4 | REV LTR —

EAMR NUMBER	QTY REQD	QTY REQD	QTY REQD	QTY REQD	QTY REQD	QTY REQD -1	FIND NUMBER	PART OR IDENTIFYING NUMBER	NOMENCLATURE OR DESCRIPTION	ZONE	MATERIAL AND SPECIFICATION	CODE IDENT NUMBER	HT TR	FINISH	PT MK	REV LTR
						-		-1	TEST PANEL-ASSY	A4-1						
						4		-2	DOUBLER	C6-1	.16 X 6.5 X 8.5 7075-T6 ALUM. SHEET				M	
						4		-3	DOUBLER	C7-1	.375 X 6.5 X 11.5 7075-T6 ALUM. PLATE OR T651 BARE OR CLAD				M	
						2		-4	DOUBLER	C9-1	.16 X 12.5 X 14.8 7075-T6 ALUM. SHEET				M	
						2		-9	OPP-4	C9-1	.16 X 12.5 X 14.8 7075-T6 ALUM. SHEET				M	
						2		-5	DOUBLER	C10-1	.375 X 12.5 X 16.3 7075-T6 ALUM. PLATE OR T651 BARE OR CLAD				M	
						2		-6	OPP-5	C10-1	.375 X 12.5 X 16.3 7075-T6 ALUM. PLATE OR T651 BARE OR CLAD				M	
						4		-7	DOUBLER	C12-1	.071 X 5.1 X 19.1 7075-T6 ALUM. SHEET				M	
						A.R		BACS40R9F64F	SHIM							
						A.R		BACS40R64F84F	SHIM							
						1		64-36286-7	PANEL-ASSY							
						3		64-36249-5	CURVED ANGLE		9					

PARTS LIST

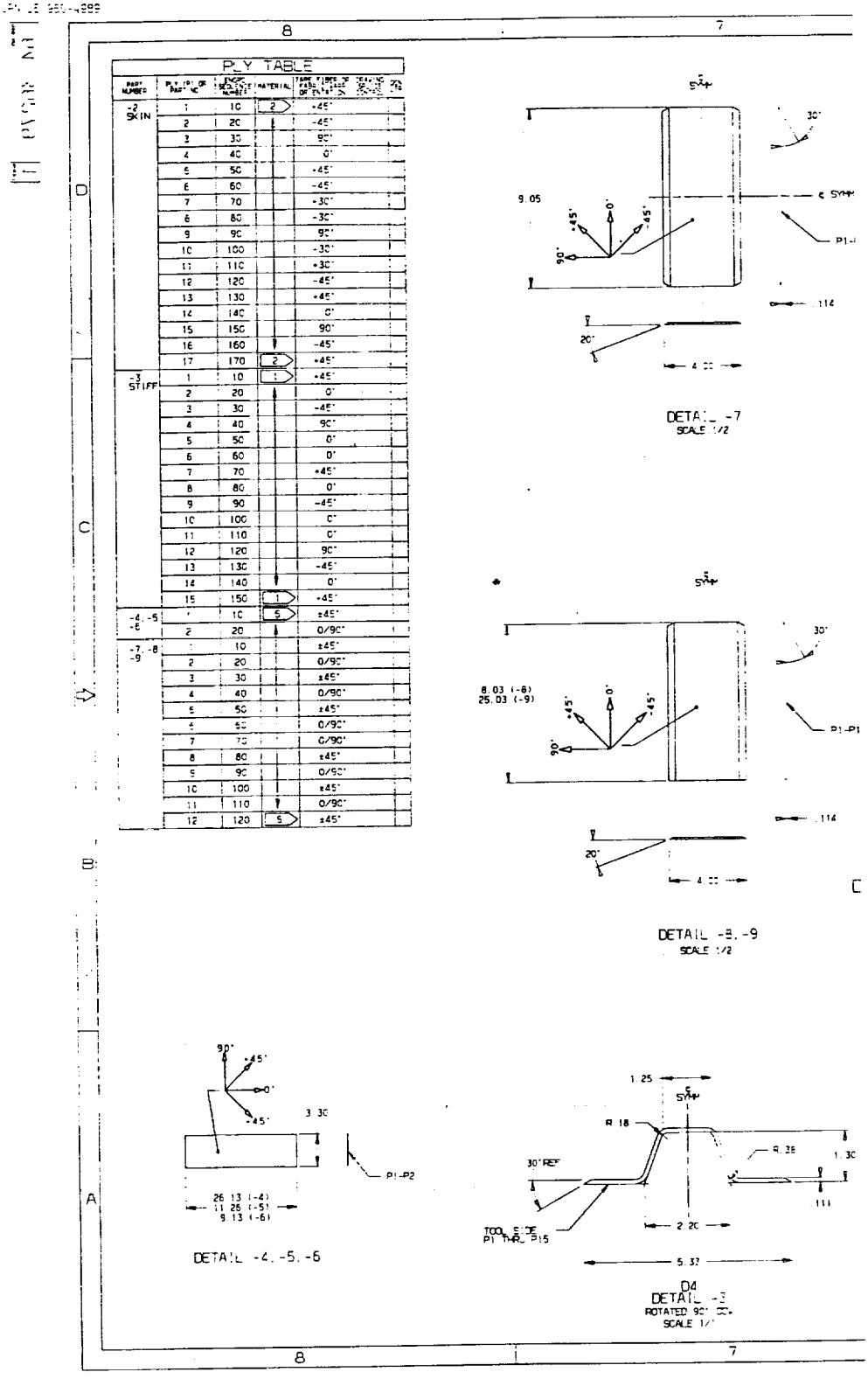
THE BOEING COMPANY
STRUCTURES LABORATORY SEATTLE, WASHINGTON 98124

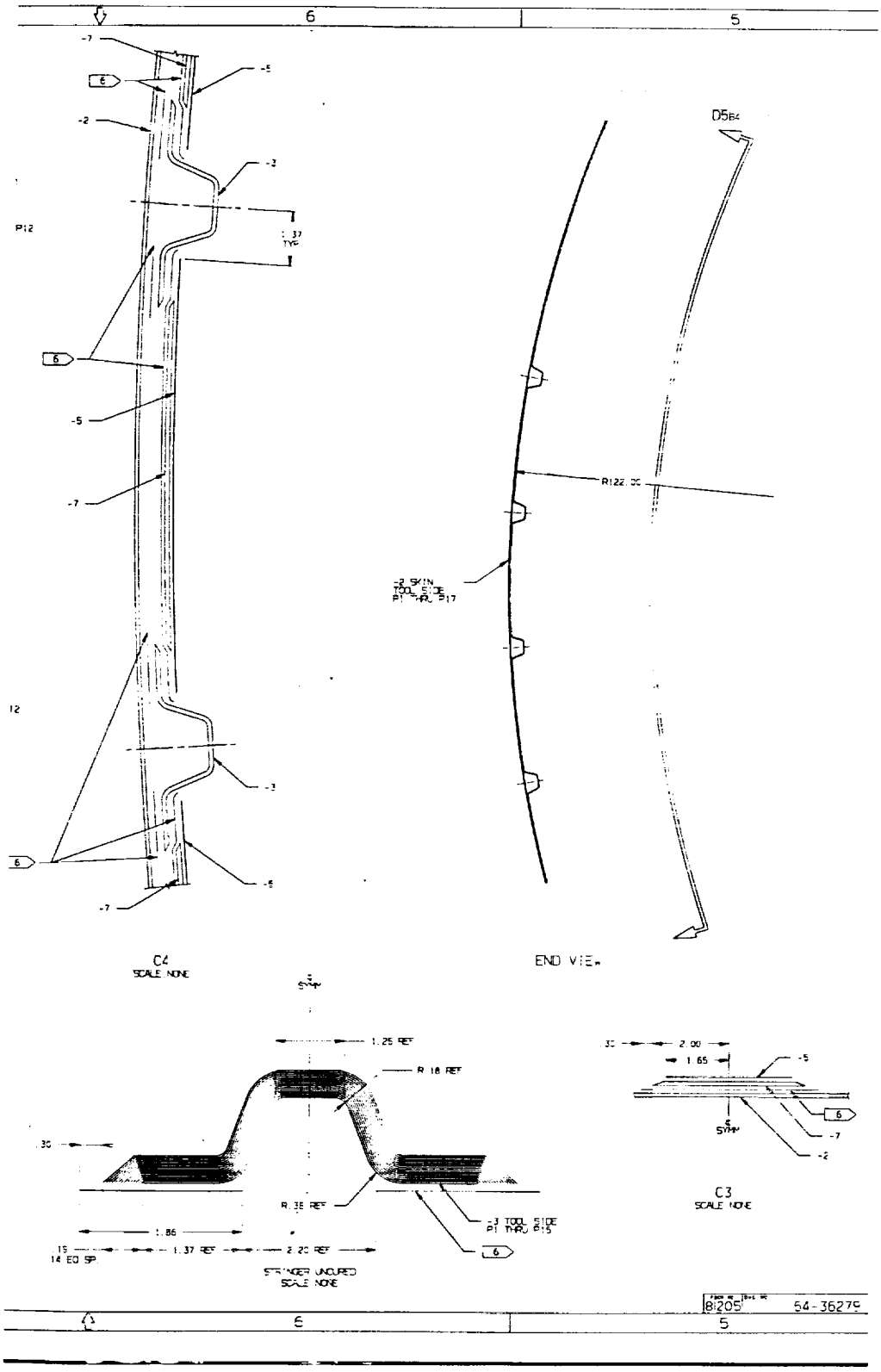
CODE IDENT NUMBER 81205 | PL 261X0369 | SHEET 5 | REV LTR –

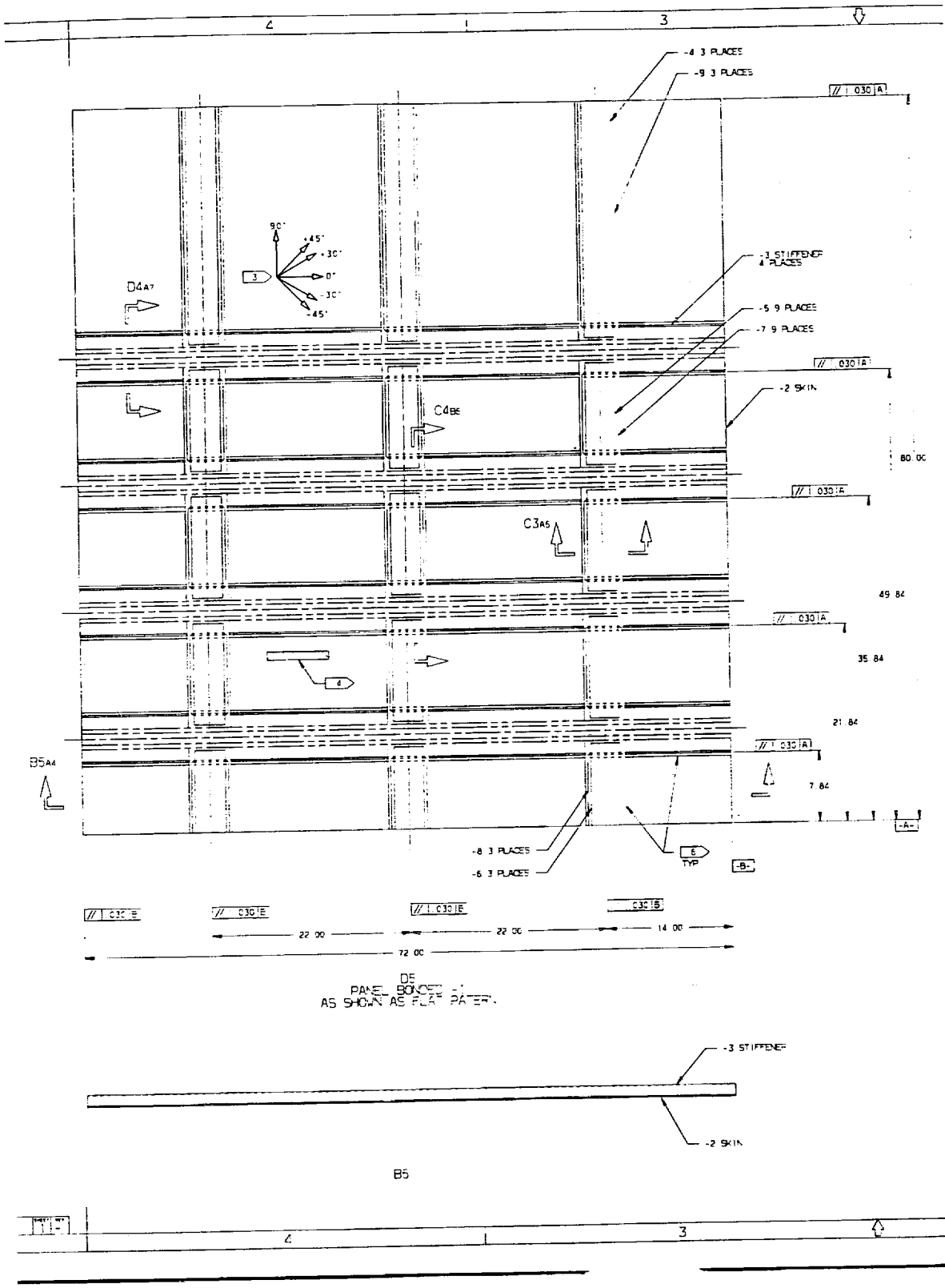
EAMR NUMBER	QTY REQD	QTY REQD	QTY REQD	QTY REQD	QTY REQD	QTY REQD -1	FIND NUMBER	PART OR IDENTIFYING NUMBER	NOMENCLATURE OR DESCRIPTION	ZONE	MATERIAL AND SPECIFICATION	CODE IDENT NUMBER	HT TR	FINISH	PI MK	REV LTR
						156		BACB30MB6A6U	BOLT		9					
						120		NAS6605-10	BOLT							
						8		NAS6605-8	BOLT							
						8		NAS6605-7	BOLT							
						48		NAS6605-4	BOLT							
						A.R.		AN960-10	WASHER		9					
						A.R.		AN960-516	WASHER							
						184		BACN10JC5CD	NUT							
						156		NAS1805-3	NUT		9					

Appendix D

Panel Bond, Cutting Diagram, and Panel Assembly Drawings for Panel 4

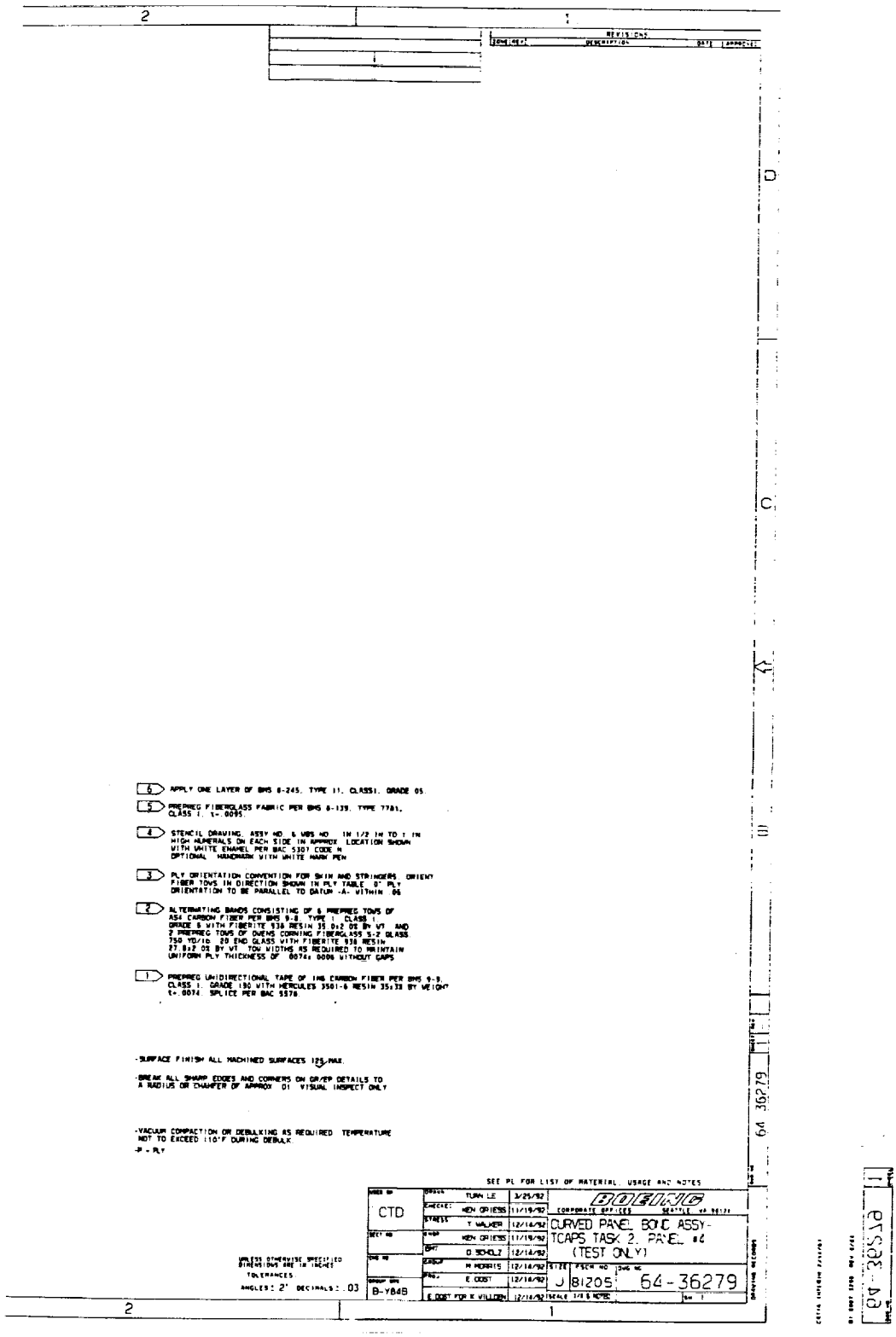

PLY TABLE
DETAIL -7
SCALE 1/2
DETAIL -8, -9
SCALE 1/2
DETAIL -4, -5, -6
DETAIL -3
ROTATED 90° CW
SCALE 1/1

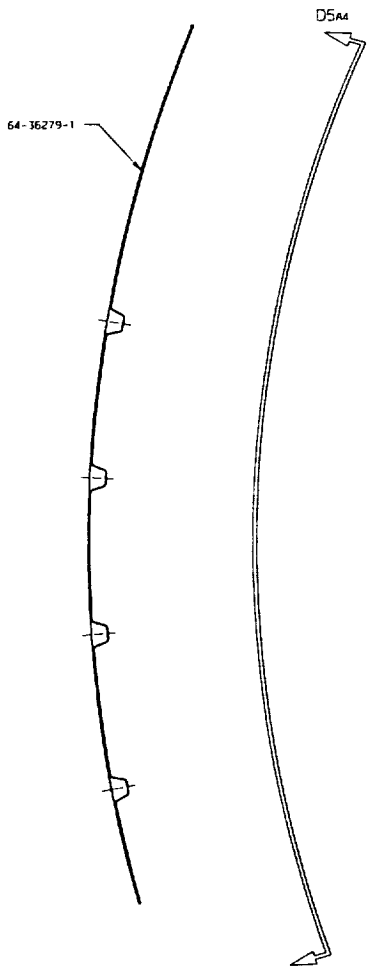

6
5
-7
-5
-2
-3
P12
.37 TYP
-5
-7
12
-3
-5
-7
C4
SCALE NONE
D5B4
R122.00
-2 SKIN TOOL SIDE P1 THRU P17
END VIEW
1.25 REF
R.18 REF
.30
R.38 REF
-3 TOOL SIDE P1 THRU P15
1.86
15
14 EQ SP
1.37 REF
2.20 REF
STRINGER UNCURED
SCALE NONE
.30
2.00
1.65
-5
-7
-2
C3
SCALE NONE
8205
54-36279
6
5



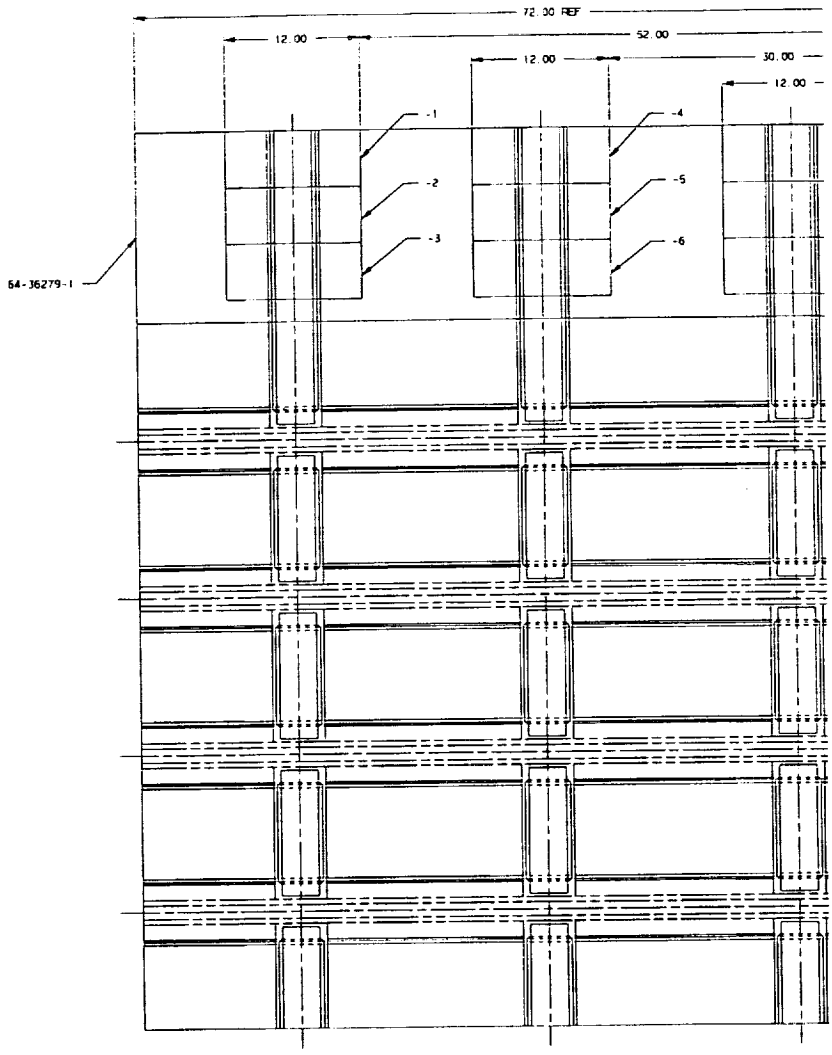
D5
PANEL BOUNDARY
AS SHOWN AS FLAT PATTERN

B5


REVISIONS
ZONE
DESCRIPTION
DATE
APPROVED
6 APPLY ONE LAYER OF BMS 8-245, TYPE II, CLASS1, GRADE 05.
5 PREPREG FIBERGLASS FABRIC PER BMS 8-139, TYPE 7781, CLASS 1, t=.0095.
4 STENCIL DRAWING, ASSY NO. & WBS NO. IN 1/2 IN TO 1 IN HIGH NUMERALS ON EACH SIDE IN APPROX. LOCATION SHOWN WITH WHITE ENAMEL PER BAC 5307 CODE N OPTIONAL: HANDMARK WITH WHITE MARK PEN
3 PLY ORIENTATION CONVENTION FOR SKIN AND STRINGERS. ORIENT FIBER TOWS IN DIRECTION SHOWN IN PLY TABLE. 0° PLY ORIENTATION TO BE PARALLEL TO DATUM -A- WITHIN .06
2 ALTERNATING BANDS CONSISTING OF 6 PREPREG TOWS OF AS4 CARBON FIBER PER BMS 9-8 TYPE I CLASS I GRADE 6 WITH FIBERITE 938 RESIN 35.0±2.0% BY WT AND 2 PREPREG TOWS OF OWENS CORNING FIBERGLASS S-2 GLASS 750 YD/LB 20 END GLASS WITH FIBERITE 938 RESIN 37.0±2.0% BY WT. TOW WIDTHS AS REQUIRED TO MAINTAIN UNIFORM PLY THICKNESS OF .0074± .0006 WITHOUT GAPS
1 PREPREG UNIDIRECTIONAL TAPE OF IMS CARBON FIBER PER BMS 9-8, CLASS 1, GRADE 190 WITH HERCULES 3501-6 RESIN 35±3% BY WEIGHT t=.0074. SPLICE PER BAC 5378.
-SURFACE FINISH ALL MACHINED SURFACES 125 μIN/IN.
-BREAK ALL SHARP EDGES AND CORNERS ON GR/EP DETAILS TO A RADIUS OR CHAMFER OF APPROX .01. VISUAL INSPECT ONLY
-VACUUM COMPACTION OR DEBULKING AS REQUIRED. TEMPERATURE NOT TO EXCEED 110°F DURING DEBULK.
-P - PLY
SEE PL FOR LIST OF MATERIAL, USAGE AND NOTES
CTD
B-Y84B
UNLESS OTHERWISE SPECIFIED DIMENSIONS ARE IN INCHES
TOLERANCES
ANGLES: 2° DECIMALS: .03
DRAWN TURAN LE 3/25/92
CHECKED KEN CRIESS 11/19/92
STRESS T WALKER 12/16/92
M MFG KEN CRIESS 11/19/92
QA D SCHOLZ 12/16/92
GROUP M MORRIS 12/16/92
PROJ E COST 12/16/92
E COST FOR R WILLSON 12/16/92
BOEING
CORPORATE OFFICES SEATTLE, WA 98124
CURVED PANEL BOLTED ASSY - TCAPS TASK 2, PANEL #2 (TEST ONLY)
SIZE J
FSCM NO 81205
DWG NO 64-36279
SCALE 1/8 SHEET 1
64-36279
D
C
B
A

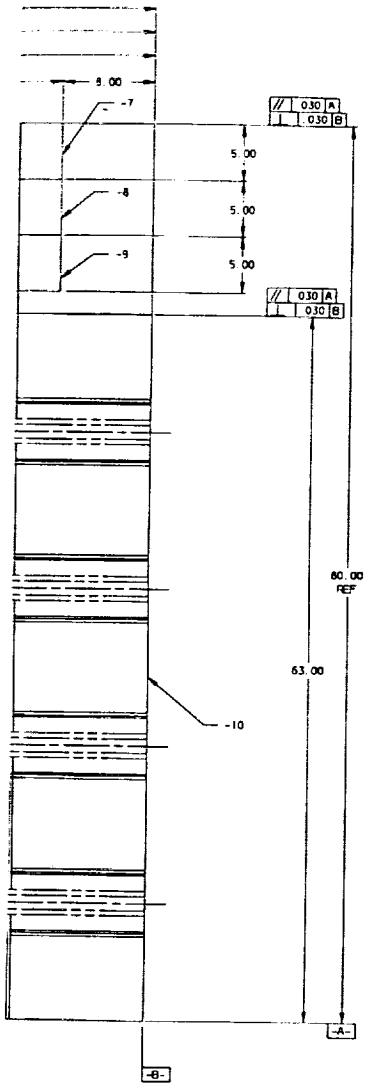


END VIEW



D5
SKIN AS SHOWN AS FLATPATERN
DIMENSION MEASURE ON
OUTSIDE MOLD LINE

81205 64-36287 1



-USE OF MANUFACTURING EXCESS MAY BE REQUIRED TO PROVIDE FOR .25 VIEW TYP.

-HAND MARK PARTS WITH WHITE MARKING PEN.

-SURFACE FINISH ALL MACHINED SURFACES 125 MAX.

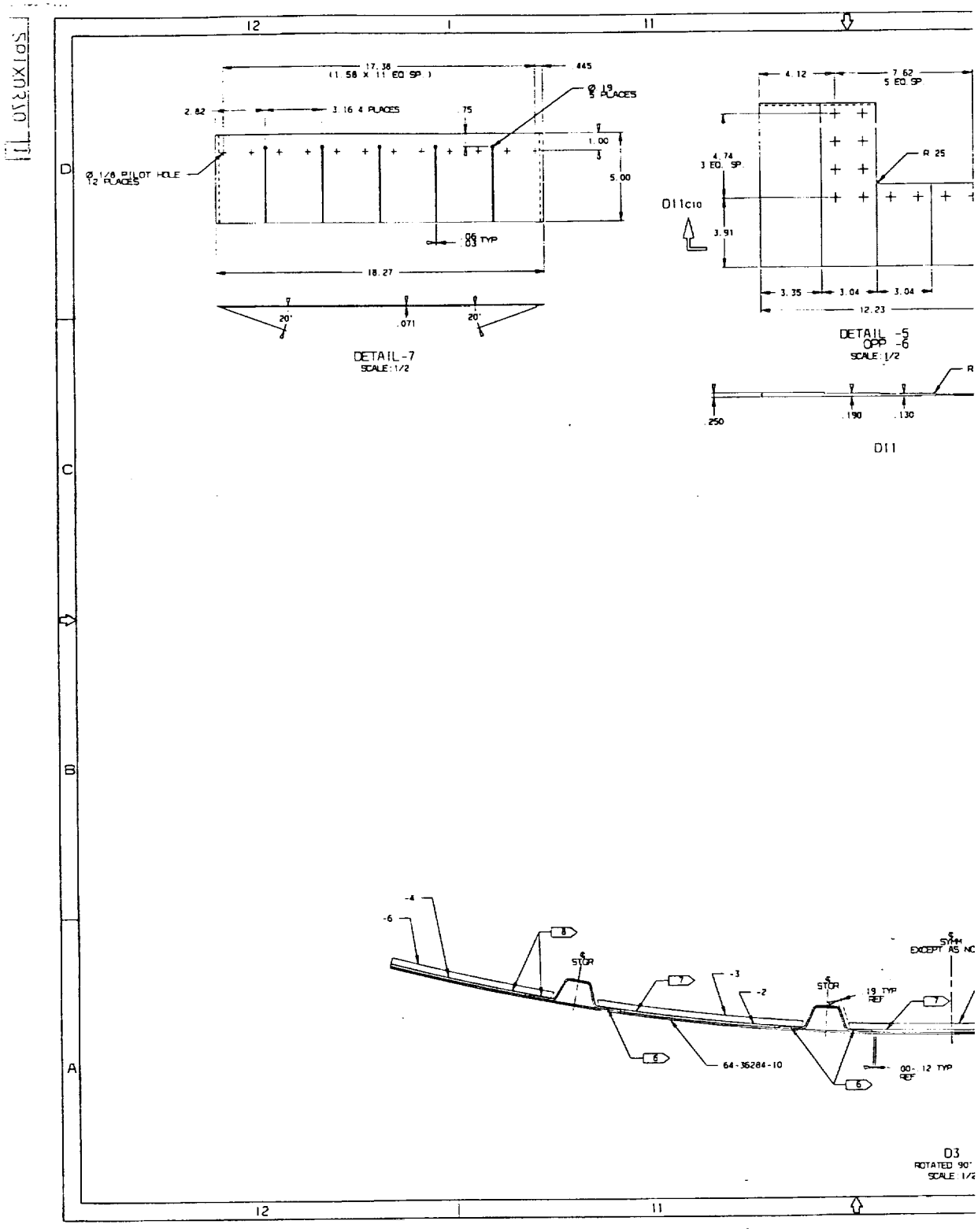
-BREAK ALL SHARP EDGES AND CORNERS ON GR/EP DETAILS TO A RADIUS OR CHAMFER OF APPROX .01. VISUAL INSPECT ONLY.

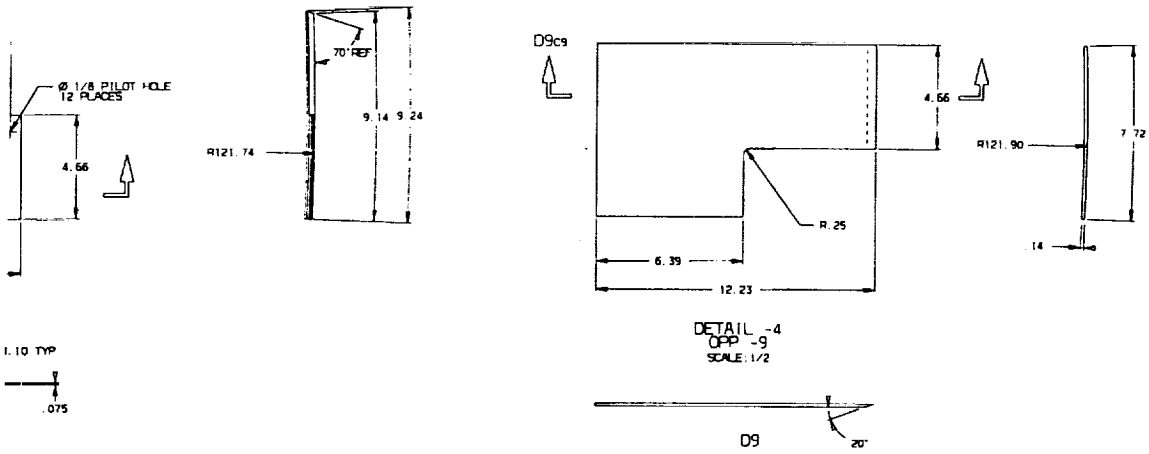
SEE PL FOR LIST OF MATERIAL, USAGE AND NOTES

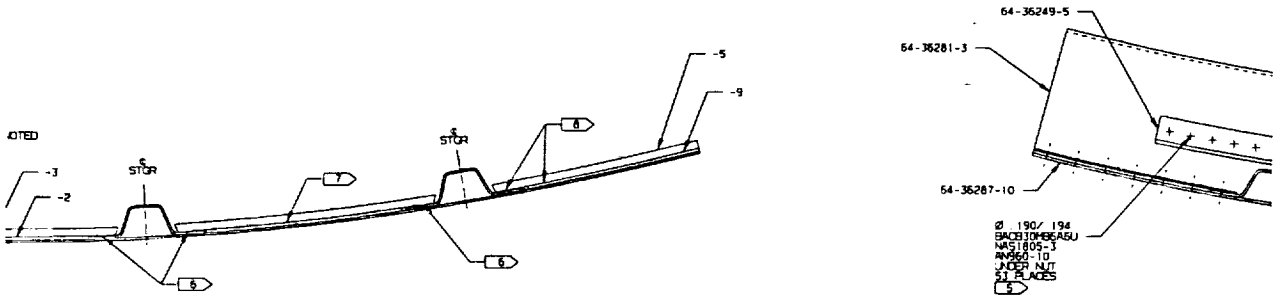
UNLESS OTHERWISE SPECIFIED DIMENSIONS ARE IN INCHES
TOLERANCES:
ANGLES ± 2° DECIMALS ± .03

CTD	DRAWN TUAN LE	7/20/92	BOEING CORPORATE OFFICES SEATTLE, WA 98124
	CHECKED		CURVED PANEL CUTTING DIAGRAM- TCAPS TASK 2, PANEL #4 (TEST ONLY)
	STRESS		
	ENGR		
	MFG		
	QUALITY		
8-Y848	ALT		SIZE D, FSCM NO. J81205, DWG NO. 64-36287, SCALE 1/4, SHT 1

64-36287


12
11
D
C
B
A
17.38
(1.58 X 11 EQ SP.)
.445
Ø .19
5 PLACES
2.82
3.16 4 PLACES
.75
1.00
5.00
Ø.1/8 PILOT HOLE
12 PLACES
.06
.03 TYP
18.27
20°
.071
20°
DETAIL-7
SCALE: 1/2
4.12
7.62
5 EQ. SP.
4.74
3 EQ. SP.
R .25
D11c10
3.91
3.35
3.04
3.04
12.23
DETAIL -5
OPP -6
SCALE: 1/2
.250
.190
.130
D11
-4
-6
8
STOR
7
-3
-2
STOR
.19 TYP
REF
7
SYM
EXCEPT AS NO
6
64-36284-10
6
.00- .12 TYP
REF
D3
ROTATED 90°
SCALE: 1/2

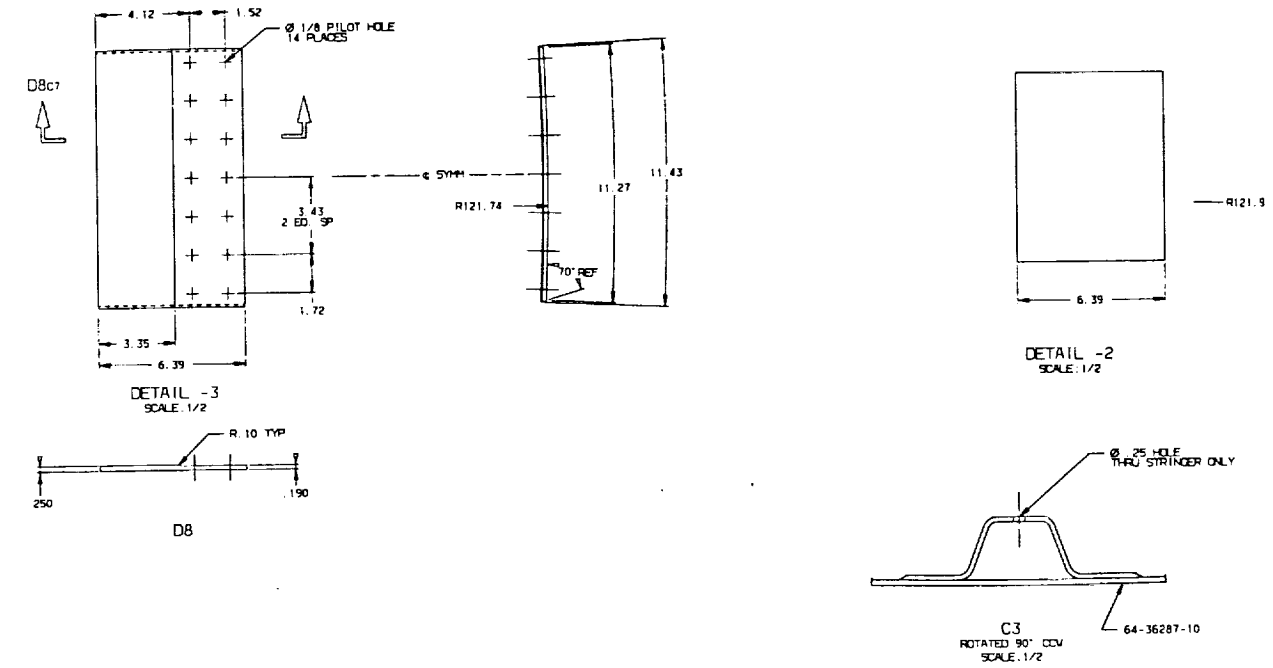


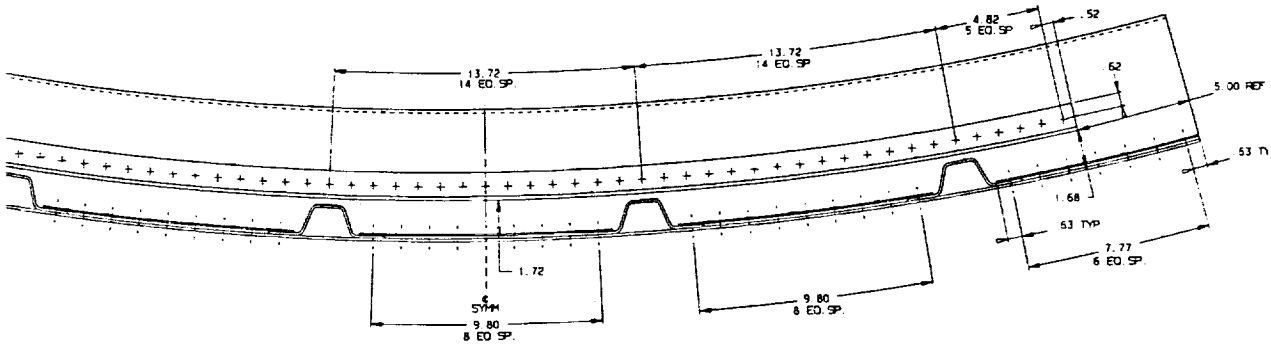


BOEING PROPRIETARY
THE INFORMATION CONTAINED HEREIN IS PROPRIETARY TO THE BOEING COMPANY AND SHALL NOT BE REPRODUCED OR DISCLOSED IN WHOLE OR IN PART OR USED FOR ANY PURPOSE EXCEPT WHEN SUCH USER POSSESSES DIRECT WRITTEN AUTHORIZATION FROM THE BOEING COMPANY

81205 261X0370 1 -

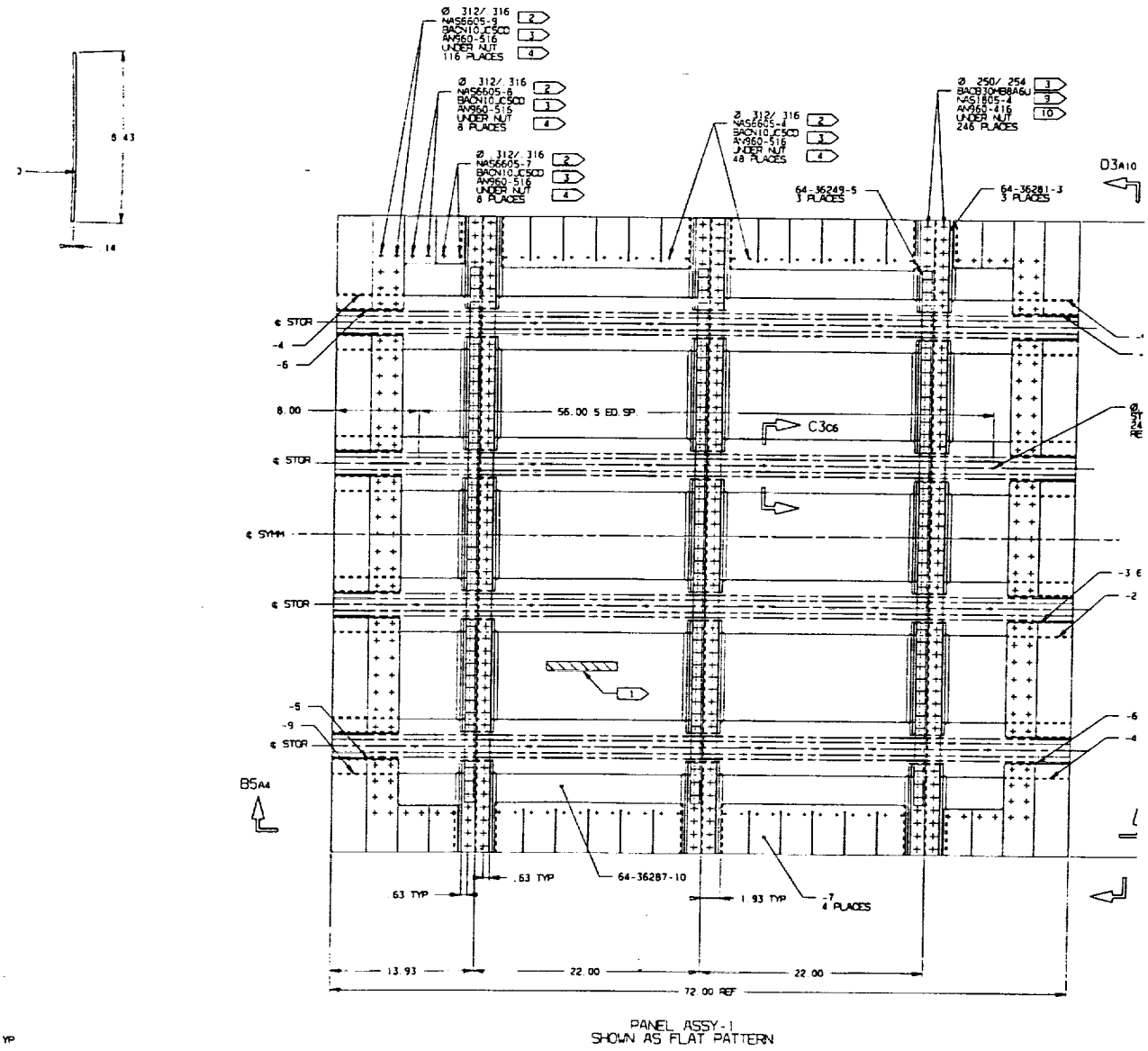
10 9 8

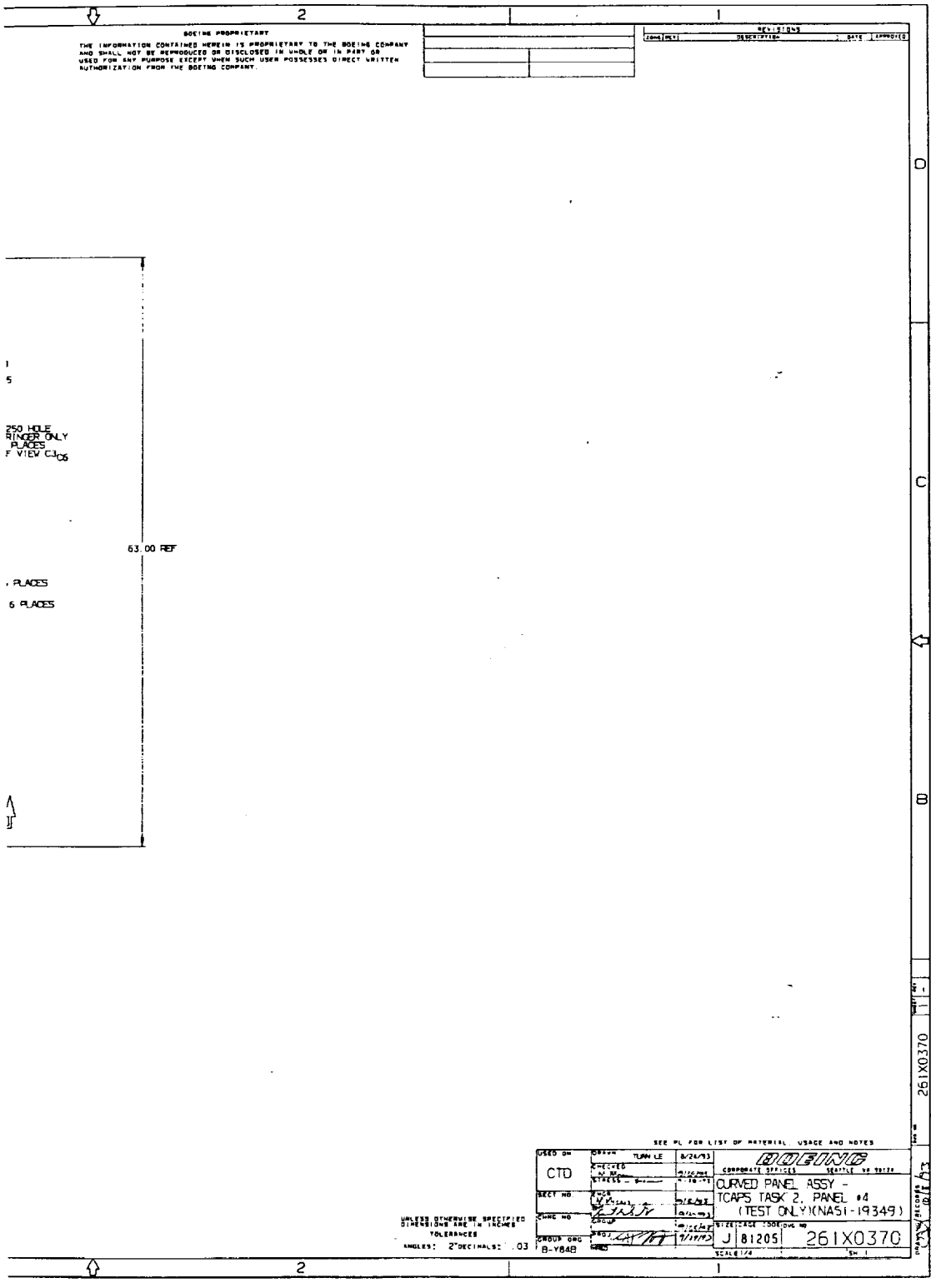




TYPICAL FRAME SECTION
SCALE: 1/2

BOEING PROPRIETARY
THE INFORMATION CONTAINED HEREIN IS PROPRIETARY TO THE BOEING COMPANY AND SHALL NOT BE REPRODUCED OR DISCLOSED IN WHOLE OR IN PART OR USED FOR ANY PURPOSE EXCEPT WHEN SUCH USER POSSESSES DIRECT WRITTEN AUTHORIZATION FROM THE BOEING COMPANY


5
4
3
Ø .312/ .316
NAS6605-9
BACN10JC5CD
AN960-516
UNDER NUT
116 PLACES
Ø .312/ .316
NAS6605-8
BACN10JC5CD
AN960-516
UNDER NUT
8 PLACES
Ø .312/ .316
NAS6605-7
BACN10JC5CD
AN960-516
UNDER NUT
8 PLACES
Ø .312/ .316
NAS6605-6
BACN10JC5CD
AN960-516
UNDER NUT
48 PLACES
Ø .250/ .254
BACB30MB8A6U
NAS1805-4
AN960-416
UNDER NUT
246 PLACES
64-36249-5
3 PLACES
64-36281-3
3 PLACES
D3A10
8.43
.14
℄ STOR
-4
-6
8.00
56.00 S ED. SP.
C3C6
℄ STOR
℄ SYMM
℄ STOR
-5
-9
℄ STOR
B5A4
.63 TYP
.63 TYP
64-36287-10
1.93 TYP
-7
4 PLACES
13.93
22.00
22.00
72.00 REF
PANEL ASSY-1
SHOWN AS FLAT PATTERN
64-36281-3
3 PLACES
64-36249-5
3 PLACES
-5
-9
-7
-7
-6
-4
64-36287-10
B5
81205
261X0370
5
4
3


BOEING PROPRIETARY
THE INFORMATION CONTAINED HEREIN IS PROPRIETARY TO THE BOEING COMPANY AND SHALL NOT BE REPRODUCED OR DISCLOSED IN WHOLE OR IN PART OR USED FOR ANY PURPOSE EXCEPT WHEN SUCH USER POSSESSES DIRECT WRITTEN AUTHORIZATION FROM THE BOEING COMPANY.
REVISIONS
250 HOLE
RINGER ONLY
PLACES
F VIEW C
63.00 REF
PLACES
6 PLACES
SEE PL FOR LIST OF MATERIAL, USAGE AND NOTES
USED ON
CTD
DRAWN TURN LE 8/24/93
CHECKED
STRESS
DES
ENGR
GROUP
PROJ
GROUP ORG
B-Y848
BOEING
CORPORATE OFFICES SEATTLE WA 98124
CURVED PANEL ASSY -
TCAPS TASK 2, PANEL #4
(TEST ONLY)(NAS1-19349)
SIZE J
CAGE CODE 81205
DWG NO 261X0370
SCALE 1/4
SH 1
UNLESS OTHERWISE SPECIFIED DIMENSIONS ARE IN INCHES
TOLERANCES
ANGLES: 2° DECIMALS: .03
261X0370

PARTS LIST

REVISION STATUS												
SHEET	LTR	ADDED SHEETS				SHEET	LTR	ADDED SHEETS			
		SHEET	LTR	SHEET	LTR			SHEET	LTR	SHEET	LTR
1	-										
2	-										
3	-										
4	-										
5	-										

PART NUMBER	APPLICATION			DWG SH NUMBER	REV LTR
	NEXT ASSY	USED ON	EFFECTIVITY		
-1	113X9004	TEST ONLY			

CAD DRAWING
(NO DATASET RELEASED)

ENGINEERING REFERENCE ONLY
CAD FILE NAME: CATIAX.V2R2.NSTGRPAT.MAP
DATASET NAME:261X0370M01-- CURVED PANEL ASSY TCAPS PANEL #4

DWG ORIG BY B-Y84B

CONTR		THE BOEING COMPANY STRUCTURES LABORATORY SEATTLE, WASHINGTON 98124
DRN TUAN LE	8/24/93	
CHK	9/15/93	CURVED PANEL ASSY- TCAPS TASK 2, PANEL #4 (TEST ONLY) (NAS1-19349)
ENGR J. Bodine	9-28-93	
ORG		
PROJ	9/29/93	
BMT	9/29/93	CODE IDENT NO 81205 | PL 261X0370 | SH 1 OF 5 | REV LTR -

PARTS LIST	THE BOEING COMPANY STRUCTURES LABORATORY SEATTLE, WASHINGTON 98124	CODE IDENT NUMBER 81205	PL 261X0370	SHEET 2	REV -

REVISIONS				REVISIONS			
LTR	DESCRIPTION	DATE	APPROVED	LTR	DESCRIPTION	DATE	APPROVED

PARTS LIST	THE BOEING COMPANY STRUCTURES LABORATORY SEATTLE, WASHINGTON 98124	CODE IDENT NUMBER 81205	PL 261X0370	SHEET 3	REV -

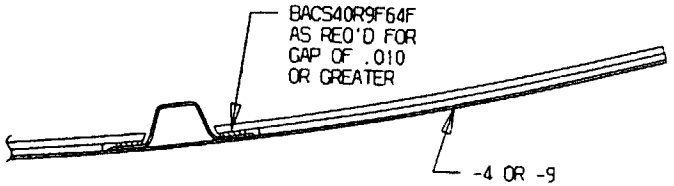
NOTES

- INSTALL BOLT AND NUT FASTENERS PER BAC 5009 & BAC 5063.
- SURFACE FINISH ALL MACHINED SURFACES 125 MAX.
- TRIM AND MACHINE GR/EP PARTS TO THE REQUIREMENTS OF BAC 5578.
- BREAK ALL SHARP EDGES AND CORNERS ON GR/EP DETAILS TO A RADIUS OR CHAMFER OF APPROX .01. VISUAL INSPECT ONLY.
- FORM, PUNCH, STRAIGHTEN, BREAK SHARP EDGES AND FIT METAL PARTS PER BAC5300.

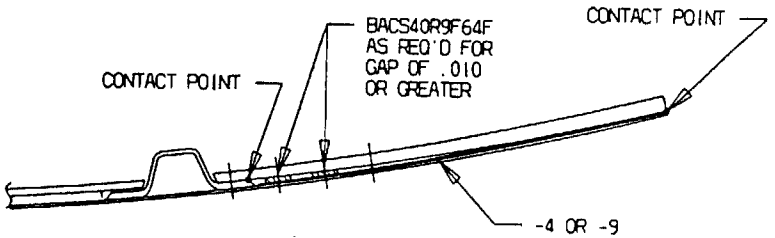
1. STENCIL DRAWING, ASSY NO. IN 1/2 IN TO 1 IN HIGH NUMERALS ON EACH SIDE IN APPROX. LOCATION SHOWN WITH WHITE ENAMEL PER BAC 5307. OPTIONAL: HANDMARK WITH WHITE MARK PEN.
2. FASTENER HEAD NEAR SIDE.
3. UP TO (2) WASHERS UNDER NUT IS ACCEPTABLE FOR LONGER GRIP LENGTH FASTENERS.
4. TORQUE FASTENERS 90-125 IN-LBS.
5. TORQUE FASTENERS 30-40 IN-LBS.
6. FOR GAP .010 OR GREATER USE BACS40R9F64F SHIM AS REQ'D. LOCATE AND CENTER TO EXISTING HOLES IN DOUBLERS. Ø .375 HOLES THRU BACS40R9F64F SHIM ONLY.
7. FOR GAP .010 OR GREATER USE BACS40R64F84F SHIM AS REQ'D. LOCATE AND CENTER TO EXISTING HOLES IN DOUBLERS. Ø .375 HOLES THRU BACS40R64F84F SHIM ONLY.

NOTES

8. IF -4 OR -9 HIGHER THAN STRINGER FLANGE USE OPT#1 BELOW. IF -4 OR -9 LOWER THAN STRINGER FLANGE USE OPT#2 BELOW. FOR GAP .010 OR GREATER USE BACS40R9F64F SHIM AS REQ'D. LOCATE AND CENTER TO EXISTING HOLES IN DOUBLERS. Ø .375 HOLES THRU SHIMS ONLY.



OPTION #1



OPTION #2

9. MAXIMUM FRAME/SKIN GAP BEFORE INSTALLATION BOLTS = .030 CONTACT ATCAS ENGINEERING FOR INSTRUCTIONS IF GAP EXCEEDS .030.
10. TORQUE FASTENERS 50-75 IN-LBS.

PARTS LIST

THE BOEING COMPANY
STRUCTURES LABORATORY SEATTLE, WASHINGTON 98124

CODE IDENT NUMBER 81205 | PL 261X0370 | SHEET 4 | REV LTR –

EAMR NUMBER	QTY REQD	QTY REQD	QTY REQD	QTY REQD	QTY REQD	QTY REQD - 1	FIND NUMBER	PART OR IDENTIFYING NUMBER	NOMENCLATURE OR DESCRIPTION	ZONE	MATERIAL AND SPECIFICATION	CODE IDENT NUMBER	HT TR	FINISH	PT MK	REV LTR
						-		-1	TEST PANEL-ASSY	A4-1						
						6		-2	DOUBLER	C6-1	.14 X 6.5 X 8.5 7075-T6 ALUM. SHEET				M	
						6		-3	DOUBLER	C7-1	.25 X 6.5 X 11.5 7075-T6 ALUM. PLATE OR T651 BARE OR CLAD				M	
						2		-4	DOUBLER	C9-1	.14 X 7.8 X 12.3 7075-T6 ALUM. SHEET				M	
						2		-9	OPP-4	C9-1	.14 X 7.8 X 12.3 7075-T6 ALUM. SHEET				M	
						2		-5	DOUBLER	C10-1	.25 X 9.3 X 12.3 7075-T6 ALUM. PLATE OR T651 BARE OR CLAD				M	
						2		-6	OPP-5	C10-1	.25 X 9.3 X 12.3 7075-T6 ALUM. PLATE OR T651 BARE OR CLAD				M	
						4		-7	DOUBLER	C12-1	.071 X 5.1 X 18.3 7075-T6 ALUM. SHEET				M	
						A.R		BACS40R9F64F	SHIM							
						A.R		BACS40R64F84F	SHIM							
						1		64-36287-10	PANEL-ASSY							
						3		64-36281-3	FRAME							
						3		64-36249-5	CURVED ANGLE							

PARTS LIST

THE BOEING COMPANY
STRUCTURES LABORATORY SEATTLE, WASHINGTON 98124

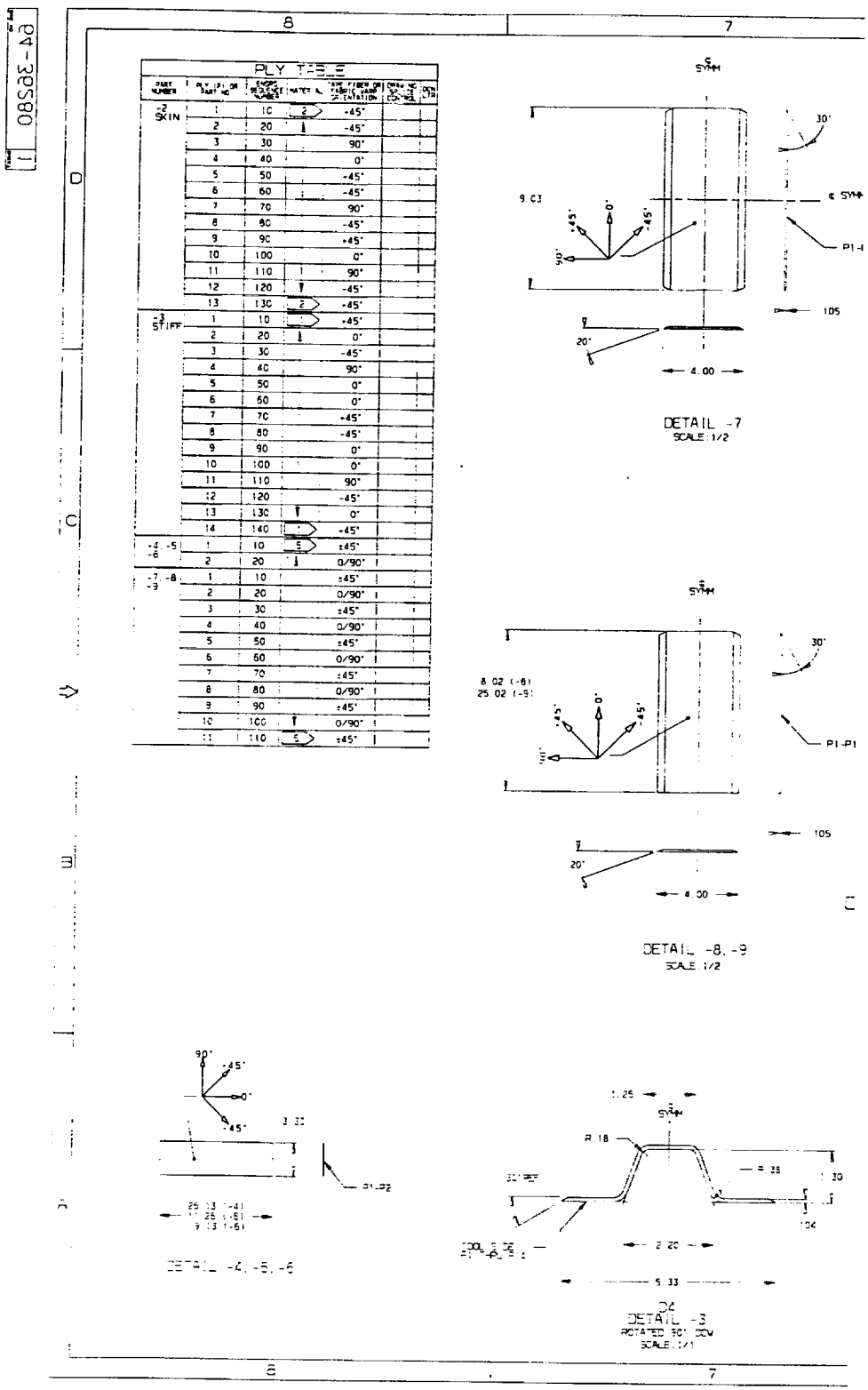
CODE IDENT NUMBER 81205 | PL 261X0370 | SHEET 5 | REV LTR –

EAMP NUMBER	QTY REQD	QTY REQD	QTY REQD	QTY REQD	QTY REQD	QTY REQD -1	FIND NUMBER	PART OR IDENTIFYING NUMBER	NOMENCLATURE OR DESCRIPTION	ZONE	MATERIAL AND SPECIFICATION	CODE IDENT NUMBER	HT TR	FINISH	PT MK	REV LTR
						159		BACB30MB6A6U	BOLT							
						246		BACB30MB8A6U	BOLT							
						116		NAS6605-9	BOLT							
						8		NAS6605-8	BOLT							
						8		NAS6605-7	BOLT							
						48		NAS6605-4	BOLT							
						A.R.		AN960-10	WASHER							
						A.R.		AN960-416	WASHER							
						A.R.		AN960-516	WASHER							
						180		BACN10JC5CD	NUT							
						159		NAS1805-3	NUT							
						246		NAS1805-4	NUT							

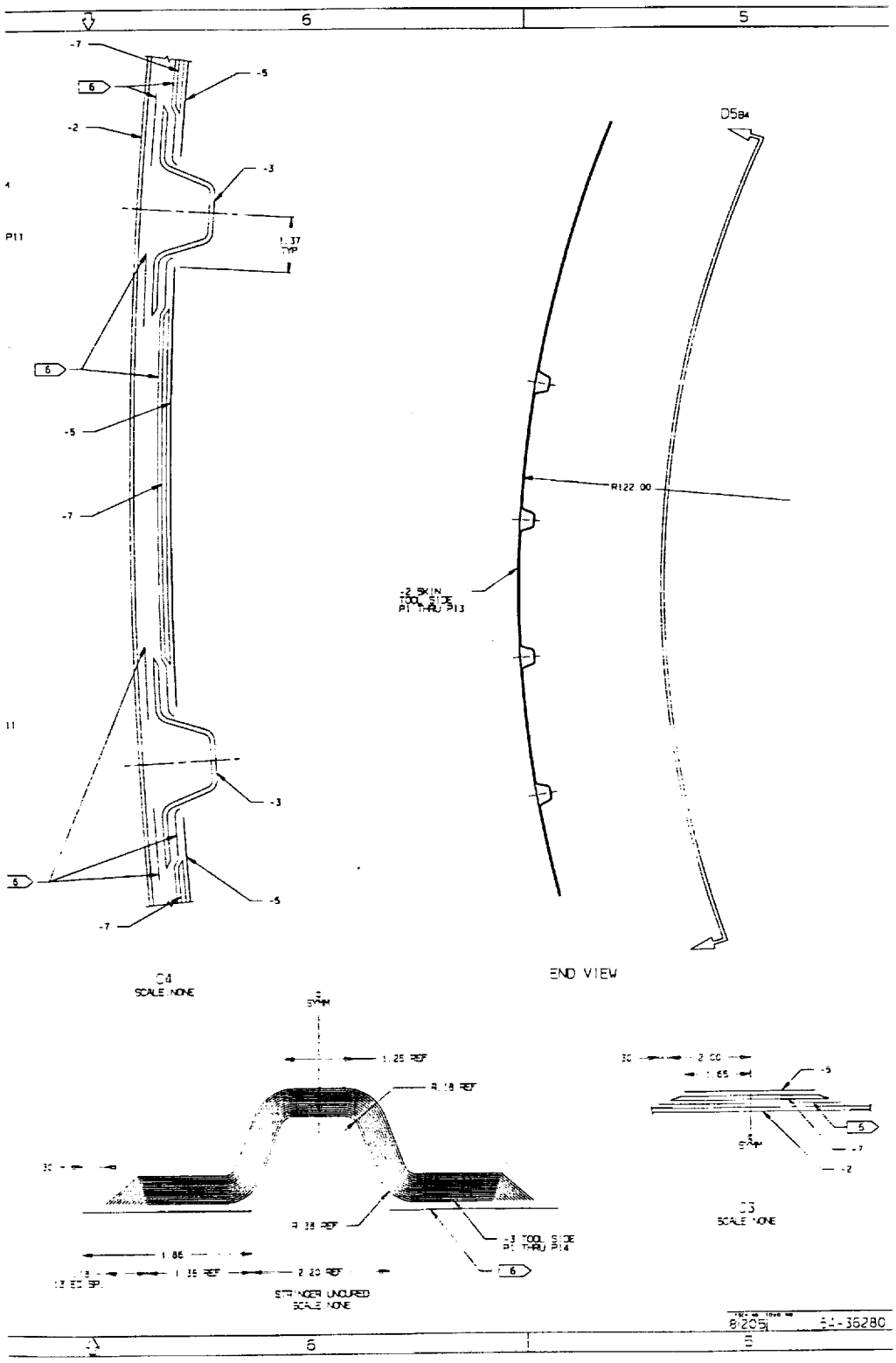
Appendix E

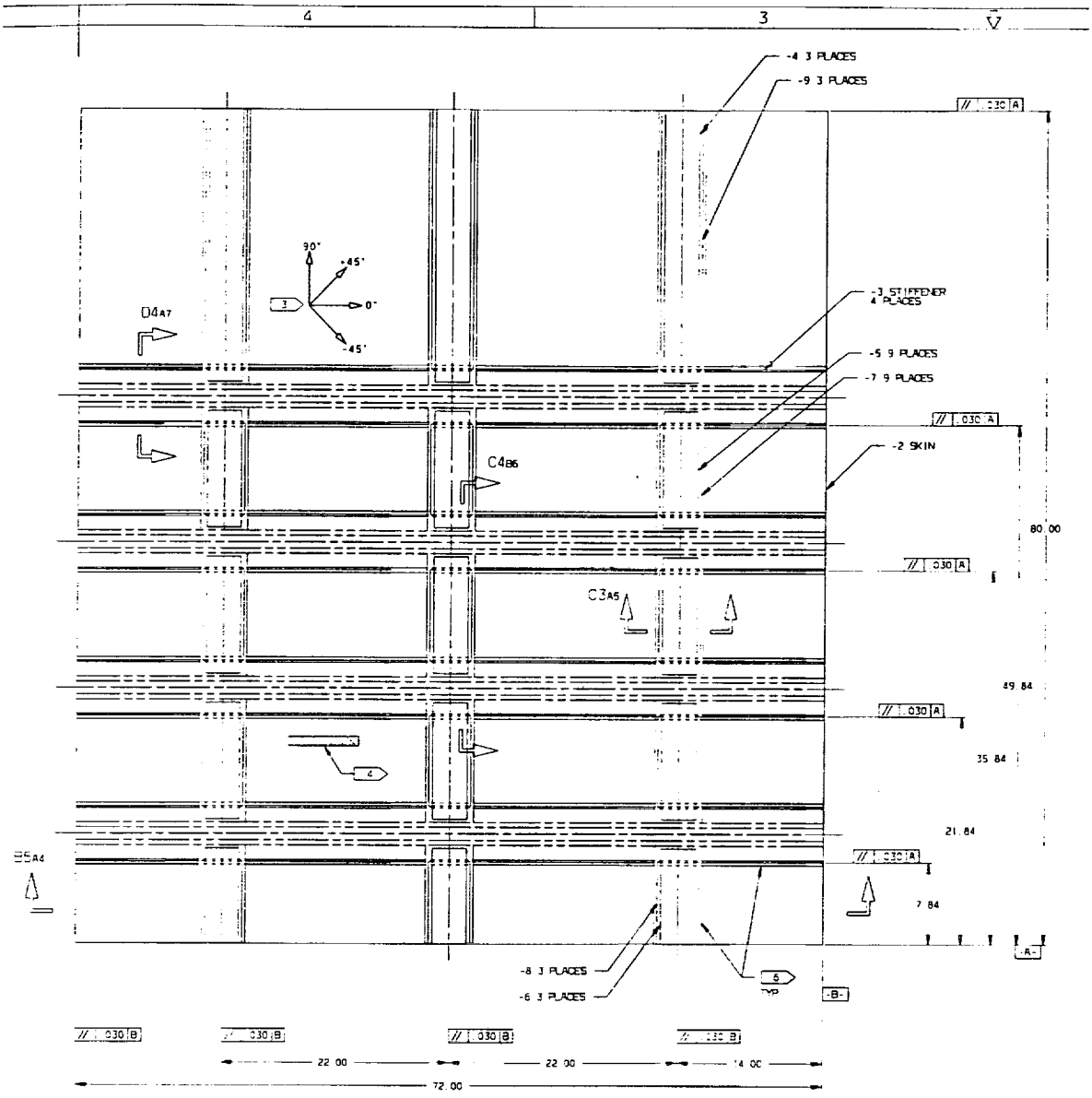
Panel Bond, Cutting Diagram, and Panel Assembly Drawings for Panel 5

TUAN LE 965-4989



ORIGINAL PAGE IS
OF POOR QUALITY

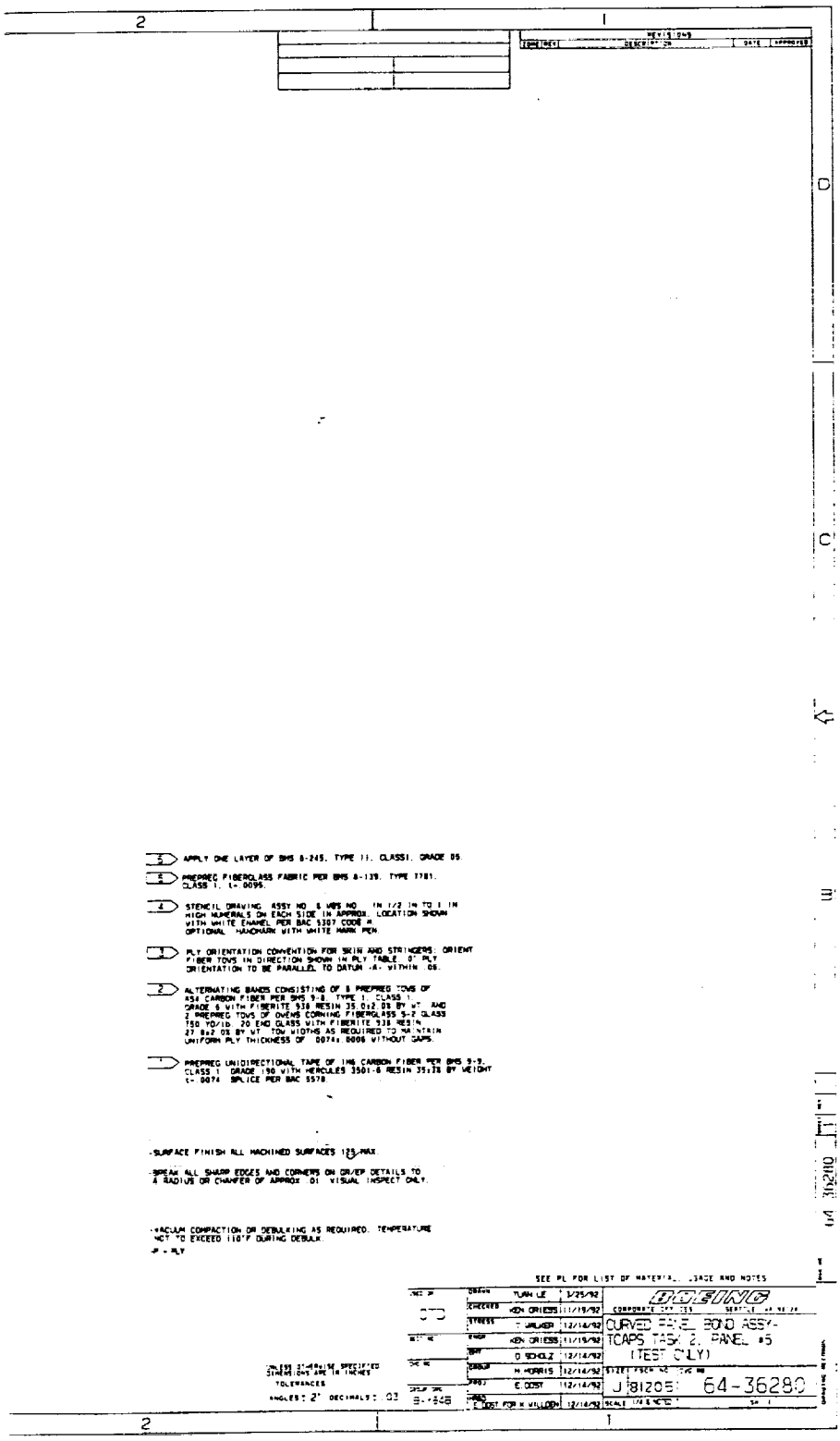

6
5
-7
-5
6
-2
-3
P11
1.37 TYP
6
-5
-7
-3
6
-5
-7
D5B4
R122.00
-2 SKIN TOOL SIDE PLY THRU P13
END VIEW
C4
SCALE NONE
1.25 REF
R.18 REF
R.38 REF
-3 TOOL SIDE PLY THRU P14
6
1.86
1.35 REF
2.20 REF
STRINGER UNCURED
SCALE NONE
2.00
1.65
-5
5
-7
-2
D3
SCALE NONE
8/205
54-36280
6
5



D5
PANEL BONDED -1
AS SHOWN AS FLAT PATERN



ORIGINAL PAGE IS
OF POOR QUALITY



5 APPLY ONE LAYER OF BMS 8-245, TYPE II, CLASS1, GRADE B5

6 PREPREG FIBERGLASS FABRIC PER BMS 8-139, TYPE 7781, CLASS 1, t= .0095.

4 STENCIL DRAWING ASSY NO. & VBS NO. IN 1/2 IN TO 1 IN HIGH NUMERALS ON EACH SIDE IN APPROX. LOCATION SHOWN WITH WHITE ENAMEL PER BAC 5307 CODE W OPTIONAL HANDMARK WITH WHITE MARK PEN.

3 PLY ORIENTATION CONVENTION FOR SKIN AND STRINGERS: ORIENT FIBER TOWS IN DIRECTION SHOWN IN PLY TABLE. 0° PLY ORIENTATION TO BE PARALLEL TO DATUM -A- WITHIN .05.

2 ALTERNATING BANDS CONSISTING OF 8 PREPREG TOWS OF AS4 CARBON FIBER PER BMS 9-8, TYPE 1, CLASS 1, GRADE 6 WITH FIBERITE 938 RESIN 35.0±2.0% BY WT AND 2 PREPREG TOWS OF OWENS CORNING FIBERGLASS S-2 GLASS 750 YD/LB 20 END GLASS WITH FIBERITE 938 RESIN 27.0±2.0% BY WT TOW WIDTHS AS REQUIRED TO MAINTAIN UNIFORM PLY THICKNESS OF .0074± .0008 WITHOUT GAPS.

1 PREPREG UNIDIRECTIONAL TAPE OF 1MIL CARBON FIBER PER BMS 9-8, CLASS 1 GRADE 190 WITH HERCULES 3501-6 RESIN 35±3% BY WEIGHT t= .0074 SPLICE PER BAC 5578.

-SURFACE FINISH ALL MACHINED SURFACES 125 MAX.

-BREAK ALL SHARP EDGES AND CORNERS ON DR/EP DETAILS TO A RADIUS OR CHAMFER OF APPROX .01 VISUAL INSPECT ONLY.

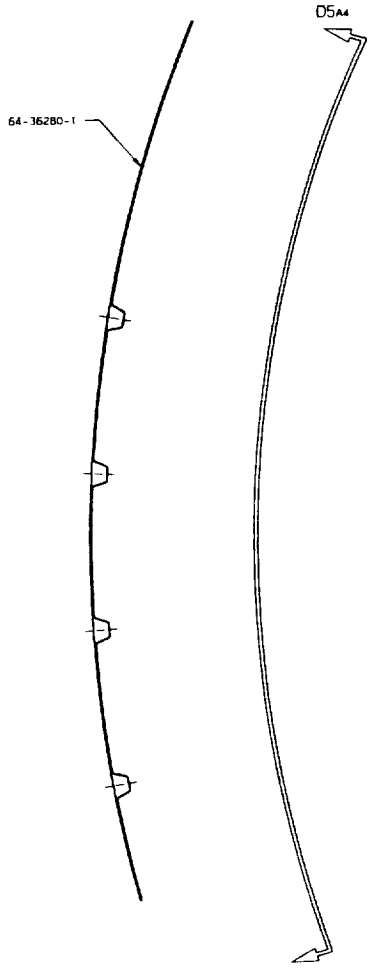
-VACUUM COMPACTION OR DEBULKING AS REQUIRED. TEMPERATURE NOT TO EXCEED 110°F DURING DEBULK.

P - PLY

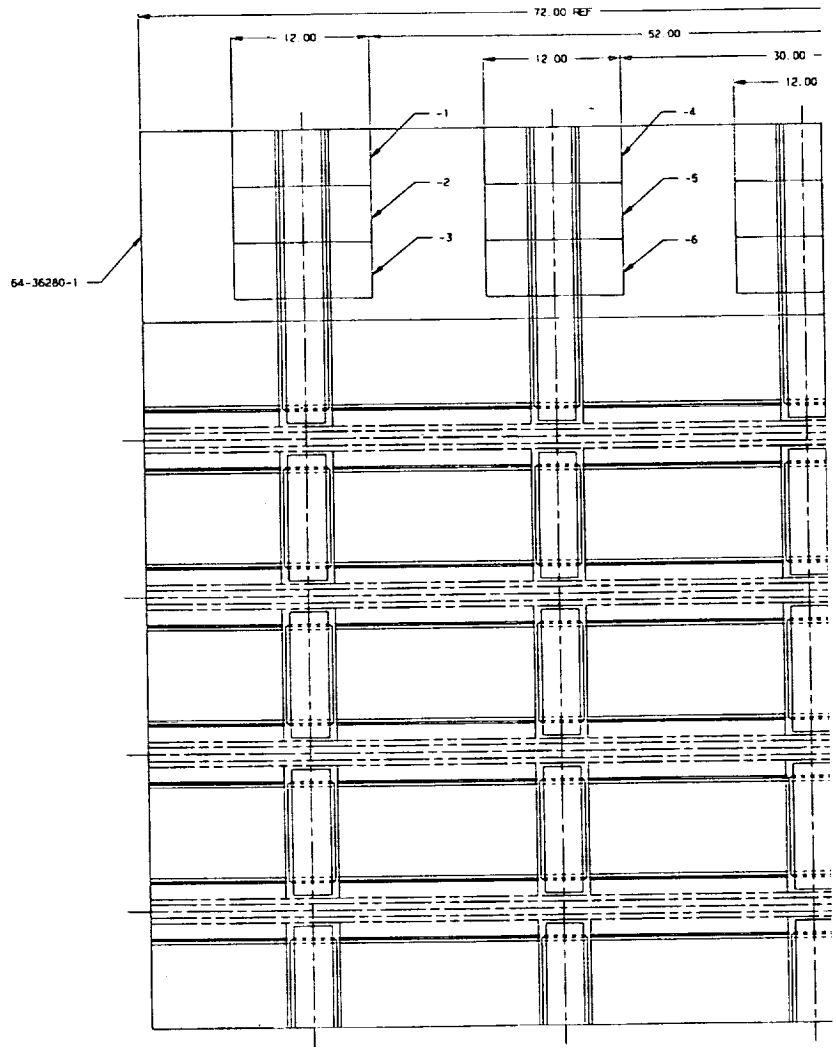
SEE PL FOR LIST OF MATERIAL, USAGE AND NOTES

DRAWN	YUAN LE	1/25/92	BOEING
CHECKED	KEN CRIESS	11/19/92	
STRESS	T JAUHER	12/14/92	CURVED PANEL BOND ASSY-
ENGR	KEN CRIESS	11/19/92	TCAPS TASK 2, PANEL #5
QA	D SCHOLZ	12/14/92	(TEST ONLY)
DRAFT	H HORRIS	12/14/92	
PROJ	E COST	12/14/92	J181205 64-36280
APPD	E COST FOR K WILLOUGHBY	12/14/92	SCALE 1/4 SHEET 1 OF 1

UNLESS OTHERWISE SPECIFIED DIMENSIONS ARE IN INCHES
TOLERANCES
ANGLES ± 2° DECIMALS ± .03

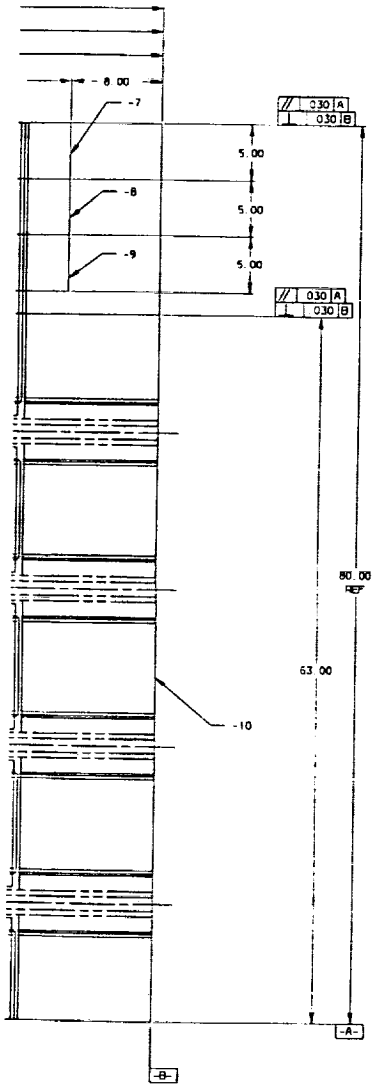


END VIEW



D5
SKIN AS SHOWN AS FLATPATERN
DIMENSION MEASURE ON
OUTSIDE MOLD LINE

81205	64-36288	1	-



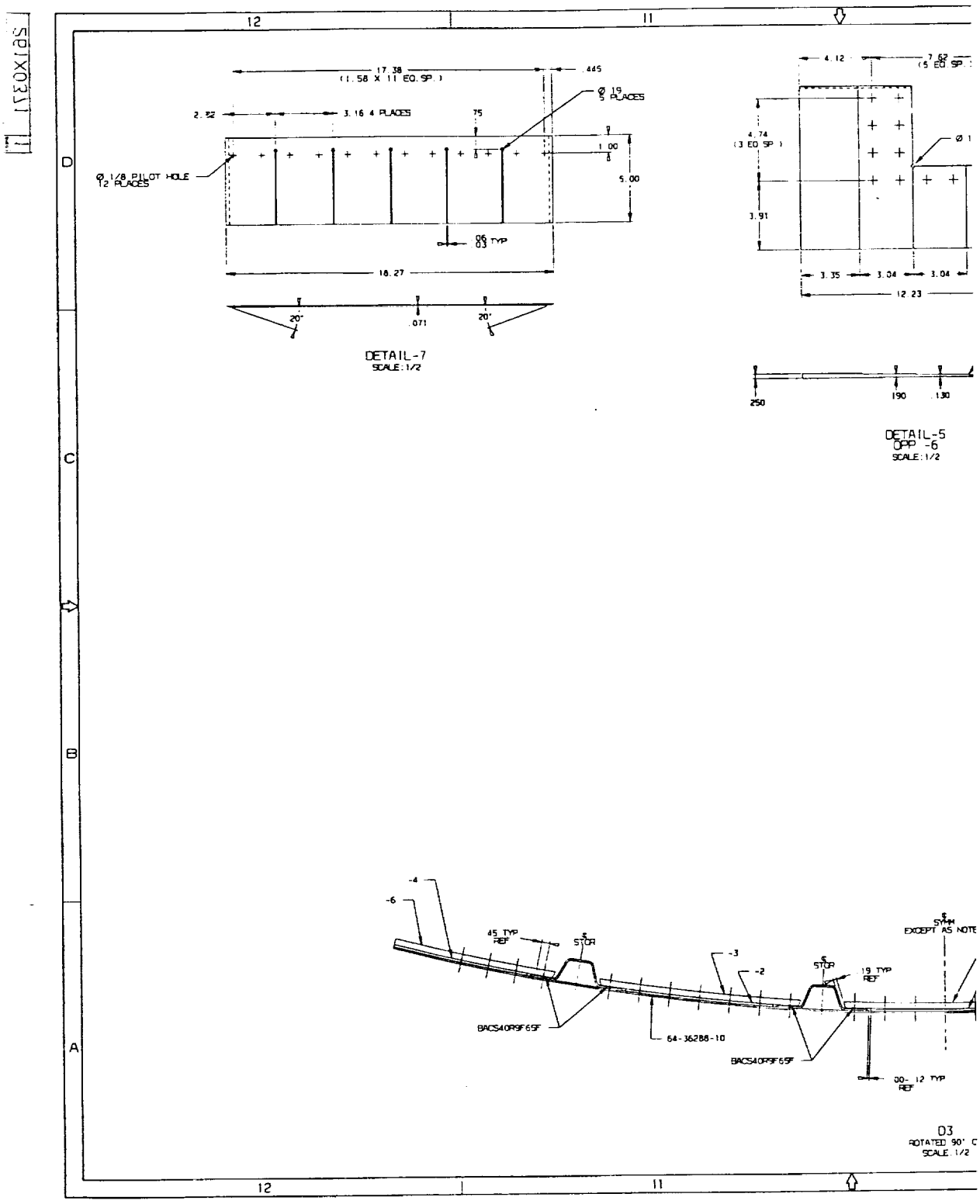
- USE OF MANUFACTURING EXCESS MAY BE REQUIRED TO PROVIDE FOR .25 KERF TYP
- HAND MARK PARTS WITH WHITE MARKING PEN
- SURFACE FINISH ALL MACHINED SURFACES 125 MAX
- BREAK ALL SHARP EDGES AND CORNERS ON OR/EP DETAILS TO A RADIUS OR CHAMFER OF APPROX .01. VISUAL INSPECT ONLY.

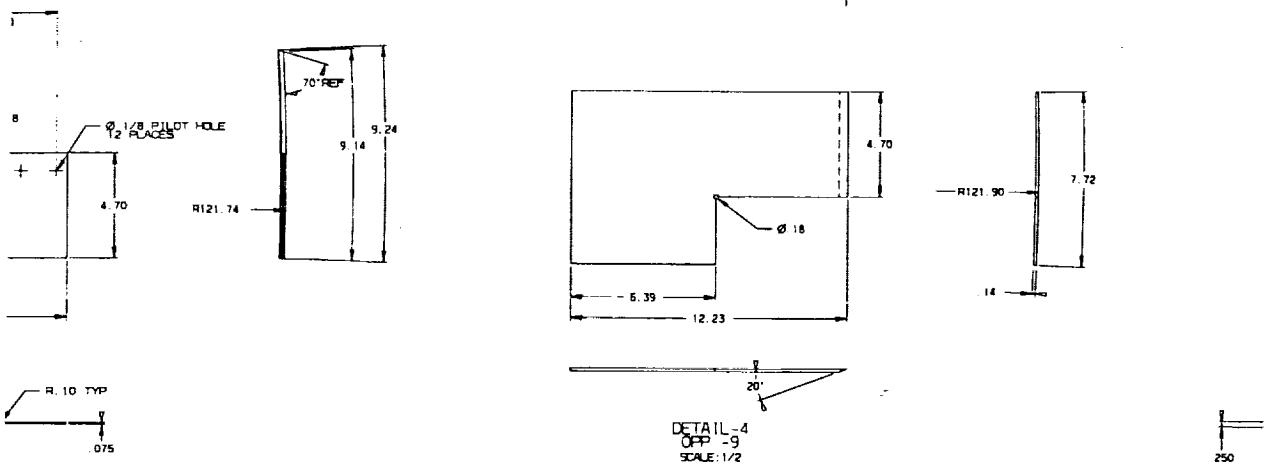
SEE PL FOR LIST OF MATERIAL, USAGE AND NOTES

UNLESS OTHERWISE SPECIFIED DIMENSIONS ARE IN INCHES
TOLERANCES
ANGLES: 2° DECIMALS: .03

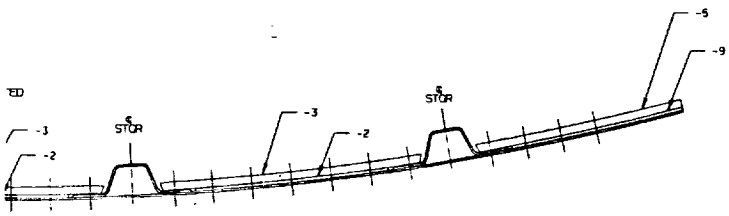
CTD	DRAWN TIAN LE	1/20/92	BOEING CORPORATE OFFICES SEATTLE, WA 98124
	CHECKED		CURVED PANEL CUTTING DIAGRAM TCAPS TASK 2, PANEL #5 (TEST ONLY)
	ENGR APPR		
	STRESS	9/15/92	
	PROJ	9/11/92	SIZE J 81205 DWG NO 64-36288
B-Y848	GROUP ENGR		SCALE 1/8

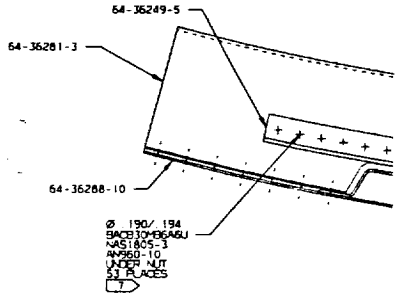
64-36288


12
11
D
C
B
A
17.38
(1.58 X 11 EQ. SP.)
.445
Ø .19
5 PLACES
2.52
3.16 4 PLACES
.75
1.00
5.00
Ø.178 PILOT HOLE
12 PLACES
.06
.03 TYP
18.27
20°
.071
20°
DETAIL-7
SCALE: 1/2
4.12
7.62
(5 EQ SP.)
4.74
(3 EQ SP.)
3.91
3.35
3.04
3.04
12.23
.250
.190
.130
DETAIL-5
OPP -6
SCALE: 1/2
-4
-6
45 TYP
REF
STOR
-3
-2
STOR
.19 TYP
REF
SYMM
EXCEPT AS NOTE
BACS40R9F65F
64-36288-10
BACS40R9F65F
.00-.12 TYP
REF
D3
ROTATED 90° C
SCALE: 1/2



DETAIL-4
OPP -9
SCALE: 1/2



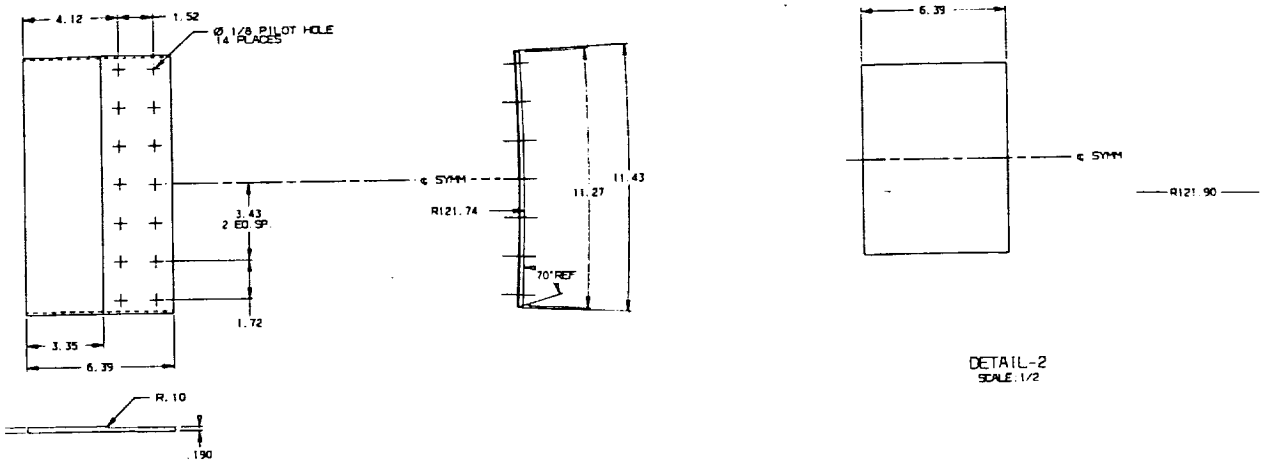


BOEING PROPRIETARY
THE INFORMATION CONTAINED HEREIN IS PROPRIETARY TO THE BOEING COMPANY AND SHALL NOT BE REPRODUCED OR DISCLOSED IN WHOLE OR IN PART OR USED FOR ANY PURPOSE EXCEPT WHEN SUCH USER POSSESSES DIRECT WRITTEN AUTHORIZATION FROM THE BOEING COMPANY

CV

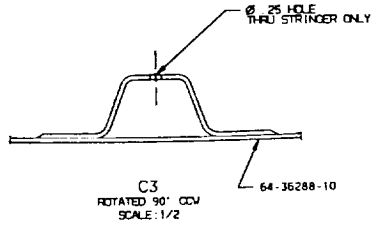
CAGE CODE	DWG NO.	SHEET NO.
81205	261X0371	1

10 | 9 | 8

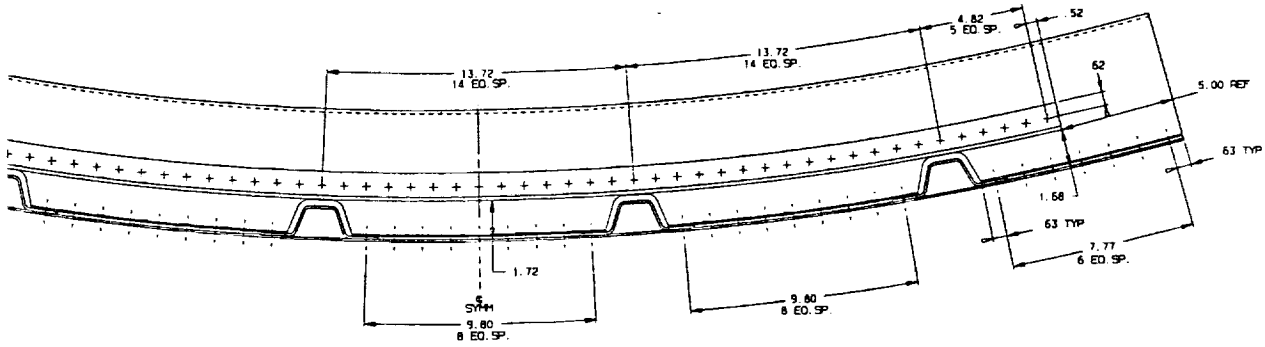


DETAIL-3
SCALE: 1/2

DETAIL-2
SCALE: 1/2



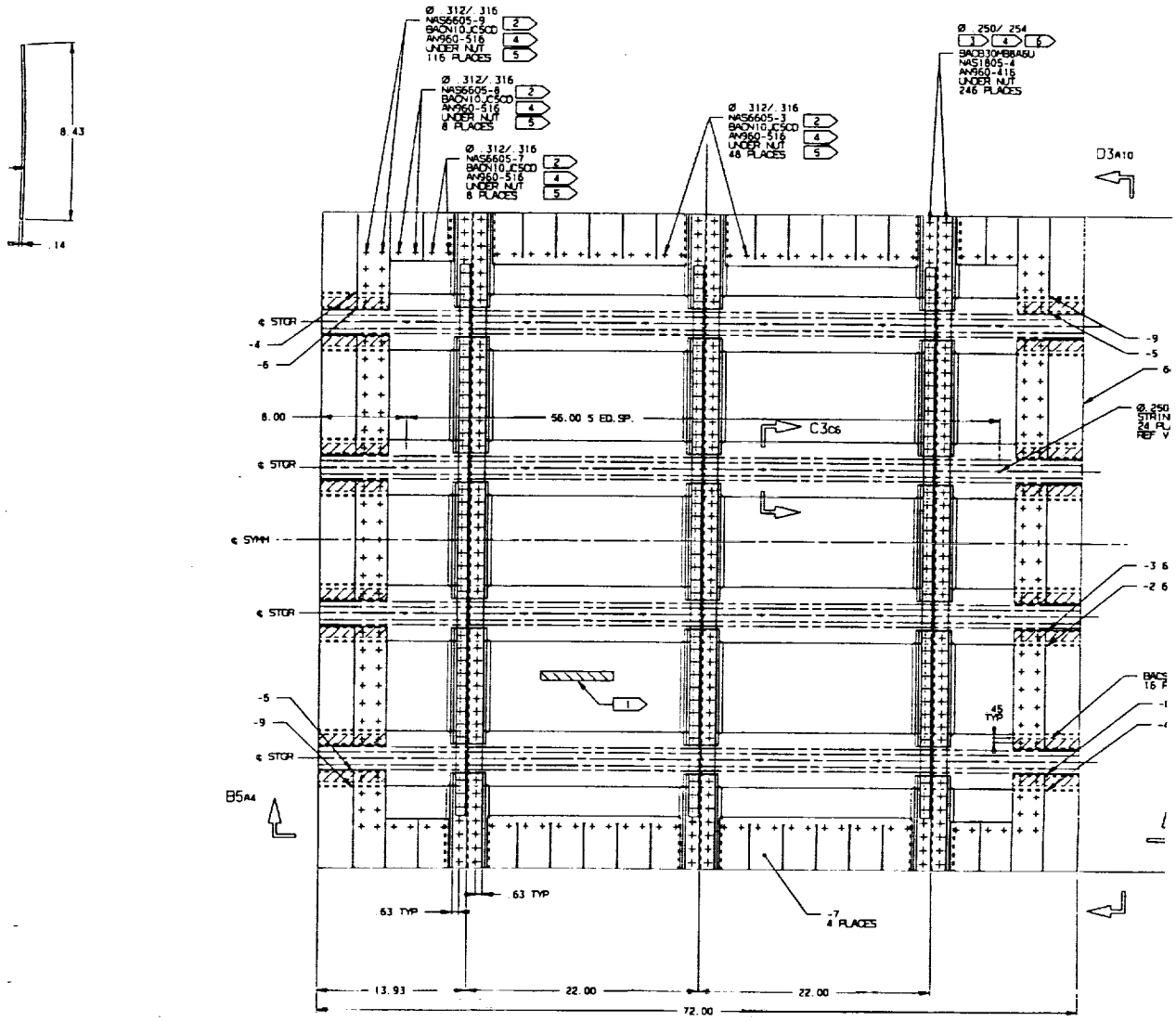
C3
ROTATED 90° CCW
SCALE: 1/2



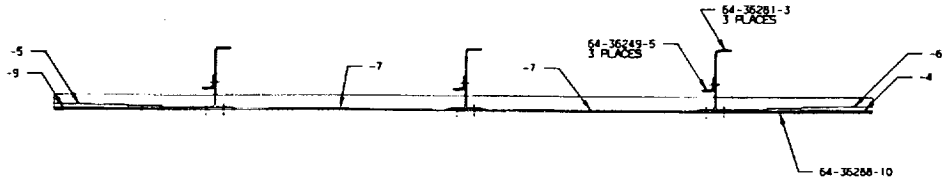
TYPICAL FRAME SECTION
SCALE: 1/2

BOEING PROPRIETARY
THE INFORMATION CONTAINED HEREIN IS PROPRIETARY TO THE BOEING COMPANY AND SHALL NOT BE REPRODUCED OR DISCLOSED IN WHOLE OR IN PART OR USED FOR ANY PURPOSE EXCEPT WHERE SUCH USE POSSESSES DIRECT WRITTEN AUTHORIZATION FROM THE BOEING COMPANY

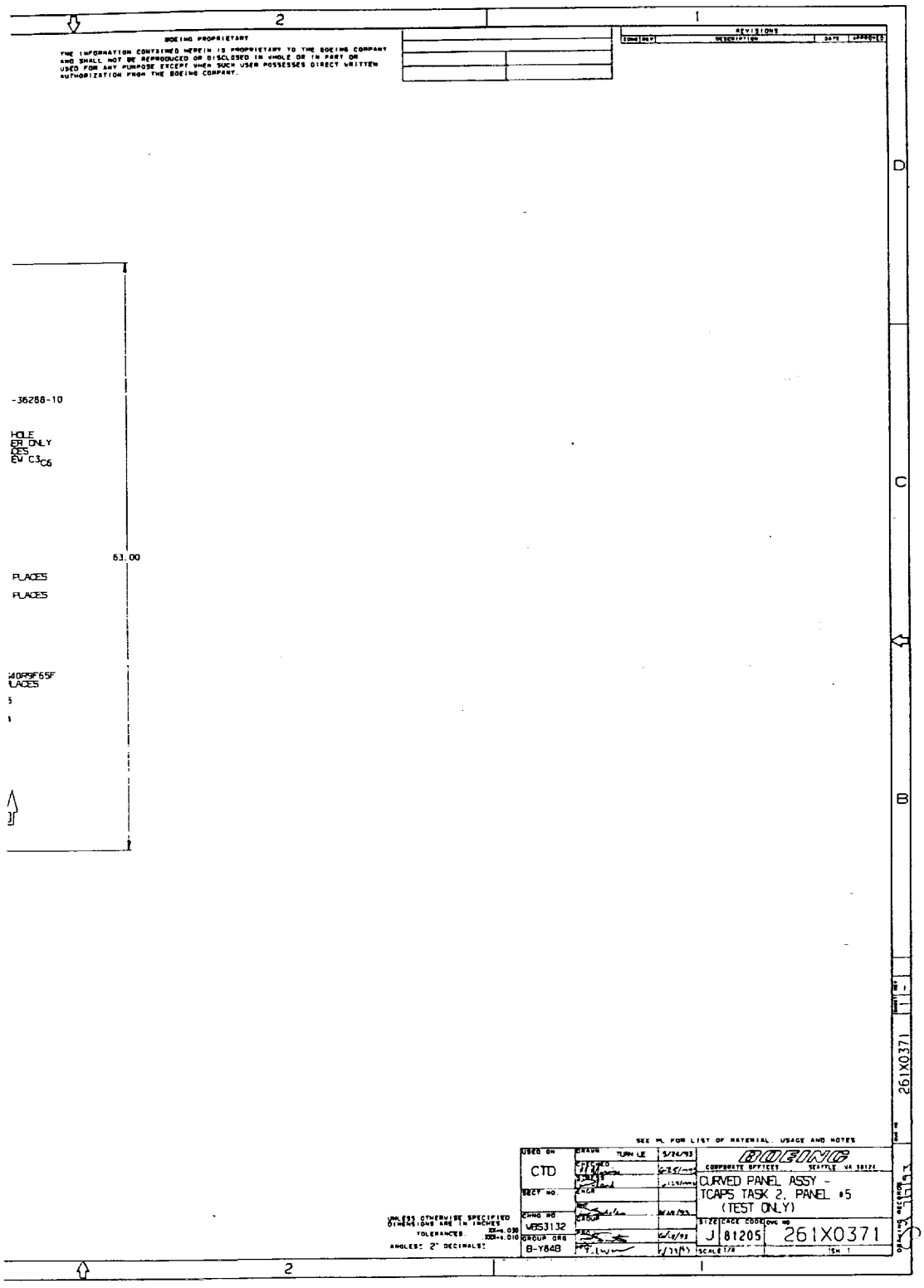
7
6



PANEL ASSY-1
SHOWN AS FLAT PATTERN



B5


BOEING PROPRIETARY
THE INFORMATION CONTAINED HEREIN IS PROPRIETARY TO THE BOEING COMPANY AND SHALL NOT BE REPRODUCED OR DISCLOSED IN WHOLE OR IN PART OR USED FOR ANY PURPOSE EXCEPT WHEN SUCH USER POSSESSES DIRECT WRITTEN AUTHORIZATION FROM THE BOEING COMPANY.
REVISIONS
-36288-10
HOLE
BY ONLY
PLACES
PLACES
63.00
SEE HL FOR LIST OF MATERIAL, USAGE AND NOTES
CTD
V853132
B-Y848
BOEING
CURVED PANEL ASSY -
TCAPS TASK 2, PANEL #5
(TEST ONLY)
J 81205
261X0371

PARTS LIST

REVISION STATUS

SHEET	LTR	ADDED SHEETS				SHEET	LTR	ADDED SHEETS			
		SHEET	LTR	SHEET	LTR			SHEET	LTR	SHEET	LTR
1	-										
2	-										
3	-										
4	-										
5	-										

PART NUMBER	APPLICATION			DWG SH NUMBER	REV LTR
	NEXT ASSY	USED ON	EFFECTIVITY		
-1	113X9005	TEST ONLY			

CAD DRAWING
(NO DATASET RELEASED)

ENGINEERING REFERENCE ONLY
CAD FILE NAME: CATIAX.V2R2.NSTGRPAT.MAP
DATASET NAME:261X0371M01-- CURVED PANEL ASSY TCAPS PANEL #5

EWA NO. WBS3132

DWG ORIG BY B-Y848

CONTR		
DRN TUAN LE	5/25/93	
CHK M. MORRIS	6/25/93	
ENGR D. POLLAND	6/25/93	
ORG		
PROJ P. SMITH	6/29/93	
BMT D. SCHOLZ	6/29/93	
K. WILLDEN	6/29/93	

THE BOEING COMPANY
STRUCTURES LABORATORY SEATTLE, WASHINGTON 98124

CURVED PANEL ASSY-
TCAPS TASK 2, PANEL #5
(TEST ONLY)

CODE IDENT NO		SH	REV LTR
81205	PL 261X0371	1 OF 5	-

PARTS LIST

THE BOEING COMPANY
STRUCTURES LABORATORY SEATTLE, WASHINGTON 98124

CODE IDENT NUMBER		SHEET	REV LTR
81205	PL 261X0371	2	-

REVISIONS

LTR	DESCRIPTION	DATE	APPROVED

REVISIONS

LTR	DESCRIPTION	DATE	APPROVED

PARTS LIST	THE BOEING COMPANY STRUCTURES LABORATORY SEATTLE, WASHINGTON 98124	CODE IDENT NUMBER 81205	PL 261X0371	SHEET 3	REV LTR –

NOTES

-INSTALL BOLT AND NUT FASTENERS PER BAC 5009 & BAC 5063.

-SURFACE FINISH ALL MACHINED SURFACES 125 MAX.

-TRIM AND MACHINE GR/EP PARTS TO THE REQUIREMENTS OF BAC 5578.

-BREAK ALL SHARP EDGES AND CORNERS ON GR/EP DETAILS TO A RADIUS OR CHAMFER OF APPROX .01. VISUAL INSPECT ONLY.

-FORM, PUNCH, STRAIGHTEN, BREAK SHARP EDGES AND FIT METAL PARTS PER BAC5300.

NOTES

1. STENCIL DRAWING, ASSY NO. & WBS NO. IN 1/2 IN TO 1 IN HIGH NUMERALS ON EACH SIDE IN APPROX. LOCATION SHOWN WITH WHITE ENAMEL PER BAC 5307. OPTIONAL: HANDMARK WITH WHITE MARK PEN.
2. FASTENER HEAD NEAR SIDE.
3. MAXIMUM FRAME/SKIN GAP BEFORE INSTALLING BOLTS -.030 CONTACT ATCAS ENGINEERING FOR INSTRUCTIONS IF GAP EXCEEDS .030.
4. UP TO (2) WASHERS UNDER NUT IS ACCEPTABLE FOR LONGER GRIP LENGTH FASTENERS.
5. TORQUE FASTENERS 90-125 IN-LBS.
6. TORQUE FASTENERS 50-75 IN-LBS.
7. TORQUE FASTENERS 30-40 IN-LBS.

PARTS LIST

THE BOEING COMPANY
STRUCTURES LABORATORY SEATTLE, WASHINGTON 98124

CODE IDENT NUMBER 81205 | PL 261X0371 | SHEET 4 | REV LTR —

EMR NUMBER	QTY REQD	QTY REQD	QTY REQD	QTY REQD	QTY REQD	QTY REQD -1	FIND NUMBER	PART OR IDENTIFYING NUMBER	NOMENCLATURE OR DESCRIPTION	ZONE	MATERIAL AND SPECIFICATION	CODE IDENT NUMBER	HT TR	FINISH	PT MK	REV LTR
						-		-1	TEST PANEL-ASSY	A4-1						
						6		-2	DOUBLER	C6-1	.14 X 6.5 X 8.5 7075-T6 ALUM. SHEET				M	
						6		-3	DOUBLER	C7-1	.25 X 6.5 X 11.5 7075-T6 ALUM. PLATE OR T651 BARE OR CLAD				M	
						2		-4	DOUBLER	C9-1	.14 X 8.0 X 12.5 7075-T6 ALUM. SHEET				M	
						2		-9	OPP-4	C9-1	.14 X 8.0 X 12.5 7075-T6 ALUM. SHEET				M	
						2		-5	DOUBLER	C10-1	.25 X 9.5 X 12.5 7075-T6 ALUM. PLATE OR T651 BARE OR CLAD				M	
						2		-6	OPP-5	C10-1	.25 X 9.5 X 12.5 7075-T6 ALUM. PLATE OR T651 BARE OR CLAD				M	
						4		-7	DOUBLER	C12-1	.071 X 5.1 X 18.5 7075-T6 ALUM. SHEET				M	
						16		BACS40R9F65F	SHIM							
						1		64-36288-10	PANEL-ASSY							
						3		64-36281-3	FRAME							
						3		64-36249-5	CURVED ANGLE							

PARTS LIST

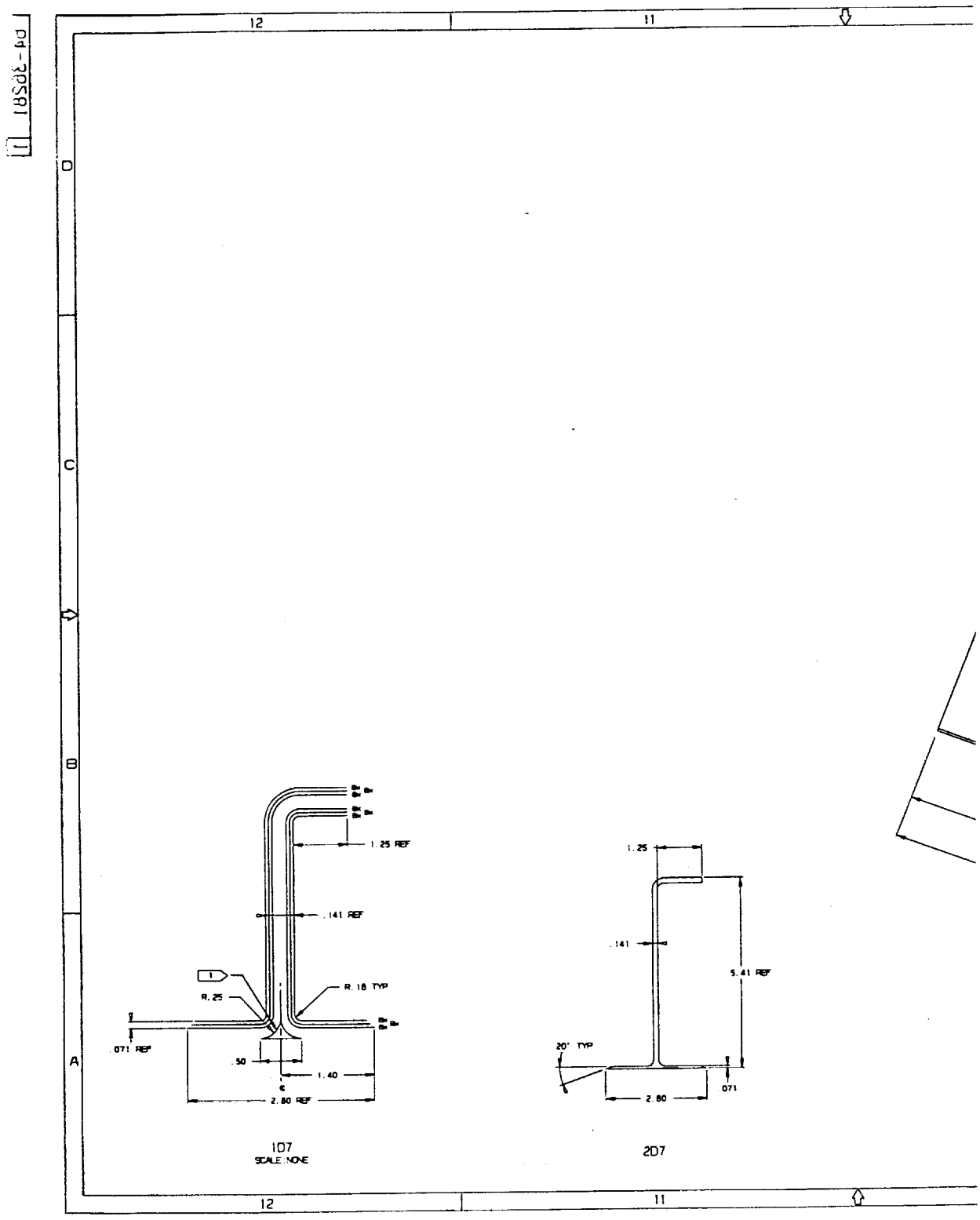
THE BOEING COMPANY
STRUCTURES LABORATORY SEATTLE, WASHINGTON 98124

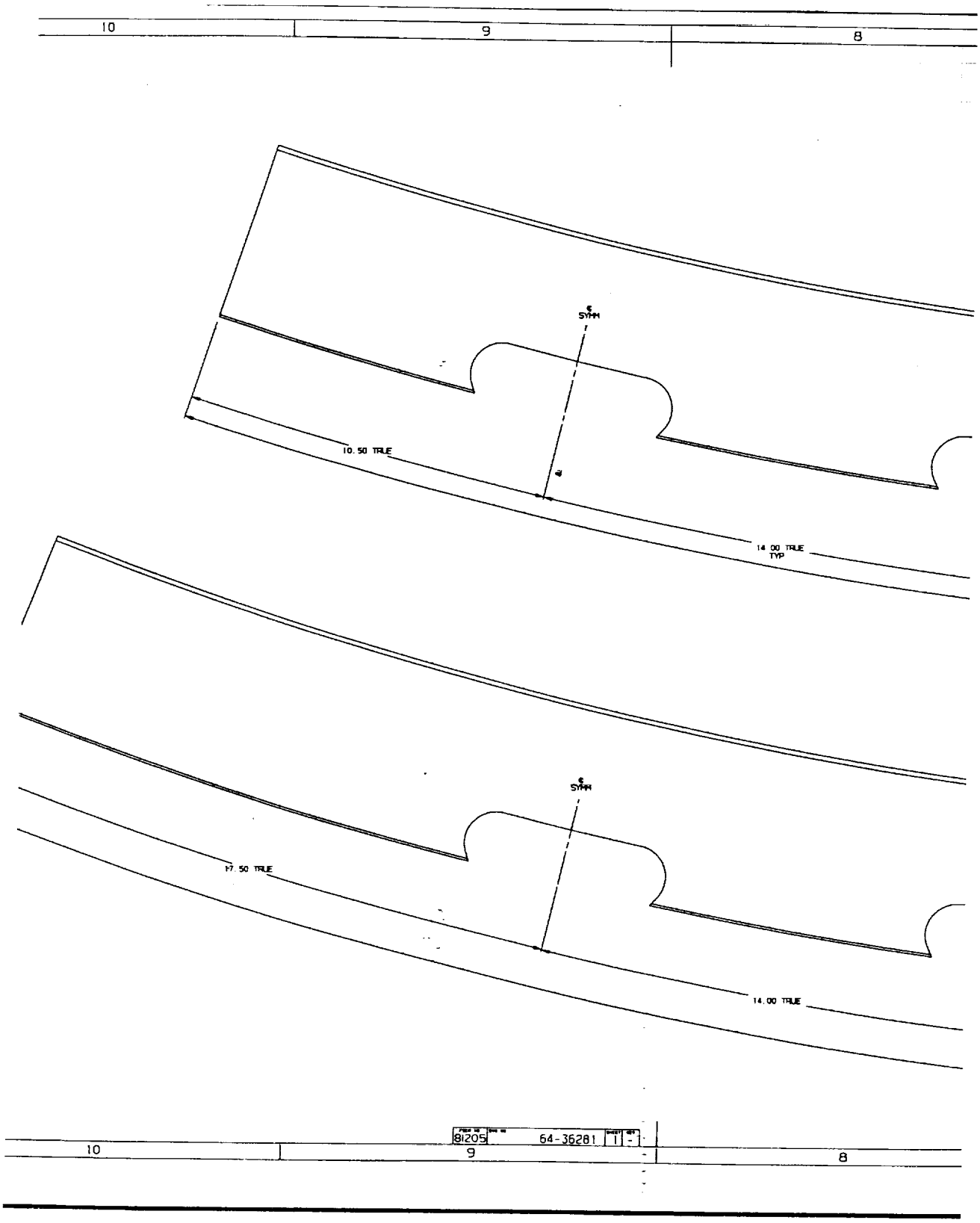
CODE IDENT NUMBER 81205 | PL 261X0371 | SHEET 5 | REV LTR —

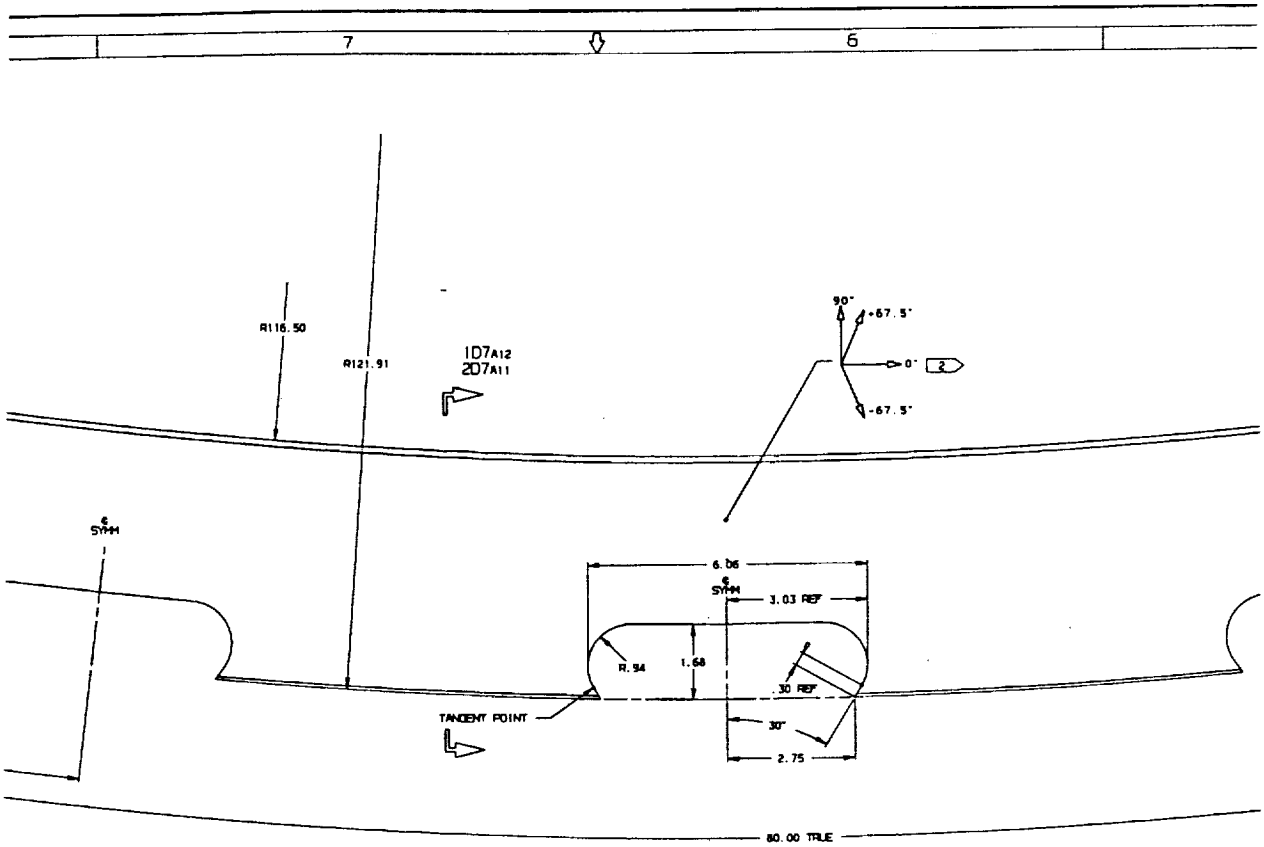
ENGR NUMBER	QTY REQD	QTY REQD	QTY REQD	QTY REQD	QTY REQD	QTY REQD -1	FIND NUMBER	PART OR IDENTIFYING NUMBER	NOMENCLATURE OR DESCRIPTION	ZONE	MATERIAL AND SPECIFICATION	CODE IDENT NUMBER	HT TR	FINISH	PT NK	REV LTR
						246		BACB30MB8A6U	BOLT							
						159		BACB30MB6A6U	BOLT							
						116		NAS6605-9	BOLT							
						8		NAS6605-8	BOLT							
						8		NAS6605-7	BOLT							
						48		NAS6605-3	BOLT							
						A.R.		AN960-10	WASHER							
						A.R.		AN960-416	WASHER							
						A.R.		AN960-516	WASHER							
						180		BACN10JC5CD	NUT							
						246		NAS1805-4	NUT							
						159		NAS1805-3	NUT							

Appendix F

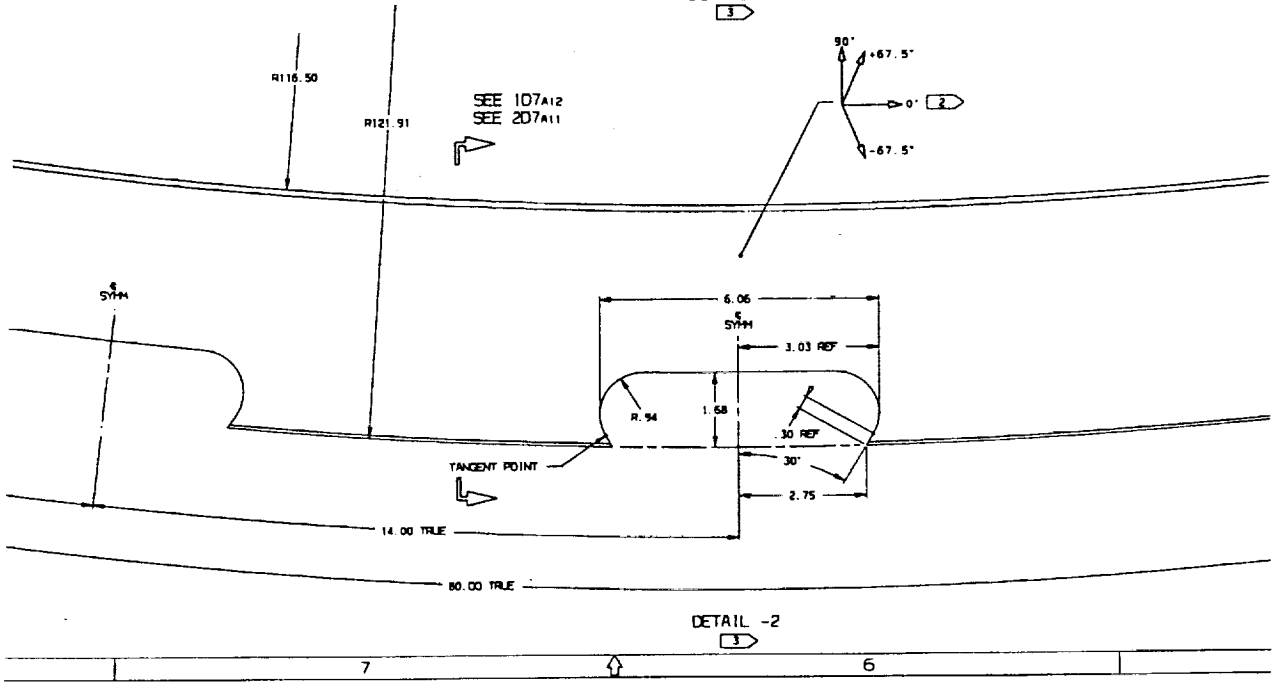
Frame Fabrication Drawing


12
11
D
C
B
A
1.25 REF
.141 REF
1
R.25
R.18 TYP
.071 REF
.50
1.40
2.80 REF
1.25
.141
5.41 REF
20° TYP
2.80
.071
1D7
SCALE NONE
2D7


10
9
8
℄
SYMM
10.50 TRUE
14.00 TRUE
TYP
℄
SYMM
17.50 TRUE
14.00 TRUE
81205
64-36281
11
10
9
8

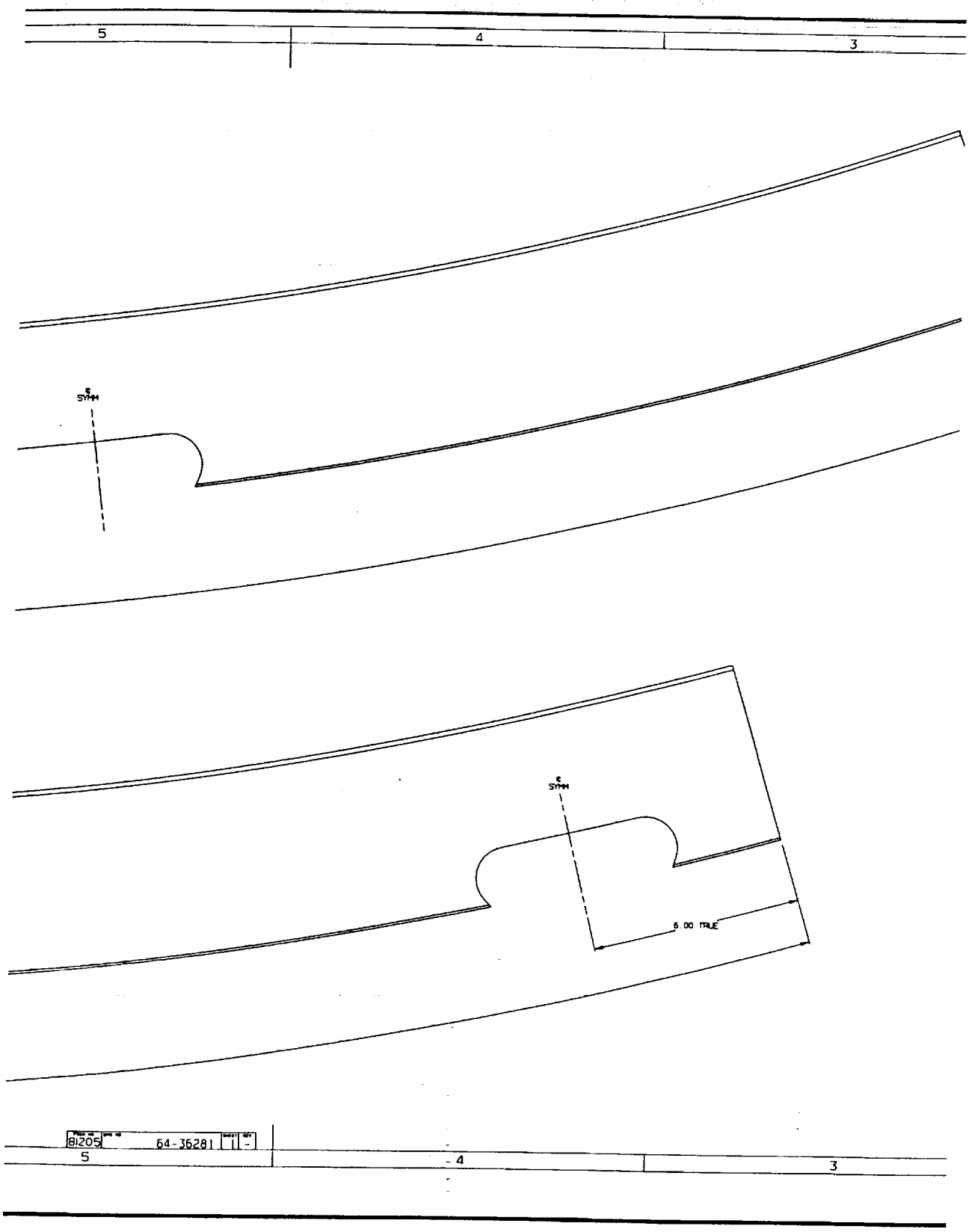


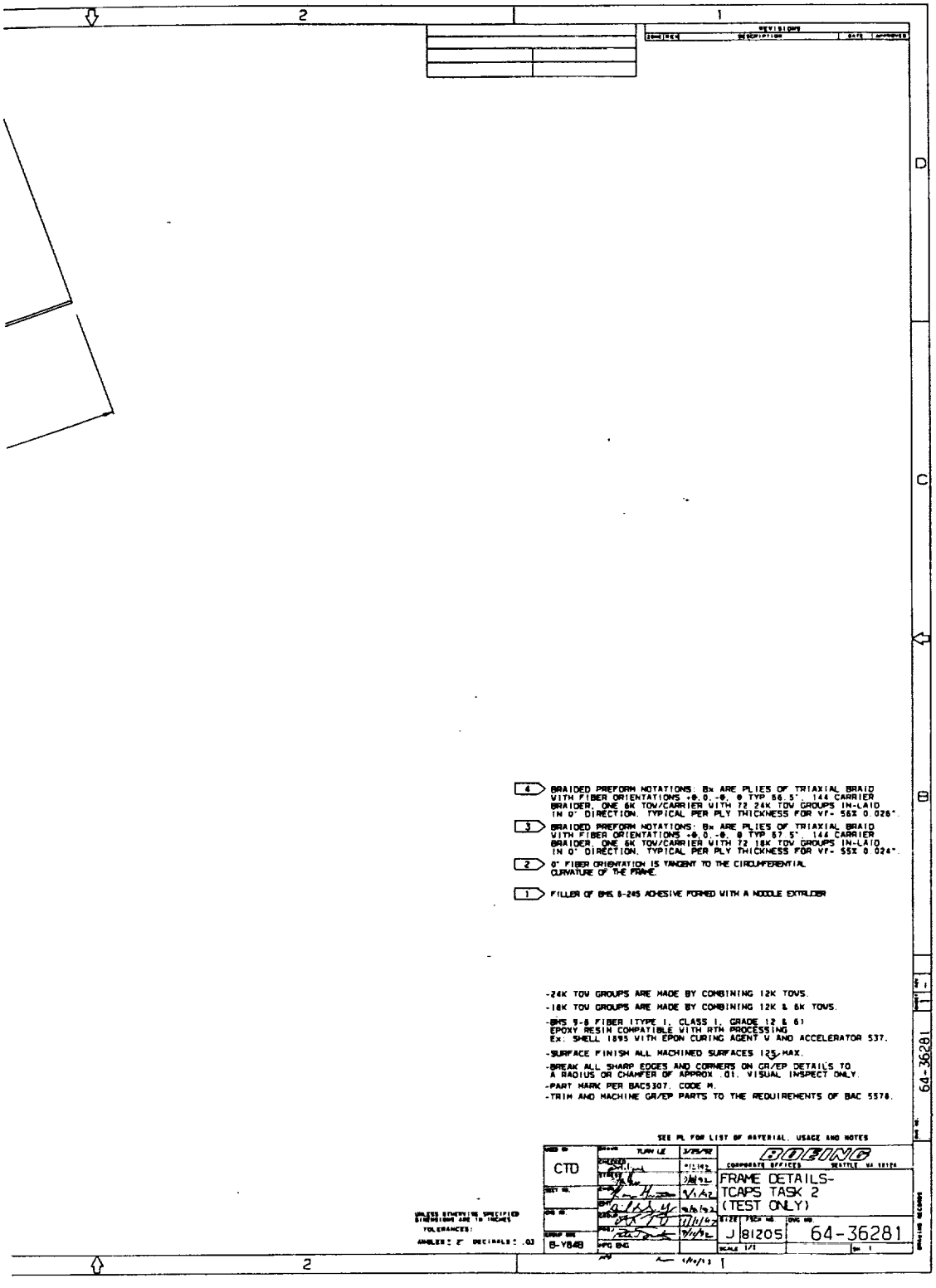
DETAIL -1
3

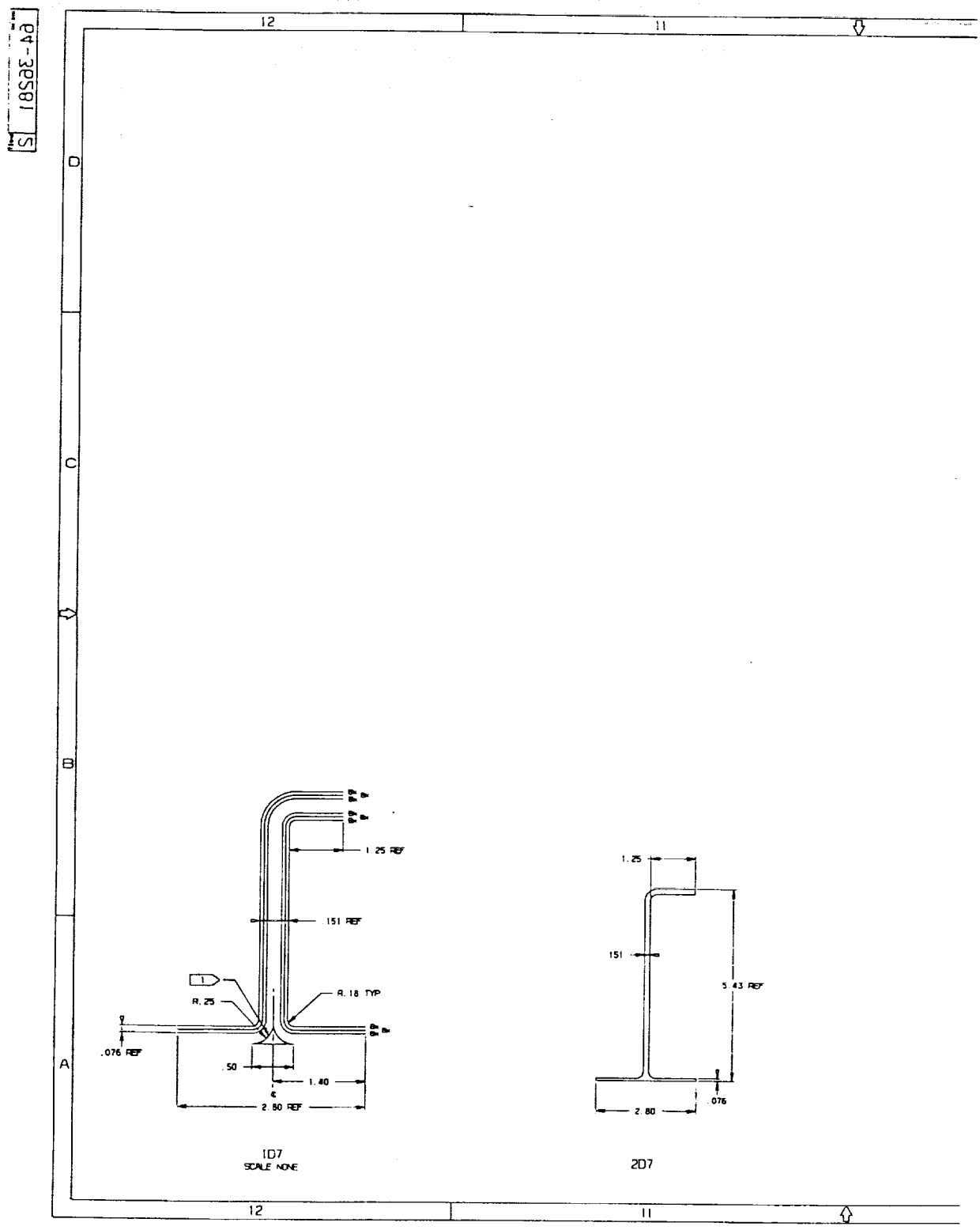


DETAIL -2
3

7
6


5
4
3
℄
SYMM
℄
SYMM
6.00 TRUE
81205
64-36281
5
4
3

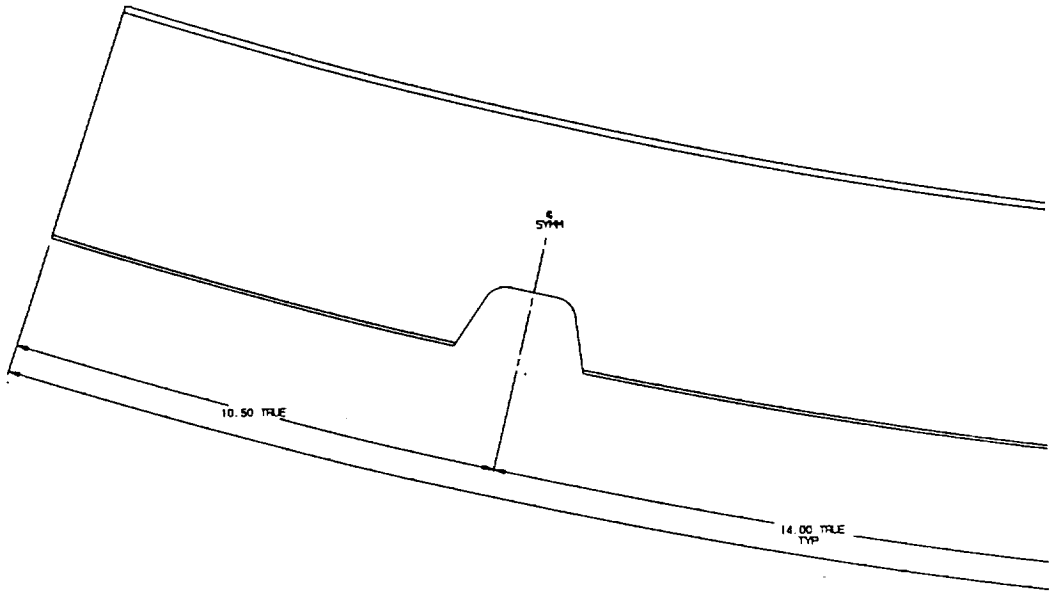

2
1
D
C
B
A
REVISIONS
DESCRIPTION
DATE
APPROVED
4 BRAIDED PREFORM NOTATIONS: Bx ARE PLIES OF TRIAXIAL BRAID WITH FIBER ORIENTATIONS +θ,0,-θ, θ TYP 66.5°. 144 CARRIER BRAIDER, ONE 6K TOW/CARRIER WITH 72 24K TOW GROUPS IN-LAID IN 0° DIRECTION. TYPICAL PER PLY THICKNESS FOR Vf= 56% 0.026".
3 BRAIDED PREFORM NOTATIONS: Bx ARE PLIES OF TRIAXIAL BRAID WITH FIBER ORIENTATIONS +θ,0,-θ, θ TYP 67.5°. 144 CARRIER BRAIDER, ONE 6K TOW/CARRIER WITH 72 18K TOW GROUPS IN-LAID IN 0° DIRECTION. TYPICAL PER PLY THICKNESS FOR Vf= 55% 0.024".
2 0° FIBER ORIENTATION IS TANGENT TO THE CIRCUMFERENTIAL CURVATURE OF THE FRAME.
1 FILLER OF BMS 8-245 ADHESIVE FORMED WITH A NOODLE EXTRUDER
-24K TOW GROUPS ARE MADE BY COMBINING 12K TOWS.
-18K TOW GROUPS ARE MADE BY COMBINING 12K & 6K TOWS.
-BMS 9-8 FIBER (TYPE I, CLASS I, GRADE 12 & 6) EPOXY RESIN COMPATIBLE WITH RTM PROCESSING Ex: SHELL 1895 WITH EPON CURING AGENT V AND ACCELERATOR 537.
-SURFACE FINISH ALL MACHINED SURFACES 125 MAX.
-BREAK ALL SHARP EDGES AND CORNERS ON GR/EP DETAILS TO A RADIUS OR CHAMFER OF APPROX .01. VISUAL INSPECT ONLY.
-PART MARK PER BAC5307, CODE M.
-TRIM AND MACHINE GR/EP PARTS TO THE REQUIREMENTS OF BAC 5578.
SEE PL FOR LIST OF MATERIAL, USAGE AND NOTES
CTD
B-Y848
BOEING
CORPORATE OFFICES SEATTLE WA 98124
FRAME DETAILS-
TCAPS TASK 2
(TEST ONLY)
J81205
64-36281
SCALE 1/1
SHT 1
64-36281
UNLESS OTHERWISE SPECIFIED DIMENSIONS ARE IN INCHES
TOLERANCES:
ANGLES ± 2° DECIMALS ± .03



1D7
SCALE NONE

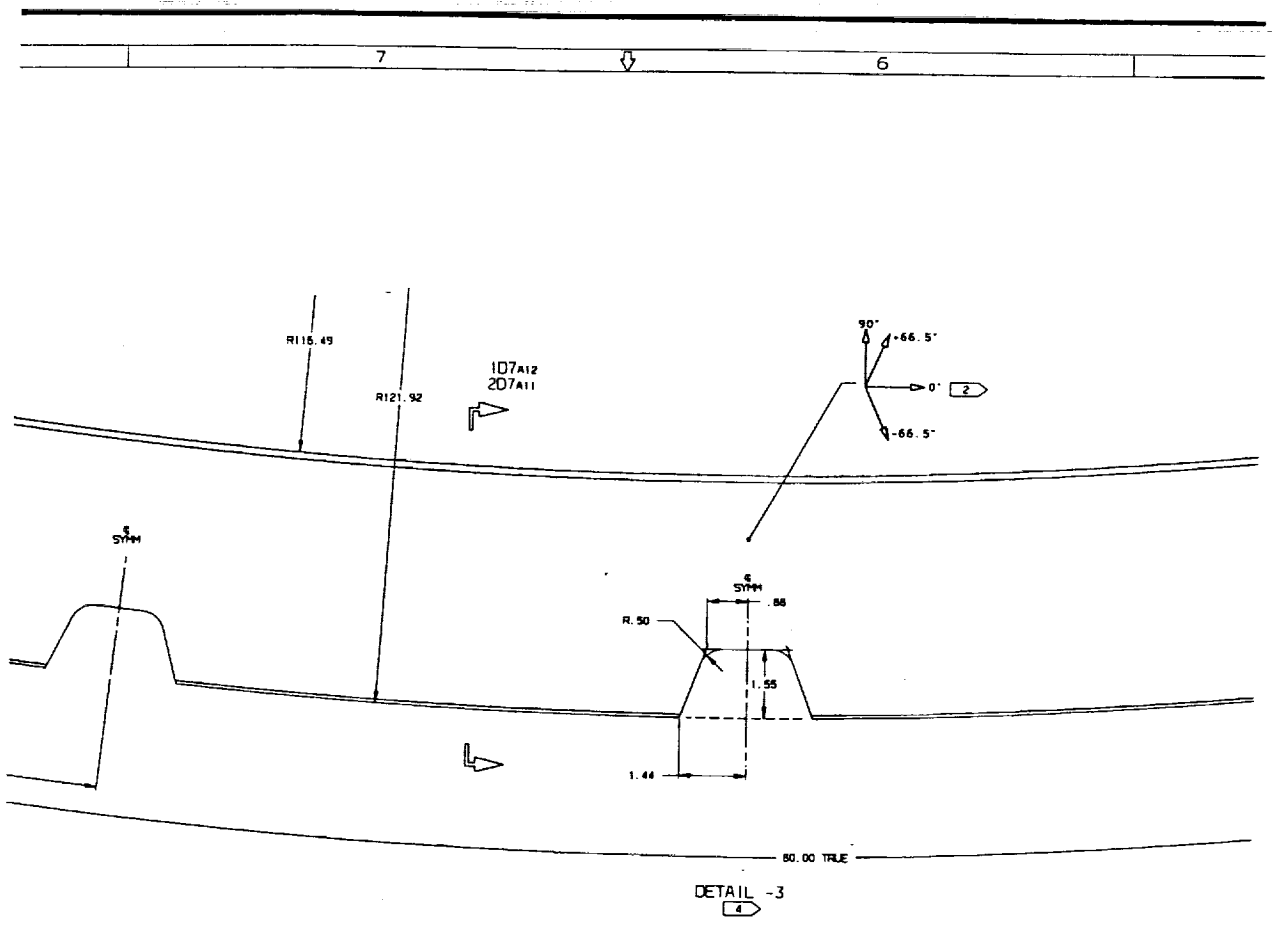
2D7

10	9	8

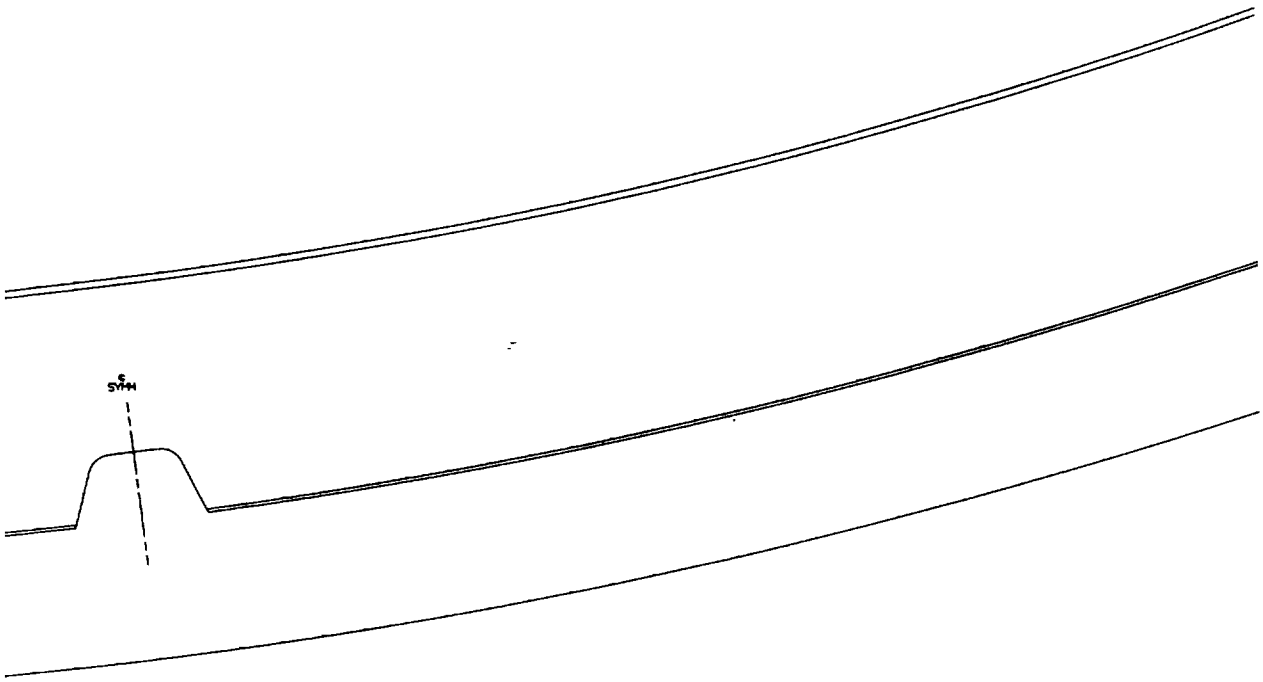


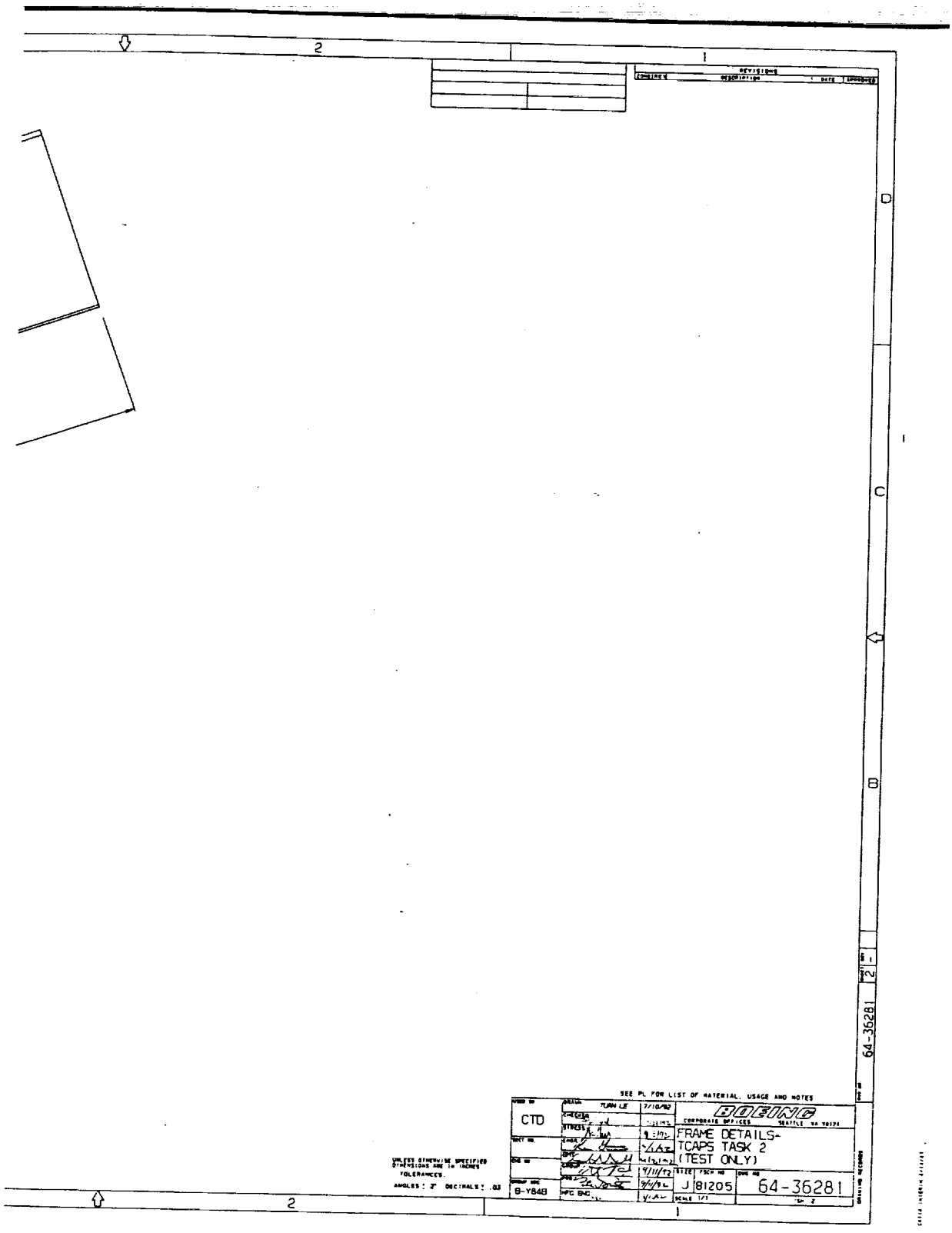
81205	54-36281	21

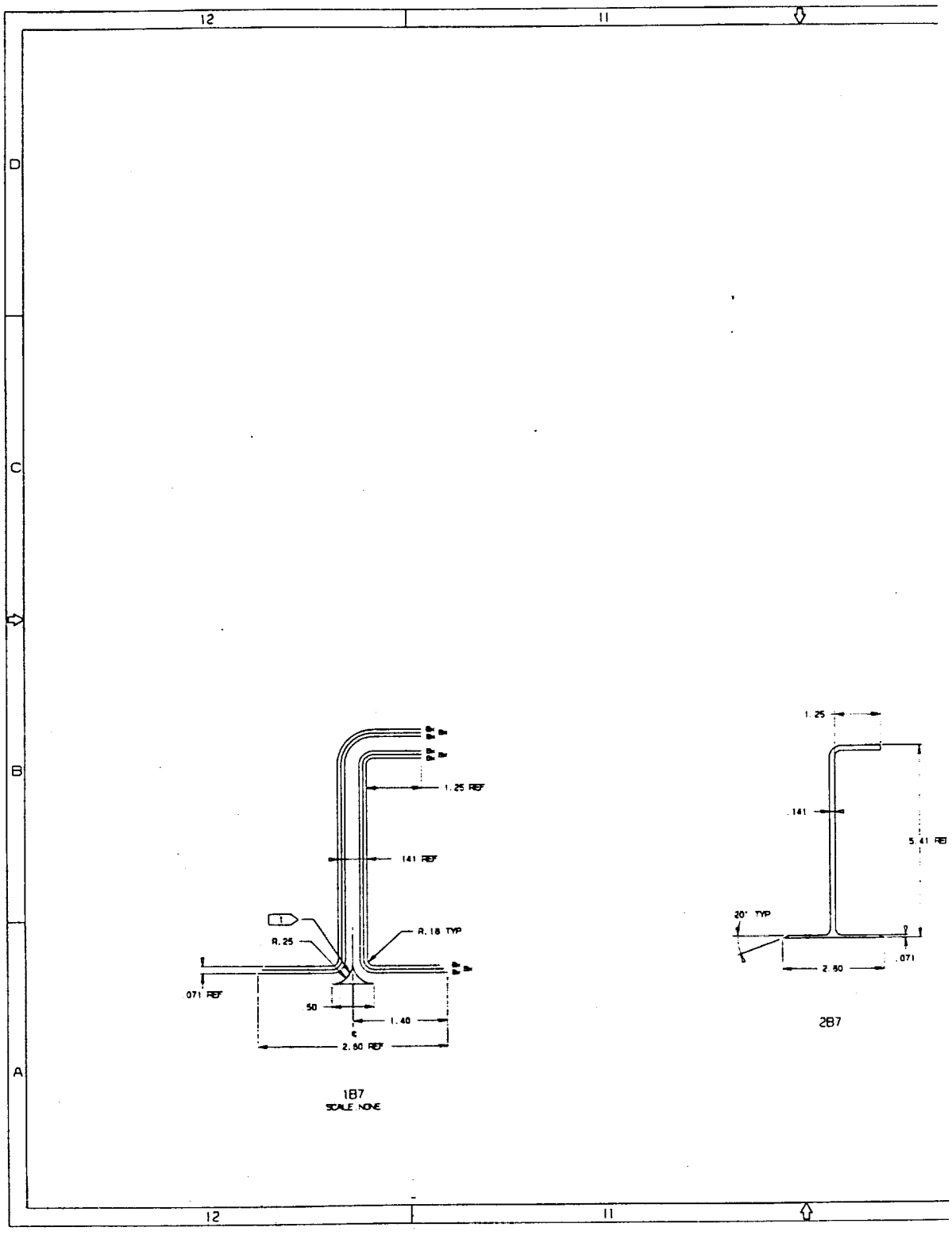
10	9	8


7
6
R115.49
R121.92
107A12
207A11
90°
+66.5°
0°
2
-66.5°
℄ SYMM
℄ SYMM
.88
R.50
1.55
1.44
80.00 TRUE
DETAIL -3
4

7
6

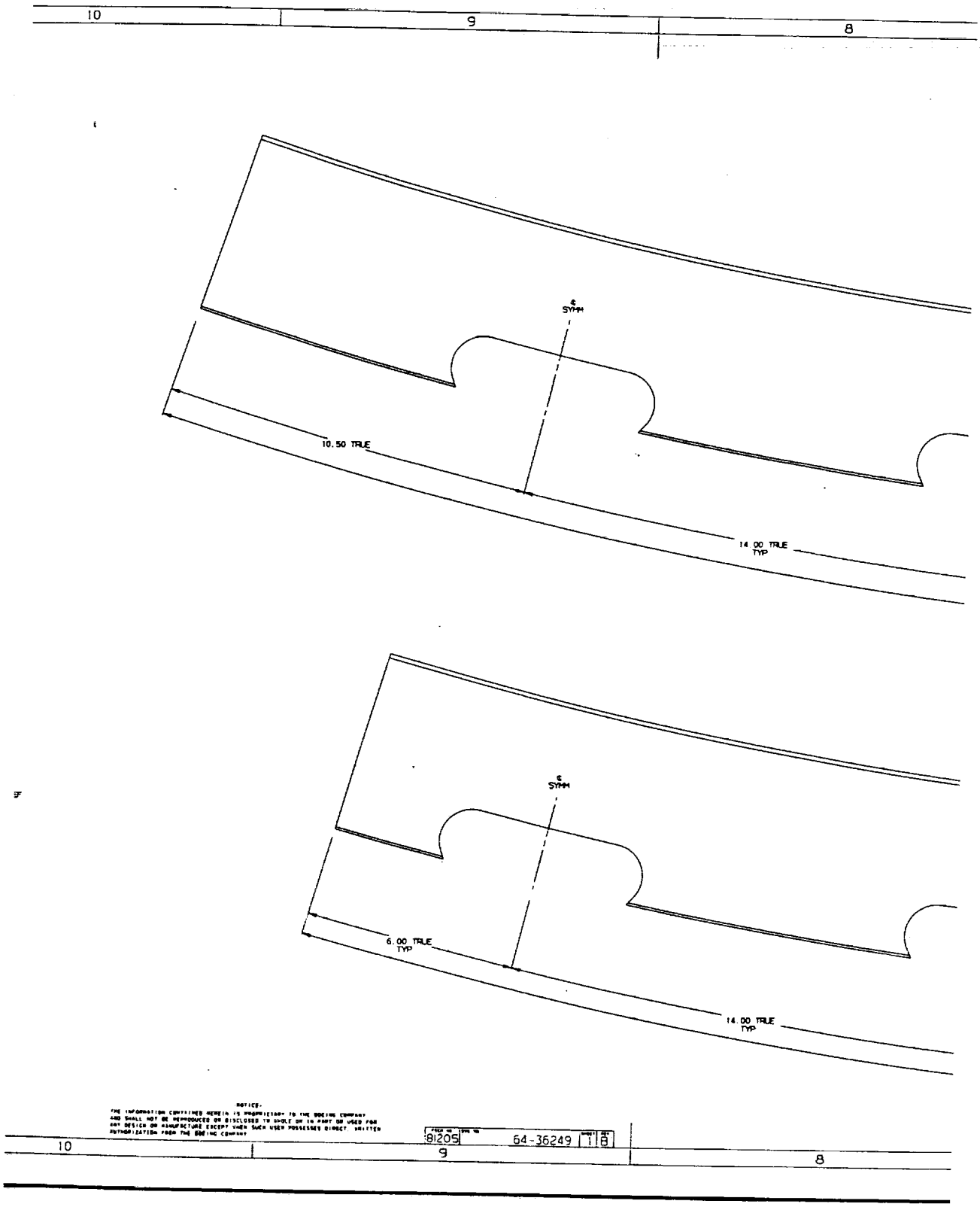

5
4
3
℄
SYM

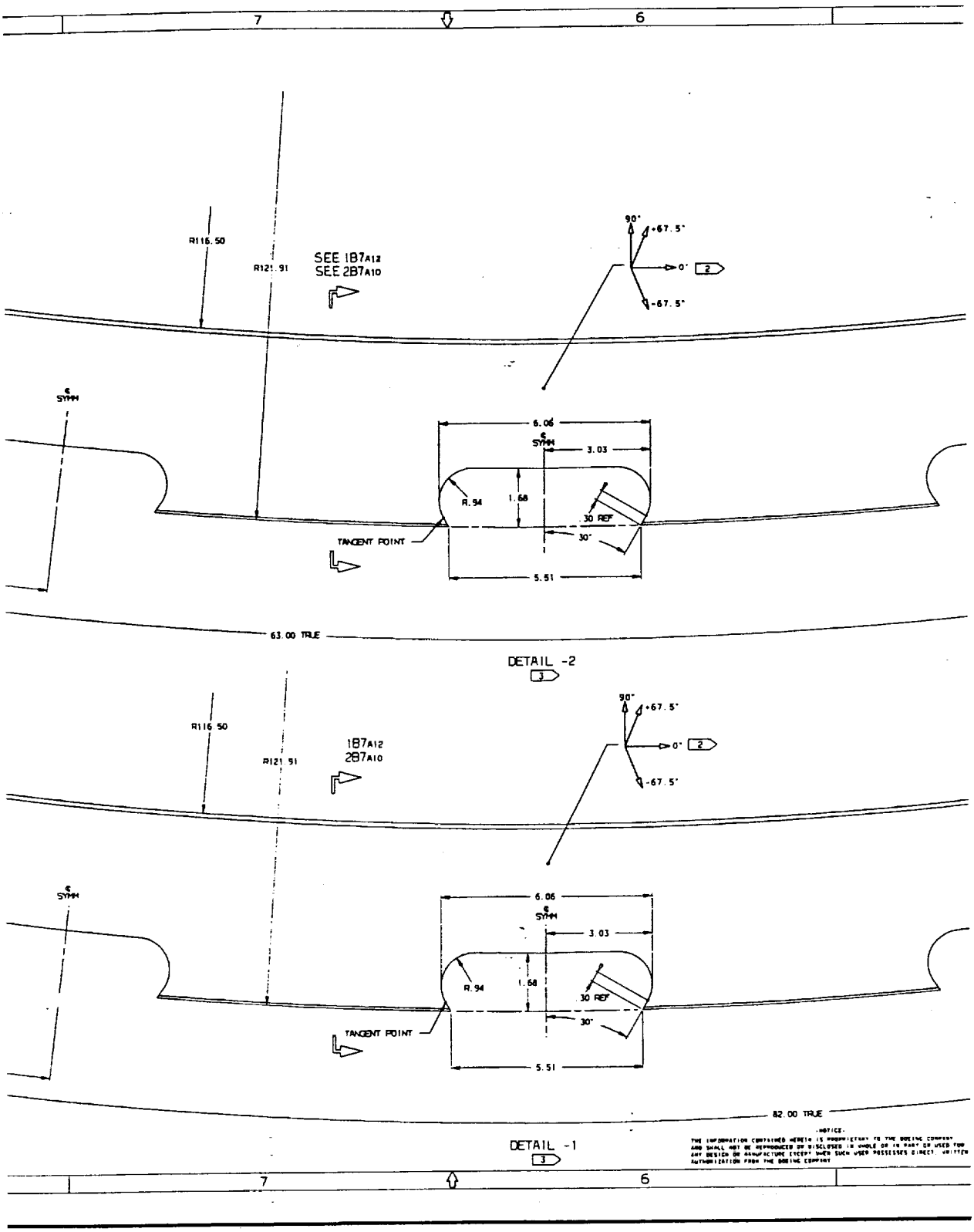

2
1
D
C
B
2
1
SEE PL FOR LIST OF MATERIAL, USAGE AND NOTES
CTD
TURN LE
7/10/92
BOEING
CORPORATE OFFICES SEATTLE, WA 98124
FRAME DETAILS-
TCAPS TASK 2
(TEST ONLY)
B-Y848
J 81205
64-36281
64-36281



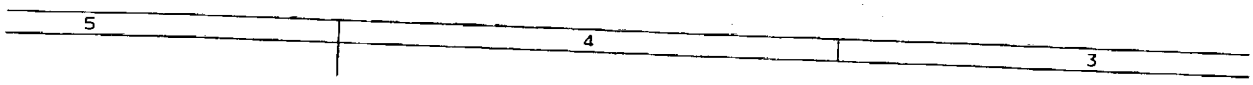
1B7
SCALE NONE

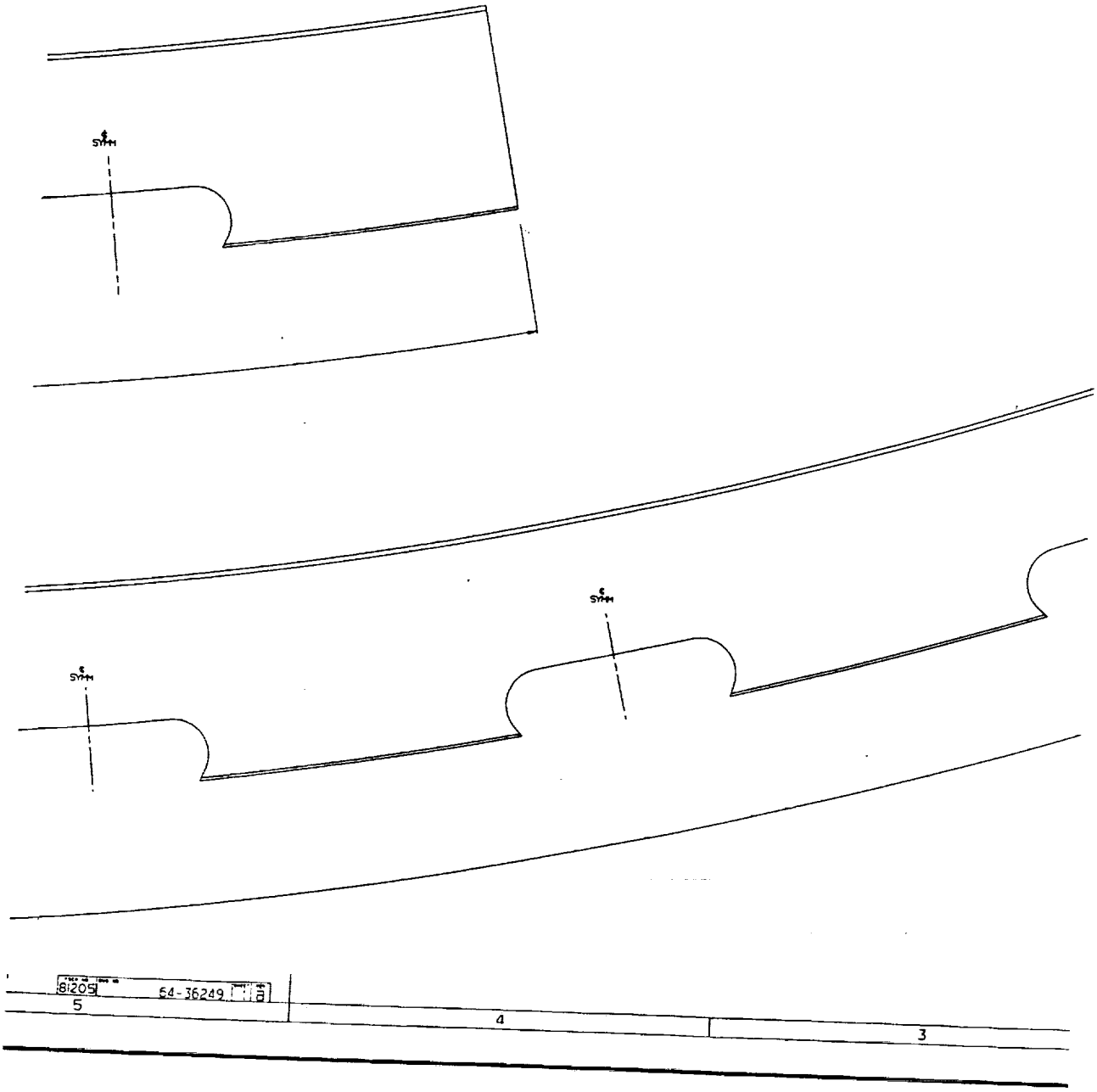
2B7

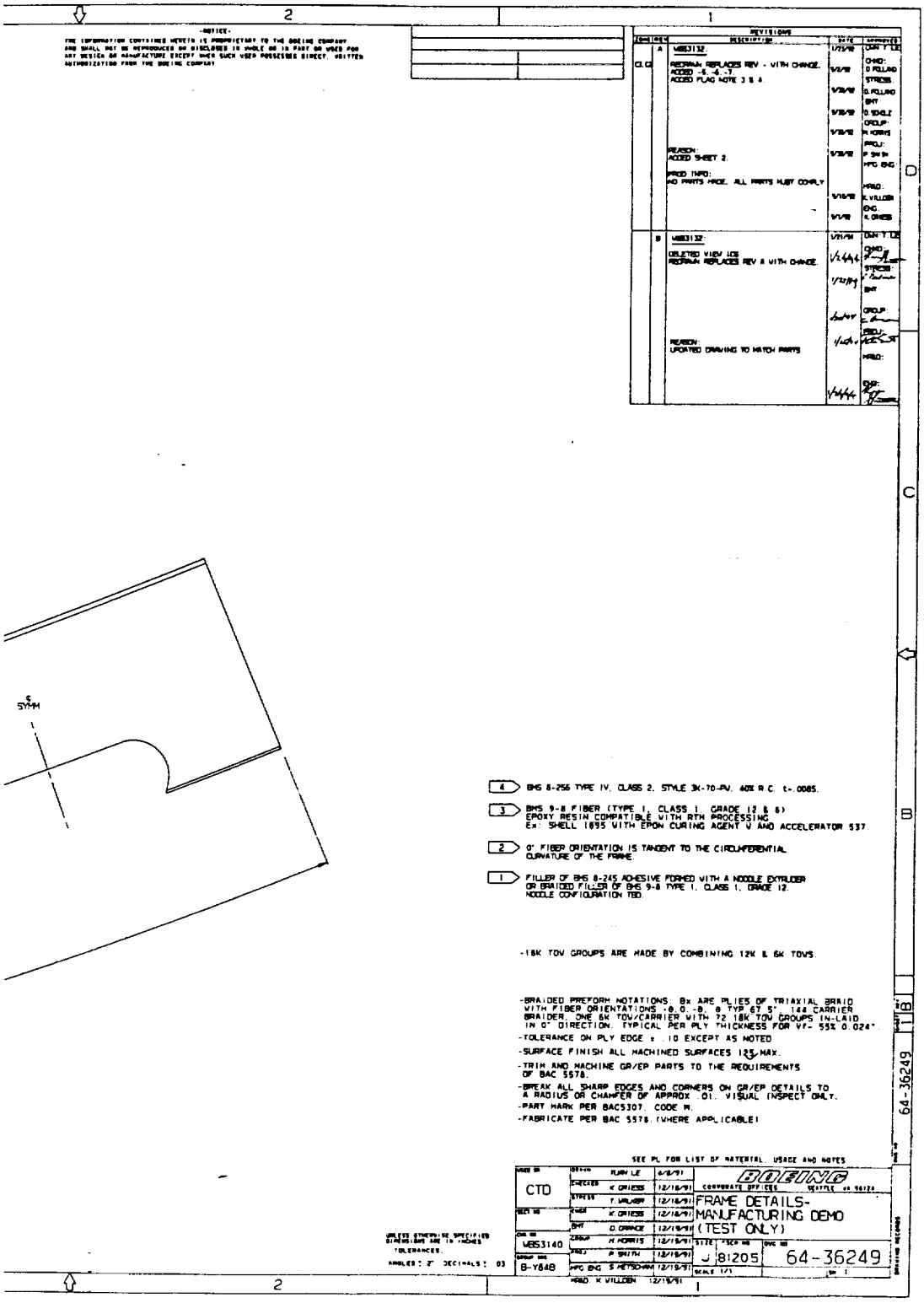

10
9
8
℄ SYMM
10.50 TRUE
14.00 TRUE TYP
℄ SYMM
6.00 TRUE TYP
14.00 TRUE TYP
NOTICE:
THE INFORMATION CONTAINED HEREIN IS PROPRIETARY TO THE BOEING COMPANY AND SHALL NOT BE REPRODUCED OR DISCLOSED IN WHOLE OR IN PART OR USED FOR ANY DESIGN OR MANUFACTURE EXCEPT WHEN SUCH USER POSSESSES DIRECT WRITTEN AUTHORIZATION FROM THE BOEING COMPANY
8120S
64-36249
10
9
8

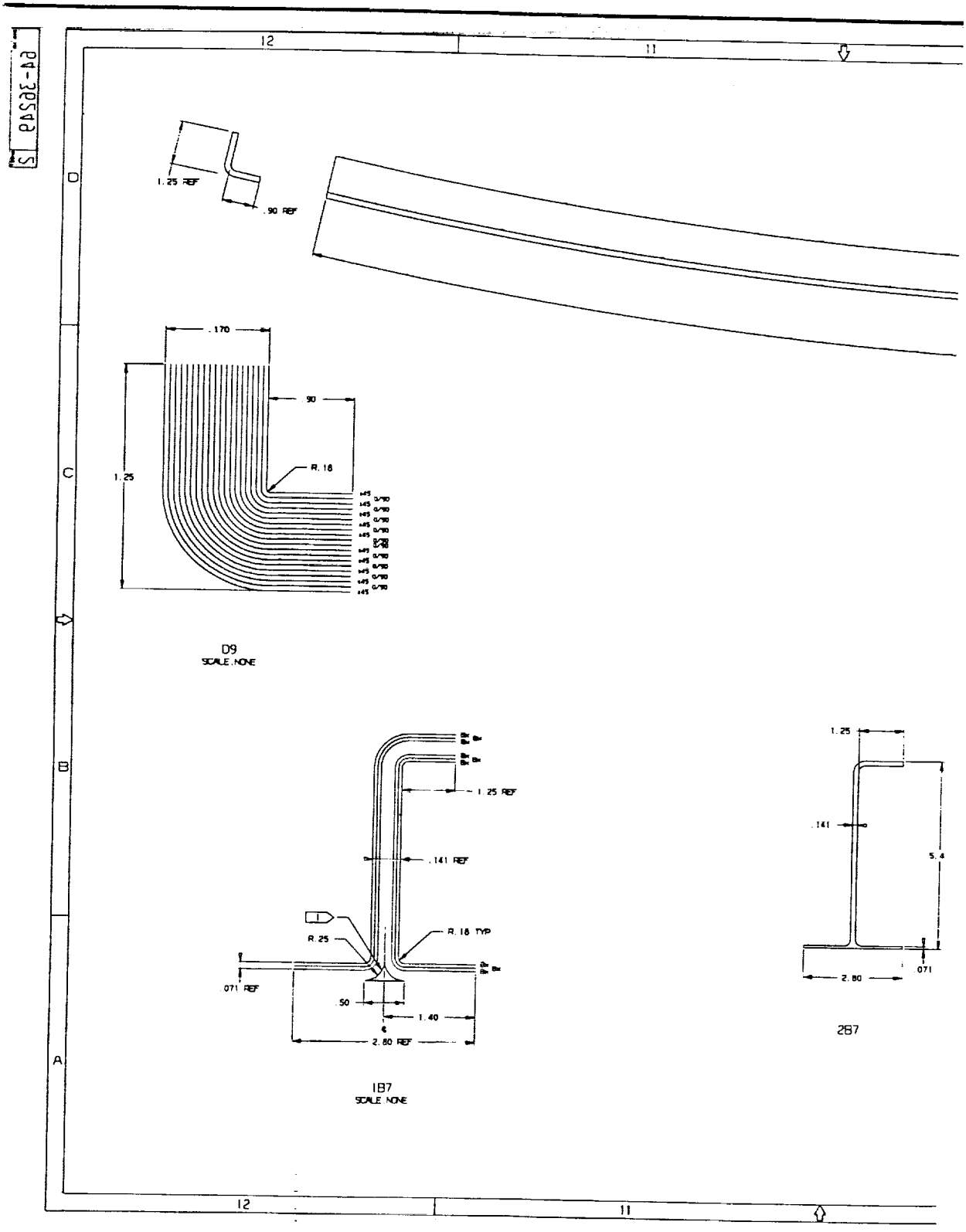


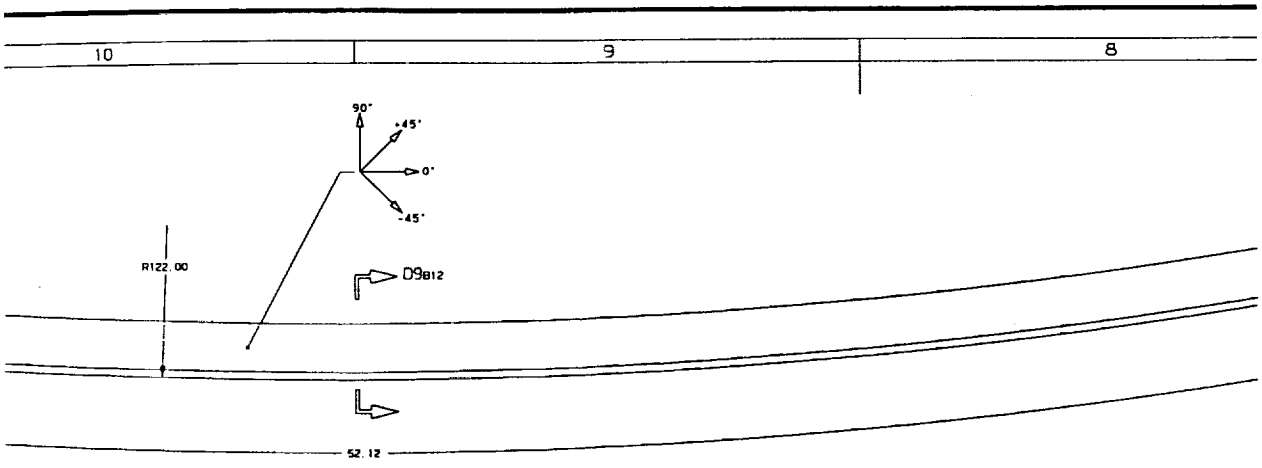
-NOTICE-
THE INFORMATION CONTAINED HEREIN IS PROPRIETARY TO THE BOEING COMPANY AND SHALL NOT BE REPRODUCED OR DISCLOSED IN WHOLE OR IN PART OR USED FOR ANY DESIGN OR MANUFACTURE EXCEPT WHEN SUCH USES POSSESSES DIRECT, WRITTEN AUTHORIZATION FROM THE BOEING COMPANY


5
4
3

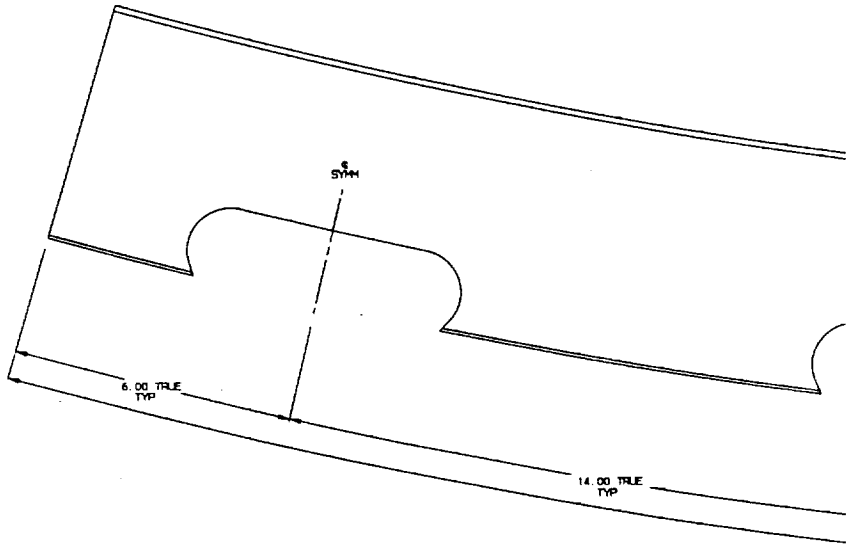

℄
SYM
℄
SYM
℄
SYM
81205
54-36249
5
4
3


-NOTICE-
THE INFORMATION CONTAINED HEREIN IS PROPRIETARY TO THE BOEING COMPANY AND SHALL NOT BE REPRODUCED OR DISCLOSED IN WHOLE OR IN PART OR USED FOR ANY DESIGN OR MANUFACTURE EXCEPT WHEN SUCH USE POSSESSES DIRECT, WRITTEN AUTHORIZATION FROM THE BOEING COMPANY
REVISIONS
A
B
REASON:
ADDED SHEET 2.
REASON:
UPDATED DRAWING TO MATCH PARTS
℄ SYMM
4 BMS 8-256 TYPE IV, CLASS 2, STYLE 3K-70-PW, 40% R.C. t=.0085.
3 BMS 9-8 FIBER (TYPE I, CLASS 1, GRADE 12 & 6) EPOXY RESIN COMPATIBLE WITH RTM PROCESSING. Ex: SHELL 1895 WITH EPON CURING AGENT U AND ACCELERATOR 537.
2 0° FIBER ORIENTATION IS TANGENT TO THE CIRCUMFERENTIAL CURVATURE OF THE FRAME.
1 FILLER OF BMS 8-245 ADHESIVE FORMED WITH A NOODLE EXTRUDER OR BRAIDED FILLER OF BMS 9-8 TYPE 1, CLASS 1, GRADE 12. NOODLE CONFIGURATION TBD.
-18K TOW GROUPS ARE MADE BY COMBINING 12K & 6K TOWS.
-BRAIDED PREFORM NOTATIONS: 8x ARE PLIES OF TRIAXIAL BRAID WITH FIBER ORIENTATIONS -θ,0,-θ, θ TYP 67.5° 144 CARRIER BRAIDER. ONE 6K TOW/CARRIER WITH 72 18K TOW GROUPS IN-LAID IN 0° DIRECTION. TYPICAL PER PLY THICKNESS FOR Vf- 55% 0.024".
-TOLERANCE ON PLY EDGE ± .10 EXCEPT AS NOTED
-SURFACE FINISH ALL MACHINED SURFACES 125 MAX.
-TRIM AND MACHINE GR/EP PARTS TO THE REQUIREMENTS OF BAC 5578.
-BREAK ALL SHARP EDGES AND CORNERS ON GR/EP DETAILS TO A RADIUS OR CHAMFER OF APPROX .01. VISUAL INSPECT ONLY.
-PART MARK PER BAC5307, CODE M.
-FABRICATE PER BAC 5578. (WHERE APPLICABLE)
SEE PL FOR LIST OF MATERIAL, USAGE AND NOTES
CTD
V853140
8-Y848
BOEING
FRAME DETAILS-
MANUFACTURING DEMO
(TEST ONLY)
J 81205
64-36249
SCALE 1/1
SHT 1
64-36249 REV B
2
1


12
11
D
C
B
A
1.25 REF
.90 REF
.170
.50
R.18
1.25
D9
SCALE: NONE
1.25 REF
.141 REF
R.25
R.18 TYP
.071 REF
.50
1.40
2.80 REF
1B7
SCALE: NONE
1.25
.141
5.4
.071
2.80
2B7



DETAIL -5
4

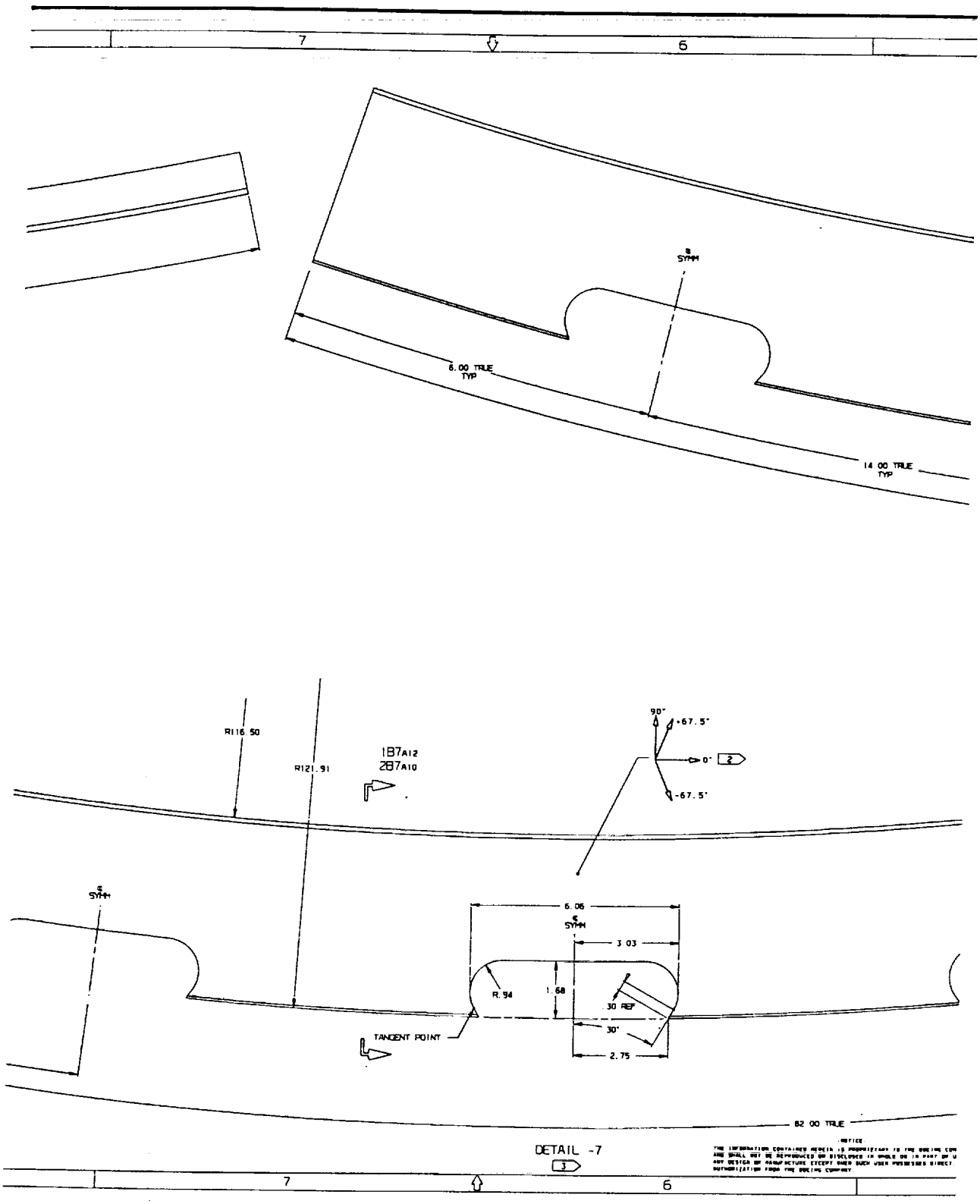


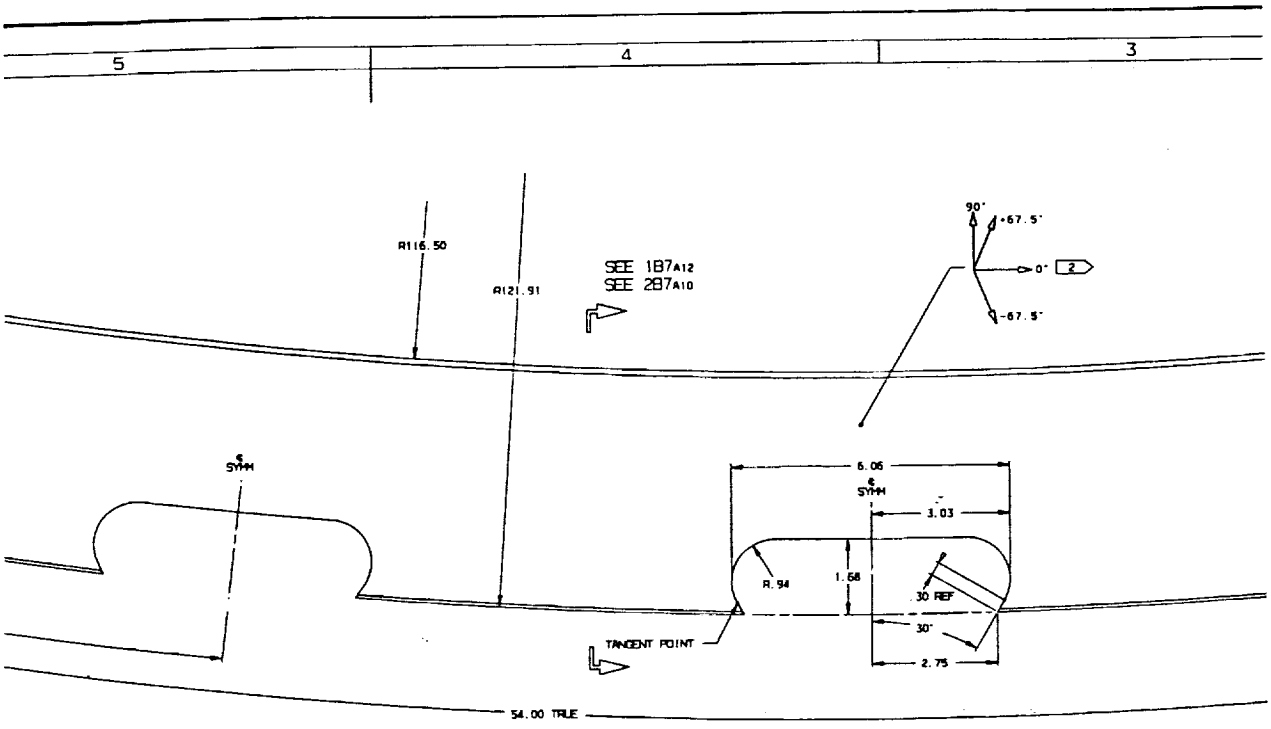
11 REF

-NOTICE-
THE INFORMATION CONTAINED HEREIN IS PROPRIETARY TO THE BOEING COMPANY AND SHALL NOT BE REPRODUCED OR DISCLOSED IN WHOLE OR IN PART OR USED FOR ANY DESIGN OR MANUFACTURE EXCEPT WHEN SUCH USES POSSESSES DIRECT, WRITTEN AUTHORIZATION FROM THE BOEING COMPANY

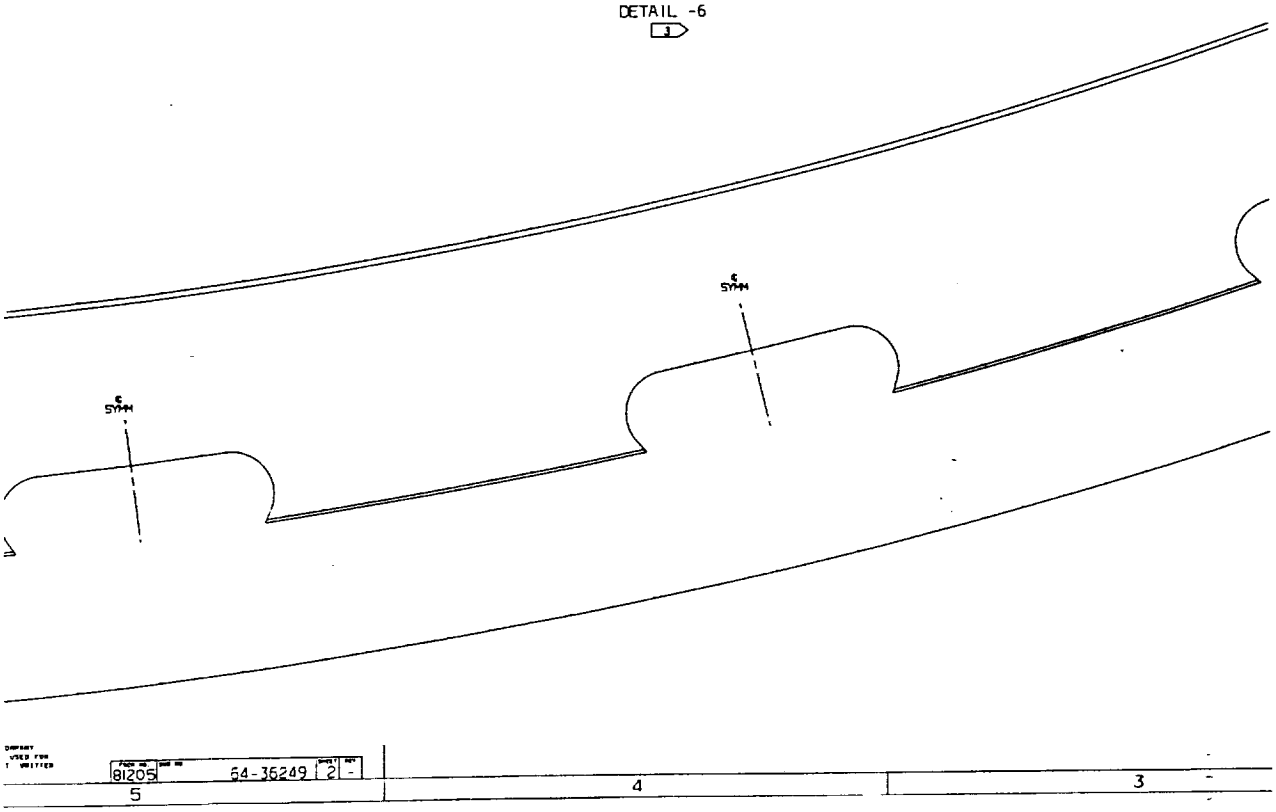
81205 64-36249 2

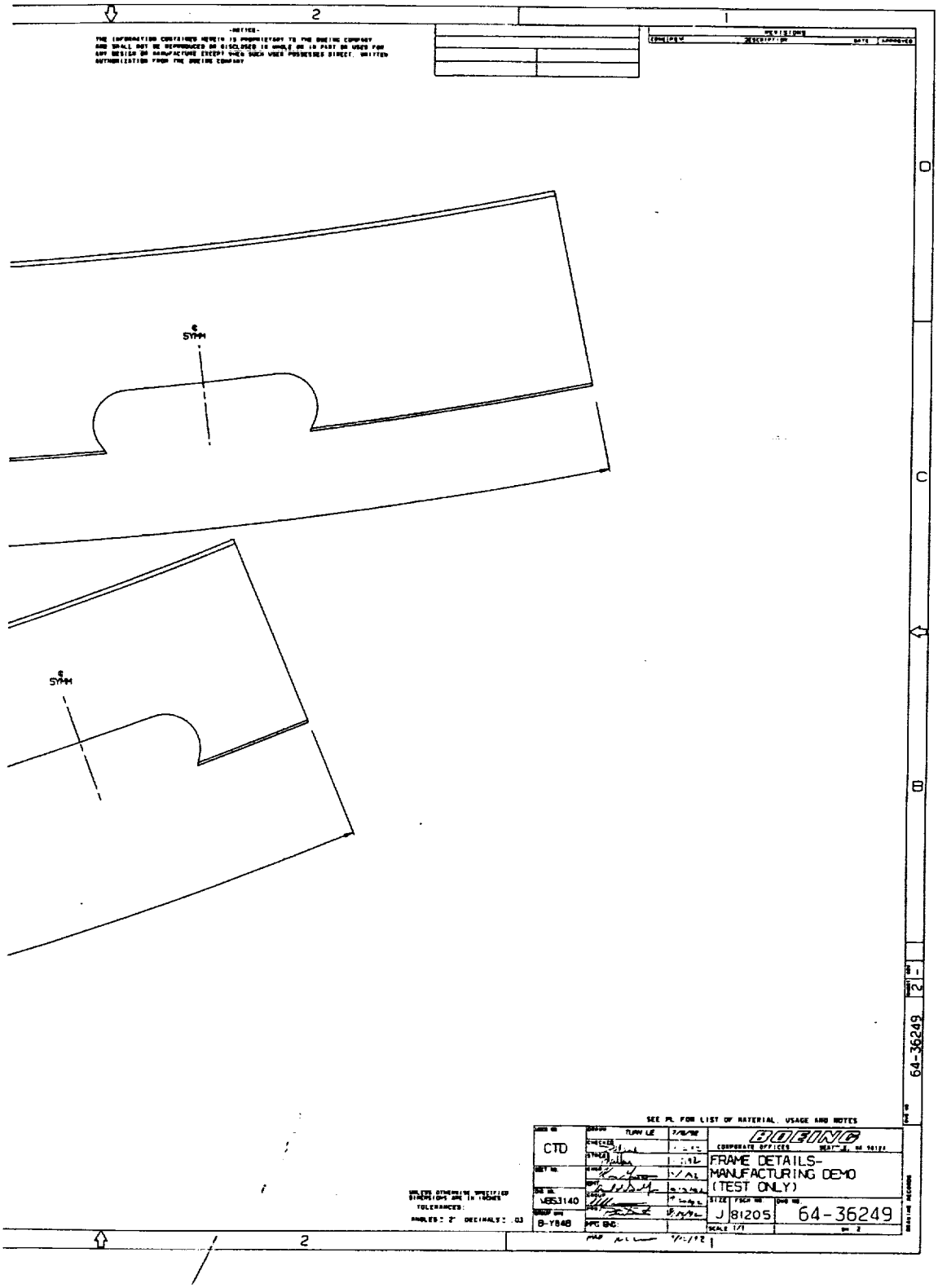
10
9
8


7
6
℄ SYMM
6.00 TRUE TYP
14.00 TRUE TYP
R116.50
R121.91
187A12
287A10
90°
+67.5°
0°
2
-67.5°
℄ SYMM
6.06
℄ SYMM
3.03
R.94
1.68
30 REF
30°
2.75
TANGENT POINT
82.00 TRUE
DETAIL -7
3
7
6


5
4
3
R116.50
R121.91
SEE 187A12
SEE 287A10
90°
+67.5°
0°
2
-67.5°
℄ SYMM
6.06
℄ SYMM
3.03
R.94
1.68
.30 REF
30°
2.75
TANGENT POINT
54.00 TRUE

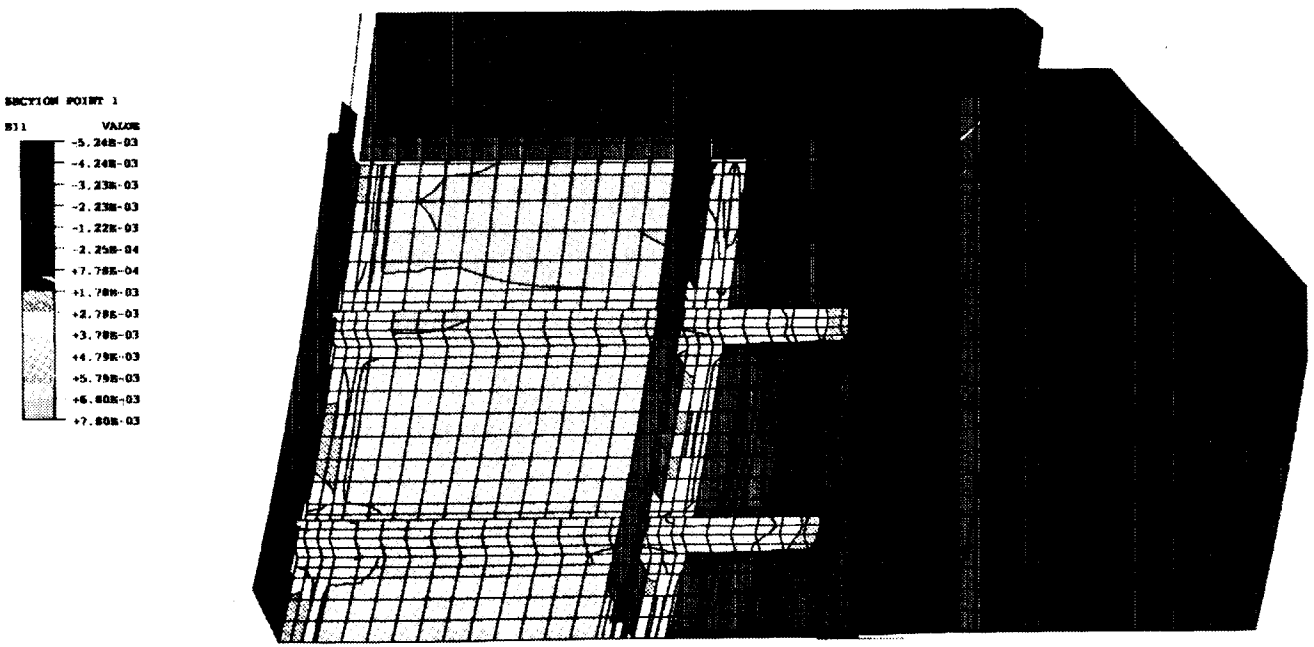
DETAIL -6
3


℄ SYMM
℄ SYMM


2
1
D
C
B
SYMM
SYMM
SEE PL FOR LIST OF MATERIAL, USAGE AND NOTES
BOEING
CORPORATE OFFICES
FRAME DETAILS-
MANUFACTURING DEMO
(TEST ONLY)
CTD
V853140
B-Y848
J 81205
64-36249
64-36249
2

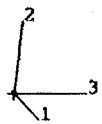
Appendix G

Finite Element Results for Undamaged Panel 1



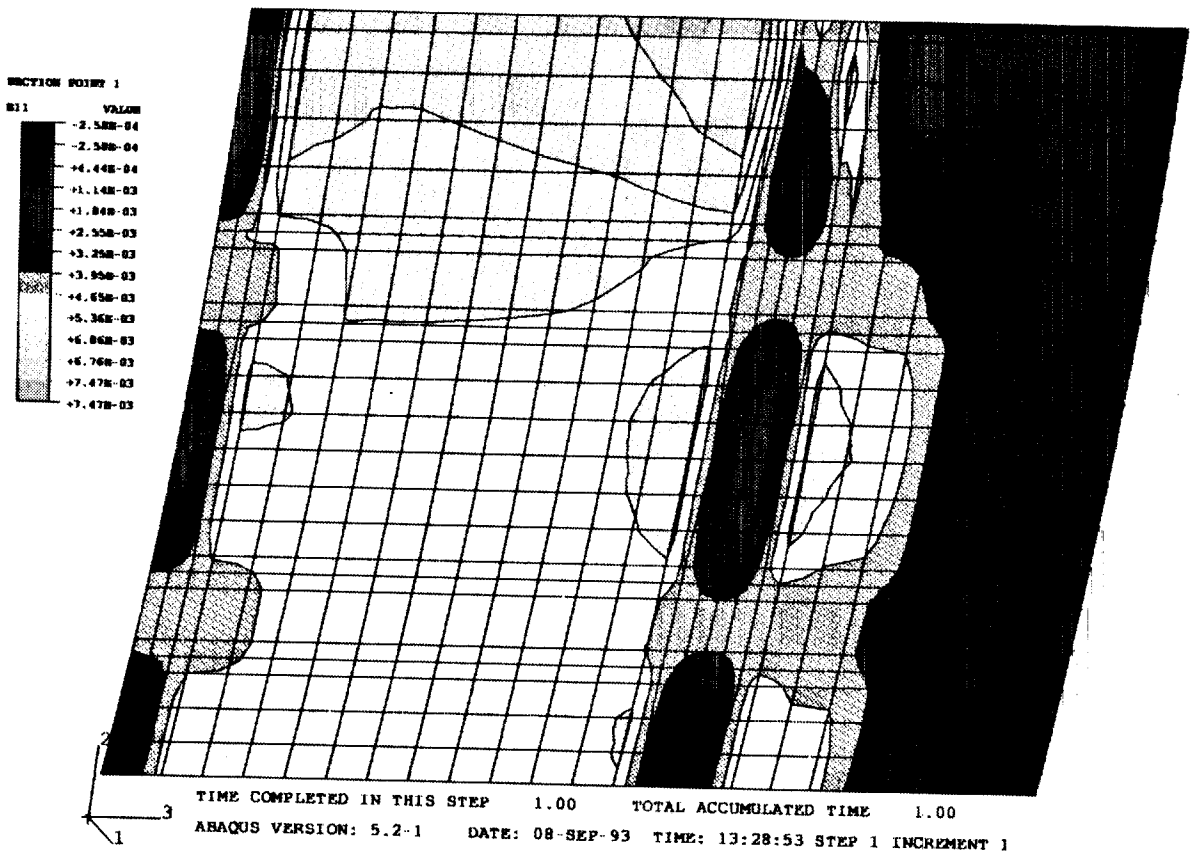
TCAPS1: SLOTTED AXIAL DOUBLERS

P=13.8 psi, Axial Load=5000 lb/in

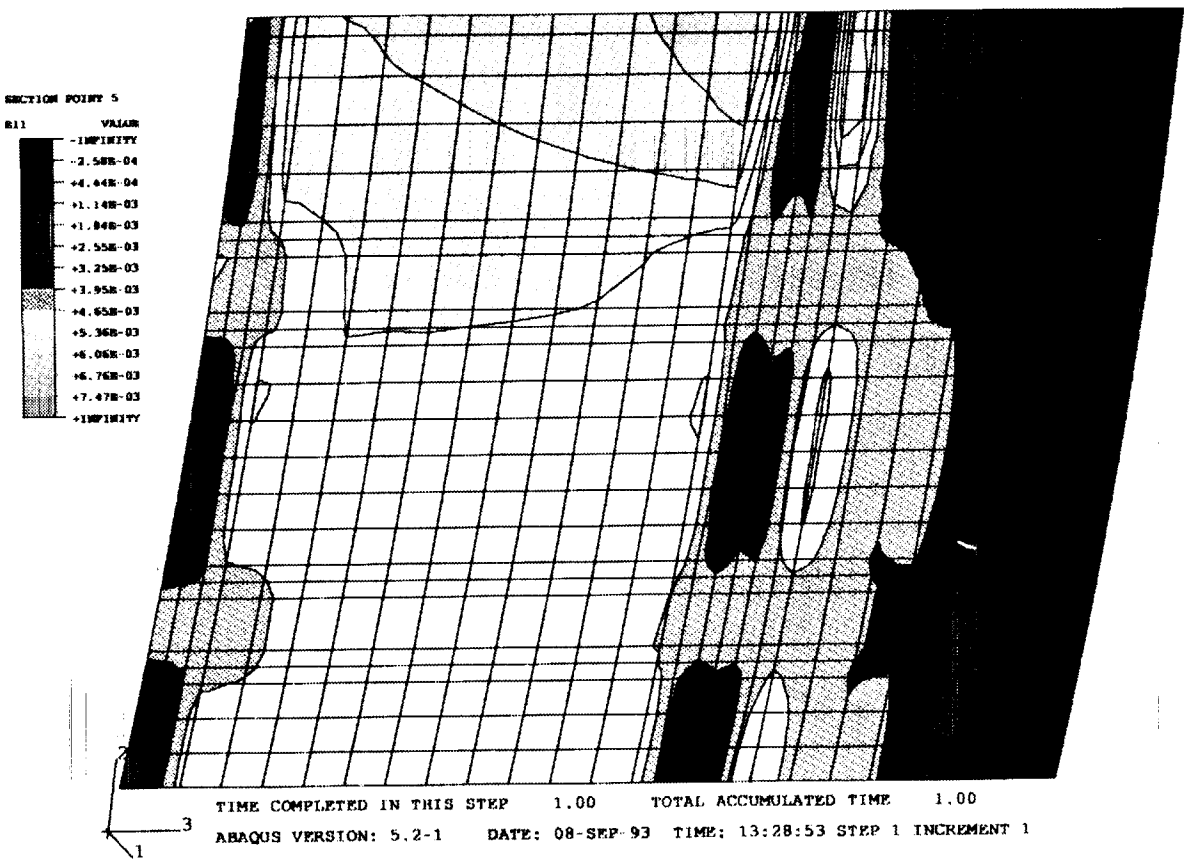


TIME COMPLETED IN THIS STEP 1.00 TOTAL ACCUMULATED TIME 1.00

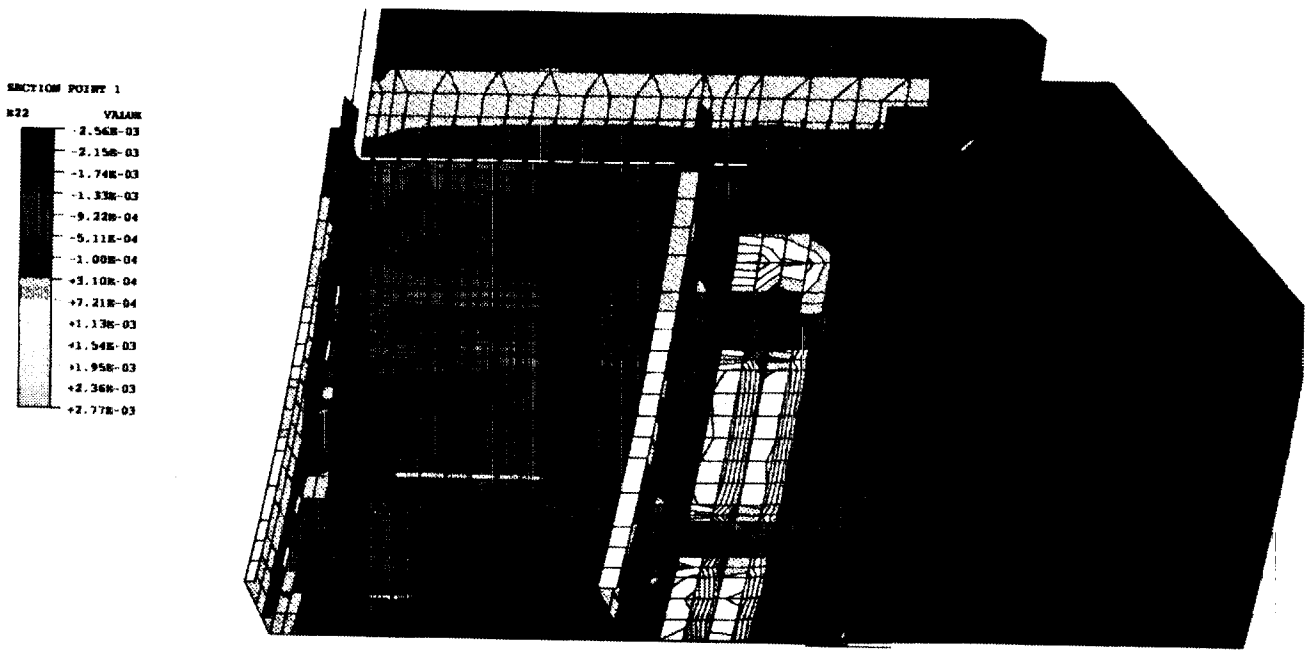
ABAQUS VERSION: 5.2-1 DATE: 08-SEP-93 TIME: 13:28:53 STEP 1 INCREMENT 1



TCAPS1: SLOTTED AXIAL DOUBLERS
p = 13.8 psi, Axial Load = 5000 lb/in

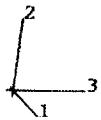


TCAPS1: SLOTTED AXIAL DOUBLERS
p = 13.8 psi, Axial Load = 5000 lb/in



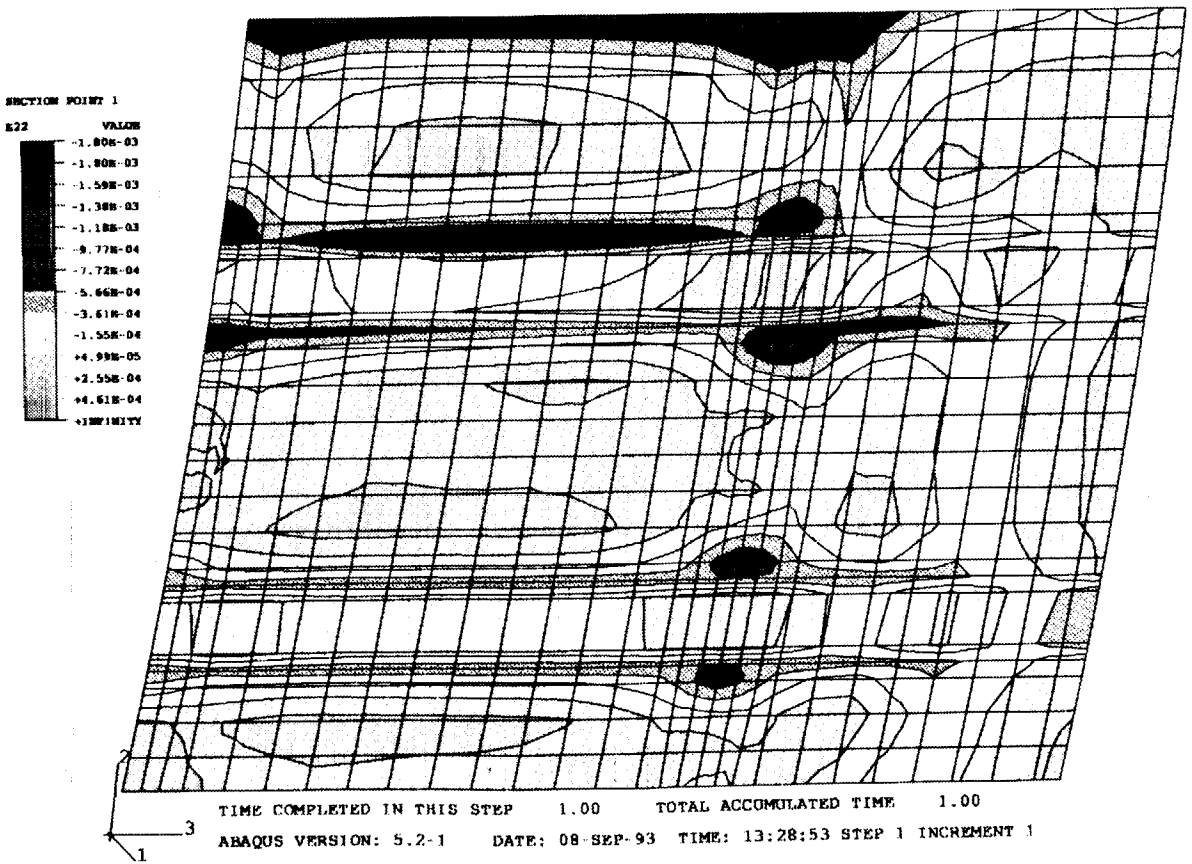
TCAPS1: SLOTTED AXIAL DOUBLERS

p=13.8 psi, Axial Load = 5000 lb/in

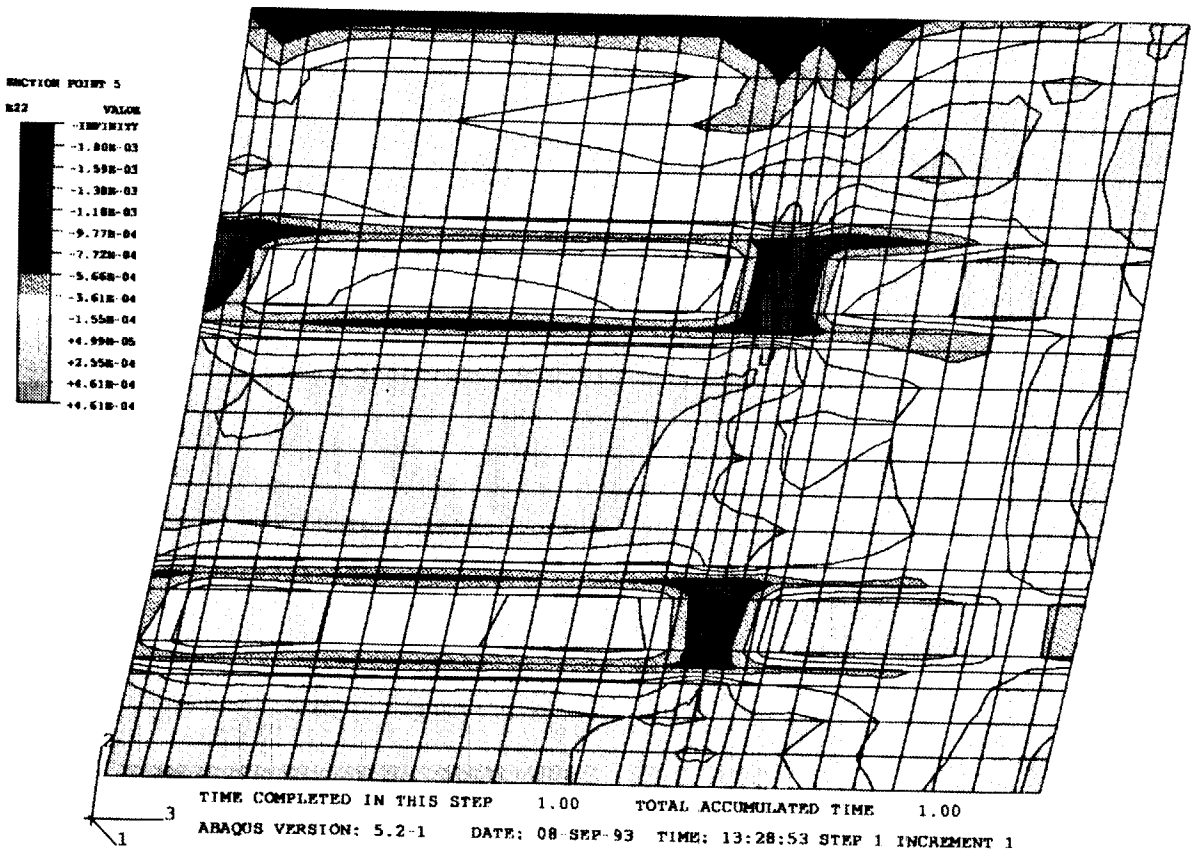


TIME COMPLETED IN THIS STEP 1.00 TOTAL ACCUMULATED TIME 1.00

ABAQUS VERSION: 5.2-1 DATE: 08-SEP-93 TIME: 13:28:53 STEP 1 INCREMENT 1

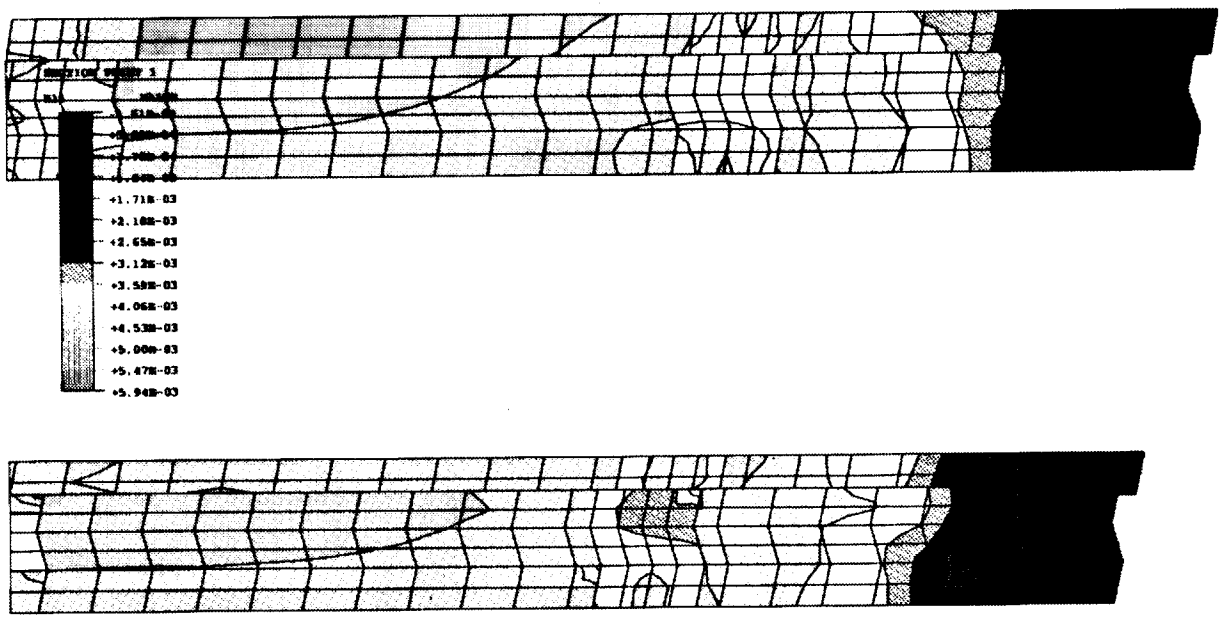


TCAPS1: SLOTTED AXIAL DOUBLERS
p = 13.8 psi, Axial Load = 5000 lb/in

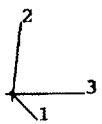


TCAPS1: SLOTTED AXIAL DOUBLERS
p = 13.8 psi, Axial Load = 5000 lb/in

AB

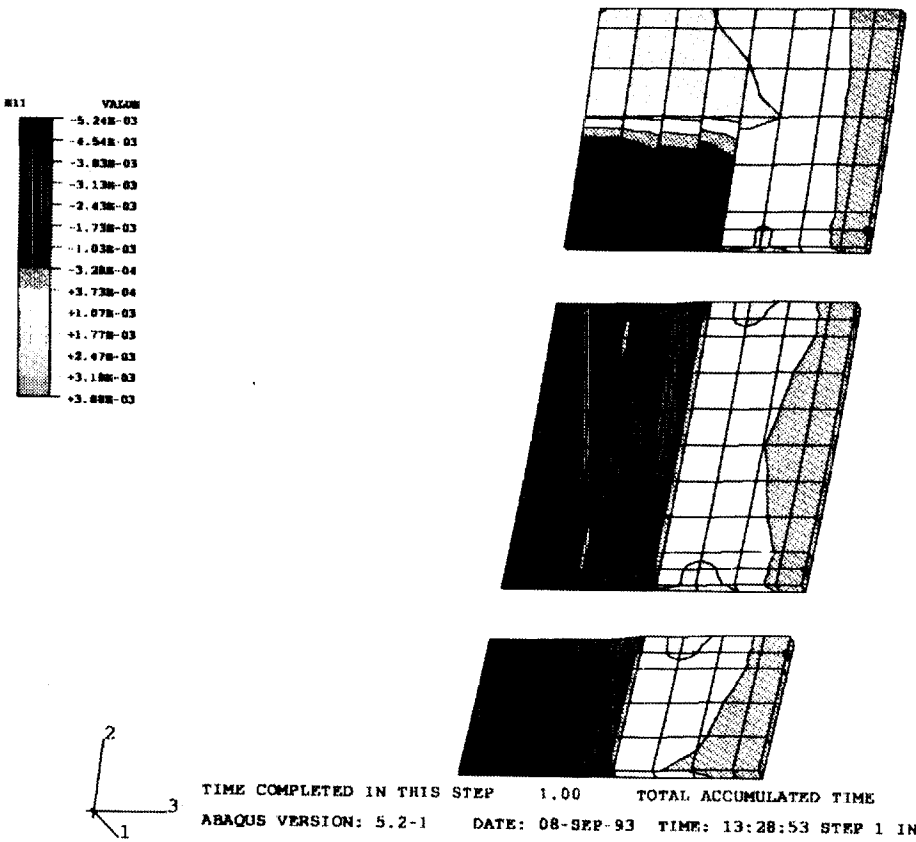


TCAPS1: SLOTTED AXIAL DOUBLERS
p=13.8 psi, Axial Load=5000 lb/in

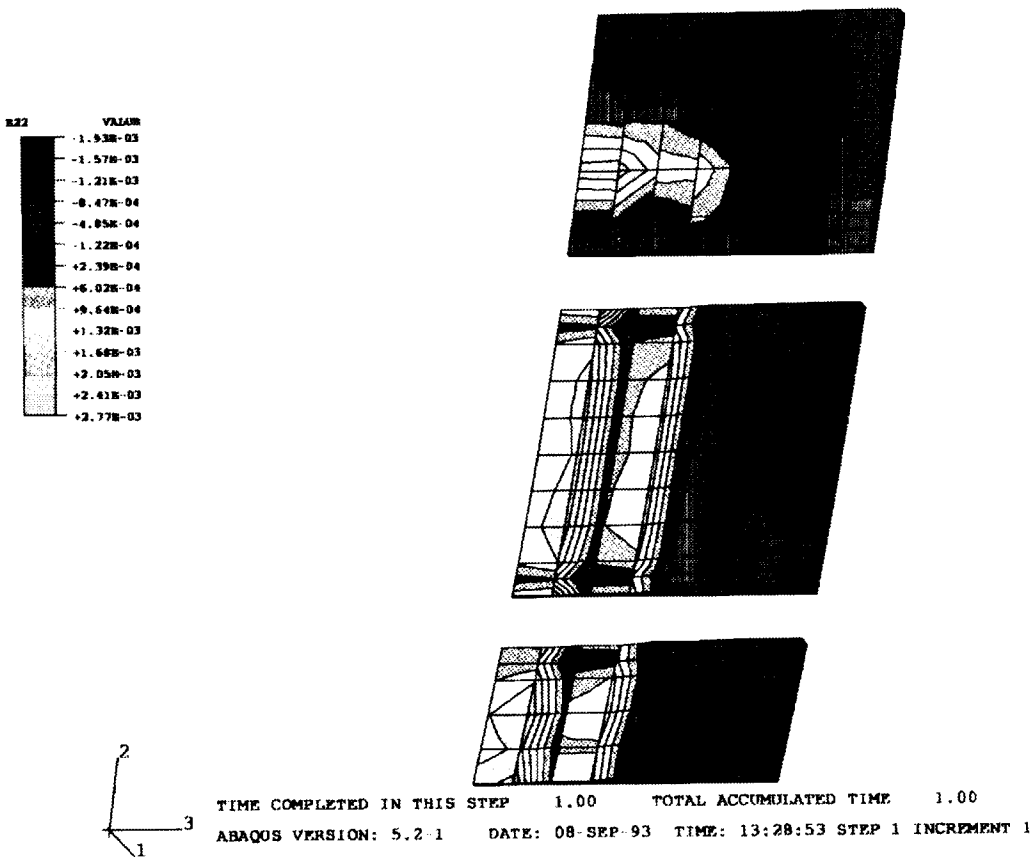


TIME COMPLETED IN THIS STEP 1.00 TOTAL ACCUMULATED TIME 1.00
ABAQUS VERSION: 5.2-1 DATE: 08-SEP-93 TIME: 13:28:53 STEP 1 INCREMENT 1

C-3.



TCAPS1: SLOTTED AXIAL DOUBLERS
p = 13.8 psi, Axial Load = 5000 lb/in

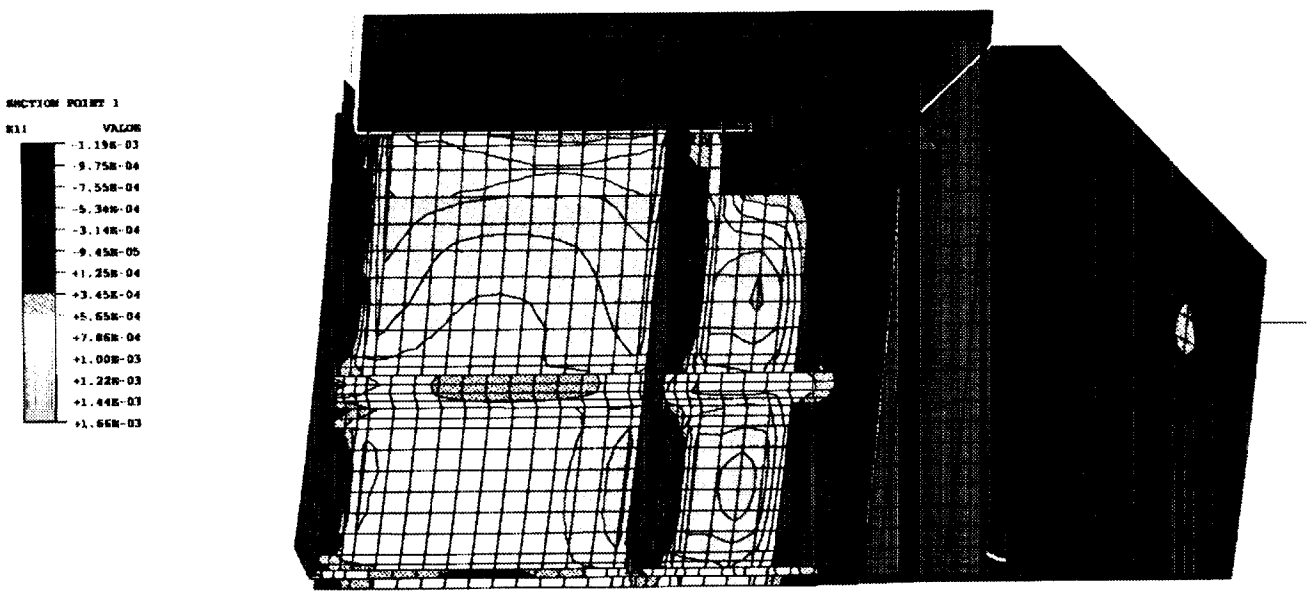


TCAPS1: SLOTTED AXIAL DOUBLERS
p = 13.8 psi, Axial Load = 5000 lb/in

Appendix H

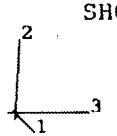
Finite Element Results for Undamaged Panel 2

ABAQUS



TCAPS2: Axial Strain, p=18.2 psi, Ax Ld=1110 lb/in

SHORT DOUBLERS, Nonlinear Sol'n

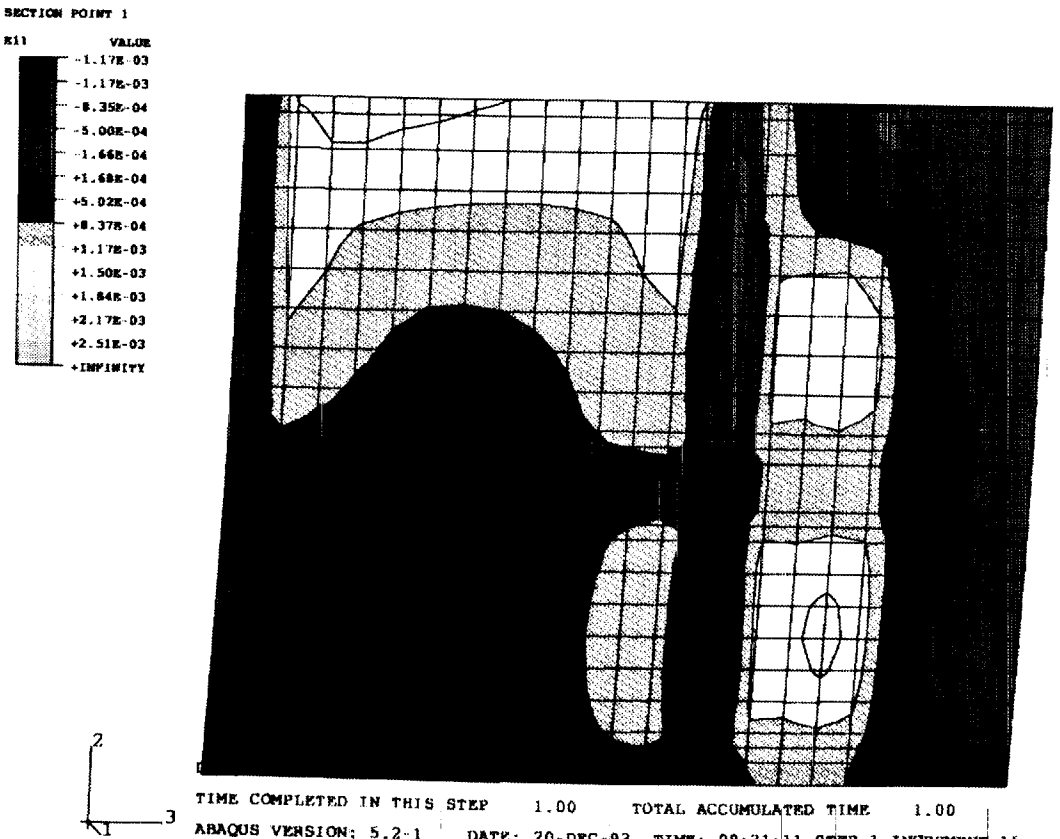


DISPLACEMENT MAGNIFICATION FACTOR = 1.00

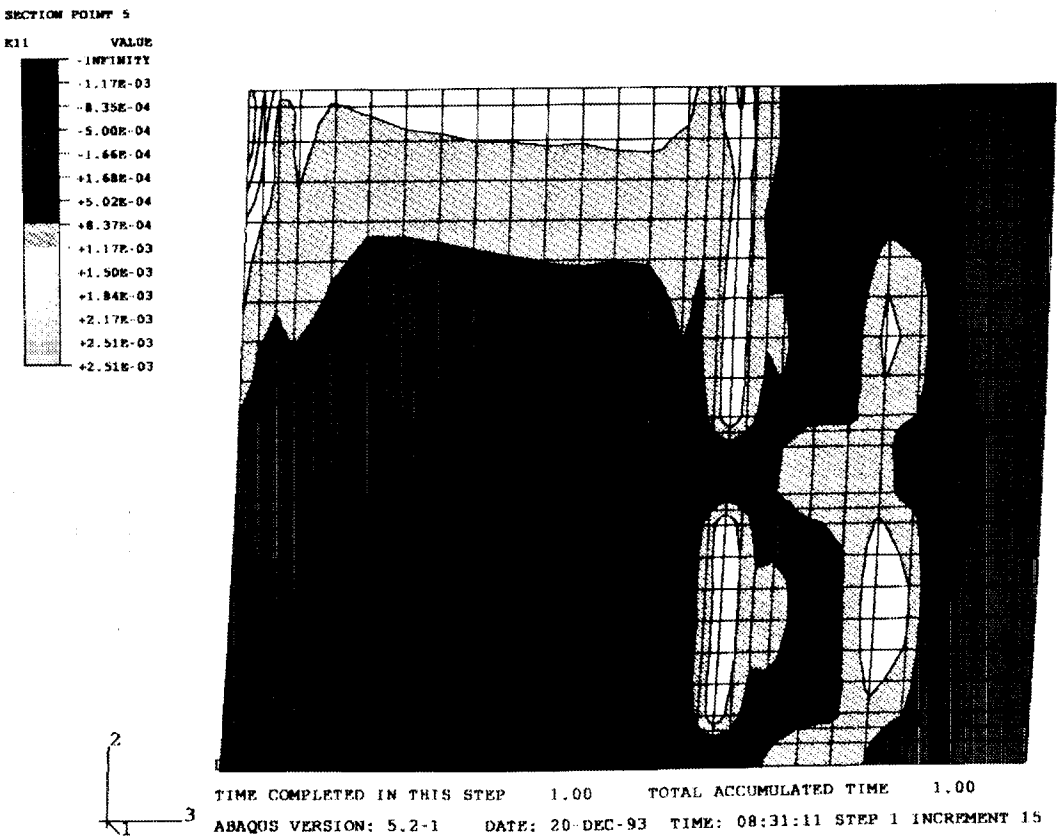
TIME COMPLETED IN THIS STEP 1.00 TOTAL ACCUMULATED TIME 1.00

ABAQUS VERSION: 5.2-1 DATE: 20-DEC-93 TIME: 08:31:11 STEP 1 INCREMENT 15

ABAQUS

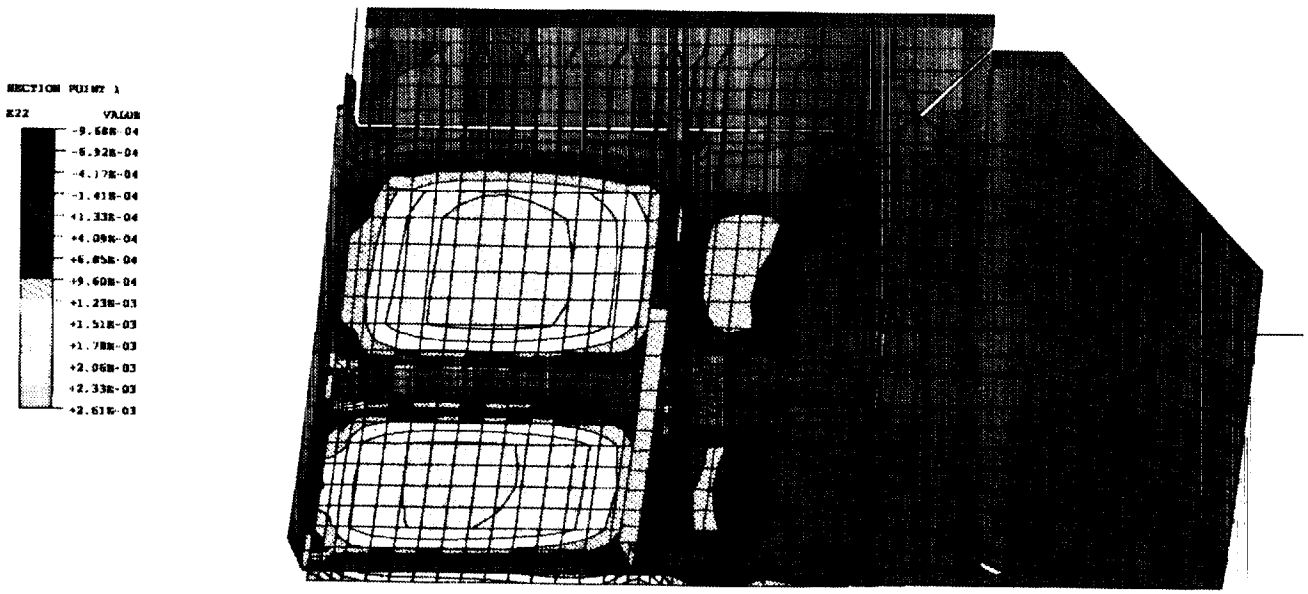


TCAPS2: Axial Strain, Outer Surf, p=18.2 psi Ax Ld=1110 lb/in
SHORT DBLRS, Strain Range set by Inner & Outer Surf Limits, NONLINEAR



TCAPS2: Axial Strain, Inner Surf, p=18.2 psi, Ax Ld=1110 lb/in
SHORT DBLRS, Strain Range set by Inner & Outer Surf Limits, NONLINEAR

ABAQUS



TCAPS2: Hoop Strain, p=18.2 psi, Ax Ld=1110 lb/in

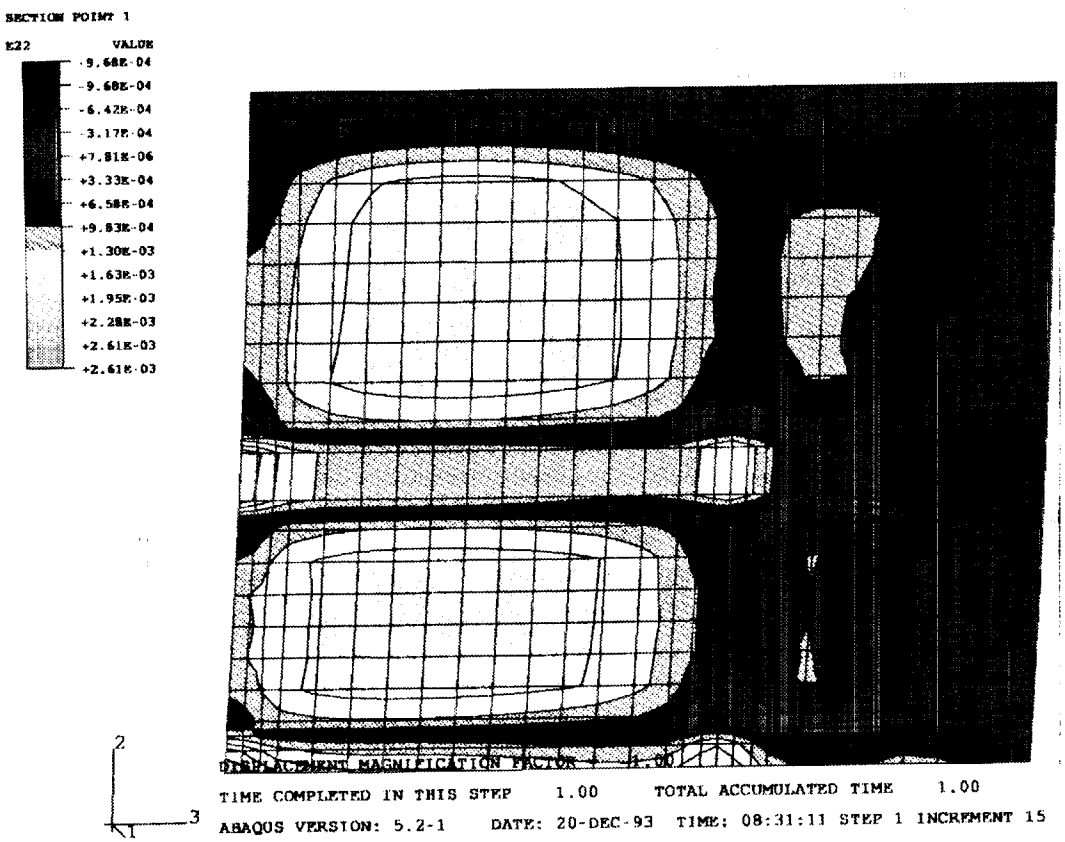
SHORT DOUBLERS, Nonlinear Sol'n

2
3
1

DISPLACEMENT MAGNIFICATION FACTOR = 1.00

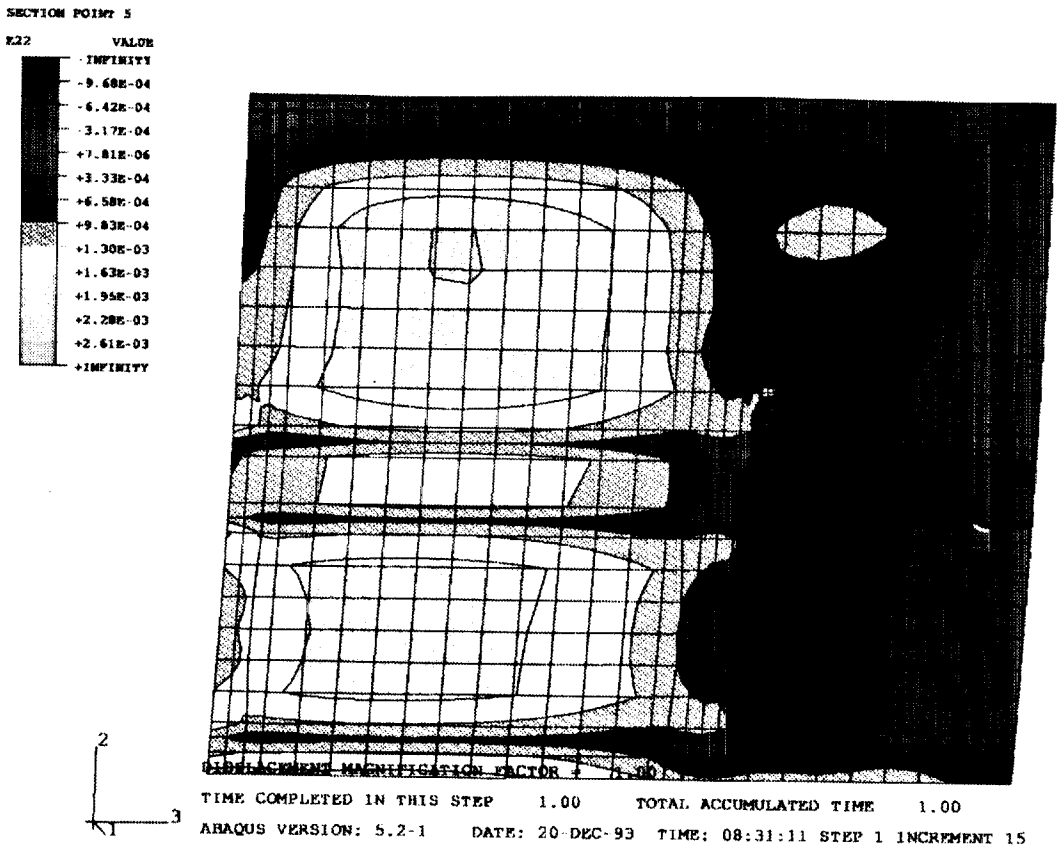
TIME COMPLETED IN THIS STEP 1.00 TOTAL ACCUMULATED TIME 1.00

ABAQUS VERSION: 5.2-1 DATE: 20-DEC-93 TIME: 08:31:11 STEP 1 INCREMENT 15

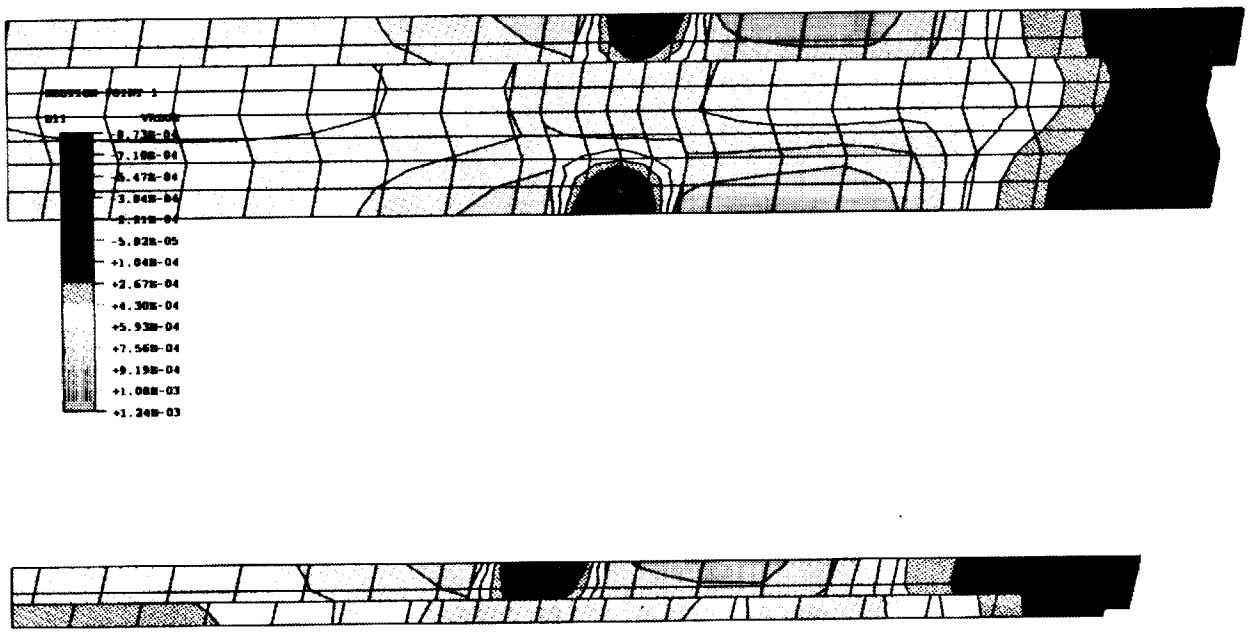


TCAPS2: Hoop Strain, Outer Surf, p=18.2 psi, Ax Ld=1110 lb/in
SHORT DBLRS, Strain Range set by Inner & Outer Surf Limits, NONLINEAR

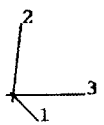
ABAQUS



TCAPS2: Hoop Strain, Inner Surf, p=18.2 psi, Ax Ld=1110 lb/in
SHORT DBLRS, Strain Range set by Inner & Outer Surf Limits, NONLINEAR



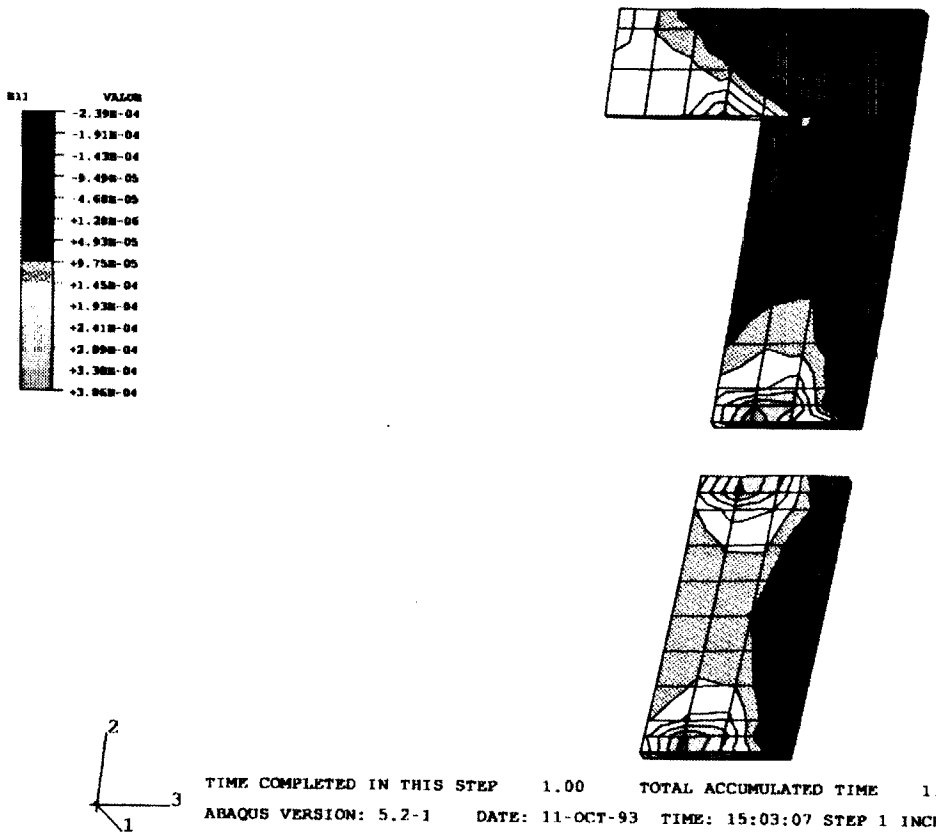
TCAPS2: SHORT DBLRS, p=18.2 psi, Ax Ld=1110 lb/in



TIME COMPLETED IN THIS STEP 1.00 TOTAL ACCUMULATED TIME 1.00

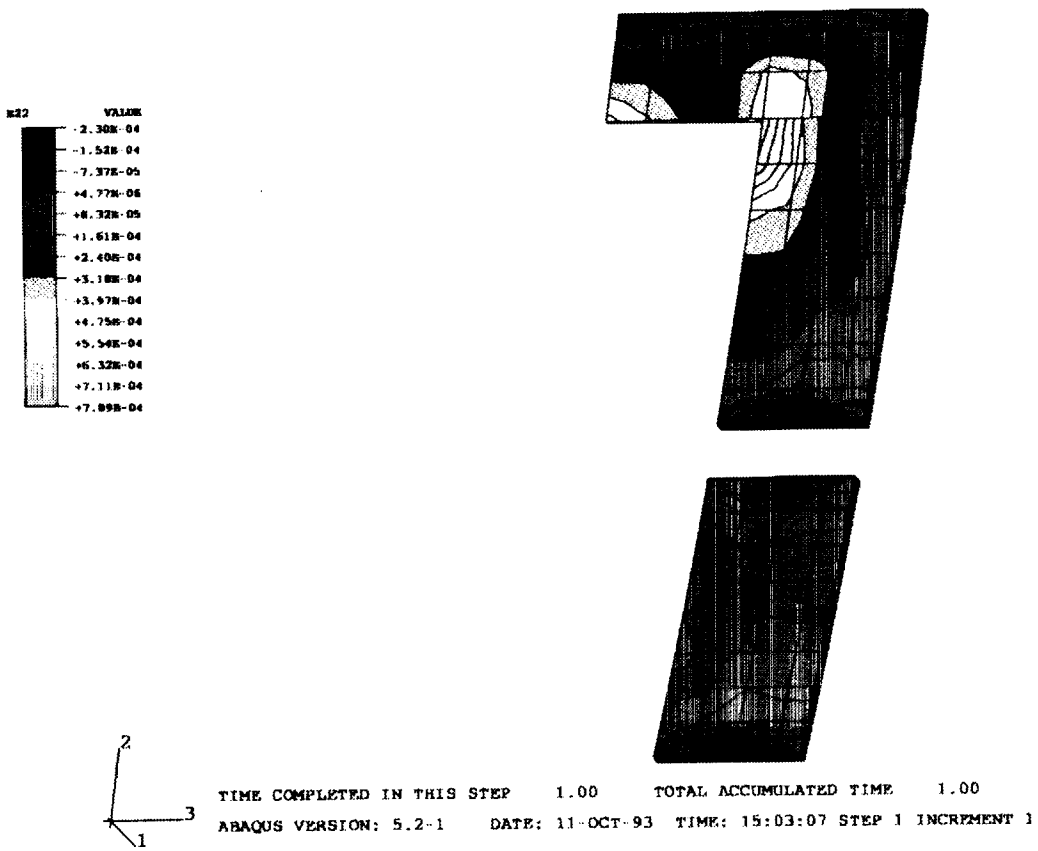
ABAQUS VERSION: 5.2-1 DATE: 11-OCT-93 TIME: 15:03:07 STEP 1 INCREMENT 1

ABAQUS



TCAPS2: SHORT DBLRS, p=18.2 psi, Ax Ld=1110 lb/in

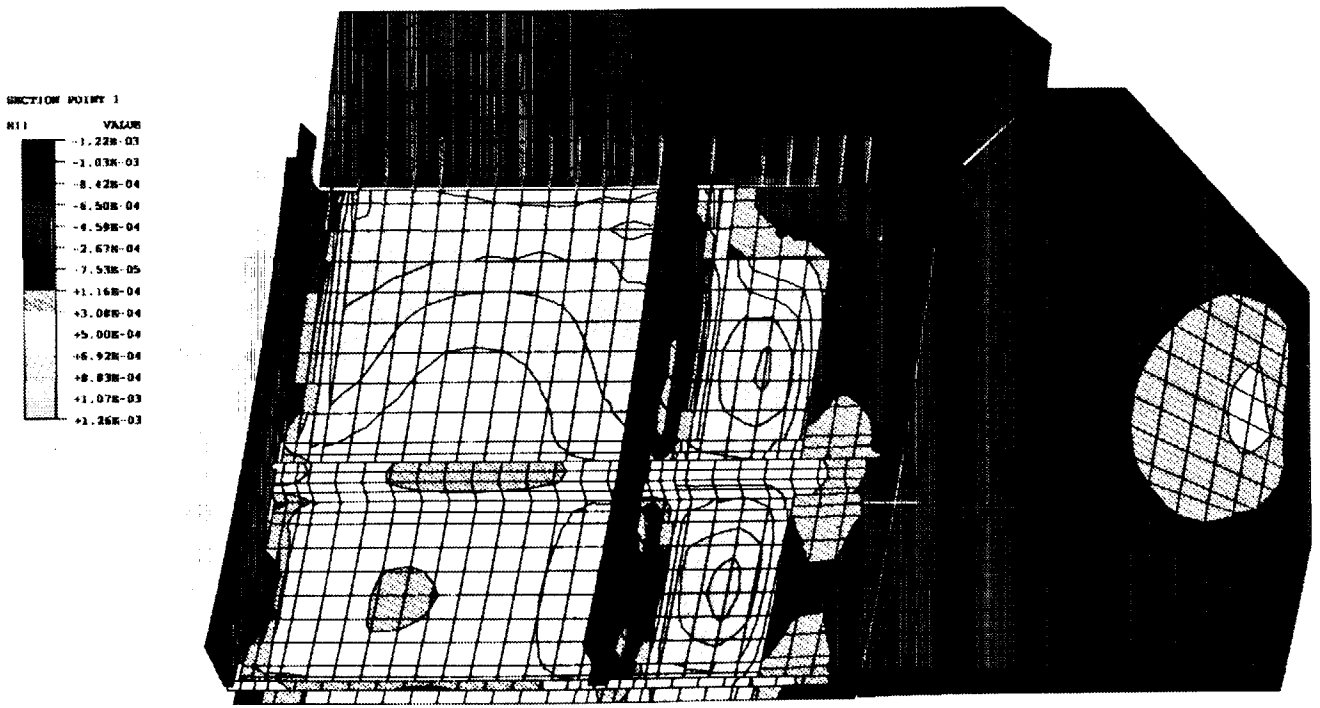
ABAQUS

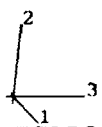


TCAPS2: SHORT DBLRS, p=18.2 psi, Ax Ld=1110 lb/in

Appendix I

Finite Element Results for Undamaged Panel 3





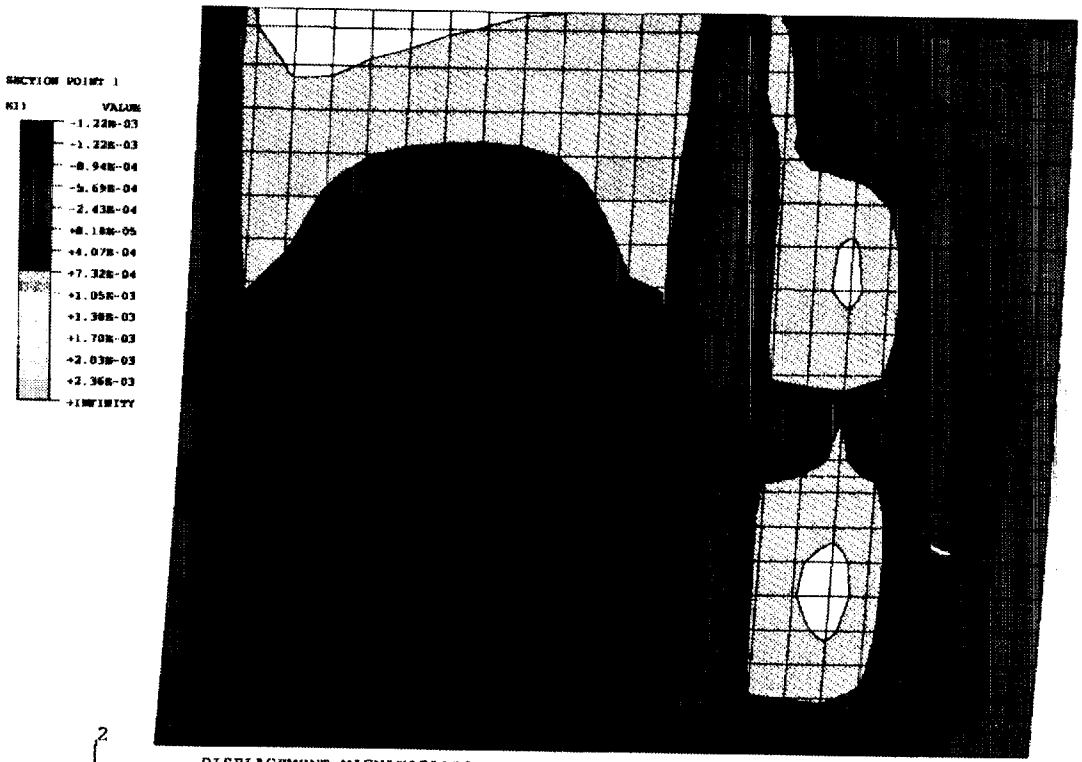
DISPLACEMENT MAGNIFICATION FACTOR = 1.00

TIME COMPLETED IN THIS STEP 1.00 TOTAL ACCUMULATED TIME 1.00

ABAQUS VERSION: 5.2-1 DATE: 29-SEP-93 TIME: 17:07:31 STEP 1 INCREMENT 14

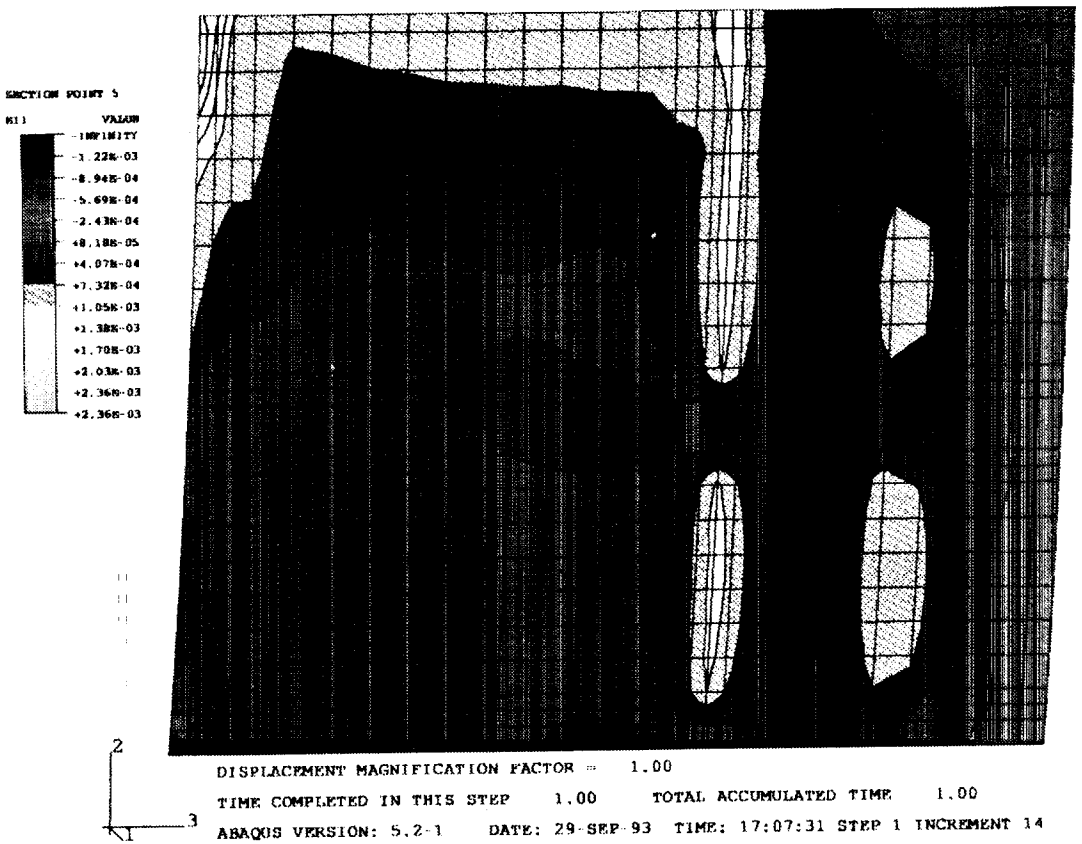
TCAPS3: Axial Strain, p = 18.2 psi, Ax Ld = 1110 lb/in

SHORT DOUBLERS, NONLINEAR SOLUTION



TCAPS3: Axial Strain, Outer Surf, p=18.2 psi, Ax Ld=1110 lb/in

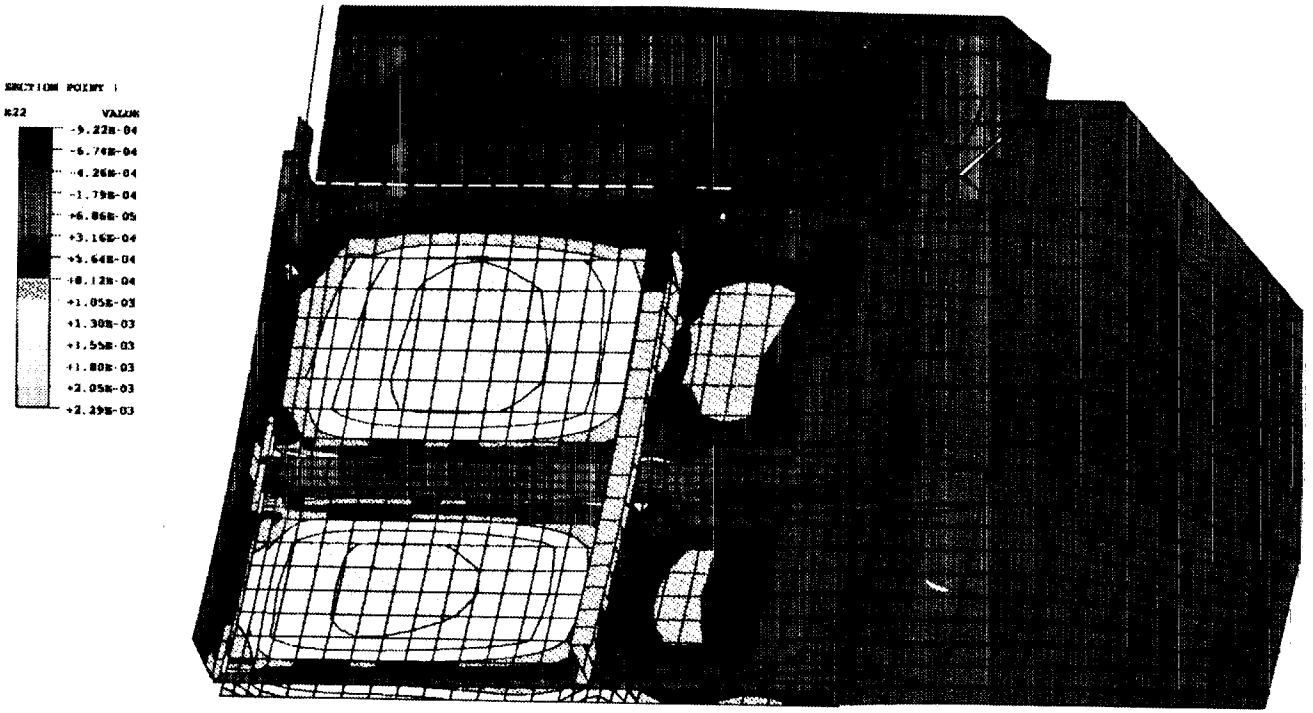
SHORT DBLRS, Strain Range set by Inner & Outer Surf Limits, NONLINEAR



TCAPS3: Axial Strain, Inner Surf, p=18.2 psi, Ax Ld=1110 lb/in

SHORT DBLRS, Strain Range set by Inner & Outer Surf Limits, NONLINEAR

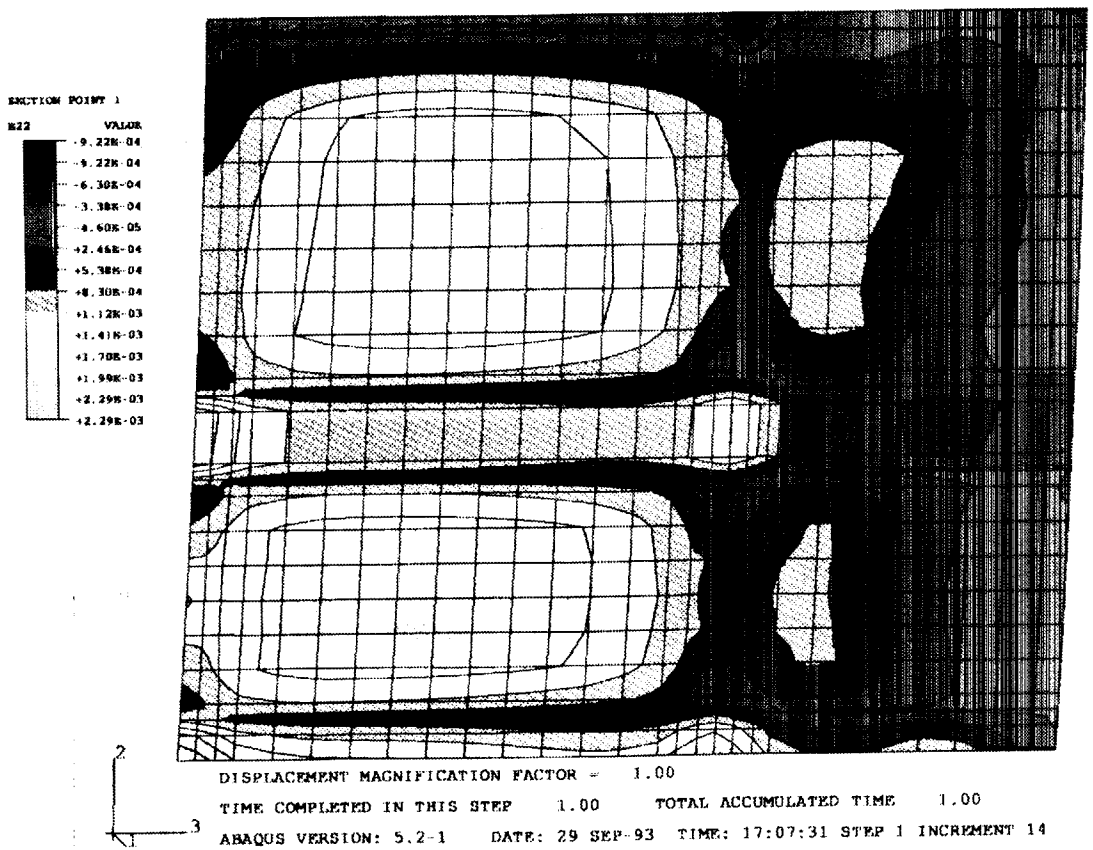
ABAQUS



TCAPS3: Hoop Strain, p = 18.2 psi, Ax Ld = 1110 lb/in

SHORT DOUBLERS, NONLINEAR SOLUTION

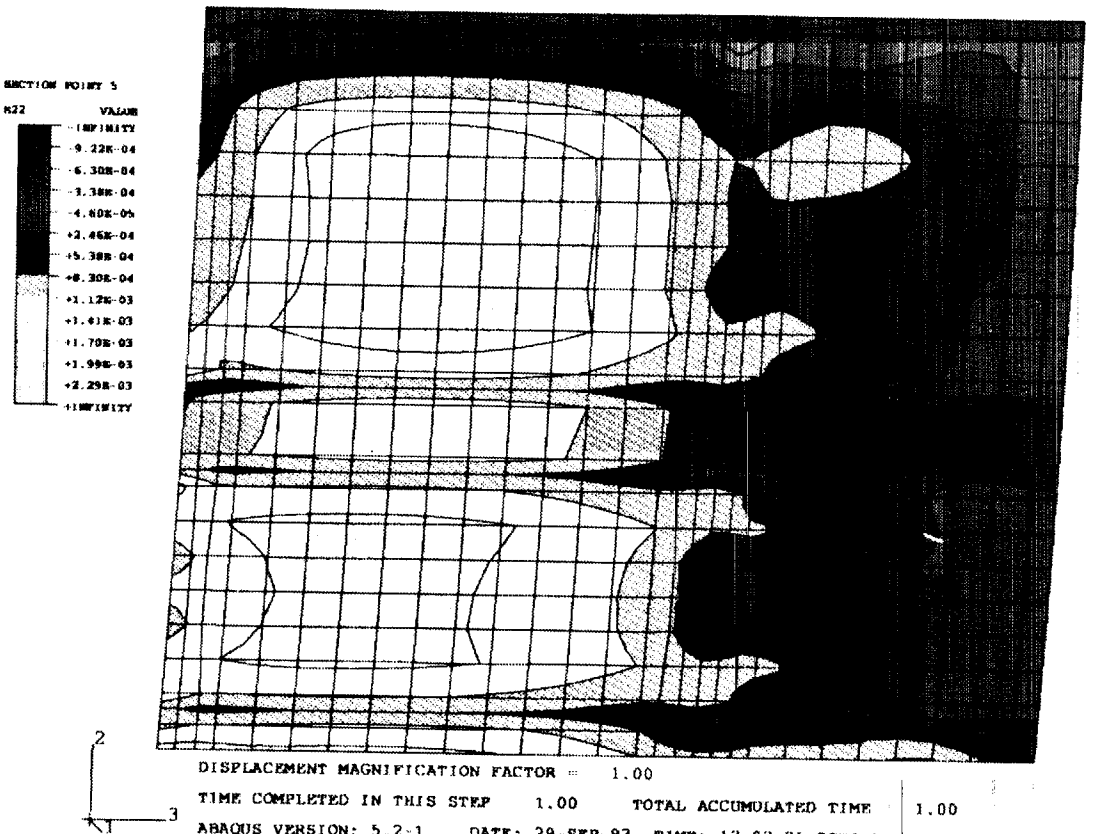
ABAQUS



TCAPS3: Hoop Strain, Outer Surf, p=18.2 psi, Ax Ld=1110 lb/in

SHORT DBLRS, Strain Range set by Inner & Outer Surf Limits, NONLINEAR

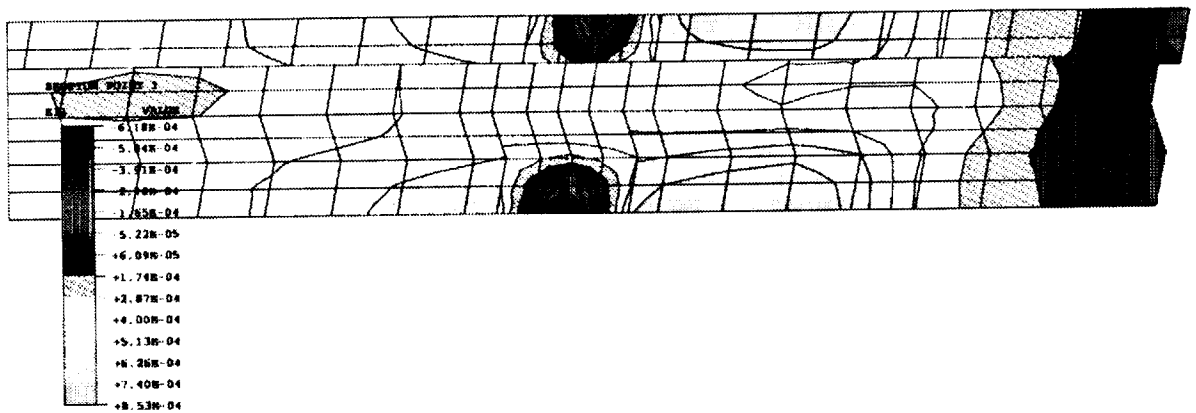
ABAQUS

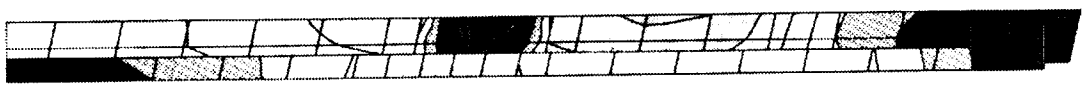


TCAPS3: Hoop Strain, Inner Surf, p=18.2 psi, Ax Ld=1110 lb/in

SHORT DBLRS, Strain Range set by Inner & Outer Surf Limits, NONLINEAR

ABAQUS





TCAPS3: Axial Strain, p = 18.2 psi, Ax Load = 1110 lb/in

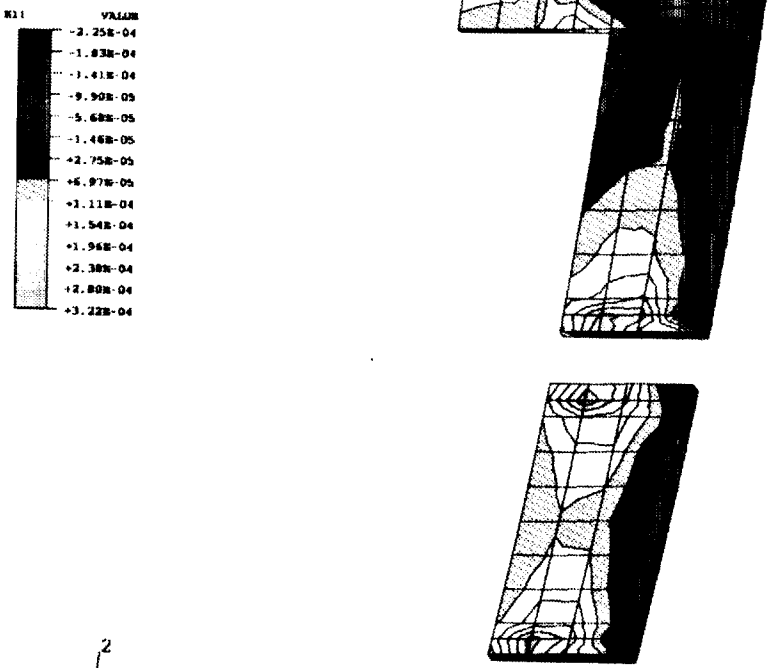
SHORT DOUBLERS, Linear Elastic Sol'n



TIME COMPLETED IN THIS STEP 1.00 TOTAL ACCUMULATED TIME 1.00

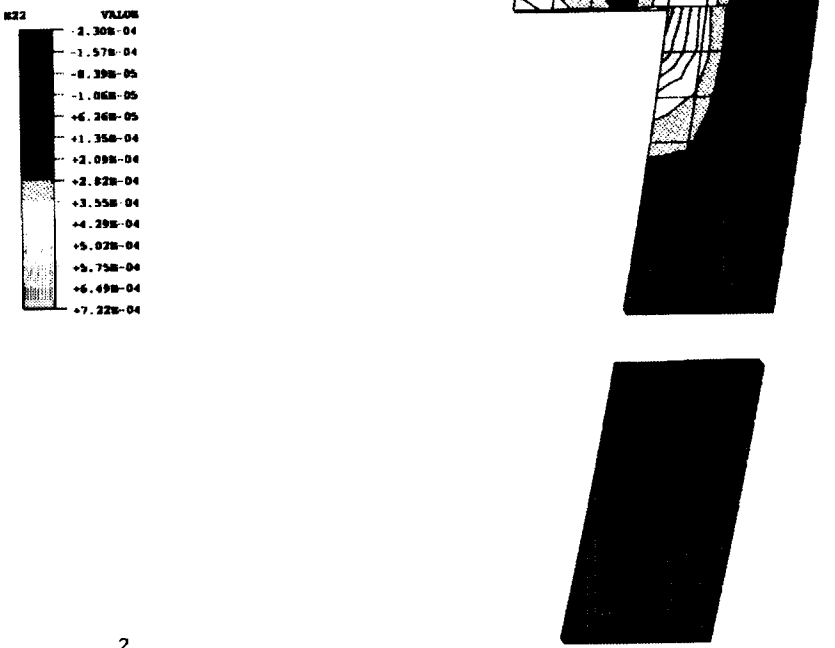
ABAQUS VERSION: 5.2-1 DATE: 06-OCT-93 TIME: 12:59:56 STEP 1 INCREMENT 1

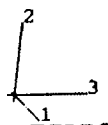
ABAQUS



TCAPS3: Axial Strain, p = 18.2 psi, Ax Load = 1110 lb/in
SHORT DOUBLERS, Linear Elastic Sol'n

ABAQUS





TIME COMPLETED IN THIS STEP 1.00 TOTAL ACCUMULATED TIME 1.00

ABAQUS VERSION: 5.2-1 DATE: 06-OCT-93 TIME: 12:59:56 STEP 1 INCREMENT 1

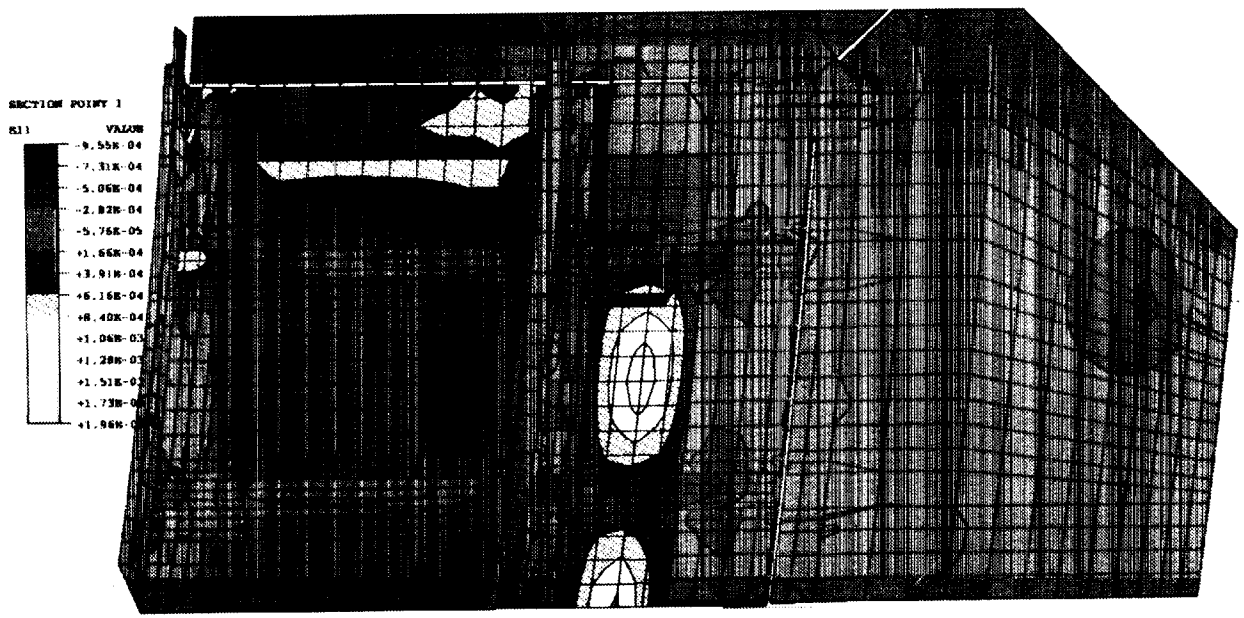
TCAPS3: Hoop Strain, p = 18.2 psi, Ax Load = 1110 lb/in

SHORT DOUBLERS, Linear Elastic Sol'n

Appendix J

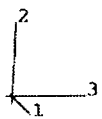
Finite Element Results for Undamaged Panel 4

ABAQUS



TCAPS4: Axial Strain, p=18.2 psi, Ax Ld=1110 lb/in

SHORT DOUBLERS, NONLINEAR SOLUTION

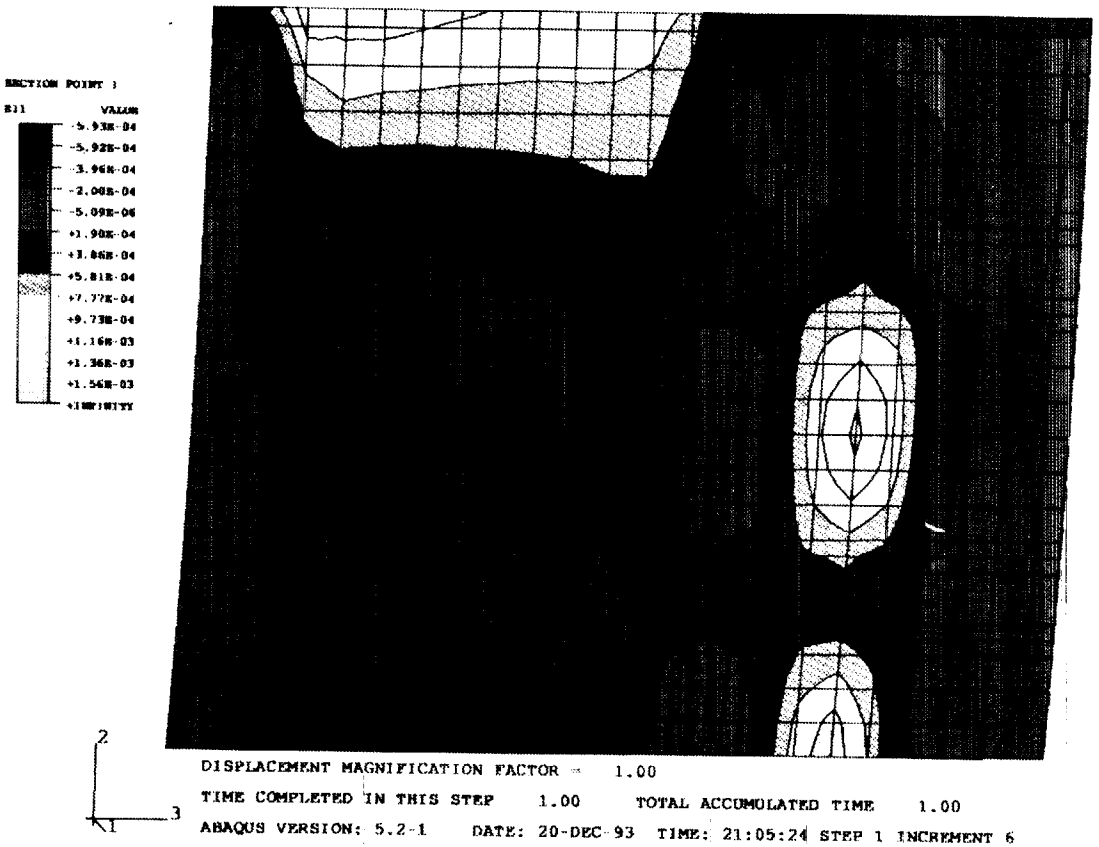


DISPLACEMENT MAGNIFICATION FACTOR = 1.00

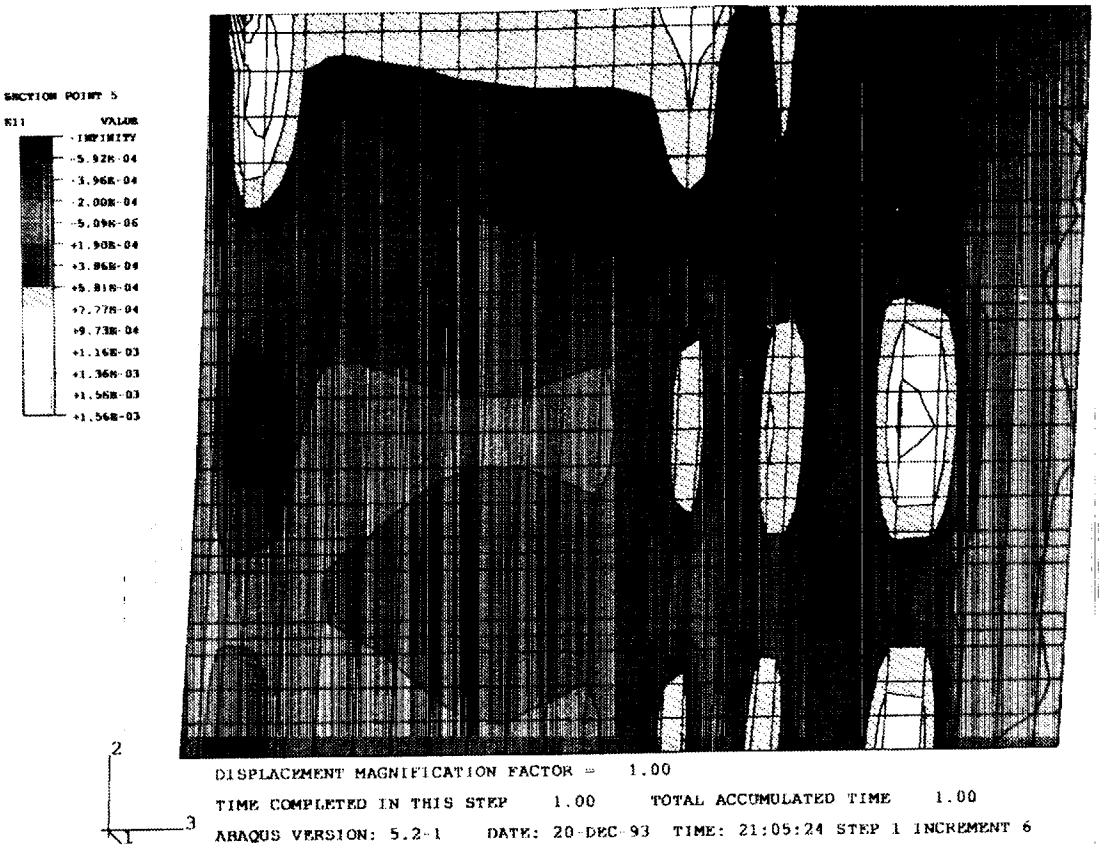
TIME COMPLETED IN THIS STEP 1.00 TOTAL ACCUMULATED TIME 1.00

ABAQUS VERSION: 5.2-1 DATE: 20-DEC-93 TIME: 21:05:24 STEP 1 INCREMENT 6

ABAQUS



TCAPS4: Axial Strain, Outer Surface, p=18.2 psi, Ax Ld=1110 lb/in
SHORT DBLRS, Strain Range set by Inner & Outer Surf Limits, NONLINEAR



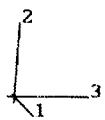
TCAPS4: Axial Strain, Inner Surface, p=18.2 psi, Ax Ld=1110 lb/in
SHORT DBLRS, Strain Range set by Inner & Outer Surf Limits, NONLINEAR

ABAQUS



TCAPS4: Hoop Strain, p=18.2 psi, Ax Ld=1110 lb/in

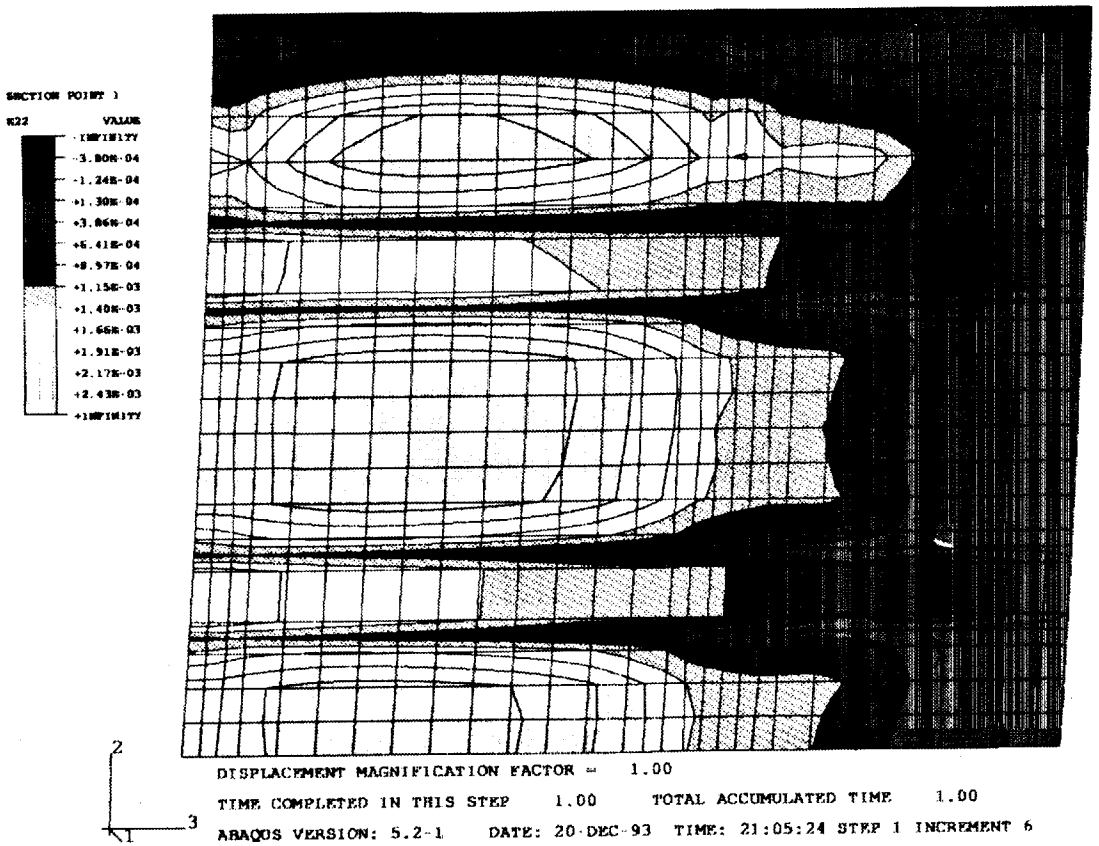
SHORT DOUBLERS, NONLINEAR SOLUTION



DISPLACEMENT MAGNIFICATION FACTOR = 1.00

TIME COMPLETED IN THIS STEP 1.00 TOTAL ACCUMULATED TIME 1.00

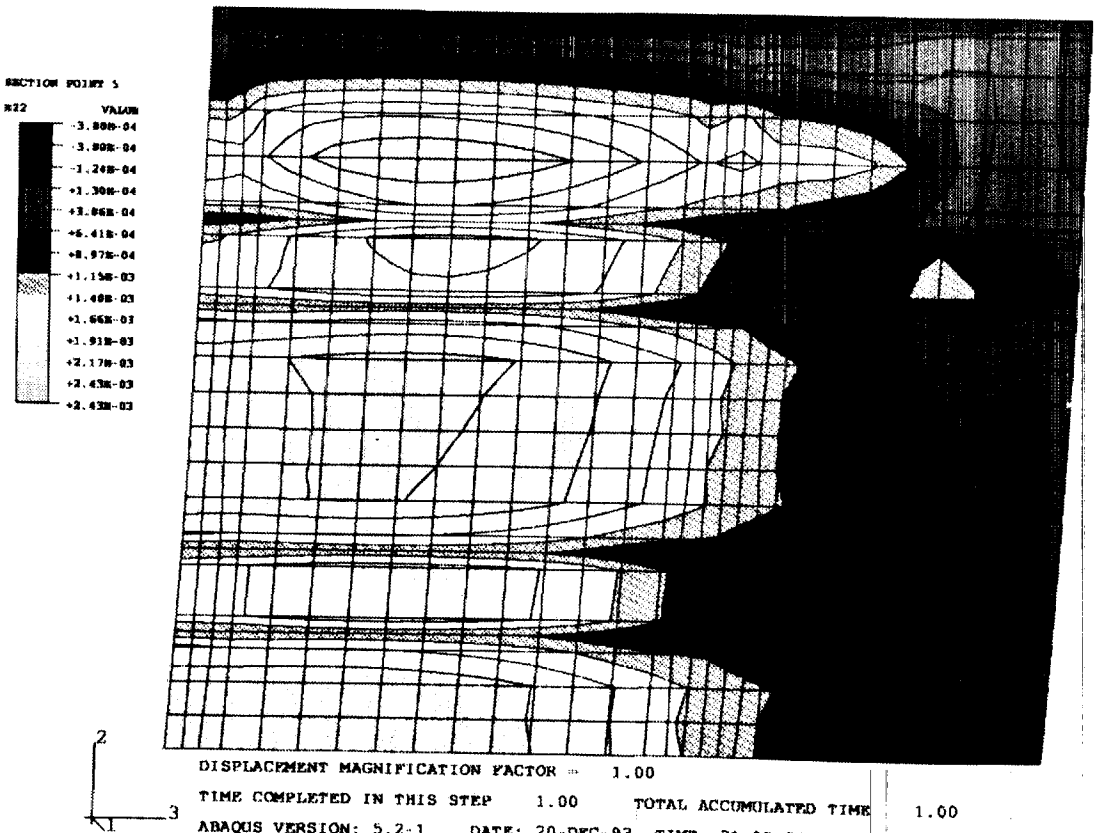
ABAQUS VERSION: 5.2-1 DATE: 20-DEC-93 TIME: 21:05:24 STEP 1 INCREMENT 6



TCAPS4: Hoop Strain, Outer Surface, p=18.2 psi, Ax Ld=1110 lb/in

SHORT DBLRS, Strain Range set by Inner & Outer Surf Limits, NONLINEAR

ABAQUS

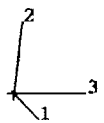


TCAPS4: Hoop Strain, Inner Surface, p=18.2 psi, Ax Ld=1110 lb/in

SHORT DBLRS, Strain Range set by Inner & Outer Surf Limits, NONLINEAR



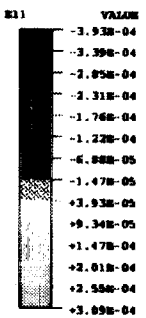
TCAPS4: SHORT DBLRS, p = 18.2 psi, Ax Ld = 1110 lb/in

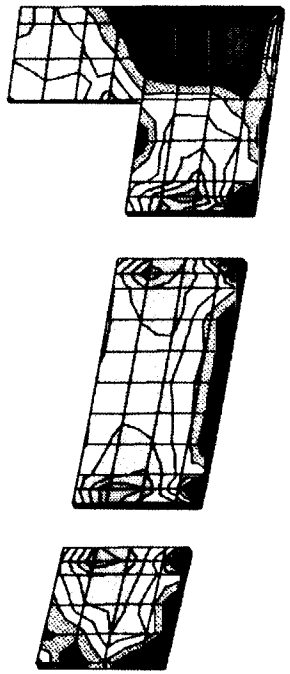


TIME COMPLETED IN THIS STEP 1.00 TOTAL ACCUMULATED TIME 1.00

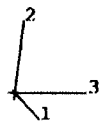
ABAQUS VERSION: 5.2-1 DATE: 24-AUG-93 TIME: 10:36:08 STEP 1 INCREMENT 1

ABAQUS





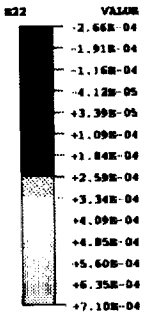
TCAPS4: SHORT DBLRS, p = 18.2 psi, Ax Ld = 1110 lb/in



TIME COMPLETED IN THIS STEP 1.00 TOTAL ACCUMULATED TIME 1.00

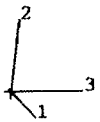
ABAQUS VERSION: 5.2-1 DATE: 24-AUG-93 TIME: 10:36:08 STEP 1 INCREMENT 1

ABAQUS





TCAPS4: SHORT DBLRS, p = 18.2 psi, Ax Ld = 1110 lb/in



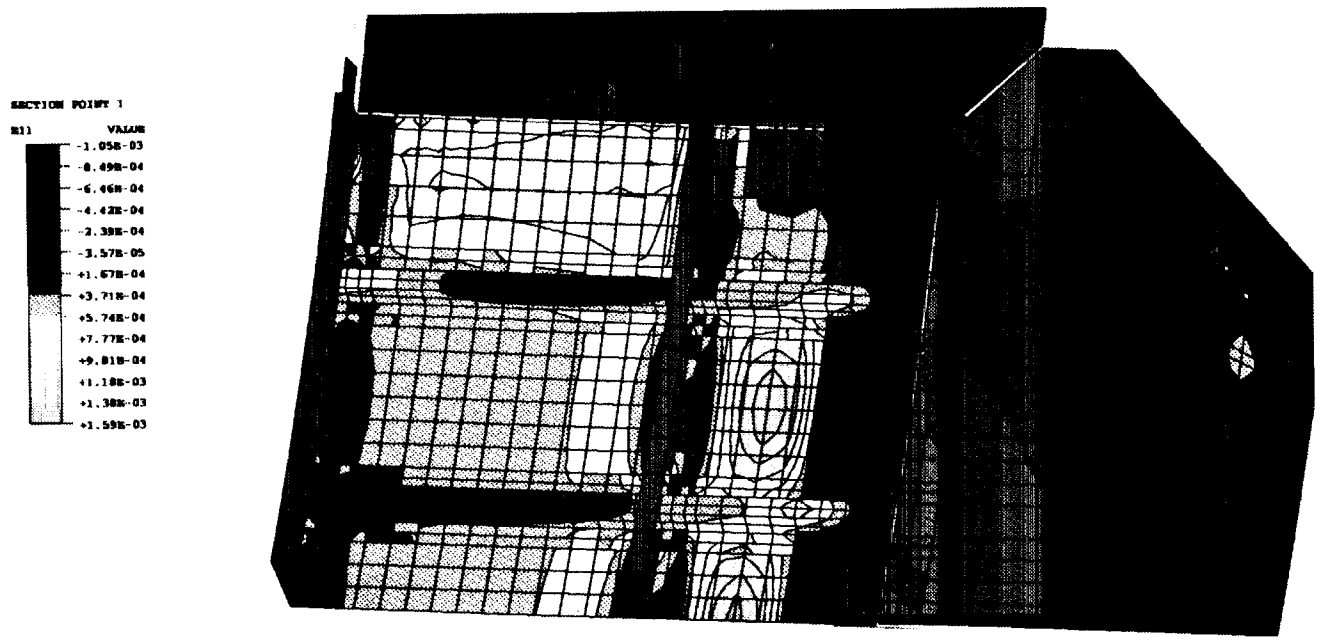
TIME COMPLETED IN THIS STEP 1.00 TOTAL ACCUMULATED TIME 1.00

ABAQUS VERSION: 5.2-1 DATE: 24-AUG-93 TIME: 10:36:08 STEP 1 INCREMENT 1

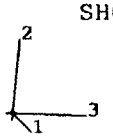
Appendix K

Finite Element Results for Undamaged Panel 5

ABAQUS



TCAPS5: Axial Strain, p=18.2 psi, Ax Load=1110 lb/in
SHORT DOUBLERS, Nonlinear Sol'n

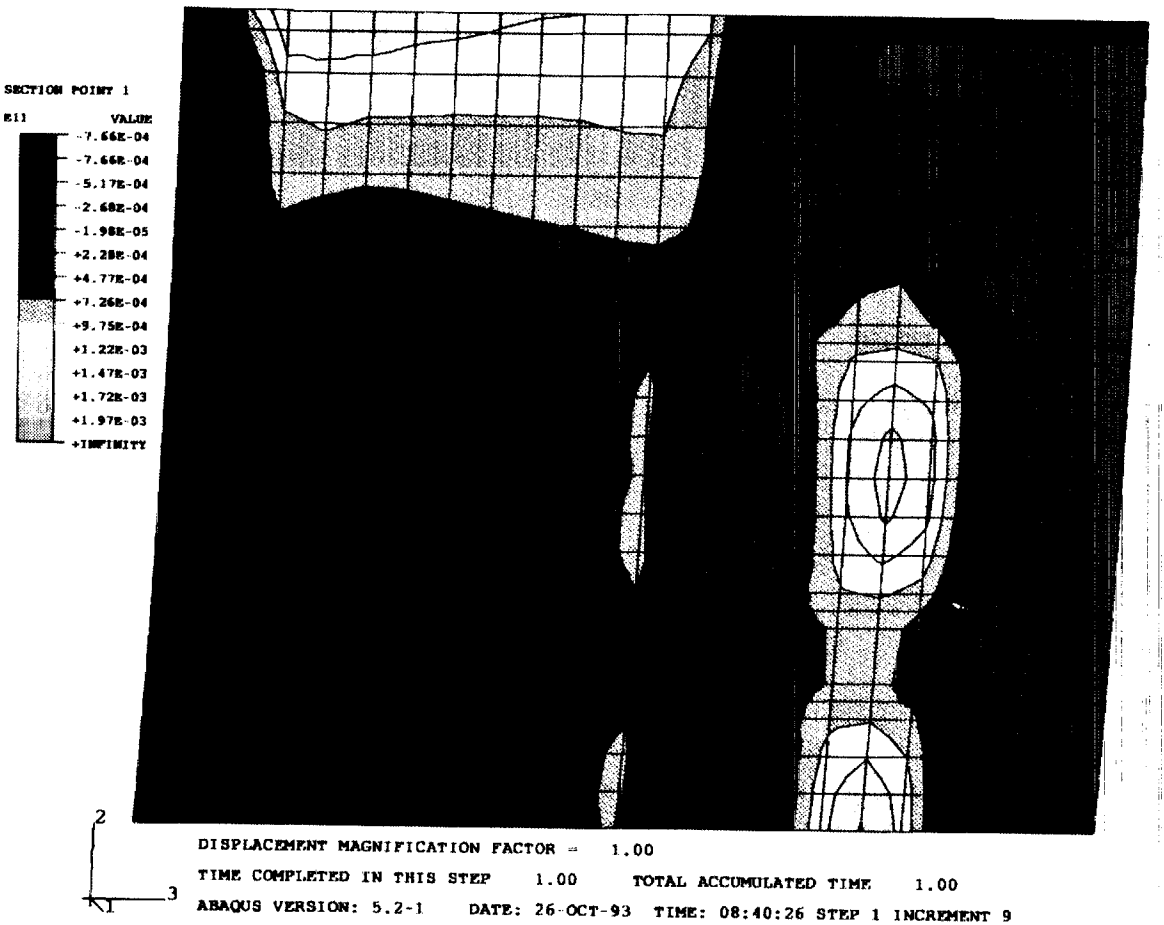


DISPLACEMENT MAGNIFICATION FACTOR = 1.00

TIME COMPLETED IN THIS STEP 1.00 TOTAL ACCUMULATED TIME 1.00

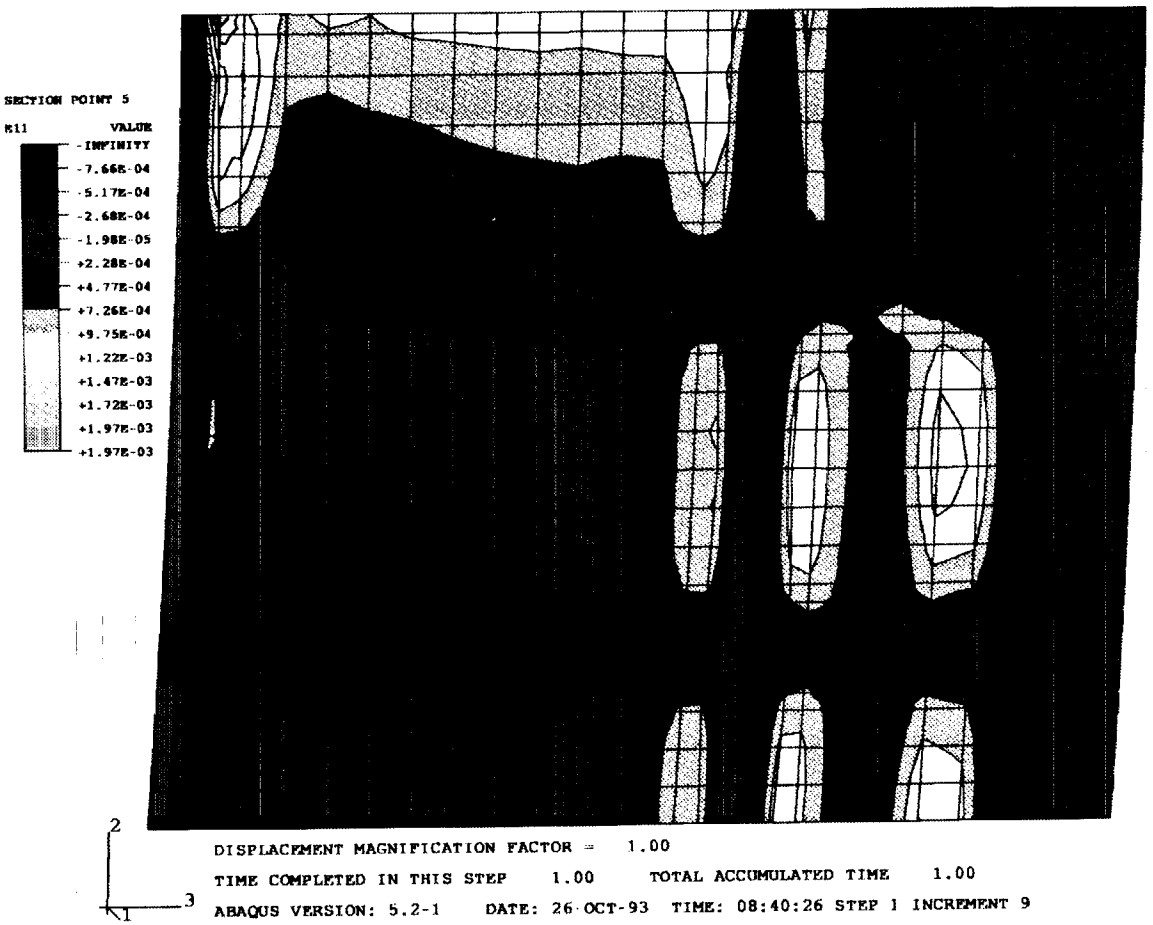
ABAQUS VERSION: 5.2-1 DATE: 26-OCT-93 TIME: 08:40:26 STEP 1 INCREMENT 9

ABAQUS



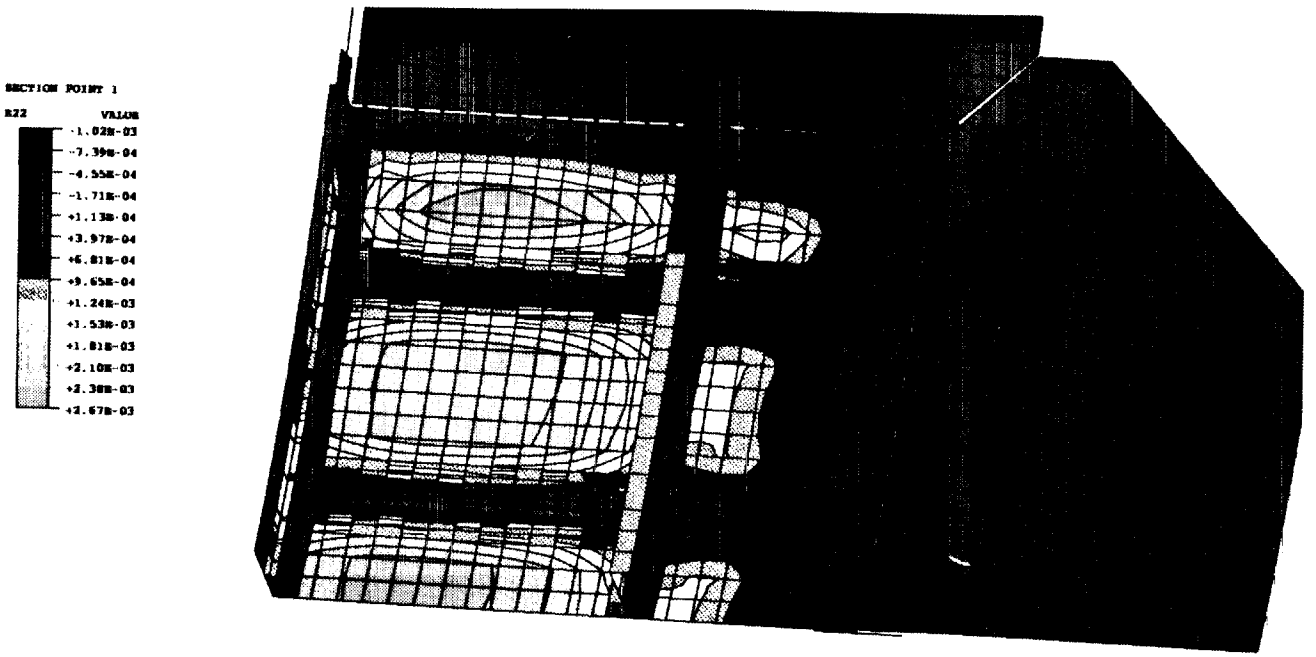
TCAPS5: Axial Strain, Outer Surf, p=18.2 psi Ax Ld=1110 lb/in
SHORT DBLRS, Strain Range set by Inner & Outer Surf Limits, NONLINEAR

ABAQUS

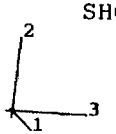


TCAPS5: Axial Strain, Inner Surf, p=18.2 psi, Ax Ld=1110 lb/in
SHORT DBLRS, Strain Range set by Inner & Outer Surf Limits, NONLINEAR

ABAQUS



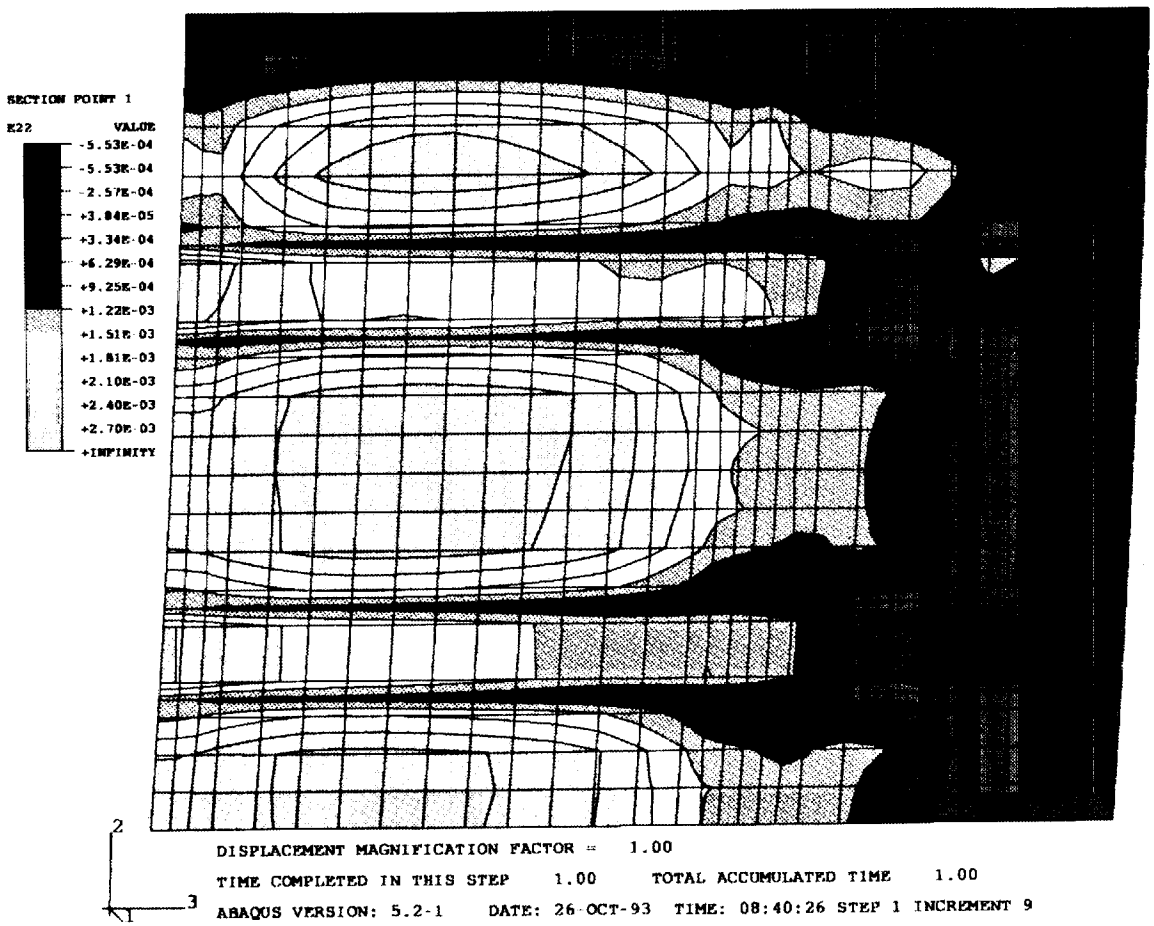
TCAPS5: Hoop Strain, p=18.2 psi, Ax Load=1110 lb/in
SHORT DOUBLERS, Nonlinear Sol'n



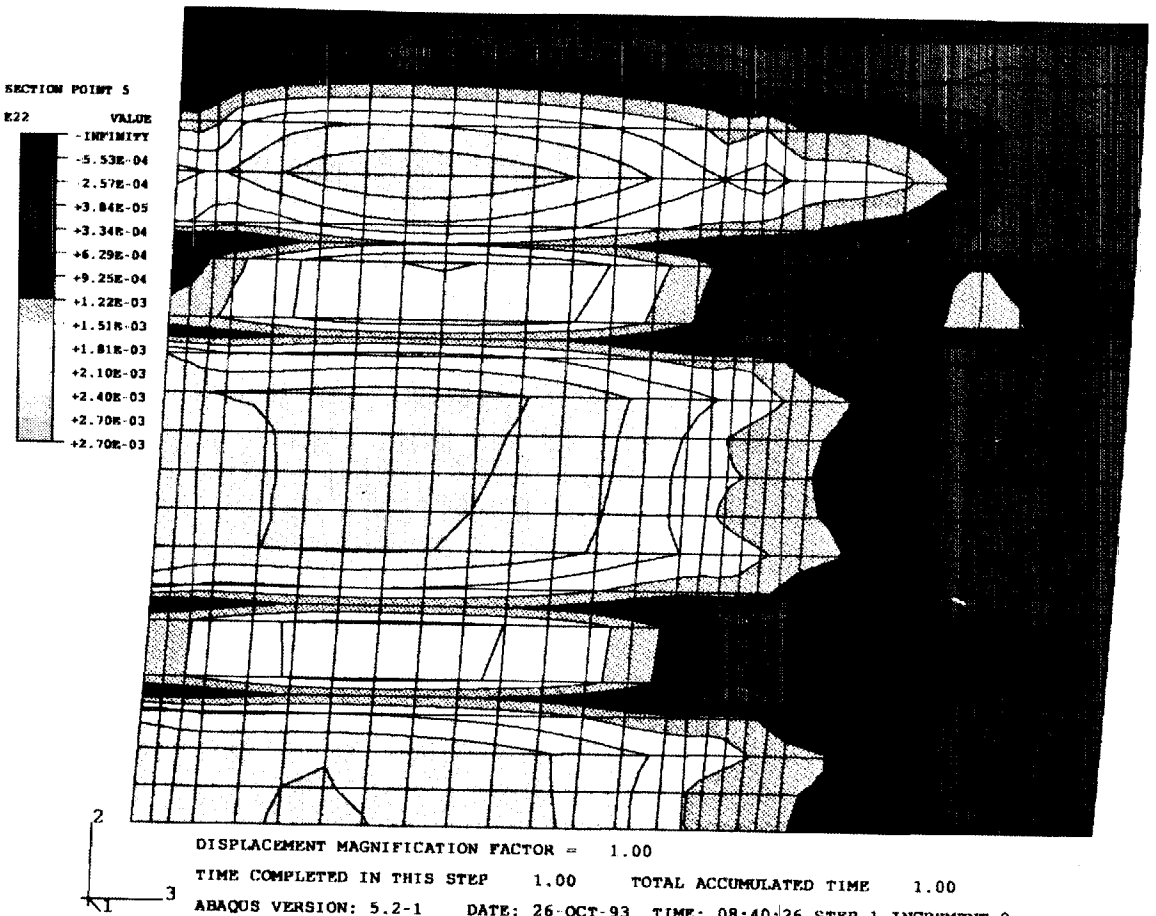
DISPLACEMENT MAGNIFICATION FACTOR = 1.00

TIME COMPLETED IN THIS STEP 1.00 TOTAL ACCUMULATED TIME 1.00

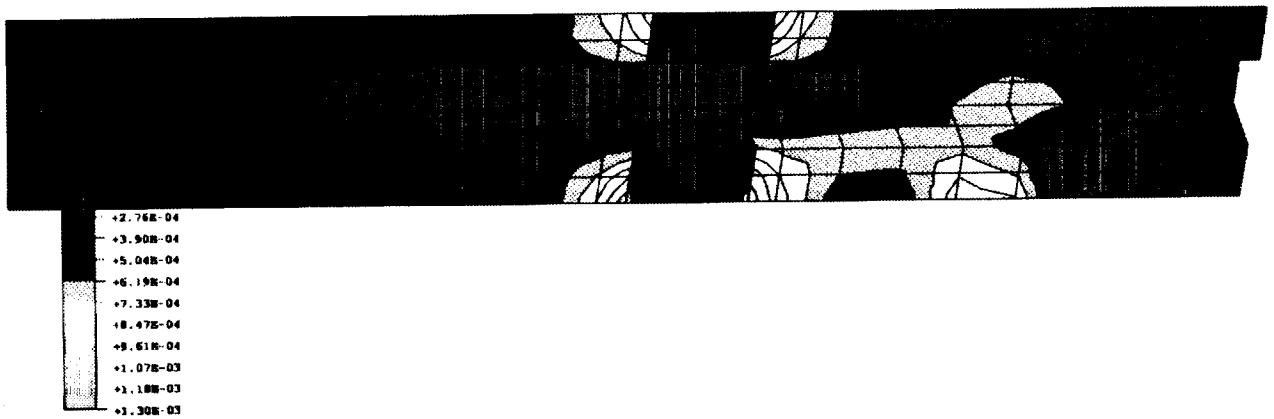
ABAQUS VERSION: 5.2-1 DATE: 26-OCT-93 TIME: 08:40:26 STEP 1 INCREMENT 9

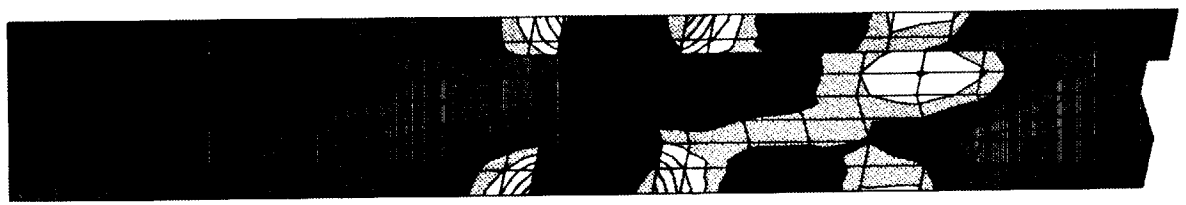


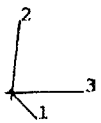
TCAPS5: Hoop Strain, Outer Surf, p=18.2 psi, Ax Ld=1110 lb/in
SHORT DBLRS, Strain Range set by Inner & Outer Surf Limits, NONLINEAR



TCAPS5: Hoop Strain, Inner Surf, p=18.2 psi, Ax Ld=1110 lb/in
SHORT DBLRS, Strain Range set by Inner & Outer Surf Limits, NONLINEAR



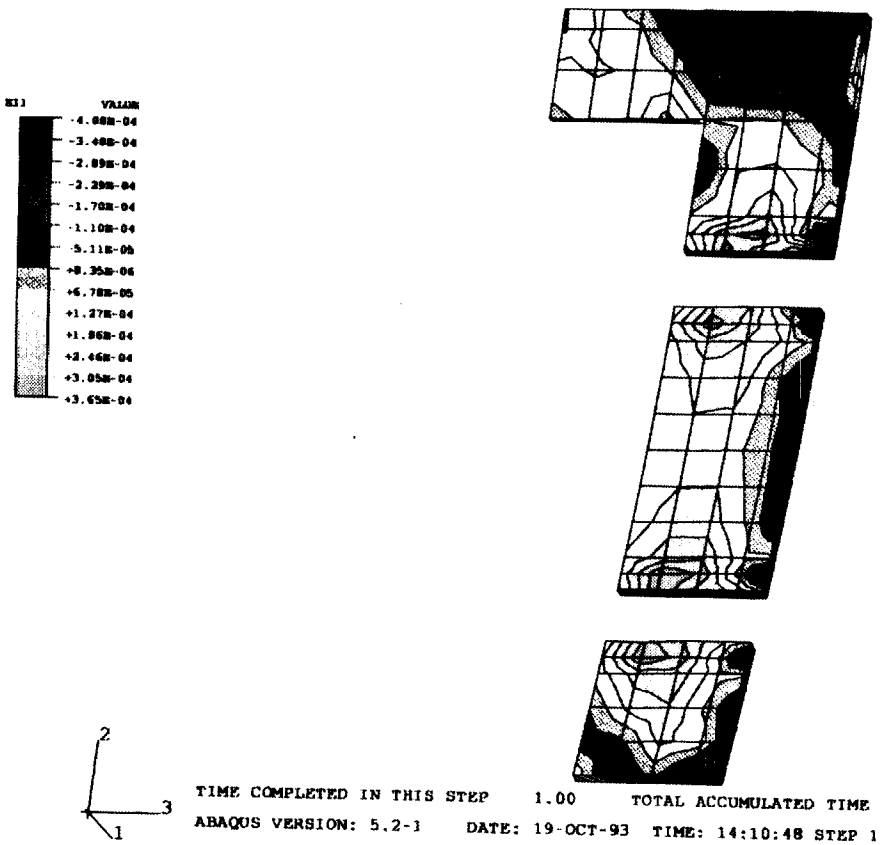




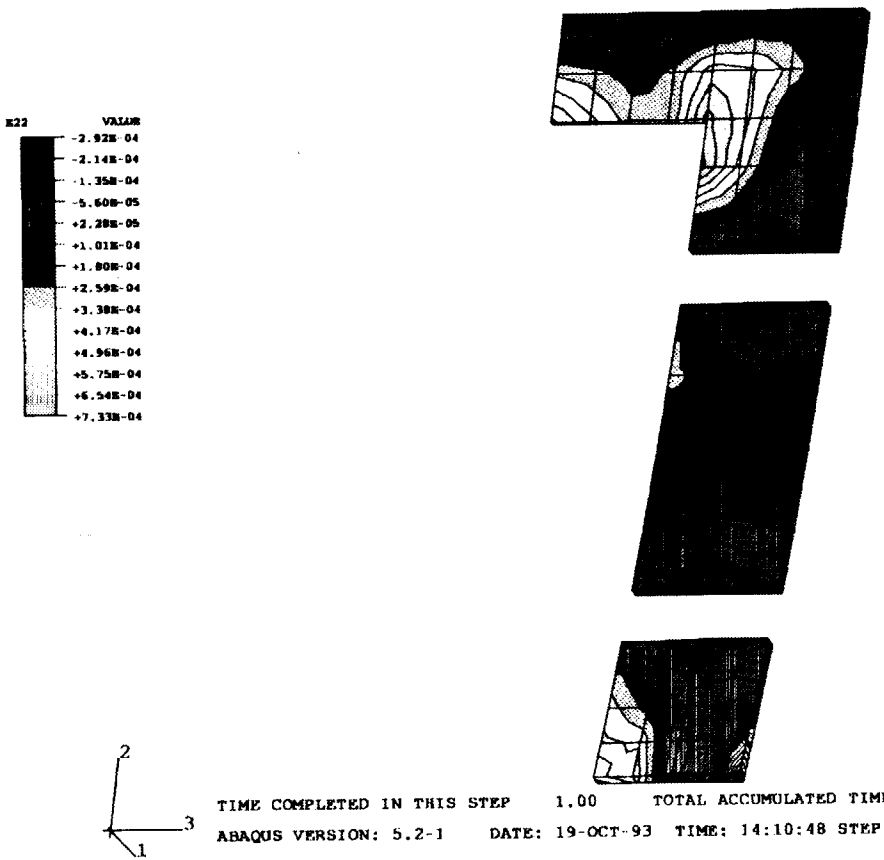
TIME COMPLETED IN THIS STEP 1.00 TOTAL ACCUMULATED TIME 1.00

ABAQUS VERSION: 5.2-1 DATE: 19-OCT-93 TIME: 14:10:48 STEP 1 INCREMENT 1

TCAPS5: SHORT DOUBLERS, p = 18.2 psi, Ax Ld = 1110 lb/in



TCAPS5: SHORT DOUBLERS, p = 18.2 psi, Ax Ld = 1110 Lb/in



TCAPS5: SHORT DOUBLERS, p = 18.2 psi, Ax Ld = 1110 Lb/in

REPORT DOCUMENTATION PAGE

Form Approved
OMB No. 0704-0188

Public reporting burden for this collection of information is estimated to average 1 hour per response, including the time for reviewing instructions, searching existing data sources, gathering and maintaining the data needed, and completing and reviewing the collection of information. Send comments regarding this burden estimate or any other aspect of this collection of information, including suggestions for reducing this burden, to Washington Headquarters Services, Directorate for Information Operations and Reports, 1215 Jefferson Davis Highway, Suite 1204, Arlington, VA 22202-4302, and to the Office of Management and Budget, Paperwork Reduction Project (0704-0188), Washington, DC 20503.

1. AGENCY USE ONLY (*Leave blank*)	2. REPORT DATE	3. REPORT TYPE AND DATES COVERED
	August 1994	Contractor Report

4. TITLE AND SUBTITLE
Benchmark Models

5. FUNDING NUMBERS
C NAS1-19349
TA 2

WU 505-02-13-01

6. AUTHOR(S)
T. H. Walker, L. B. Ilcewicz, J. B. Bodine, D. P. Murphy, and E. F. Dost

7. PERFORMING ORGANIZATION NAME(S) AND ADDRESS(ES)
Boeing Commercial Airplane Group
P. O. Box 3707
Seattle, WA 98124-2207

8. PERFORMING ORGANIZATION REPORT NUMBER

9. SPONSORING / MONITORING AGENCY NAME(S) AND ADDRESS(ES)
NASA Langley Research Center
Hampton, VA 23681-0001

10. SPONSORING / MONITORING AGENCY REPORT NUMBER
NASA CR-194969

11. SUPPLEMENTARY NOTES
Langley Technical Monitor: Mark J. Shuart
Final Report

12a. DISTRIBUTION / AVAILABILITY STATEMENT
FEDD

Subject Category 24

12b. DISTRIBUTION CODE

13. ABSTRACT (*Maximum 200 words*)

Results are presented for an analytical and experimental study of curved, stiffened composite panels for a commercial transport aircraft. Five panels representative of fuselage crown design alternatives were fabricated for concept evaluation. These panels are scheduled to be tested in the Pressure Box Test Machine at NASA Langley Research Center. The panels are characterized by a 122 in. radius, tow-placed skins, hot-drape-formed hat-section stringers, and braided/RTM J-section frames. A geometrically nonlinear finite element analysis was conducted to support the development of test fixturing and to provide predictions of undamaged panel response. A strain softening model for damaged structures is described and used to predict the response of damaged panels. Results for a study of the stringer-frame intersection ("mousehole") design detail are also presented. Bonded frame pull-off tests and supporting analyses are described.

14. SUBJECT TERMS
Composite structures; curved panels; stiffened panels; fuselage structures; nonlinear analysis; damage tolerance

15. NUMBER OF PAGES
235

16. PRICE CODE

17. SECURITY CLASSIFICATION OF REPORT	18. SECURITY CLASSIFICATION OF THIS PAGE	19. SECURITY CLASSIFICATION OF ABSTRACT	20. LIMITATION OF ABSTRACT
Unclassified	Unclassified	Unclassified	